Emanuel Andrada

A new model of the human trunk mechanics in walking

Berichte aus der Biomechatronik

Herausgegeben von Prof. Dr. Hartmut Witte
Fachgebiet Biomechatronik an der TU Ilmenau

Band 1

A new model of the human trunk mechanics in walking

von Emanuel Andrada

Universitätsverlag Ilmenau
2008

Impressum

Bibliografische Information der Deutschen Nationalbibliothek
Die Deutsche Nationalbibliothek verzeichnet diese Publikation in der Deutschen Nationalbibliografie; detaillierte bibliografische Angaben sind im Internet über http://dnb.d-nb.de abrufbar.

Diese Arbeit hat der Fakultät Maschinenbau als Dissertation vorgelegen

Tag der Einreichung:	16. Mai 2007
1. Gutachter:	Prof. Dr. phil. nat. Dr. h.c. Holger Preuschoft
2. Gutachter:	Dr. Naomichi Ogihara
3. Gutachter:	Prof. Dr. med. Hartmut Witte
Tag der Verteidigung:	30. Oktober 2007

Technische Universität Ilmenau/Universitätsbibliothek
Universitätsverlag Ilmenau
Postfach 10 05 65
98684 Ilmenau
www.tu-ilmenau.de/universitaetsverlag

Herstellung und Auslieferung
Verlagshaus Monsenstein und Vannerdat OHG
Am Hawerkamp 31
48155 Münster
www.mv-verlag.de

ISBN 978-3-939473-25-1
ISSN 1865-9136
urn:nbn:de:gbv:ilm1-2007000262

Danksagung (Acknowledgments)

Deutsch

Ich bin sehr glücklich, dass ich meine Ideen mit dieser Doktorarbeit realisieren konnte. Ich möchte die Gelegenheit nutzen und hiermit all den Personen meinen Dank ausdrücken, die einen wesentlichen Anteil am Gelingen hatten.

An erster Stelle möchte ich mich bei Prof. Witte nicht nur für seine fachliche und kompetente Betreuung bedanken, sondern auch für seine Menschlichkeit, sein Vertrauen und seine Hilfsbereitschaft. Über den ganzen Bearbeitungszeitraum gab er mir wichtige Anstöße zum Nachdenken und ermöglichte es mir, meine Ideen zu verfolgen.

Ich möchte mich auch bei allen Kollegen und Mitarbeitern bedanken, welche mir bei der Durchführung meiner Arbeit mit Ideen und Ratschläge behilflich waren. Besonders dankbar bin ich in diesem Zusammenhang Herrn Daniel Pérez Marcos und Herrn Omar Jimenez.

Der Dank richtet sich auch an die Studenten, welche mich bei der Zuarbeitung unterstützt haben. Besonders betonen möchte ich an dieser Stelle Herrn Juan Carlos Moreno Sagaon, der mir bei der ersten Korrektur dieser Arbeit in englischer Sprache behilflich war.

Ein wichtiger Dank richtet sich an meine Frau Silvia Verónica Lehmann, die mir besonders in den schwierigen Monaten mit viel Liebe beigestanden hat und eine wichtige moralische Stütze für mich war. Sie hat mir viele Tipps für die Gestaltung meiner Arbeit gegeben.

English

I would like to thank Dr. Naomichi Ogihara emphatically for helping me with the first steps of the model. He gave me also very valuable suggestions during this time.

I express my gratitude to my beloved parents Ana Maria and Carlos Alberto Andrada for their permanent support. Thank you for teaching me what the most important things in life really are.

Zusammenfassung

Titel: Ein neues Modell der Mechanik des menschlichen Rumpfes beim Gehen
Verfasser: Emanuel Andrada

Beim menschlichen Gehen interagiert der Rumpf systematisch mit den Extremitäten. Aus diesem Grund kann man Rumpfamplituden, Frequenzen und Phasen als eine Funktion der Fortbewegungsgeschwindigkeit beobachten. Das Bewegungsbild des Rumpfes aber ist individuell.
Um die Ursachen der intra- und interindividuellen Variation der Kinematik des Rumpfes zu finden, wurden zwei Hypothesen geprüft: 1) die intra- und interindividuelle Variation der Kinematik des Rumpfes ist eine Funktion der Massenverteilung, 2) hat man eine bestimmte Masseverteilung und eine gegebene Geschwindigkeit, dann wird die intra- und interindividuelle Variation in der Kinematik des Rumpfes durch die Änderungen in den visco-elastischen Eigenschaften des Bewegungsapparates realisiert.
Um Hypothese 1 zu testen, wurde eine Studie mit 106 Probanden (50 w, 56 m) durchgeführt. Bei dieser Studie wurde keine einfachen Zusammenhänge zwischen den 48 anthropometrischen und den kinematischen Parametern der Rumpfbewegung (Freiheitsgrad 6) bei 4 km/h (energetische Optimalgeschwindigkeit nach Cavagna) gefunden.
Die in der vorliegenden Arbeit präsentierten kinematischen Ergebnisse stellen dar, dass die Dämpfungsmechanismen (Dm) in der Frontalebene betont sind, und auch, dass die Dm bei den Frauen stärker ausgeprägt sind als bei den Männern. Außerdem zeigen die Ergebnisse, dass die so genannten „Kompensationsmechanismen“ zwischen Kopfrotationen und Schultertranslationen geschwindigkeitsabhängig sind, und auch, dass Frauen und Männer unterschiedliche Strategien nutzen.
Um die Hypothese 2 zu testen, wurde ein Morpho-Funktionaelles Modell des Rumpfes mit Freiheitsgrad 14, basierend auf den Hanavan Modell, vorgeschlagen.
Die Ergebnisse der Simulationen konnten nicht widerlegen, dass die visco-elastischen Parameter, die bei der Simulation berechnet werden, eine solide erklärende Kenngröße für die Änderungen der Amplituden, Frequenzen und Phasen der verschiedenen Körpersegmenten des Rumpfes beim Gehen sind. Sie sind auch in der Lage, die intra- und interindividuellen kinematischen Variationen zu erklären.
Die hier vorliegende Arbeit stellt zwei unterschiedliche Anwendungsfelder für die visco-elastischen Parameter dar. Das erste ist eine medizinisch orientierte Applikation, während sich das zweite auf bionisch inspirierte Robotik oder morpho-funktionell Maschinen bezieht.

Abstract

Title: A new model of the human trunk mechanics in walking

Author: Emanuel Andrada

During human motion, the trunk systematically interacts with the extremities. Changes of trunk amplitudes, frequencies and phases can be depicted as a function of gait's velocity. These changes, however, vary among human beings.

In order to find the causes of these intra and inter-individual variations, two possible hypotheses were tested: 1) intra and inter-individual variations of trunk kinematics are due to the segmental mass distribution represented by anthropometry, 2) For a defined mass distribution, and a given velocity, the variations of trunk kinematics are generated due to the changes in the visco-elastic properties of the locomotor system.

To check hypothesis 1 a study on 106 volunteers (50 f, 56 m) was performed. No simple relations between 48 anthropometric parameters and the 6 DOF kinematic parameters of the trunk motion during walking at 4 km/h could be identified.

Kinematical results of the present work show that the damping mechanisms towards the head (caudo-cranially) vary in dependence of anatomical planes and gender. In addition, the findings of this work display that the so called "compensation mechanism" between head rotations and body or shoulder translations are at first velocity dependent, but also that women and men use different strategies.

In order to check hypothesis 2, a 14 DOF functional morphological model of the trunk based on Hanavan's model was proposed.

Results of the simulations could not disprove that visco-elastic parameters, which are obtained by the simulations, are a solid base to explain the change in amplitudes, phases and frequencies of the different body segments in normal walking. They also are able to explain inter and intra-individual kinematical variations.

The present work introduces also two different application fields for the simulations and the visco-elastic parameters. The first one is a medically oriented application, while the second is oriented to bionically inspired robots or morphofunctional machines.

Table of contents

Index of figures

Index of Tables

"…that chance does not exist, for everything that occurs will be found to do so far a reason"
Hippocrates *(from Sarton, 1953)*

Chapter 1: Introduction

1.1 Motivation

Phylogenetical ancestors of humans produce up to 50% of their locomotion by movements of the trunk (Fischer & Witte 1998). These movements are coordinated with those of the extremities to optimize the behaviour of the whole system (Hackert 2003). Observing that, it surprises that since Weber & Weber (1836) biomechanical observations and models were restricted to the extremities' behaviour. It is improbable that the principle of task sharing between trunk and extremities, successfully since about 140 million years, and still in use in vertebrate animals, could be forgotten or neglected in a couple of million years of human history. On the contrary, there is important evidence of a systematical use of the trunk during walking (Hoffmann 2001).
The aim of the present work is, by using kinematical and dynamical models, to summarize and develop the available knowledge in trunk biomechanics. Direct practical applications can be found equally in medicine and robotics.

1.2 The long way to trunk mechanics

During evolution, locomotion tasks like walking or running became for human beings normal and easy. But, these at first view, "easy tasks" hide complex neurological, physiological, anatomical and biomechanical actions, which have to be precisely performed, in order to produce a "normal" gait.
Today, the understanding of these precisely multitask actions is significant, but still incomplete, especially in case of the trunk and its contribution to locomotion. As we will see, it was necessary about 2300 years of biomechanical history to realize that

the trunk is more than an static element that sustains the head and joins this with the arms and lower limbs.

During the "Golden Age" of Greek science in the 4th century B.C, Aristotle wrote the first book about human movement (About the Movements of Animals), a first scientific analysis of human and animal movement, based on observation, and describing muscular action and movement, and explaining ground reaction forces. In the Hellenistic Age after Alexander the Great, Herophilos and Erasistratis initiated the foundation of modern anatomy, and Archimedes' application of Euclidean methodology to mechanics formed the basis of rational mechanics. The search continued in Rome, where Galen wrote De Motu Musculorum (On the Movements of Muscles), establishing the science of myology and producing enormous advances in the understanding of muscles.

Unfortunately, this process of observation, experiments, and development of mathematical and mechanical laws was interrupted during the dark times of the Middle Ages (200 B.C. -1450 A.D.).

During the Italian Renaissance (1450 A.D. - 1527 A.D.), new pieces were added: da Vinci and Vesalius laid the foundation for modern anatomy and physiology by basing their knowledge on observation and dissection of human cadavers.

The Scientific Revolution produced a change in the understanding of nature and the way of doing scientific analysis. The foundations for Biomechanics were created as scientist such as Galileo, Borelli, and Harvey used experimentation as a way to understand the human body and its movements. Newton's laws established a new approach of studying human motion, and the tools to understand it.

Mathematical analysis during the 18^{th} century advanced the study of mechanics. Thanks to the contribution of Euler, Lagrange, and d'Alembert, the concepts of force, conservation of momentum and energy became clearly understood. In addition, muscle contraction and action became an event influenced by mechanical, bio-chemical, and electrical forces.

The transformation of biomechanics from an observational and intuitive science, to one based on quantification and mathematical analysis took place in the 19^{th} century. Instrumentation developed by Marey, Muybridge, and Braune and Fischer, allowed the quantification of locomotion for the first time. Additionally, muscle action could be quantified with EMG measurements, opening new ways for the understanding of muscle function.

The 20th century provided an explosion of sophisticated experimental methods and, with the development of the computer, a wealth of numerical mathematical methods which could be applied to biomechanical research. Furthermore, it was characterized by an increasing complex understanding of bone, cartilage, tendon, ligament, and specially muscle [7, 8, 66].

As we can see, it was a long trip full of brilliant people and ideas.

But what do we know today about locomotion?

Neurological point of view: Different structures within the brain drive the movement. Locomotion is controlled in a region of the midbrain, which is known as the mesencephalic locomotor region or MLR (see Whelan 1996). This region however, does not generate the locomotion patterns. On the basis of experiments on “spinal” cats (Grillner 1981; Pearson & Rossignol 1991) at the present the hypothesis is that the basic locomotor’s patterns are generated in the spinal cord. The so called CPGs (Central Pattern Generator) produce and module excitation waves running down the spinal cord, which distributes them to the muscles through specific cable networks called the “neural plexus”.

By observing locomotion from a mechanical point of view, motions of the upper and lower limbs will appear at first sight as the most important and obvious. This Paradigm imprinted biomechanical studies during the second half of the 20th century. Following this direction, and thanks to the application of numerical methods, many scientists developed extremity and body models (e.g. Cavagna et al.1977, Mochon & McMahon 1980, Hatze 1981, Pandy 1990) without trunk or in the best cases, representing the trunk as an static element. Normal paradigms that describe the motion of the legs during walking are the pendulum and the inverted pendulum. Upper limbs oscillate forward and backward, while the lower ones like a pendulum during the swing and like an inverted pendulum during the stance.

First in the last decade of the 20th century (more than 2300 years after Aristotle), thanks to the work of scientists like Wagenaar, van Emmerik, Beek, Taylor, Feipel, Hoffmann and Witte, it was demonstrated that the trunk is systematically used not only for stability, but also for locomotion. Therefore, locomotion is more than only arm’s and leg’s motion. Pelvic girdle, abdominal muscles, thoracic girdle and spine build up together with upper and lower limbs, a functional unit. This fact is until today included neither in medical practice nor in theoretical models nor in the robotics. The idea that the trunk builds up an static connexion between legs and arms can not be

sustained any more. On the contrary, the trunk is a dynamic interlinking element, which couples dynamically the motions and forces coming from arms, legs, shoulder, and pelvic girdle.

After about 15 years of “dynamical” trunk studies, too many questions stay unexplained, and too many kinematical and dynamical aspects unexplored. For example: we know from the studies from Wagenaar et al. 1992 and Hoffmann & Witte 2002 that trunk amplitudes, frequencies and phases are related to velocity. But we do not know how. In addition, can these amplitudes or phases be predicted? Are the changes in the amplitudes, frequencies or phases a function of anthropometry? Or something else? Why a person has its own gait? Could it be possible to find objective parameters in order to describe intra- and inter-individual variations of trunk amplitudes, frequencies and phases?

The present work tries, from a mechanical point of view, to find answers to these questions. First expanding our kinematical knowledge and relating this to anthropometry and then introducing a new model of the human trunk mechanics in walking.

1.3 Mechanics of trunk motion

In the next sections, the basic propaedeutics of spine mechanics as well as studies of the trunk using motion analyses are introduced and discussed. This information will be used to identify lacking points in previous approaches as well as a basis for the formulation of new hypotheses and work methods.

1.3.1 The spine

The spine consists of seven cervical vertebrae, twelve thoracic vertebrae, five lumbar vertebrae, five fused sacral vertebrae, and three to four fused coccygeal segments. As the spine is viewed in the frontal plane, it generally appears straight and symmetrical. In the lateral or sagittal plane there are four normal curvatures. These curves are anteriorly convex in the cervical and lumbar regions (lordosis) and posteriorly convex in the thoracic and sacral regions (kyphosis). There is a mechanical basis for these normal anatomic curves; they give the spinal column

increased flexibility and augmented, shock-absorbing capacity, while at the same time maintaining adequate stiffness and stability at the intervertebral joint level [12].
The spine is a mechanical structure. Vertebrae articulate with each other in a controlled manner through a complex of levers (vertebrae), pivots (facets and discs), passive restrains (ligaments) and actors (muscles). The long, slender, ligamentous bony structure is markedly stiffened by the rib cage. Although the spine has some inherent ligamentous stability, the major portion of the mechanical stability is due to the highly developed, dynamic neuromuscular control system [12].
The spine has three fundamental biomechanical functions:

1. To transfer the weights and the resultant bending moments of the head, trunk and upper extremities.
2. To allow sufficient physiologic motions between these body segments.
3. To protect the delicate spinal cord from potentially damaging forces.

1.3.2 Literature Review

In the last decades, multiple clinical tests were performed, in order to obtain the mechanical properties and the range of motion of the spine. Most of them, especially in early times, are statical test performed in vitro or in vivo (Gregersen & Lucas 1967, Kummer 1981, Panjabi et al. 1989, Gunzburg et al. 1991, Macintosh et al.1993, Wessel et al. 1994, Panjabi et al. 1994, Kumar et al. 1995, Kumar & Panjabi 1995, Dvořák et al. 1994, Marras & Granata 1995, McGregor et al. 1995).
Gregersen & Lucas (1967) performed an “in vivo” study, in which they implanted Steinmann-nails in the thoracic lumbar spine process of seven young men. The aim of the study was to find in which segments of the spine motions occur. They depicted significant torsion values between vertebrae neighbour bodies at the thoracic region, while walking. On the other hand, the torsion at lumbar level was clearly smaller. Gunzburg et al. (1990) performed a similar study. In this case, the number of subjects was eight and the Steinmann-nails were only implanted at the lumbar level. The observed relative motions were similar to those published by Gregersen & Lucas. Putz (1981) depicted that trunk frontal bending occurs principally at the level of the thoracolumbal junction. Kummer (1981) added to these observations. His results also show that rotations and lateral bending are performed principally at the level of the thoracic spine.

By using a motion model (from Capozzo 1983) and comparable data of motion analyses (form Thurston & Harris 1983) in combination with results of EMG-measures (from Vink & Karssemeeijer 1988), Vink et al. (1988) depicted possible energy storage in trunk back muscles. Mussa-Ivaldi (1988) demonstrated that cortical cells encode muscle state variables and not necessary that this cells encode the planning of multi-joint arm movements in terms of the desired hand direction. Therefore he interpreted Georgopoulos et al.'s (1982 &1983) results by assuming that cortical cells encode the desired rate of shortening of muscles. Scholle et al. (2001) showed, based on experiments with rats, that as a consequence of the regionalization of the electrical activation patterns of muscles, muscles may form a tunable spring. In the human trunk, these muscles springs are situated crosswise, at some 45° to the longitudinal axis. In their ideal form, they actively, and elastically, drive trunk torsion (Witte et al. 2004).

Dynamical analyses of the spine and pelvis are normally performed using treadmills or walking lanes. Interesting on this point are the pelvic, thoracic and trunk amplitude, frequency and phase variations with velocity variations. Stokes et al., 1989; Crosbie et al., 1997; Vogt & Banzer 1999, Syczewska et al., 1999 studied trunk kinematics using one and up to three different velocities. Motions and behaviours were analyzed during restricted phases of the motion's cycle. Complete phases or more motion cycles can be found in the works published by Taylor et al., 1999 and Feipel et al. 2000. These works are focussed on pelvic and thoracic oscillations and therefore, we will not really find spine kinematics (like torsion or lateral flexion).
Spine kinematics can be found in the works of Wagenaar & Beek (1992), Van Emmerik & Wagenaar (1996), Hoffmann (2001), McGibbon & Krebs (2001), Witte et al. (2002 & 2004) and Van Emmerik et al. (2005).
Wagenaar & Beek (1992) examined the transverse plane of the trunk of 4 subjects at different velocities (from 0,25 m/s to 1,50 m/s). Their calculations included torsion and phase shift variations between pelvis and thorax on the transverse plane. Van Emmerik & Wagenaar (1996) studied the trunk phase dynamics of seven healthy subjects, while the walking velocity was gradually increased and decreased. They found differences in amplitudes and phases between upward and downward profiles.
Hoffmann (2001) published a study with thirty males and thirty females as test-persons. They walked on a treadmill at velocities from 2 km/h to 6 km/h. The motion

paths of pelvis and thorax were acquired using an ultrasonic system adjusted at a sampling frequency of 24 Hz. Amplitudes, frequencies of pelvic and thoracic motions on transverse and frontal planes were analyzed as well as the relative motions between them. In addition, the phase shift angles between pelvis and thorax on planes at each velocity were computed.

Witte et al. (2002 & 2004) based on Hoffman's data and a pilot study of 5 subjects, presented similar results, focussing the results on trunk resonance and morpho-functional mechanisms used in bipedal locomotion.

McGibbon & Krebs (2001) published a study from 93 healthy adults with an age range from 20 to 90 years. The aim of the study was to investigate age-related changes in lower trunk coordination and energy during gait. Investigations were done between pelvic and lower trunk rotations and angular velocities on the sagittal plane. Subjects walked with self-selected speed.

Van Emmerik et al. (2005) published a study based on 30 subjects, who walked on a treadmill at velocities from 0,2 to 1,8 m/s and were divided into three groups with mean ages of 23,3, 49,3 and 72,6 years. The purpose of the experiment was to examine age-related changes in range of motion and coordination of segments of the upper body during locomotion, and the effects of systematic walking velocity manipulation on rotational motion and coordination.

1.4 Lacking points and hypotheses

1.4.1 Lacking points and a question

On the basis of the reviewed literature, and in order to better understand trunk biomechanics, some not yet sufficiently studied points in field kinematical description of trunk motions have to be investigated:

- There is until today not any information about the coupling angles (phase shift angles) between rotations, translations and rotation-translations within each segment. For instance the phase between pelvic axial rotation and pelvic lateral tilt or between thoracic sagittal tilt and thoracic longitudinal translation.
- Although amplitudes, frequencies and some coupling angles between pelvis and thorax or thorax and head were analyzed, they were mostly focussed on

age related changes and not on gender differences. Only in the works of Hoffmann (2001) and Witte et al. (2002 & 2004), these differences were considered, but only in frontal and transverse planes. In addition, the calculations were performed using projection angles. In this point the examinations form Hoffmann & Witte must be extended to 3D calculations, including also trunk sagittal plane and head motions. It has to be remembered that gender differences were significant in the works of Hoffmann & Witte, and therefore, they should also be introduced in further age related change tests.

In addition, there is one very important question, which until today could not be answered and it is from crucial meaning:

- Which is the cause of the intra and inter individual differences of amplitudes, frequencies and phases in trunk motions while walking?

Without answering this question, it will be impossible to understand trunk and control mechanisms used in locomotion.

1.4.2 Formulation of hypotheses

From earlier studies from Witte (1996) and Hoffmann (2001), it is possible to find first sources for hypotheses' formulation. In one pilot study, Witte found that the torsion of the trunk has a minimum at the energetically optimal velocity from Cavagna et al. (1977), which agrees with the theory that the trunk constitutes a resonant system (see fig 1-1 A). It also shows that the torsion has lower values than the sum of the pelvic and thoracic axial rotation, which indicates that their phase shift angle can not be 180°, which is implied by the terms "symmetrical gait" or "diagonal" for walking. At this point, it will be useful to remember that when a resonator system reaches the resonation frequency less energy is needed to continue working. This individual minimum disappears in later studies (Hoffmann, 2001) when means of 30 male and female volunteers were computed (see fig 1-1 B). If we compare these results with mechanical concepts of resonant systems currently under discussion for human locomotion like suspended, inverted and torsion pendula, spring-mass systems, two hypotheses may be presented:

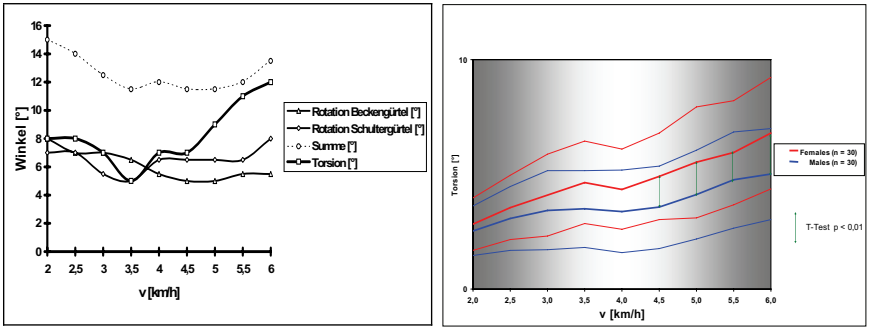

Figure 1- 1 Left: pilot study from Witte (1996). Right: Gender trunk torsion differences (Witte et al. 2002) from data of Hoffmann.

Hypotheses:

1 **Trunk amplitudes, frequencies and phases are due to the segmental mass distribution. Therefore, a high correlation between anthropometry and trunk kinematics may be hypothesized.**

2 **For a defined mass distribution, and a given velocity, the variations of amplitudes, frequencies and phases of the trunk are generated due to the changes in the visco-elastic properties of the locomotor system.**

The first one is based on the following assumptions:

- The resonant dent of the trunk torsion disappears in Hofmann studies because different mass distributions may build up different resonator systems, and therefore their minimal torsional values vary.
- Inverted and torsion's pendula motions and their frequency equations display dependencies on length and mass.

Assumptions for the second hypothesis:

- Anthropometry is necessary but not enough to predict motion patterns of a person.
- In muscles it is possible to store energy (Vink et al 1988), and they can also be used as tunable springs (Mussa-Ivaldi, 1988, Scholle et al 2001). Therefore, different activation patterns in combination with anthropometry may produce different motion amplitudes, frequencies and phases.

1.5 Goal and contents of this work

The goals of the present work are: 1. to expand the actual kinematical knowledge about the trunk, 2. to present a new mechanical model of the trunk based on trunk's morphological, functional, kinematical and dynamical studies, and 3. to explain, first by using kinematical models and then the above mentioned model of the trunk mechanics in walking, the cause of the intra- and inter-individual variation in trunk amplitudes, frequencies and phases during walking.

In order to fill-out lacking points, kinematical analyses on a large cohort of subjects should be performed. Each test-person should walk in upward and downward profiles and with very wide velocity ranges. The kinematical data should be computed using 3-D coordinates and be post-processed with elements of signal analysis (like FFT and cross-correlations), in order to obtain also frequencies and phases between the motion components. To test hypothesis 1 an important quantity of anthropometrical measurements on each subject have to be done. To test hypothesis 2 an elasto-mechanic multi-body model of the trunk has to be developed.

Chapter 2 introduces first the experiments, which were divided in two sections: motion analysis and anthropometry. To this part follow the data computation methods, where the different mathematical as well as signal analysis methods are presented.

Chapter 3 presents results from more than 100.000 kinematical calculations, including pelvic, thoracic and head motions, frequencies and phases.

In chapter 4, the results of correlations, regressions and multivariate ANOVAs between anthropometrical measures and kinematical data are presented and implemented to check hypothesis 1.

In chapter 5, chapters 2 to 4 are reviewed and discussed.

Chapter 6 introduces the construction of a morpho-functional model of the trunk and the results of its simulations, which are systematically used to test hypothesis 2.

In chapter 7, the automated routine, the model, along with their results are employed to present two different usage fields as medicine and robotics.

Chapter 8 discusses chapter 6 and 7, and finally, chapter 9 presents general conclusions involving the complete work.

"The strongest arguments prove nothing so long as the conclusions are not verified by experience. Experimental science is the queen of sciences and the goal of all speculation."
***Roger Bacon**, Opus Tertium*

Chapter 2: Methods and materials

2.1 Tracking motion

In order to get the kinematical paths of the gait of a test-person, the motion of limbs and body segments can be represented by multiplicity of invasive and (or) non-invasive methods. If it's desired to calculate the dynamics, biometrical data (mass and dimensions) have to be measured, too. The way, in which those analyses are performed, could have a determinant influence on the quality of the experimental results. The scientist must choose not only between the diverse invasive or non-invasive above mentioned methods, but also between the diversity of calculation procedures, which usually do not conduce to the same results.
These diverse tracking methods will be shortly discussed in the first part of chapter 2, later in a more detailed way, the infrared motion system which was used as the acquisition method in our experiment. Afterwards the experiment will be explained, which was divided in two sections, anthropometry and motion analysis. In the anthropometry section the measurement methods will be detailed. In the motion's analysis section, the motion analysis set-up will be explained in detail, and the different conditions under which the motion of the trunk and the head was tracked.
The second part of this chapter will be focussed on the calculation methods, the spectrum analysis, cross-correlations and finally how data were stored, in order to perform further calculations.

2.1.1 Different tracking methods

This section discusses the different and most frequently used invasive and non-invasive methods in biomechanical assessment.
If we talk about the invasive methods, the most used for analysis of movements are:

- X-ray cinematography, with this approach is possible to observe directly the motion of the bones and is mostly used to quantify kinematics of small animals (45 kV…48kV) [86].
- MRI (Magnetic Resonance Imaging) is used to obtain cross-sectional images of structures. MRI uses the change in orientation of the magnetic moment of hydrogen nuclei for a particular tissue that is generated when the tissue is placed in a magnetic field and stimulated with a radio frequency wave. This method is appropriated for very slow motion. In general to compare different body positions (e.g., sitting, standing). [8, 86].
- If we join the osteosynthesis material (Kirschner-wires, Steinmann-pins, Schanz-screws) with the external world, is possible to measure the movements of bones with a great accuracy. [8, 28]

The methods described bellow are non-invasive. In these methods the motion of the skeletal element will be measured on the skin surface. There are two non-invasive methods to measure a point or segment of interest: the first uses active markers and the second passive markers.

Active markers and passive cameras: light emitting diodes (LED) are attached to the point of interest of a segment. They emit signal ´s with a distinct frequency in the IR part of the spectrum. Each LED attached to the segment of interest has its own specific frequency and can easily be identified at every point in time during a measurement. Cameras that quantify IR signals, take the emission of the LEDs and using triangulation calculate the 3d position of the LED.

Passive markers and active cameras: In this case, the cameras send an IR flash with a determined sample frequency, which is reflected on the markers. Each camera takes the reflection and provides a two-dimensional image of the markers. With a combination of a minimum of two cameras, it is possible to compute the three-dimensional position of the markers. This transformation is commonly performed using the DLT (direct linear transformation) method (Abdel-Aziz and Karara, 1971) [8].

The Qualisys® Pro-Reflex® - System is one of the systems, which belong to this category. This motion measurement equipment was chosen, because it has many advantages. Some of them are:

- Great accuracy and reliability.

- Possibility to measure motions at higher sampling frequencies (up to 1000 Hz)
- Advanced computer algorithms and user friendly interfaces
- Direct export to Matlab®.

The last point was one of the most important decision's factor, due to the amount of volunteers and tests (see page 19).

2.2 Experiments

2.2.1 Previous studies

This experiment was made following previous examinations from (Hoffmann, Witte, 2001) and (Witte et al., 2004). These two experiments were focussed on the motion paths of the spine, using not only direct calculations of the kinematics of the spine but also spectrum analyses. The spectrum analysis facilitates by using FFTs and cross-correlations to calculate the maximal amplitude and frequency of the dominant mode of the periodical motions of the trunk as well as the interaction of the principal mode with his harmonics (Q-Q values from Witte et al. 2003) and the phase angle between the different rotations and translations, which have the same dominant mode.

2.2.2 Present examination

The study presented here was part of a motion study on overall 300 volunteers, which was approved by the ethic committee of Friedrich-Schiller- Universität Jena (0558-11/00).
The clinical examination was accomplished in the KIP-Labor of the Friedrich-Schiller-Universität Jena. The number of test-persons, who have participated in the experiment as volunteers, was 106 (50 females and 56 males). One of the most important points of this experiment was to accept only anamnestically healthy volunteers. To be sure of that, each volunteer filled a questionnaire before the experiment. In this questionnaire, the test-person was asked to answer whether he/she had got any previous spinal injuries or back-pain during walking, running or in

sitting posture. In other parts of the questionnaire, it was asked about the sport activities and hours a day spent in sitting posture.
The last part of the acceptance protocol consisted in a visual control of the state of the spine.
The mean age of the volunteers was 24 y (range 20 y to 31 y), most of them students of the universities of Jena and Ilmenau. This age interval was chosen, because teen-ager's spine is not yet stabile and on the other hand, because of the difficulty in finding people over 30 y without spinal diseases.

2.2.3 Anthropometry

In order to achieve the dynamics and to check whether correlations between biometrical data and the kinematics of the trunk could exist [chapter 4], 48 biometrical data hypothesized as relevant have been measured in each test person. From the 48 measurements, 37 were achieved with the test-person standing and 11 in sitting position. All the measurements were done following Rudolf Martin (1914) and DIN 33402 (parts I and II).

Materials

- Beam-compass (BC)
- Balance (B)
- Anthropometer -Vernier calliper long scale- (AVClS)
- Anthropometer -Vernier calliper short scale- (AVCsS)
- Calliper (Tasterzirkel) (C)
- Measuring tape (MT)

In table 2-1, the different measurements are presented with their corresponding measuring instrument.

Table 2- 1 Anthropometrical measures and measuring instruments

Arm circumference	left and right	Measuring instrument
Pelvis width, sitting		AVCsS
Pelvis width, standing		AVCsS
Pelvis circumference		MT
Leg length	left and right	AVCIS
Leg circumference	left and right	MT
Ribcage width, sitting		AVCsS
Ribcage width, standing		AVCsS
Thoracic circumference		MT
Finger-ground distance		AVCIS
Finger pick height	left and right	AVCIS
Foot length, sitting	left and right	AVCsS
Foot length, standing	left and right	AVCsS
Weight, sitting		B
Weight, standing		B
Knee height, sitting	left and right	AVCIS
Knee height, standing	left and right	AVCIS
Ankle height, sitting	left and right	AVCIS
Ankle height, standing	left and right	AVCIS
Head width		C
Head height		C
Head depth		C
Body height		AVCIS
Upper arm height	left and right	AVCIS
Thigh length	left and right	AVCsS
Spine height (C7)		AVCIS
Shoulder width (bi acromial)		AVCsS
Shoulder height	left and right	AVCIS
height sitting		AVCIS
Scretch of arms		AVCsS
Waist width, sitting		AVCsS
Waist width, standing		AVCsS
Waist circumference		MT
forearm height	left and right	AVCIS

2.2.3 Motion Analysis

Motion analysis test

In order to track the motion of the head, shoulder girdle and pelvic girdle, each test-person walked without shoes on a treadmill at velocities of 2 km/h – 6 km/h, with an ascending and descending ramp of 0.5 km/h increment resp. decrement. That totalizes 16 tests per volunteer. The motion of the head was represented with a marker triplet over Osfrontale, the movements of the pectoral girdle were represented with a marker triplet over Sternum and those of the pelvic girdle were tracked by marker triplet over Sacrum (Spinal process L4 and Spinae iliacae post. supp.) (figure 2-1) [5].

The lab coordinate system was positioned over the treadmill and was set in the following way: motion direction –x, positive lateral translation y (to the right) and positive vertical displacement z (up direction) (figure 2-2).

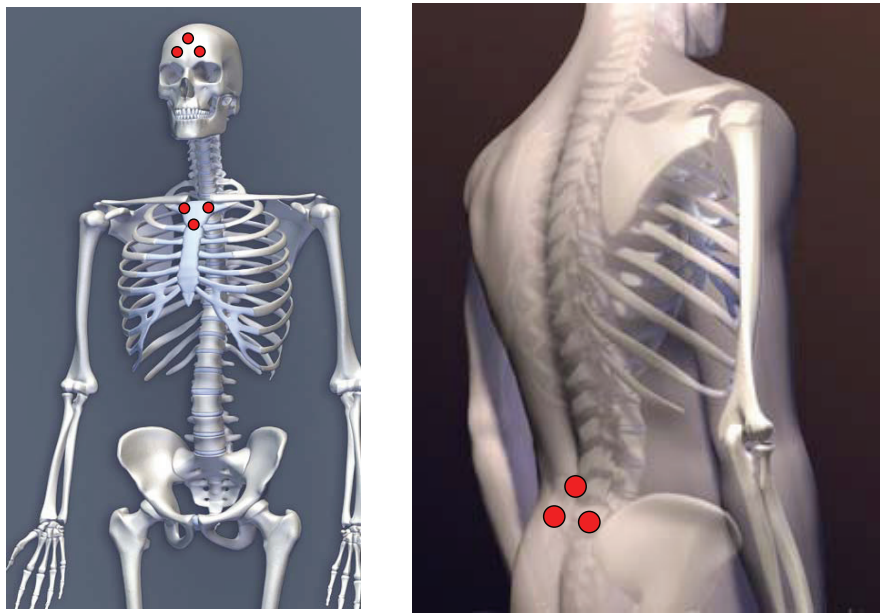

a) **b)**

Figure 2- 1 a) shows the marker-triplet over Os-frontale and sternum, b) shows marker triplet over sacrum. Figures courtesy 3Dscience.com

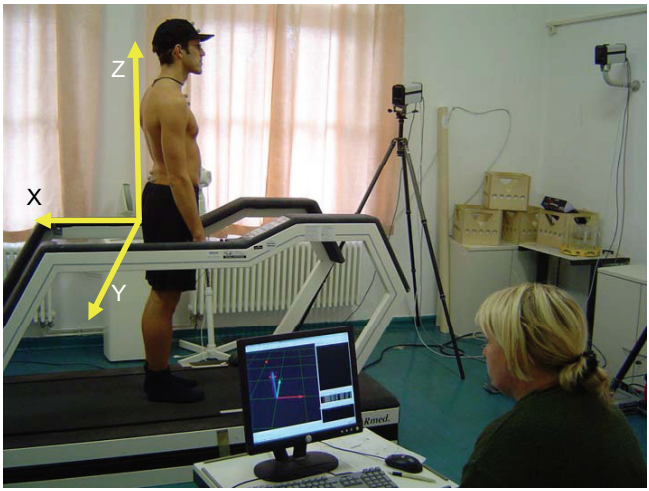

Figure 2- 2 Labs coordinate system: motion direction –x, positive lateral translation y (to the right) and positive vertical displacement z (upward direction).

The motion of the pectoral and pelvic girdle and the motion of the head at each velocity were taken in periods of 15 sec. with 6 Qualisys® infrared cameras at a sampling frequency of 120 Hz. Figure 2-3 shows the position of the cameras in relation to the position of the treadmill.

The tracking from 2-D data to 3d data and the posterior identification of the data was made using the tool Qualisys® Track Manager®. This tool is Windows®-based software. Qualisys® Track Manager® receives the 2-D data information from each camera and performs automatically the transformation into 3-D data.

It is usual that the cameras register unwanted reflections; the identification of the markers and the discarding of the unwanted reflections must be made manually.

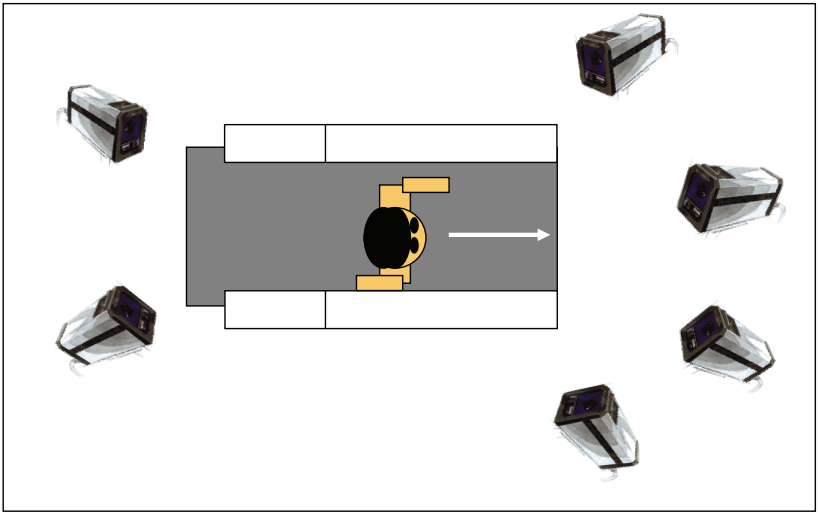

Figure 2- 3 Position of the 6 Qualisys® infrared cameras in relation to the treadmill. The white arrow indicates motion direction. As shown, motions paths of the head and the pectoral girdle were tracked with 4 cameras and those of the pelvic girdle with 2.

The normal procedure is the following: as soon as the tracking from 2-D into 3-D is performed, Qualisys® Track Manager® locates the markers and reflections into the "Unidentified trajectories" box. It must be explained, that markers as well as reflexes are shown as markers. The markers that correspond to the experiment must be moved to "Labeled trajectories", those that correspond to reflections must be moved to "Discarded trajectories".

All 2-D and 3-D data can be easily exported from QTM® to different formats such as TSV, C3D and directly into Matlab® [98].

In fig. 2-4 the graphic user interface QTM® is presented.

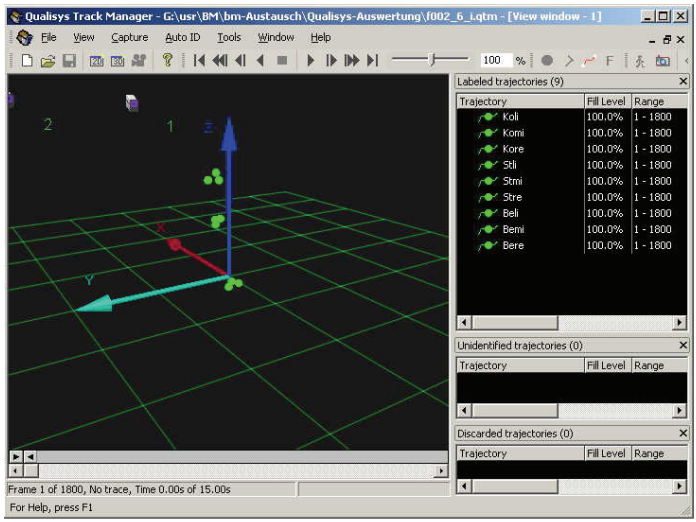

Figure 2- 4 QTM® Graphic user interface. The spheres showed in green represent the triplet-makers from the pelvis (below), thorax (middle) and head (above).

2.3 Calculating kinematical data

One of the objectives of this work was to get the most accurately possible description of the kinematics of the trunk. To fulfil this requirement, 103 kinematical parameters from the pelvis, thorax and head were computed. In order to manage the great quantity of data (106 volunteers*16 experiments per volunteers *103 calculations per experiment = 174688 calculations) resulting of the experiments, it was necessary to write an automated routine. This routine was written in Matlab®.

The automated routine is composed for 4 modules: the first module performs the automated load, the construction of the body coordinate systems and the first quality control of the data. The second performs the calculations of the translations and the absolute and relative rotations as well as interpolation and filtering. The absolute and relative rotations are computed with Cardan angles.

The third one computes the FFTs and the cross-correlations, in order to calculate the amplitude and frequency of the highest basic oscillation frequency and the phases between the different translations and rotations. Finally the fourth module saves the results into a specially designed structure.

Another module, which doesn't belong to the automated routine, was programmed, in order to make possible the exportation of the saved data to Excel® and SPSS®[1].

In the following pages, it will be discussed about the different modules of the automated routine and how the different calculations were achieved.

2.3.1 First module

Automated load

As mentioned earlier, the quantity of experiments were 106 vol.x 16 experiments per vol. = 1696 experiments. That means 1696 different *.qtm files. All these files must be loaded and their data processed. To make the automatic load of the files easier, the qtm files were exported to Matlab® with the following names:

ga-b.mat

Where *g* is the gender of the vol. (m=male, f=female), *a* is the number of the volunteer (from 01 to 56 in the case of the males vol. and from 01 to 50 in the case of the females vol.) and *b* is a number, which represent the different velocities and profiles.

Construction of the body coordinate systems

In order to calculate 3-D absolute and relative rotations between rigid bodies, a set of axes must be attached to each body. To do that, the routine uses the following method: On each body (pelvis, thorax and head) a marker triplet was attached (a, b, c, fig. 2-5).

[1] Not discussed in this work.

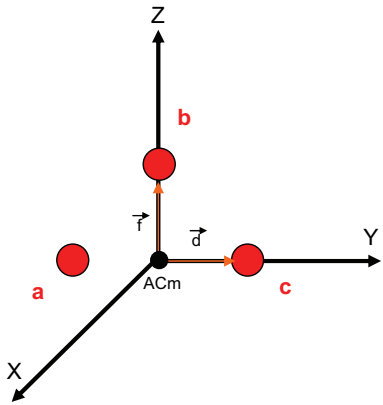

Figure 2- 5 Construccion of the body coordinate system from three markers.

The middle point between a and c is,

$$[(a_x, a_y, a_z)^T + (c_x, c_y, c_z)^T] / 2 = (acm_x, acm_y, acm_z)^T \quad \text{eq.(2.1)}$$

The vectors acm-b and acm-c can be calculated as

$$(f_x, f_y, f_z)^T = (b_x, b_y, b_z)^T - (ac_{mx}, ac_{my}, ac_{mz})^T \quad \text{eq.(2.2)}$$

$$(d_x, d_y, d_z)^T = (c_x, c_y, c_z)^T - (ac_{mx}, ac_{my}, ac_{mz})^T \quad \text{eq.(2.3)}$$

With the cross-product between the vectors e und d, the fist orthogonal axe is obtained, this vector x_b is perpendicular to the plane formed by e and d and its direction is determined via the right-hand rule.

$$(x_{bx}, x_{by}, x_{bz})^T = (d_x, d_y, d_z)^T \times (f_x, f_y, f_z)^T \quad \text{eq.(2.4)}$$

Using the same approach, the third axe is expressed as

$$(y_{bx}, y_{by}, y_{bz})^T = (f_x, f_y, f_z)^T \times (x_{bx}, x_{by}, x_{bz})^T \quad \text{eq.(2.5)}$$

At this point, the three directions of the body coordinate systems were calculated, where x and y are respectively the x and y directions and f represents the z direction. In order to make the calculations of the rotation matrix easier, the use of unit vectors is recommended. They will be obtained from the division between each vector and its norm.

$$e_x = (x_{bx}, x_{by}, x_{bz})^T / \left| (x_{bx}, x_{by}, x_{bz})^T \right| \quad \text{eq.(2.6)}$$

$$e_y = (y_{bx}, y_{by}, y_{bz})^T / \left| (y_{bx}, y_{by}, y_{bz})^T \right| \quad \text{eq.(2.7)}$$

$$e_z = (f_{bx}, f_{by}, f_{bz})^T / \left| (f_{bx}, f_{by}, f_{bz})^T \right| \quad \text{eq.(2.8)}$$

These three vectors together configure the position matrix of each rigid body, or in other words the body coordinate system.

$$Mp = \begin{pmatrix} e_{xx} & e_{yx} & e_{zx} \\ e_{xy} & e_{yy} & e_{zy} \\ e_{xz} & e_{yz} & e_{zz} \end{pmatrix} \quad \text{eq. (2.9)}$$

This procedure assumes that the position of the three points is error-free.

First quality control of a row-data

One common problem in motion analyses using makers and infrared cameras are the missing values in the data. These “holes” are produced, because during the sampling one or more markers were not taken by at least two of the cameras. This fact produces a problem during the transformation of the sampled data from 2-D into 3-D. The reason is, that the DLT method, and any similar method, determinate three-dimensional spatial coordinates from several two-dimensional sets of information.
If the holes are located between numerical data, different interpolation methods can be used to rectify the raw-data. But when the holes are at the beginning or at the end of the raw-data, the interpolation methods are not useful and the holes must be erased. When the raw-data is exported to Matlab®, these holes are taken as NaN (not a number) [97].

In order to process these NaN at the beginning and/or at the end of the raw-data, the function *antinan* was programmed.

antinan searches NaNs at the beginning and/or at the end of the raw-data, and returns the vector positions of the first and the last numerical data.
Since calculations between different bodies are made and the raw-signals from each body can show different holes paths at the beginning and/or at the end of the data, the function *match* was programmed.

The *match* function matches two body coordinate systems in the best possible way, by using the first and the last numerical data obtained from the function *antinan* of each body. Fig. 2-6 introduces the logical diagram of the function.

2.3.2 Second module

Basic principles – Joint kinematics

The joint kinematics is normally used for the description of the relative motion between two bodies. The mechanics of rigid bodies provide multiple ways to numerically represent these relative movements. For example:

- Euler-Cardan angles
- Joint Coordinate Systems (JCS)
- Finite helical axes and rotations
- Helical angles

Why to choose Cardan Angles to calculate the rotation of the trunk?

Cardan angles are widely used in biomechanics because they provide a representation of joint orientation analogous to the anatomical representation that both clinicians and researchers are accustomed to use (which is not the case from finite helical and helical angles). [8, 9]

The fact that Cardan angles are sequence dependent has sometimes been viewed as a disadvantage. An appropriate standardization of the sequence is one simple solution to this problem [8, 9, 91].

One mayor disadvantage of Cardan angles is gimbal lock, a mathematical singularity that occurs when the second rotation equals ±π/2 [8]. This problem can be avoided by selecting the smaller rotation as second rotation.

In mostly used Euler sequences, the gimbal lock occurs when the second rotation equals 0. This problem can not be avoided in trunk rotations (they will always pass through cero).

The advantages and disadvantages of the JCS for representing three-dimensional joint orientation are identical to those described for Cardan angles [8]. This method is mostly used to represent joint kinematics of the legs and was originally presented for the specific application to the knee joint (Groot and Sunday, 1983).

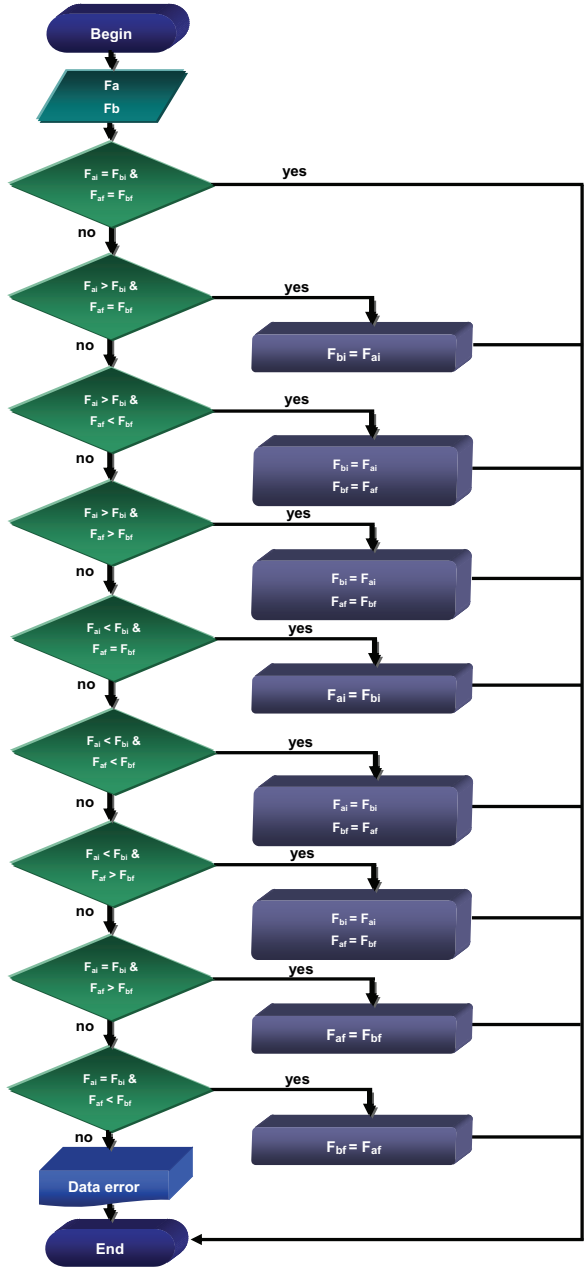

Figure 2- 6 Algorithm of the function *match*. F_a and F_b are the input functions, F_{ai} and F_{bi} are the first numerical data of each vector and F_{af} and F_{bf} are the last. The first and last numerical values are obtained from the function *antinan*.

Calculation of the Cardan angles (proposed method):

In order to calculate the rotations from a body relative to the labor frame (LF) and the relative motion between two of them, the functions *cardanang* and *cardan2* were programmed.

cardanang returns the Cardan angles of the motion of a single body, relative to the LF [1 0 0, 0 1 0, 0 0 1].

cardan2 returns the Cardan angles of the relative motion of two bodies.

These two functions use and follow the next mathematical and biomechanical principles:
The Cardan angle representation of three-dimensional motion uses three sets of independent rotations to transform one set of coordinates into another. These three independent rotations are usually represented as (α) about ***x***, (β) about ***y*** and (γ) about ***z*** (fig.2-7).

$$[R_j]= [R_\alpha] [R_\beta] [R_\gamma] \quad \text{eq. (2.10)}$$

The angles R_x, R_y, R_z or R_α, R_β, R_γ are often called *Euler angles*[2] (Panjabi et. al.,1993; Panjabi et. al., 1981; Oxland et. al. 1992). They are also referred to as *Bryant-Euler angles*[3] (Goel et. al. 1988, Nowinsky et. al. 1993), *Cardan angles* (Woltring 1991), *Dexter angles* (Grood and Suntay, 1983), or *Roll*, *Pitch*, and *Yaw* (Paul, 1982) [13].
In the present work, the sequence of three rotations using three different axes will be always called Cardan angles following (Woltring, 1991).

[2] In his original work, published in 1748, Euler recognized that a sequence of three rotations using two axes was sufficient to describe motion of an object from initial to final orientation. That suggests that a sequence of three rotations using three different axes should not be called Euler sequence.

[3] A sequence of three rotations will be called Bryant-angles only if the sequence is 3-2-1. The Bryant-angles mostly are used in commercial aviation.

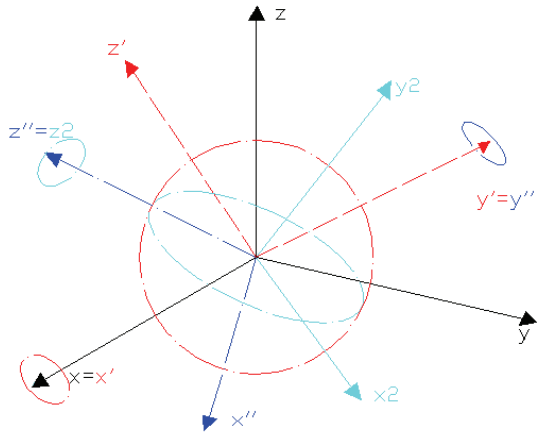

Figure 2- 7 shows the rotation from a set of coordinates (X,Y,Z) to (X2, Y2, Z2) using Cardan angles with the sequence (α, β, γ).

In eq. (2.10), $[R_j]$ is the parametric representation of the rotation matrix. Therefore to transform one set of coordinates (A) into another (B) yields

$$[B] = [R_j]\,[A] \quad \text{eq. (2.11)}$$

The parametric rotation matrices for rotations around ***x***, ***y***, and ***z*** axes of Cartesian coordinate system are defined as:

$$R_\alpha = \begin{pmatrix} 1 & 0 & 0 \\ 0 & \cos\alpha & \sin\alpha \\ 0 & -\sin\alpha & \cos\alpha \end{pmatrix} \quad \text{eq. (2.12)}$$

$$R_\beta = \begin{pmatrix} \cos\beta & 0 & -\sin\beta \\ 0 & 1 & 0 \\ \sin\beta & 0 & \cos\beta \end{pmatrix} \quad \text{eq. (2.13)}$$

$$R_{\gamma}=\begin{pmatrix} \cos\gamma & \sin\gamma & 0 \\ -\sin\gamma & \cos\gamma & 0 \\ 0 & 0 & 1 \end{pmatrix} \quad \text{eq. (2.14)}$$

For practical use in biomechanics, the sequences of ordered rotations should be chosen, so that the anatomical definitions are satisfied. Taking in account the orientation of the LF (fig. 2-2), the component ***y*** represents the transverse axis and the rotation around this axis (β) will be the flexion-extension. The sagittal axis is represented by ***x*** and the rotation around this axis (α) will be the lateral-flexion. The longitudinal axis will be ***z*** and the rotation around them (γ) will represent the torsion.
As mentioned in the previous section, the second rotation should represent the smaller rotation to prevent the gimbal lock. In normal gait, the smaller trunk rotation is the flexion-extension. Therefore the chosen sequence for the calculation of the rotation matrix will be the following: the first rotation about ***x***, the second about ***y'*** and the third about ***z''***.

$$[R_j]= [R_{x,\alpha}]\,[R_{y',\beta}]\,[R_{z'',\gamma}] = [R_{\alpha}]\,[R_{\beta}]\,[R_{\gamma}] \quad \text{eq. (2.15)}$$

The rotation will be expressed as

$$[R_j]= \begin{pmatrix} \cos\beta\cos\gamma & -\cos\beta\sin\gamma & \sin\beta \\ \sin\alpha\sin\beta\cos\gamma+\cos\alpha\sin\gamma & -\sin\alpha\sin\beta\sin\gamma+\cos\alpha\cos\gamma & -\sin\alpha\cos\beta \\ -\cos\alpha\sin\beta\cos\gamma+\sin\alpha\sin\gamma & \cos\alpha\sin\beta\sin\gamma+\sin\alpha\cos\gamma & \cos\alpha\cos\beta \end{pmatrix}$$

eq.(2.16)

The Cardan angles α, β and γ can be obtained from the following trigonometric equations:

$$\alpha = -\,\text{atan}\,(R_j(2,3)/R_j(3,3)); \quad \text{eq. (2.17)}$$

$$\beta = \text{asin}\,(R_j(1,3)); \quad \text{eq. (2.18)}$$

$$\gamma = -\text{atan}\,(R_j\,(1,2)/\,R_j\,(1,1)); \quad \text{eq. (2.19)}$$

where α represents the lateral-flexion, β the flexion-extension and γ the torsion.

The next problem to be solved was the selection of the reference frame. In case of the trunk, both inferior and superior segment (resp. pelvis and thorax) could be selected as reference frame. The motion of the spine often is calculated using the motion of each vertebra with respect to the vertebra below it [13, 20, 55]. In those calculations the markers are attached on the same plane (back). In case of the present study, the markers are attached in two parallel planes (back: sacrum and front: sternum). To take a decision, calculations of the Cardan angles, using the function *cardan2*, of the relative rotation between pelvis and thorax from the majority of the test persons were performed. First the pelvis was chosen as reference frame and then the thorax. Following, these data were compared with the calculation of the lateral-flexion, flexion-extension and the torsion obtained from the subtraction of the absolute motions between the pelvis and the thorax, using *cardanang*.

Great discrepancies were observed when the pelvis was used as reference frame. The amplitude of the rotations was twice as big as those calculated from the base of the absolute rotations. In many cases this amplitude was so big, that the motion became cuasi non-anatomical. On the other hand, the rotations computed using the thorax as reference frame returned only very small amplitude differences. The shape of the functions matches, which means, that the phase was not affected. In fig. 2-8, the discrepancies between pelvis and sternum as reference frame are shown.

The same experiment was achieved between thorax and head. No significant discrepancies were found. In this case the markers were placed on the same plane (front).

Although the questions, why the discrepancies are so big? And why this occurs only between pelvis and thorax? Were not answered, this experiment showed that, in the case of the trunk by using marker triplet attached on the sacrum and sternum, the upper segment (superior) should be used as reference frame. This approach is also recommended and used by Capozzo [75] in the case of the legs, which uses the upper or proximal segment as reference frame.

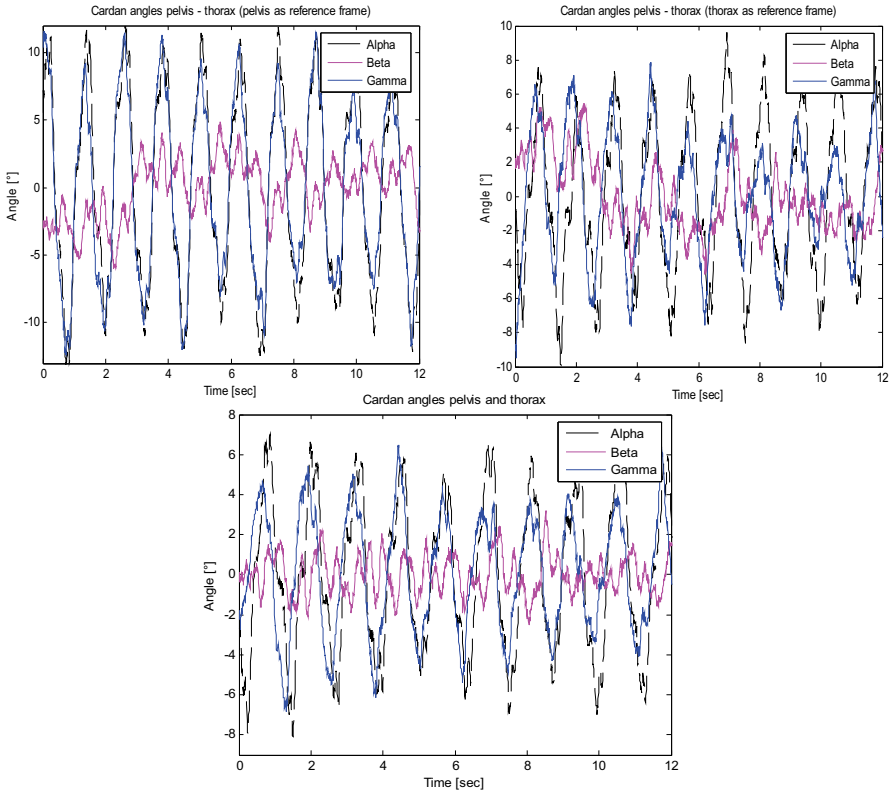

Figure 2- 8 Display the differences in the amplitude of the lateral-flexion, torsion and flexion-extension calculated with the same sequence of Cardan angles by using different reference frames. a) Pelvis as reference frame. b) Thorax as reference frame and c) Cardan angles from thorax relative to the Lab frame - Cardan angles from pelvis relative to the Lab frame. It is easy to see that in figure a) the amplitude of the torsion (Gamma) is twice as big as in the figures b) and c), but between b) and c), the discrepancies are minimal.

Using the thorax coordinate system as reference frame, equation (2.11) can be expressed as

$$[\text{pelvis}] = [R_j]\,[\text{thorax}] \quad \text{eq. (2.20)}$$

which implies

$$[R_j] = [\text{pelvis}]\,[\text{thorax}]^{-1} \quad \text{eq. (2.21)}$$

Equ. 2.21 $[R_j]$ represents the rotation matrix between pelvis and thorax. The function *cardan2* performs the equ. (2.16) and then computes the angles α, β and γ, using the equations (2.17, 2.18, 2.19).

Using symmetry to choose Cardan angle sequence

Crawford et al. (1996) in their work considered the question, how choose a sequence in spinal motion? They presented that this can be addressed by considering symmetry planes and types of rotations. They proposed:

1) In spinal motion the plane of symmetry is the sagittal plane. Angles should, if possible, describe the deviation from this plane. That's means that the first two rotations should be around the axes, which form this plane. In our case this will be around Z and X.
2) Lateral tilt and flexion/extension are essentially the same type of motion (bending). They are distinctly different in nature from axial rotation (twisting). Because their similarity flexion/extension and lateral tilt should be complementary motions.

Crawford et al. (1996) found that "the best" Euler or Cardan sequence for spinal motion is axial then lateral and then sagittal rotation (in our coordinate system R_z, R_x, R_y or γ, α, β). In the present point, it will be important to remember that Skalli et al. (1995), Wu & Cavanagh (1995) suggested that a single Euler sequence can be chosen arbitrarily and used as the standard for describing angular spinal motion.
The rotation matrix will be:

$$[R_j] = [R_{z,\gamma}]\ [R_{x',\alpha}]\ [R_{y'',\beta}] = [R_\gamma]\,[R_\alpha]\,[R_\beta] \quad \text{eq. (2.22)}$$

The rotation will be expressed as

$$[R_j]= \begin{pmatrix} \cos\gamma\cos\beta - \sin\gamma\sin\alpha\sin\beta & -\sin\gamma\cos\alpha & \cos\gamma\sin\beta + \sin\gamma\sin\alpha\cos\beta \\ \sin\gamma\cos\beta + \cos\gamma\sin\alpha\sin\beta & \cos\gamma\cos\alpha & \sin\gamma\sin\beta - \cos\gamma\sin\alpha\cos\beta \\ -\cos\alpha - \sin\beta & \sin\alpha & \cos\alpha\cos\beta \end{pmatrix}$$

eq. (2.23)

The Cardan angles α, β and γ can be obtained from the following trigonometric equations:

$$\alpha = \sin (R_j (3, 2)); \quad \text{eq. (2.24)}$$

$$\beta = - \operatorname{atan} (R_j (3\text{-}1)/ R_j (3,3)); \quad \text{eq. (2.25)}$$

$$\gamma = - \operatorname{atan} (R_j (1, 2)/ R_j (2,2)); \quad \text{eq. (2.26)}$$

As above expressed, the motion of the spine is calculated using the motion of each vertebra with respect to the vertebra below it. Therefore, pelvis has to be used as reference frame.

To compare both approaches, data from nine volunteers were computed first using our proposed sequence and after that the one proposed by Crawford et al. (1996). Tables 2-2 and 2-3 introduce the results of amplitude and phase computed with xyz resp. zxy sequence.

Table 2- 2 Results and means using xyz sequence (thorax as reference frame)

	α_{thorax}	γ_{thorax}	α pelvis-thorax	γ pelvis-thorax	Phase γ p-th	Phase α p-th
	0,59	2,49	2,95	2,77	78,75	303,75
	1,64	3,42	3,91	3,53	84,375	289,69
	0,88	2,86	2,45	1,25	47,81	320,63
	1,09	2,31	2,88	1,26	30,938	278,44
	1,38	2,82	3,78	2,67	98,438	241,17
	1,68	2,24	3,80	2,41	92,813	270
	0,98	3,14	2,53	2,64	67,5	306,56
	1,02	2,89	3,87	1,16	9,8438	270,7
	2,20	3,40	3,10	2,95	51,68	246,09
Mean	1,27	2,84	3,25	2,29	62,46	280,78

Table 2- 3 Results and means using zxy sequence (pelvis as reference frame)

	α_{thorax}	γ_{thorax}	$\alpha_{pelvis\text{-}thorax}$	$\gamma_{pelvis\text{-}thorax}$	Phase $\gamma_{p\text{-}th}$	Phase $\alpha_{p\text{-}th}$
	0,56	2,32	2,82	3,69	92,81	303,75
	1,55	3,01	3,66	4,84	87,19	289,69
	0,84	2,72	2,25	2,22	11,25	320,63
	0,99	1,89	2,52	2,61	33,75	281,25
	1,29	2,72	3,00	4,70	NaN	241,17
	1,61	2,16	3,26	4,31	73,13	270,00
	0,91	2,79	2,31	3,69	59,06	306,56
	1,01	2,81	3,83	1,70	22,15	270,70
	2,15	3,09	2,93	3,98	54,14	246,09
Mean	1,21	2,61	2,95	3,53	54,18	281,09

Observing the results, we can conclude that absolute motions do not differ significantly. Lateral flexions show similar values but with the tendency that xyz sequence (main frame upper segment) are larger. On the opposite, torsions computed with xyz sequence are smaller than those computed with zxy sequence (main frame lower segment), and in this case the difference is significant. The most important point is that phases between pelvis and thorax do not differ significantly by using xyz or zxy sequences. This fact proves that to apply xyz sequence using upper segment as reference frame is correct in this case, because xyz sequence using lower segment as reference frame changes the phase between 90° and 180°.
In the light of these results, Cardan angles will be computed using eqs. (2.19), (2.17), (2.18), (2.19) and eq. (2.21).

Interpolation and filtering:

In this section, the post-processing of the data calculated with the functions *cardanang* and *cardan2* will be addressed.
To achieve the processing of the raw data, the functions *intfil* and *eliptico* were programmed.
Intfil returns two vectors (A, B) from the input function (x). The vector B contains the interpolated function from (x) and A the interpolated and filtered function from (x). In both cases, the function *intfil* centred the oscillations on zero.

[A, B] =*intfil* (x);

To interpolate, the *infilt* function uses the Matlab® function *interp1*. This function performs one dimensional data interpolation [97].Under this function is possible to use different interpolation methods. For the function *infilt*, the cubic spline method was selected.
To smooth the raw data, the *infilt* function uses two consecutive FIR filters. The first one is the 10 point averaging filter; the second one is a cubic Savitzky-Golay filter.
Because the averaging filter produces phase distortion, the 10 point averaging filter was mounted in a Matlab's FIR *filtfilt* filter function.

The *filtfilt* function performs zero-phase digital filtering by processing the input data in both the forward and reverse directions. After filtering in the forward direction, it reverses the filtered sequence and runs it back through the filter. The resulting sequence has precisely zero-phase distortion and doubles the filter order. filtfilt minimizes start-up and ending transients by matching initial conditions, and works for both real and complex inputs [97].
Savitzky-Golay smoothing filters (also called digital smoothing polynomial filters or least squares smoothing filters) are typically used to "smooth out" a noisy signal whose frequency span (without noise) is large. In this type of application, Savitzky-Golay smoothing filters perform much better than standard averaging FIR filters, which tend to filter out a significant portion of the signal's high frequency content along with the noise. Although Savitzky-Golay filters are more effective at preserving the pertinent high frequency components of the signal, they are less successful than standard averaging FIR filters at rejecting noise [97].
Considering these explanations, is easy to see, that the *intfil* function uses the better part of each filter function. That means that the noise will be filtered using very smooth average methods and the smoothing of the signal, keeping high frequency components, with the Savitzky-Golay filter.
In the last process, the *intfil* function centers the interpolated/filtrated function on zero, using:

$$Y(i) = y(i) - \text{mean}\,(y(i)) \quad \text{eq. (2.27)}$$

Where y(i) is the actual ordinate of the point and Y(i) is the centered one.

The filter function *eliptico* is an elliptic high-pass band filter, which uses the Matlab® function *ellip.* The task of *eliptico* is to filter all frequencies below 0.5 Hz.

This filter is used only to remove low frequencies from the motion of the head.

Because it was observed many times, that the test-persons, though they should have to look forward, performed a periodic rotation of the head with great amplitudes. The frequency of these rotations showed values between 0.1 and 0.4 Hz and the amplitudes between 10° and 40°.

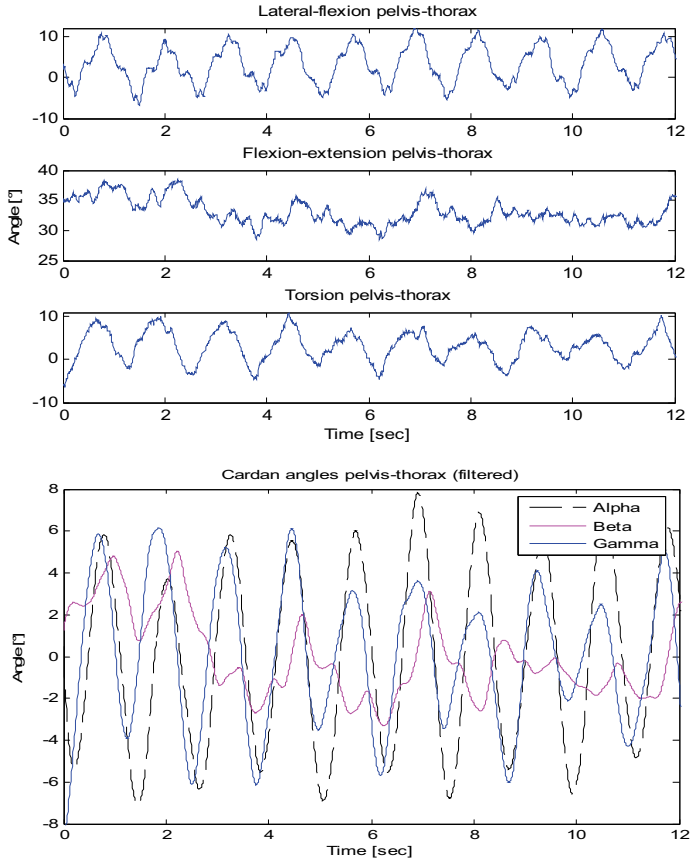

Figure 2- 9 Cardan angles between pelvis and thorax. a) Raw-data, b) filtered data using the intfil function. Alpha (lat.-flexion), beta (flexion-extension), gamma (torsion).

These rotations can not be produced by the normal gait. They are produced intentionally or not by the test-person, maybe because they were tired or not concentrated. Consequently, for the purpose of this experiment, they were taken as artefact and using *eliptico* neglected.
In fig. 2-10 the effect of *eliptico* is introduced.

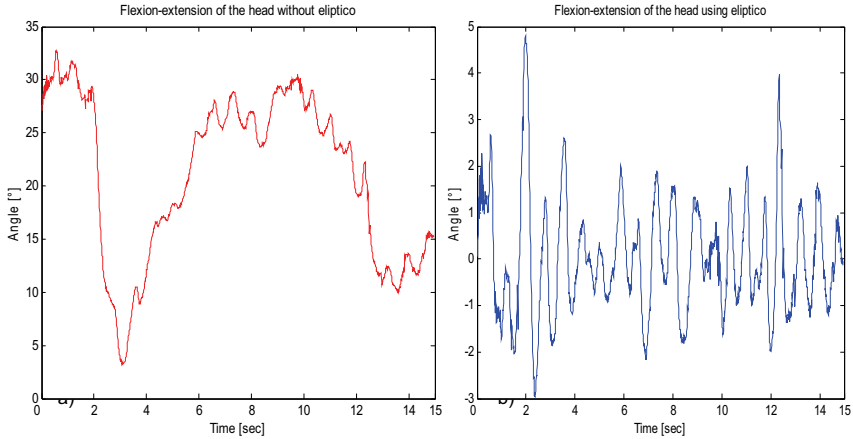

Figure 2- 10 illustrates the effect of the filter *eliptico*. In a) amplitudes bigger as 30° are showed. They could be produced, because the test-person was tired or not concentrated. b) due to the action of the filter, all these not admissible amplitudes are neglected.

2.3.3 Third module

The third module performs the spectrum analysis of the data. The goal of this module is to provide:

- maximal amplitude and the frequency of the dominant mode of the oscillation and the Q-Q values (from Witte et al. 2003)
- the phase between the oscillations, which have the same dominant mode of the frequency of the oscillation.

For the calculation of the amplitudes, the frequency and the Q-Q values, the function *amp_fre* was programmed.

[A, B,C]=amp_fre (X)

The *amp_fre* function uses the matlab's function *fft* to perform the Fast Fourier Transform of the vector X, and returns the amplitude (A) and the frequency (B) of the principal mode of the oscillation. The units for the amplitude of the rotations and translations are respectively degrees and mm, for the frequency Hz.
To perform the calculation of the Q-Q values (C) *amp_fre* uses also the *Uarea* function, programmed following (Witte et al. 2003).

$$Q_4 = \frac{\int_{0,5.f}^{1,5.f} a(f)df}{\int_{0,5.f}^{4,5.f} a(f)df} \quad \text{eq. (2.23)}$$

Where $\int_{0,5.f}^{1,5.f} a(f)df$ is the area under the curve of the FFT from the angle function, between 0,5 and 1,5 times the principal mode of the oscillation and $\int_{0,5.f}^{4,5.f} a(f)df$ is the area under the same curve but between 0,5 and 4,5 times principal mode of the oscillation. The Quartile Q_4 will take values between 0,25 (case of white-noise) and 1 (case of one pick). For normalization purposes, it is useful to take scale between 0 and 1 or from 0% to 100%.

$$S = -\frac{1}{3} + \frac{4}{3}Q_4 \quad \text{eq. (2.24)}$$

Where S is the Stereotypindex [0 to 1 or 0% to 100%]

To achieve the phase between the functions with equal frequency, the function *fase* was programmed.

Phi = fase (X, Y, Freq_X)

fase returns the phase angle in grad (0° to 360°) between the vectors X (as base) and Y, using the matlab's function *xcorr* (normalised).

The calculation method is the following:

The f*ase* function performs the normalized cross-correlation between the vectors X and y and computes the phase angle between them using the following equation:

$$\text{Phi} = \left(\frac{x\max}{Sf}\right) \times f \times 360 \ [°] \quad \text{eq. (2.25)}$$

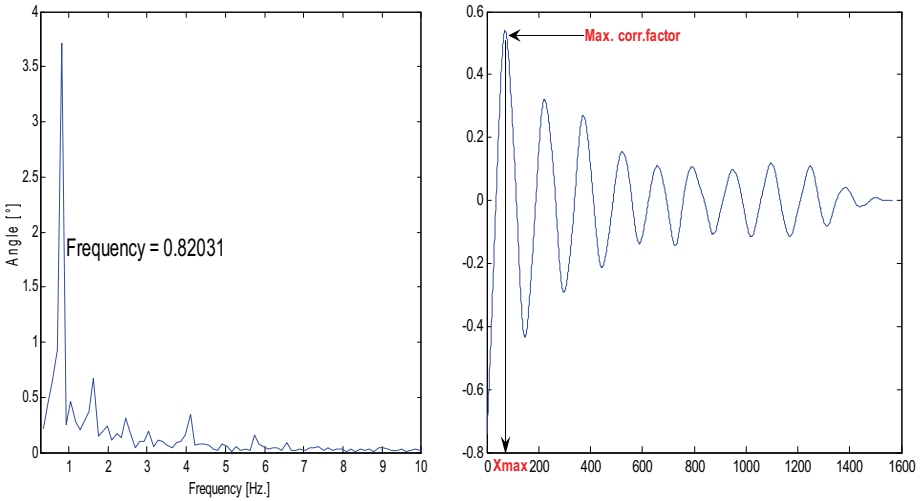

Figure 2- 11 Shows the results from the FFT and the cross-correlation function and how to obtain the information used in the function *fase.*

where xmax is the abscissa coordinate in points of the maximal correlation coefficient (see fig. 2-11). If we divide it by the sampling frequency (Sf), we will obtain the time in seconds. From the multiplication by the time (xmax/Sf) and the frequency of the oscillation of the functions (f), we will obtain a coefficient, which is a percentage value of the full vibration (from 0 to 1). To express it in degrees, it must be multiplied by 360.

The function *fase* uses also a 10 point averaging filter mounted in a Matlab's FIR *filtfilt* filter function, to prevent erroneous phase angles produced when the correlation function has a small local maximum around the absolute maximum.

It must be said, that before *fase* function processes the calculation, the routine checks previously whether the two input functions have the same frequency. Should

this be true, the phase shift angle will be computed; if not, the phase angle will be saved as NaN.

2.3.4 Fourth module

All the calculated data was automatically saved on a Structure. Structures are Matlab® arrays with named "data containers" called fields. The fields of a structure can contain any kind of data [97]. That allows saving not only numerical information (e.g. vectors, matrices) but also strings.

"I often say that when you can measure what you are speaking about and express it in numbers you know something about it, when you can cannot express it in numbers, your knowledge is of a meagre and unsatisfactory kind."
***Lord Kelvin**, 1891*

Chapter 3: Results kinematics of trunk and head

In the following pages, the results from the calculations of the kinematical paths of the trunk and head from all the 106 test-persons will be presented[4].
The results of the kinematical analysis will be displayed divided in: pelvis, thorax, head, pelvis-thorax and thorax-head. Within each subdivision, the results obtained from the male and female volunteers are compared.
From the absolute and relative motions of the trunk and head, the amplitudes of the principal oscillation mode of the three translations and rotations are shown, as well as their frequencies and phase shift angles, related to velocities.
Finally, some selected results of the descriptive statistics are presented.

3.1 Absolute motions (global frame)

3.1.1 Pelvis

Rotations and translations

Fig. 3-1 shows the amplitude of the basic oscillation mode of the pelvic rotations about the sagittal (α) and the transversal axis (β) during walking. The values represented are the means and the std. deviations of 56 males and 50 females[5].

[4] Part of the results on this chapter were published in "Interdependencies of trunk motion and Anthropometry in humans", Erfurter Tage (Andrada, Witte et al., 2006)

Kinematical calculations were performed for ascending and descending ramps (2 km/h to 6 km/h and 6 km/h to 2 km/h, resp.).

The upper left figure shows the pelvic rotation α, around the sagittal axis (males). On the ascending ramp, the amplitude starts from 4,52° at 2 km/h and decreases to 4,03° at 3,5 km/h. From 3 km/h to 6 km/h, the value of the amplitude increases to 5,62°.

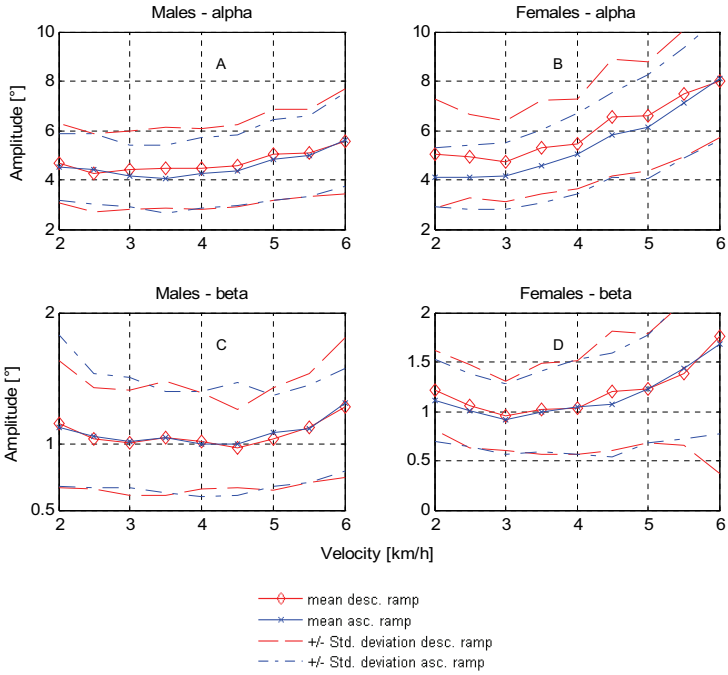

Figure 3- 1 Comparison of the rotation of the pelvis of male and female volunteers around the sagittal axis (upper left and right) and the transverse axis (bottom left and right), related to the velocity.

Amplitudes of α in males show dependencies on the change of the speed. The descending ramp starts with 5,57° at 6 km/h, has a minimum of 4,28° at 2,5 km/h and ends with 4,66° at 2 km/h.

[5] Number of test-persons. The calculations were performed using only validated quality data. This means, that the number of test-persons used to calculate the different kinematical parameters may vary. See tables.

Only with the exception of velocities (6 km/h) in males and females and 2,5 km/h in males, the means calculated for the rotations on the descending ramp are larger than those calculated for the ascending ramp. The std. deviations on the descending ramp also were larger than those of the ascending ramp.

In the case of the females (upper right), minimal and maximal amplitudes for the ascending and descending ramp are: 2,6° resp. 8,1° in ascending ramp and 3,4° resp. 8° in descending ramp.

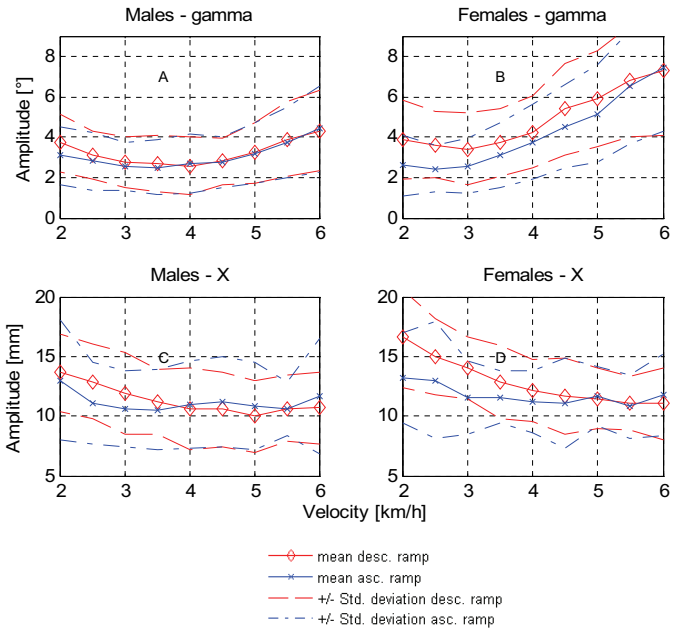

Figure 3- 2 Rotation of the pelvis from males and females volunteers around the longitudinal axis (upper left and right) and translation in the sagittal axe (bottom left and right), related to the velocity.

Rotations of the pelvis around the transverse axis (bottom) show no clear dependencies on the velocity. In the case of the male volunteers (bottom left), the amplitude for all velocities are close to 1° up to 5 km/h, then amplitudes ascend to 1,3° at 6 km/h. In case of the females (bottom right), there is an increasing ramp starting at 4 km/h up to the maximal value of 1,73°.

Fig. 3-2 shows the means and std. deviation of the pelvic rotation γ around the longitudinal axis, and the translation of the pelvis on the sagittal axis (X) of males (upper left) and females (upper right), related to velocity.

In the case of the longitudinal rotation, males do show significant amplitude differences between ascending and descending profiles from 2 km/h to 4 km/h.

At 2 km/h the values of the amplitude are 3,08° and 3,7° for the ascending resp. descending ramp.

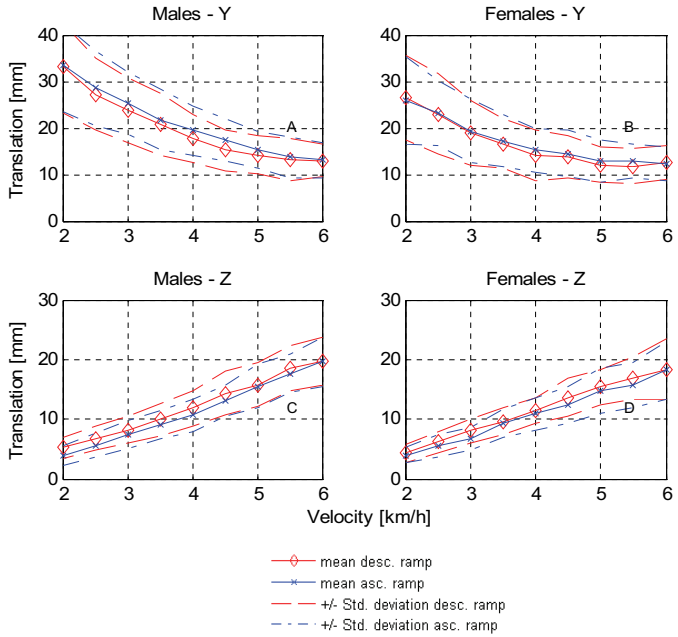

Figure 3- 3 Translation of the pelvis of males and females volunteers in the transverse axis (upper left and right) and in the longitudinal axis (bottom left and right), related to the velocity.

Both values descend to a minimum of 2,48° at 3,5 km/h for the ascending ramp and 2,56° at 4 km/h for the descending ramp. Soon both ascending and descending ramps ascend to a maximum of 4,4° respectively 4,31° at 6 km/h.

Females show only same amplitudes at 6 km/h (7,4°), then the amplitudes calculated for the descending profile are always larger. The minimal amplitudes appear at 2,5 km/h for the ascending ramp and at 3 km/h for the descending ramp (2,47° resp. 3,39°).

Translations in X for both males and females show an inverse relation to velocity. That may not be very clear in the ascending ramp but in the descending one. The means of the maximal and minimal amplitudes are: 13,65 mm at 2 km/h resp. 9,97 mm at 5 km/h (males) and 16,44 mm at 2 km/h resp. 10,99 mm at 6 km/h (females).
Fig. 3-3 shows the means and std. deviations of the translations of the pelvis in the transversal axis (Y), and in the longitudinal axis (Z) of males and females, related to velocity. Mean of amplitudes for the translations in Y of males and females (upper left and right) descend with the increment of the velocity. On the other hand, the amplitude translations in Z (bottom) increase linearly with the velocity. The mean of the maximal and minimal male's pelvic translation arise in Y direction: 33,25 mm at 2 km/h resp. 12,99 mm at 6 km/h, in Z direction: 19,7 mm at 6 km/h resp. 4 mm at 2 km/h. In females' case, the values are: in Y direction: 26,51 mm at 2 km/h resp. 11,72 mm at 5,5 km/h, in Z direction: 18,48 mm at 6 km/h resp. 3,9 mm at 2 km/h.

Table 3- 1 Pelvic rotations and translations (males)

		Speed	2 km/h	2,5 km/h	3 km/h	3,5 km/h	4 km/h	4,5 km/h	5 km/h	5,5 km/h	6 km/h
Pelvic rotations and translations (males)	Asc. Profile	Alpha [°]	4,52	4,43	4,16	4,03	4,28	4,38	4,81	4,97	5,63
		Std. deviation	1,33	1,43	1,26	1,40	1,43	1,44	1,64	1,65	1,89
		n	52	51	49	51	51	52	51	52	52
	Desc. Profile	Alpha [°]	4,66	4,28	4,39	4,48	4,44	4,57	5,02	5,10	5,57
		Std. deviation	1,62	1,60	1,61	1,65	1,66	1,67	1,84	1,77	2,13
		n	52	54	53	53	52	49	51	53	50
	Asc. Profile	Beta [°]	1,13	1,06	1,02	1,05	1,00	1,00	1,09	1,12	1,32
		Std. deviation	0,45	0,39	0,35	0,42	0,40	0,39	0,42	0,42	0,51
		n	52	51	49	51	51	52	51	52	52
	Desc. Profile	Beta [°]	1,15	1,04	1,01	1,05	1,02	0,97	1,04	1,12	1,28
		Std. deviation	0,48	0,39	0,40	0,43	0,36	0,30	0,39	0,42	0,53
		n	52	53	53	53	52	49	51	53	50
	Asc. Profile	Gamma [°]	3,08	2,81	2,56	2,49	2,66	2,76	3,21	3,74	4,40
		Std. deviation	1,42	1,44	1,20	1,37	1,47	1,23	1,48	1,76	2,10
		n	52	51	49	51	51	52	51	52	52
	Desc. Profile	Gamma [°]	3,71	3,08	2,76	2,69	2,56	2,81	3,21	3,89	4,32
		Std. deviation	1,45	1,18	1,24	1,38	1,43	1,16	1,47	1,84	2,01
		n	52	54	53	53	52	49	51	53	50
	Asc. Profile	X [mm]	13,00	11,11	10,62	10,53	10,96	11,23	10,82	10,65	11,70
		Std. deviation	5,02	3,41	3,20	3,36	3,66	3,79	3,63	2,23	4,82
		n	52	51	49	51	51	52	51	52	52
	Desc. Profile	X [mm]	13,65	12,89	11,89	11,15	10,66	10,57	9,97	10,65	10,69
		Std. deviation	3,25	3,09	3,43	2,72	3,43	3,13	3,04	2,78	3,01
		n	52	54	53	53	52	49	51	53	50
	Asc. Profile	Y [mm]	33,25	28,50	25,25	21,77	19,48	17,52	15,28	13,71	13,09
		Std. deviation	9,73	7,84	6,60	6,53	5,28	4,51	4,04	4,37	3,85
		n	52	51	49	51	51	52	51	52	52
	Desc. Profile	Y [mm]	33,05	27,26	23,79	20,73	17,71	15,22	14,20	13,28	12,99
		Std. deviation	9,72	7,62	7,08	6,63	5,15	4,38	4,12	4,53	3,59
		n	52	54	53	53	52	49	51	53	50
	Asc. Profile	Z [mm]	4,03	5,59	7,43	8,95	10,66	13,10	15,59	17,69	19,64
		Std. deviation	1,79	1,99	2,39	2,16	2,76	2,69	3,58	3,20	4,21
		n	52	51	49	51	51	52	51	52	52
	Desc. Profile	Z [mm]	5,20	6,79	8,21	9,96	11,87	14,36	15,80	18,58	19,75
		Std. deviation	1,88	1,99	2,25	2,69	2,90	3,65	3,61	3,81	4,05
		n	52	54	53	53	52	49	51	53	50

In tables 3-1 and 3-2, the values of the means and the standard deviations of the different amplitudes for each speed are shown, in addition to the amount of data used to calculate them.

Table 3- 2 Pelvic rotations and translations (females)

		Speed	2 km/h	2,5 km/h	3 km/h	3,5 km/h	4 km/h	4,5 km/h	5 km/h	5,5 km/h	6 km/h
Pelvic rotations and translations (females)	Asc. Profile	Alpha [°]	4,04	4,12	4,23	4,54	5,17	5,95	6,30	7,19	8,13
		Std. deviation	1,17	1,29	1,38	1,46	1,78	1,82	2,25	2,33	2,54
		n	49	47	48	49	49	49	48	48	47
	Desc. Profile	Alpha [°]	4,98	4,92	4,75	5,32	5,50	6,61	6,56	7,43	8,08
		Std. deviation	2,16	1,66	1,60	1,89	1,83	2,44	2,19	2,54	2,31
		n	49	47	47	48	48	48	46	45	46
	Asc. Profile	Beta [°]	1,12	1,02	0,95	1,02	1,06	1,07	1,22	1,42	1,67
		Std. deviation	0,41	0,38	0,39	0,43	0,48	0,52	0,53	0,70	0,90
		n	49	47	48	49	49	49	48	48	48
	Desc. Profile	Beta [°]	1,20	1,08	0,95	1,02	1,05	1,21	1,22	1,38	1,73
		Std. deviation	0,40	0,44	0,35	0,46	0,47	0,60	0,54	0,72	1,35
		n	48	47	47	48	48	48	46	44	48
	Asc. Profile	Gamma [°]	2,62	2,47	2,64	3,09	3,83	4,62	5,25	6,55	7,41
		Std. deviation	1,46	1,13	1,33	1,56	1,90	2,12	2,50	2,88	3,16
		n	49	47	48	49	49	49	48	48	47
	Desc. Profile	Gamma [°]	3,82	3,53	3,39	3,72	4,24	5,43	5,83	6,70	7,32
		Std. deviation	1,92	1,63	1,71	1,66	1,76	2,35	2,33	2,77	3,20
		n	48	47	47	48	48	48	46	45	46
	Asc. Profile	X [mm]	13,17	12,88	11,52	11,62	11,15	11,09	11,58	11,05	11,76
		Std. deviation	3,69	4,83	3,03	2,10	2,50	3,71	2,57	2,94	3,54
		n	49	47	48	49	49	49	48	48	48
	Desc. Profile	X [mm]	16,45	14,86	13,93	12,74	12,13	11,63	11,32	10,99	11,00
		Std. deviation	4,15	3,14	2,60	3,00	2,59	3,16	2,56	2,26	3,06
		n	49	48	48	48	49	49	47	45	48
	Asc. Profile	Y [mm]	26,02	23,13	19,39	17,25	15,19	14,48	12,94	12,86	12,30
		Std. deviation	9,41	6,92	6,84	5,61	4,71	5,04	4,61	3,67	3,57
		n	49	47	48	49	49	49	48	48	48
	Desc. Profile	Y [mm]	26,51	22,96	19,07	16,60	14,00	13,88	12,12	11,72	12,66
		Std. deviation	8,92	8,64	6,99	5,34	5,42	4,51	3,75	3,76	3,71
		n	49	48	48	48	49	49	47	45	48
	Asc. Profile	Z [mm]	3,91	5,46	6,75	9,25	10,88	12,34	14,77	15,74	18,23
		Std. deviation	1,30	1,84	1,95	2,35	2,79	3,06	3,82	3,77	4,84
		n	49	47	48	49	49	49	48	48	48
	Desc. Profile	Z [mm]	4,28	6,17	8,07	9,67	11,47	13,70	15,47	16,86	18,48
		Std. deviation	1,48	1,73	1,97	2,21	2,23	3,11	3,00	3,50	4,99
		n	49	48	48	48	49	49	47	45	48

Frequencies

Figs. 3-4 to 3-6 present the frequency means of the oscillations principal mode of the pelvic rotations and translations of male and female volunteers, related to velocity.

Fig. 3-4 shows, that the frequencies of the rotations α and β (around sagittal resp. tranverse axis) increase with the increment of the velocity. By female volunteers, around the sagittal axis (lat. tilt), a minimal frequency of 0,64 Hz at 2 km/h and a maximal frequency of 1,08 Hz at 6 km/h (upper right) was registered. Around the transverse axis (frontal tilt), the results are: 0,99 Hz at 2 km/h and 1,77 Hz at 6 km/h, minimum resp. maximum.

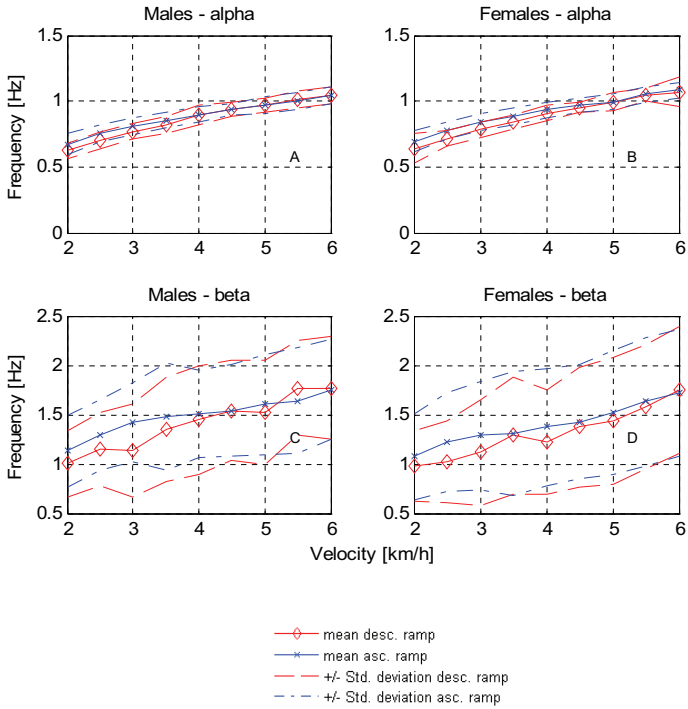

Figure 3- 4 Pelvic frequency oscillations' principal mode of males and females volunteers in the sagittal (upper left and right) and in the transverse axis (bottom left and right), related to velocity.

Minimal and maximal pelvic lateral tilt frequencies of males volunteers are: 0,62 Hz at 2 km/h resp. 1,05 Hz at 6 km/h.

Around the transverse axis (frontal tilt), the results are: 1 Hz at 2 km/h and 1,77 Hz at 6 km/h, minimum resp. maximum.

The std. deviation of the lateral tilt frequency of male and female volunteers arise very small values in both ascending and descending ramp.

Fig. 3-5 shows the frequencies of the axial rotations of the pelvis (γ) and the frequencies of their translations in the sagittal axis (X). By females volunteers a dependency on the frequency of the rotations γ related to velocity except between 3 km/h and 4 km/h in the ascending ramp is observed. The behaviour of the frequency of the translations in X is more unstable, and shows no significant variations after 4 km/h.

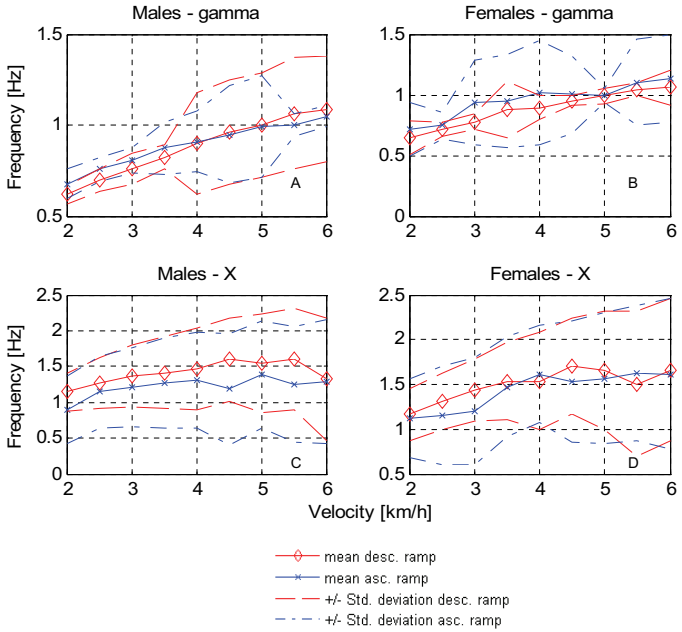

Figure 3- 5 Frequencies of the oscillations' principal mode of pelvic lateral tilt in males and females volunteers (upper left and right) and of their pelvic translations in the transverse axis (bottom left and right), related to velocity.

Minimal and maximal frequencies values of axial rotation (γ), obtained for female volunteers, are: 0,62 Hz at 2 km/h respectively 1,08 Hz at 6 km/h. Minimal and maximal values of frequencies of (X), obtained for female volunteers, are:1,13 Hz at 2 km/h resp. 1,72 Hz at 4,5 km/h.

Male volunteers show a nearly linear dependency from the frequency of the rotations γ on the velocity. A great increment of the standard deviation after 3 km/h or 3,5 km/h can be observed.

The frequencies of the translations in X grow up to 4 km/h or 4,5 km/h. In case of females, after these velocities there are no more substantial frequency variations. Minimal and maximal values of frequencies of (γ), obtained from male volunteers are: 0,61 Hz at 2 km/h resp. 1,1 Hz at 6 km/h, and of (X): 0,89 Hz at 2 km/h resp. 1,6 Hz at 4,5 km/h.

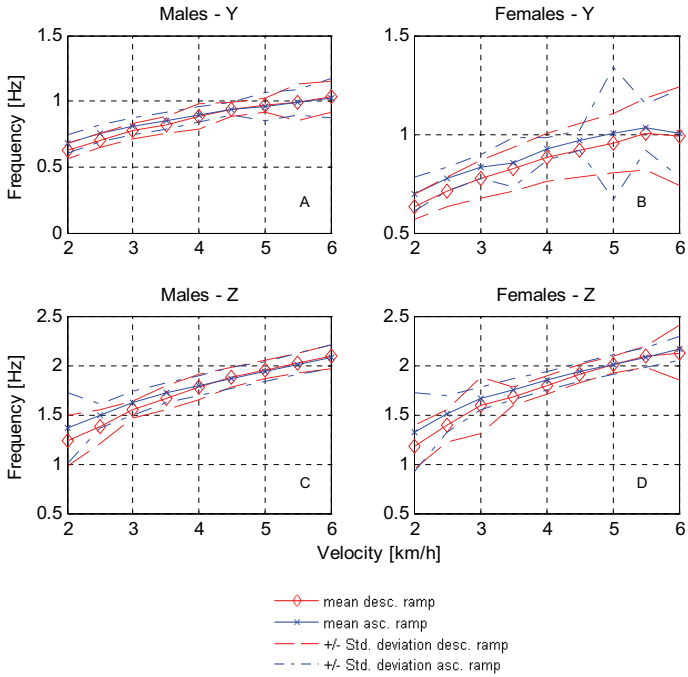

Figure 3- 6 Frequencies of the principal mode of the oscillation of the translations of the pelvis from males and females volunteers in the transverse axe (upper left and right) and in the longitudinal axe (bottom left and right), related to the velocity.

Fig. 3-6 shows the frequencies of the translations in the transverse axis (Y) and the frequencies of the translations in the longitudinal axis (Z). Both female and male test-persons show linear dependencies of their pelvic translations in Y and Z directions on velocity. Only in the female's case, the frequencies of Y translations show a decrement in their values with an increment of the velocity (1,03 Hz at 5,5 km/h and 1 Hz at 6km/h). Minimal and maximal values of frequencies obtained from female volunteers, are, for (Y): 0,63 Hz at 2 km/h resp. 1,03 Hz at 5,5 km/h, and for (Z): 1,17 Hz at 2 km/h resp. 2,17 Hz at 6 km/h.

Table 3- 3 Frequencies of pelvic rotations and translations (males)

Frequencies of pelvic rotations and translations (males)		Speed	2 km/h	2,5 km/h	3 km/h	3,5 km/h	4 km/h	4,5 km/h	5 km/h	5,5 km/h	6 km/h
	Asc. Profile	Alpha [Hz]	0,67	0,76	0,81	0,86	0,90	0,94	0,97	1,00	1,05
		Std. deviation	0,08	0,06	0,07	0,06	0,06	0,05	0,06	0,06	0,06
		n	52	51	49	51	51	52	51	52	52
	Desc. Profile	Alpha [Hz]	0,62	0,70	0,77	0,82	0,90	0,94	0,97	1,01	1,05
		Std. deviation	0,05	0,06	0,06	0,06	0,07	0,05	0,06	0,06	0,06
		n	52	54	53	53	52	49	51	53	50
	Asc. Profile	Beta [Hz]	1,13	1,29	1,42	1,48	1,50	1,54	1,60	1,64	1,75
		Std. deviation	0,36	0,36	0,40	0,54	0,44	0,46	0,51	0,54	0,51
		n	52	51	49	51	51	52	51	52	52
	Desc. Profile	Beta [Hz]	1,00	1,15	1,14	1,35	1,45	1,54	1,52	1,77	1,77
		Std. deviation	0,34	0,37	0,47	0,53	0,55	0,51	0,53	0,48	0,52
		n	52	54	53	53	52	49	51	53	50
	Asc. Profile	Gamma [Hz]	0,68	0,76	0,81	0,87	0,91	0,95	0,99	1,00	1,05
		Std. deviation	0,08	0,07	0,07	0,14	0,17	0,27	0,28	0,06	0,06
		n	52	51	49	51	51	52	51	52	52
	Desc. Profile	Gamma [Hz]	0,62	0,70	0,76	0,82	0,90	0,96	1,00	1,07	1,09
		Std. deviation	0,05	0,06	0,08	0,06	0,28	0,29	0,29	0,31	0,29
		n	52	54	53	53	52	49	51	53	50
	Asc. Profile	X [Hz]	0,89	1,14	1,21	1,27	1,31	1,18	1,39	1,25	1,29
		Std. deviation	0,47	0,50	0,56	0,63	0,67	0,78	0,76	0,80	0,87
		n	52	51	49	51	51	52	51	52	52
	Desc. Profile	X [Hz]	1,15	1,27	1,38	1,41	1,46	1,60	1,54	1,61	1,32
		Std. deviation	0,26	0,36	0,43	0,50	0,57	0,58	0,68	0,72	0,85
		n	52	54	53	53	52	49	51	53	50
	Asc. Profile	Y [Hz]	0,68	0,76	0,81	0,86	0,90	0,94	0,96	0,99	1,02
		Std. deviation	0,07	0,06	0,07	0,06	0,06	0,05	0,10	0,09	0,15
		n	52	51	49	51	51	52	51	52	52
	Desc. Profile	Y [Hz]	0,62	0,70	0,77	0,82	0,88	0,94	0,97	0,99	1,03
		Std. deviation	0,05	0,05	0,06	0,06	0,09	0,05	0,06	0,14	0,12
		n	52	54	53	53	52	49	51	53	50
	Asc. Profile	Z [Hz]	1,36	1,49	1,62	1,72	1,79	1,87	1,94	2,01	2,08
		Std. deviation	0,36	0,12	0,12	0,10	0,10	0,10	0,10	0,11	0,12
		n	52	51	49	51	51	52	51	52	52
	Desc. Profile	Z [Hz]	1,23	1,38	1,55	1,67	1,77	1,88	1,95	2,02	2,09
		Std. deviation	0,26	0,17	0,09	0,12	0,13	0,10	0,10	0,10	0,12
		n	52	54	53	53	52	49	51	53	50

Minimal and maximal values of frequencies of Y and Z obtained from male volunteers, are, for (Y): 0,62 Hz at 2 km/h respectively 1,03 Hz at 6 km/h, and for (Z): 1,23 Hz at 2 km/h respectively 2,08 Hz at 6 km/h.

In tables 3-3 and 3-4, the values of the means and the standard deviations of the different frequencies for each speed are shown, in addition to the amount of data used to calculate them.

Table 3- 4 Frequencies of pelvic rotations and translations (females)

Frequencies of pelvic rotations and translations (females)		Speed	2 km/h	2,5 km/h	3 km/h	3,5 km/h	4 km/h	4,5 km/h	5 km/h	5,5 km/h	6 km/h
	Asc. Profile	Alpha [Hz]	0,69	0,77	0,84	0,88	0,93	0,97	0,99	1,05	1,08
		Std. deviation	0,08	0,06	0,06	0,06	0,06	0,05	0,06	0,06	0,06
		n	49	47	48	49	49	49	48	48	48
	Desc. Profile	Alpha [Hz]	0,64	0,72	0,79	0,84	0,91	0,95	0,99	1,05	1,07
		Std. deviation	0,11	0,06	0,06	0,05	0,06	0,04	0,07	0,05	0,11
		n	49	48	48	48	49	49	47	45	48
	Asc. Profile	Beta [Hz]	1,09	1,24	1,31	1,33	1,40	1,46	1,55	1,66	1,74
		Std. deviation	0,43	0,49	0,55	0,62	0,58	0,57	0,62	0,64	0,63
		n	49	47	48	49	49	49	48	48	48
	Desc. Profile	Beta [Hz]	1,00	1,03	1,15	1,31	1,26	1,39	1,46	1,61	1,78
		Std. deviation	0,35	0,42	0,53	0,58	0,53	0,60	0,64	0,62	0,63
		n	49	48	48	48	49	49	47	45	48
	Asc. Profile	Gamma [Hz]	0,71	0,75	0,93	0,95	1,01	1,00	0,99	1,10	1,13
		Std. deviation	0,22	0,11	0,34	0,37	0,42	0,31	0,06	0,34	0,36
		n	49	47	48	49	49	49	48	48	48
	Desc. Profile	Gamma [Hz]	0,65	0,71	0,78	0,87	0,89	0,95	0,99	1,05	1,06
		Std. deviation	0,14	0,05	0,06	0,22	0,10	0,04	0,06	0,05	0,14
		n	49	48	48	48	49	49	47	45	48
	Asc. Profile	X [Hz]	1,13	1,15	1,23	1,49	1,63	1,55	1,59	1,59	1,64
		Std. deviation	0,43	0,55	0,59	0,55	0,54	0,67	0,71	0,78	0,83
		n	49	47	48	49	49	49	48	48	48
	Desc. Profile	X [Hz]	1,17	1,32	1,45	1,52	1,55	1,72	1,67	1,53	1,65
		Std. deviation	0,28	0,31	0,34	0,46	0,54	0,52	0,65	0,80	0,80
		n	49	48	48	48	49	49	47	45	48
	Asc. Profile	Y [Hz]	0,69	0,77	0,83	0,86	0,93	0,97	1,00	1,03	1,00
		Std. deviation	0,09	0,06	0,06	0,12	0,06	0,05	0,34	0,12	0,22
		n	49	47	48	49	49	49	48	48	48
	Desc. Profile	Y [Hz]	0,63	0,71	0,77	0,82	0,88	0,92	0,95	1,00	0,98
		Std. deviation	0,06	0,08	0,10	0,11	0,12	0,13	0,15	0,18	0,26
		n	49	48	48	48	49	49	47	45	48
	Asc. Profile	Z [Hz]	1,32	1,51	1,66	1,76	1,85	1,93	2,00	2,08	2,17
		Std. deviation	0,40	0,18	0,11	0,10	0,09	0,09	0,10	0,10	0,13
		n	49	47	48	49	49	49	48	48	48
	Desc. Profile	Z [Hz]	1,17	1,39	1,59	1,68	1,80	1,91	2,00	2,09	2,13
		Std. deviation	0,23	0,17	0,28	0,09	0,09	0,09	0,09	0,10	0,28
		n	49	48	48	48	49	49	47	45	48

Phase shift angles

Figs. 3-7 to 3-9 present the means and the std. deviations of the phase shift angles between the pelvic rotations and translations of male and female volunteers, related to velocity.

It has to be noted, that the calculation of phase angle were performed, only if the functions did have the same principal frequency (see page 38).

Figure 3-7 (upper) shows the means and the std. deviations of the phase shift angles between pelvic axial rotation γ (as base) and pelvic lateral tilt α of males and females, related to the velocity. Bottom shows the means and the std. deviations of the phase

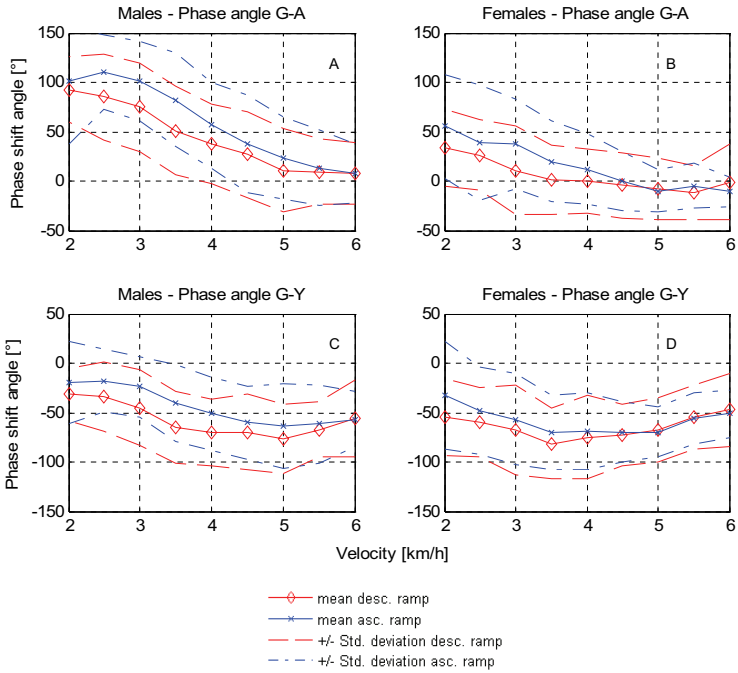

Figure 3- 7 Pelvic phase shift angle between the rotations around the longitudinal and the sagittal axis (Upper left and right) and pelvic phase shift angle between axial rotations and the translations in the transverse axe (Bottom left and right).

shift angles between pelvic axial rotation γ (as base) and the translation of the pelvis in Y direction (lateral) of males and females, related to the velocity.

Up to 5 km/h, the phase angle γ-α, for males and females, decrease with the increment of the velocity, then the phase angle does not show significant variations.

Males and females presented larger values of phase γ-α for the ascending ramp (interval: 2 km/h to 5 m/h). Minimal and maximal values of phase γ-α obtained for female volunteers, are: ascending ramp (-11° at 6 km/h resp. 55,23° at 2 km/h); descending ramp (-11,57° at 5,5 km/h respectively 33,56° at 2 km/h).

Minimal and maximal values of phase γ-α obtained from male volunteers, are: ascending ramp (7,7° at 6 km/h resp. 101,03° at 2 km/h); descending ramp (7,85° at 5,5 km/h resp. 92,48° at 2 km/h).

In the case of the men, the phase γ-Y starts with a small increase between 2 km/h and 2,5 km/h. Soon it diminishes until it reaches 5 km/h, after that, it tends to increase again (in the descending ramp there is no increment of the phase γ-Y from 2 km/h to 2,5 km/h). In the case of women, phase γ-Y descends to a minimum at 3,5 km/h in both ascending and descending ramp. After that, it increases again. Minimal and maximal values of phase γ-Y obtained for female volunteers are: ascending ramp (-32,34° at 2,5 km/h resp. -70,4° at 3,5 km/h); descending ramp (-47,38° at 6 km/h resp. -81,22° at 3,5 km/h). Minimal and maximal values of phase γ-Y obtained from male volunteers, are: ascending ramp (-17,83° at 2 km/h resp. -63,84° at 5 km/h); descending ramp (-31,78° at 2 km/h resp. -76,54° at 5 km/h).

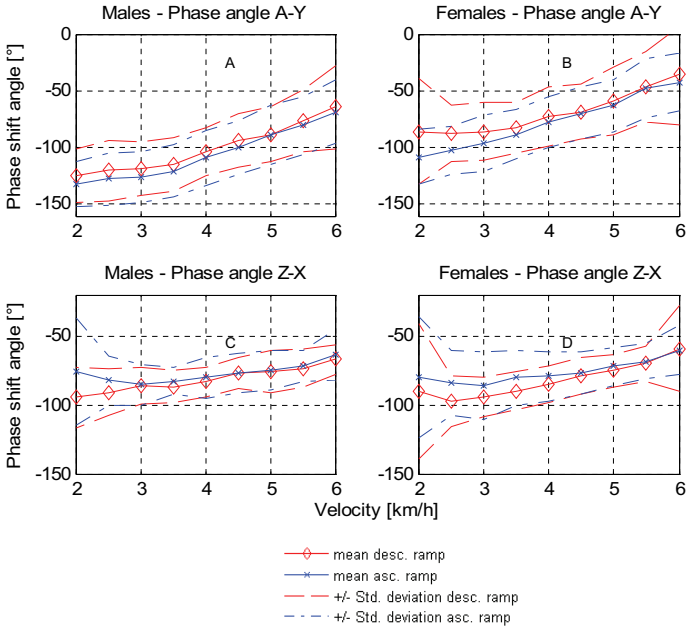

Figure 3- 8 Pelvic phase shift angles, between the rotations around the sagittal axe and the translations in Y direction, related to speed (Upper left and right). (Bottom left and right) pelvic phase shift angle between (Z) translations and (X) translations, related to speed.

Figure 3-8 (upper) shows the means and the standard deviations of the phase shift angles between the pelvic lateral tilt α (as base), and the transversal translations Y of the pelvis of males and females, related to velocity. Bottom shows the means and the std. deviations of the phase shift angles between the longitudinal translation of the

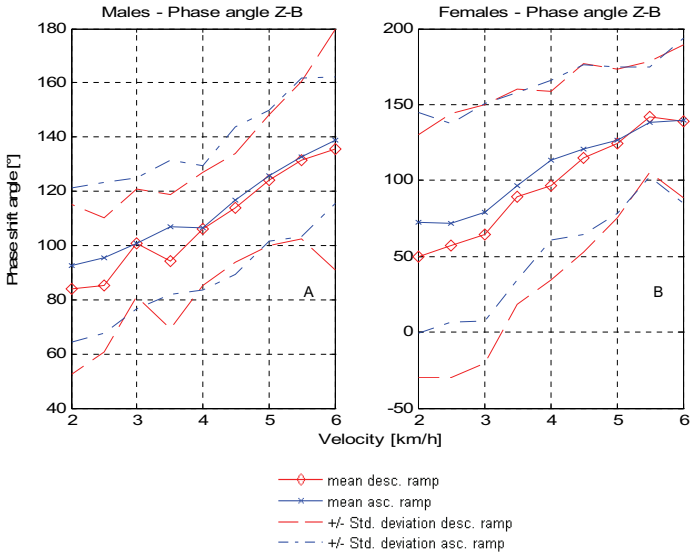

Figure 3- 9 Phase shift angles between the translations about the longitudinal axe Z and the pelvic rotation about the transverse axe, related to the speed.

pelvis in Z direction (as base), and the sagittal translation of the pelvis in X direction of males and females, related to velocity.

In the case of men as well as in that of women, Y is delayed in relation to α (interval $-\pi$; π) and the phase α-Y decreases with increasing speed.

Minimal and maximal values of phase α-Y obtained from female volunteers are: ascending ramp (-42,5° at 6 km/h resp. -107,9° at 2 km/h), and descending ramp (-35,76° at 6 km/h resp. -86° at 6 km/h).

Minimal and maximal values of phase α-Y obtained from male volunteers are: ascending ramp (-68,4° at 6 km/h resp. -131,8° at 2 km/h), and descending ramp (-64,2° at 6 km/h resp. -124,8° at 6 km/h).

The phase variation Z-X on men and women show a positive slope related to the increment of velocity. In both cases X is delayed in relation to Z. For females, the phase angle starts with a descending slope until 2,5 km/h and 3 km/h (descending resp. ascending ramp), after that it is again ascending. Males show this behaviour only for the ascending ramp (inflexion point at 3 km/h).

Minimal and maximal values of phase Z-X obtained for female volunteers are: ascending ramp (-60° at 6 km/h resp. -85,9° at 3 km/h), and descending ramp (-59,1°

at 6 km/h resp. -93,84° at 2,5 km/h). Minimal and maximal values of phase Z-X obtained for male volunteers are: ascending ramp (-63,9° at 6 km/h resp. -85,3° at 3 km/h), and descending ramp (-66,95° at 6 km/h respectively -94,7° at 2 km/h).

Figure 3-9 shows the mean and the standard deviation of the phase shift angles between the longitudinal translations Z of the pelvis (as base) and pelvic frontal tilt β, on males and females, related to velocity. Men and women increment the angle of phase Z -β, when they increase the velocity. Minimal and maximal values of phase Z-β obtained for female volunteers are: ascending ramp (72° at 2,5 km/h resp. 139° at 6 km/h), and descending ramp (50° at 2 km/h resp. 141° at 5,5 km/h).

Table 3- 5 Phases shift angles between pelvic rotations and translations (males)

		Speed	2 km/h	2,5 km/h	3 km/h	3,5 km/h	4 km/h	4,5 km/h	5 km/h	5,5 km/h	6 km/h
Phasen between pelvic rotations and translations (males)	Asc. Profile	φ(γ−α) [°]	101,03	110,23	100,99	82,22	56,95	37,88	23,47	13,29	7,71
		Std. deviation	62,72	37,40	40,55	47,18	43,44	49,72	41,40	38,17	29,75
		n	50	49	45	46	45	48	46	51	49
	Desc. Profile	φ(γ−α) [°]	92,48	85,53	74,86	50,95	37,94	27,12	11,01	9,38	7,85
		Std. deviation	33,30	43,45	44,91	44,82	40,28	43,53	41,68	33,17	31,16
		n	50	48	49	50	45	45	47	49	47
	Asc. Profile	φ(γ−Y) [°]	-19,70	-17,84	-23,93	-40,06	-51,12	-60,08	-63,84	-61,56	-56,99
		Std. deviation	41,38	31,65	30,32	39,09	37,35	37,22	42,61	39,67	27,95
		n	49	49	45	48	45	46	46	50	44
	Desc. Profile	φ(γ−Y) [°]	-31,78	-33,61	-45,22	-64,59	-69,85	-69,95	-76,55	-66,98	-56,10
		Std. deviation	26,60	35,02	38,12	36,20	33,97	38,49	35,41	28,18	38,73
		n	50	51	50	50	46	44	48	47	47
	Asc. Profile	φ(α−Y) [°]	-131,81	-127,62	-125,66	-120,49	-109,05	-99,45	-88,60	-80,54	-68,39
		Std. deviation	19,61	22,54	22,09	23,05	24,22	23,52	25,54	24,94	28,03
		n	51	51	49	49	51	50	49	49	47
	Desc. Profile	φ(α−Y) [°]	-124,83	-120,18	-118,65	-114,48	-104,16	-93,74	-88,29	-76,33	-64,18
		Std. deviation	23,43	26,83	23,68	23,54	21,07	24,01	23,83	27,05	36,40
		n	50	49	52	53	49	44	50	49	48
	Asc. Profile	φ(Z-X) [°]	-75,71	-82,43	-85,30	-82,65	-80,35	-76,63	-74,51	-71,39	-63,95
		Std. deviation	38,69	17,89	15,09	10,00	14,48	14,12	14,56	11,06	18,36
		n	26	34	33	34	33	28	33	28	27
	Desc. Profile	φ(Z−X) [°]	-94,70	-90,81	-85,86	-86,64	-83,46	-76,96	-75,72	-73,46	-66,95
		Std. deviation	22,00	16,86	13,51	12,12	10,52	11,41	15,43	14,03	10,84
		n	41	45	42	42	40	39	36	40	27
	Asc. Profile	φ(Z−β) [°]	92,72	95,44	100,70	106,79	106,62	116,69	125,69	132,63	138,95
		Std. deviation	28,36	27,95	24,23	24,83	22,89	27,23	24,18	29,31	23,23
		n	31	36	36	35	32	34	33	34	36
	Desc. Profile	φ(Z−β) [°]	83,90	85,34	100,91	94,10	106,08	113,83	124,09	131,53	135,46
		Std. deviation	31,38	24,74	19,86	24,87	20,93	20,13	24,27	29,01	44,39
		n	31	35	28	30	28	31	29	40	35

Minimal and maximal values of phase Z -β obtained for male volunteers are: ascending ramp (92,7° at 2 km/h resp. 138,9° at 6 km/h), and descending ramp (83,9° at 2 km/h resp. 135,5° at 6 km/h).

In tables 3-5 and 3-6, the values of the means and the standard deviations of the phases between rotations and translation for each speed are shown, in addition to the amount of data used to calculate them.

Table 3- 6 Phases shift angles between pelvic rotations and translations (females)

		Speed	2 km/h	2,5 km/h	3 km/h	3,5 km/h	4 km/h	4,5 km/h	5 km/h	5,5 km/h	6 km/h
Phasen between pelvic rotations and translations (females)	Asc. Profile	φ(γ–α) [°]	55,23	39,07	37,37	20,07	12,31	-0,19	-10,07	-4,78	-11,01
		Std. deviation	51,99	58,87	45,30	41,39	36,14	29,52	21,27	22,70	14,89
		n	39	37	42	41	46	47	48	47	46
	Desc. Profile	φ(γ–α) [°]	33,56	26,52	10,91	1,23	-0,07	-4,53	-7,92	-11,57	-0,91
		Std. deviation	39,04	36,24	44,98	34,86	32,74	32,70	31,60	27,79	38,56
		n	44	47	45	47	45	49	46	44	46
	Asc. Profile	φ(γ–Y) [°]	-32,34	-47,93	-56,53	-70,40	-69,31	-69,54	-69,55	-55,84	-51,16
		Std. deviation	54,31	44,43	45,81	37,49	38,96	30,84	25,68	26,35	24,34
		n	40	39	42	40	45	47	40	42	40
	Desc. Profile	φ(γ–Y) [°]	-54,81	-59,24	-67,70	-81,23	-75,00	-73,00	-67,17	-54,31	-47,39
		Std. deviation	38,60	35,19	45,74	35,27	42,52	31,25	32,75	32,25	37,50
		n	42	44	43	45	42	46	40	39	38
	Asc. Profile	φ(α–Y) [°]	-107,94	-101,88	-96,24	-88,15	-77,81	-69,47	-62,76	-47,45	-42,50
		Std. deviation	24,36	21,10	24,46	21,42	22,21	22,85	22,99	25,81	25,66
		n	47	45	46	47	46	49	40	42	41
	Desc. Profile	φ(α–Y) [°]	-85,98	-87,60	-85,88	-82,41	-72,47	-68,23	-59,32	-46,73	-35,76
		Std. deviation	46,63	24,40	25,21	22,29	25,54	23,84	29,74	30,63	44,02
		n	45	45	44	46	44	46	39	40	40
	Asc. Profile	φ(Z-X) [°]	-80,02	-84,06	-85,91	-80,08	-78,96	-77,08	-72,20	-68,17	-60,00
		Std. deviation	43,78	23,35	24,43	19,91	17,83	15,30	13,61	13,02	18,02
		n	31	31	31	40	41	37	36	33	34
	Desc. Profile	φ(Z–X) [°]	-90,33	-97,55	-93,84	-89,62	-85,02	-78,83	-75,09	-70,03	-59,14
		Std. deviation	49,20	18,33	14,29	14,24	13,27	12,99	11,98	12,66	31,34
		n	39	41	44	40	41	43	36	30	34
	Asc. Profile	φ(Z–β) [°]	72,26	72,04	79,10	96,24	113,68	120,47	126,56	138,58	139,33
		Std. deviation	72,69	65,47	71,35	61,71	52,68	55,93	48,30	35,89	54,45
		n	32	26	25	25	29	27	30	29	31
	Desc. Profile	φ(Z–β) [°]	50,13	57,17	64,70	89,06	96,70	114,56	124,19	141,84	138,80
		Std. deviation	80,38	86,94	84,87	71,05	62,01	62,19	49,06	36,38	50,63
		n	27	23	23	25	19	22	25	26	33

3.1.2 Thorax

Rotations and translations

Figures 3-10 to 3-12 show the means and the std. deviations of the thoracic rotations and translations of males and females, in both ascending and descending profiles, related to velocity.

Figure 3-10 (upper) shows the thoracic lateral tilt α of males and females related to velocity. Bottom shows the thoracic frontal tilt β of males and females, related to velocity. Male volunteers show a decrement of their lat. tilt from 2 km/h to 4 km/h. After that, they do not show significant variations of α related to velocity, although it

tends to grow again. Females also start with speed decrements up to 3,5km/h, and then like in the males' case, the amplitudes stay around 1°.

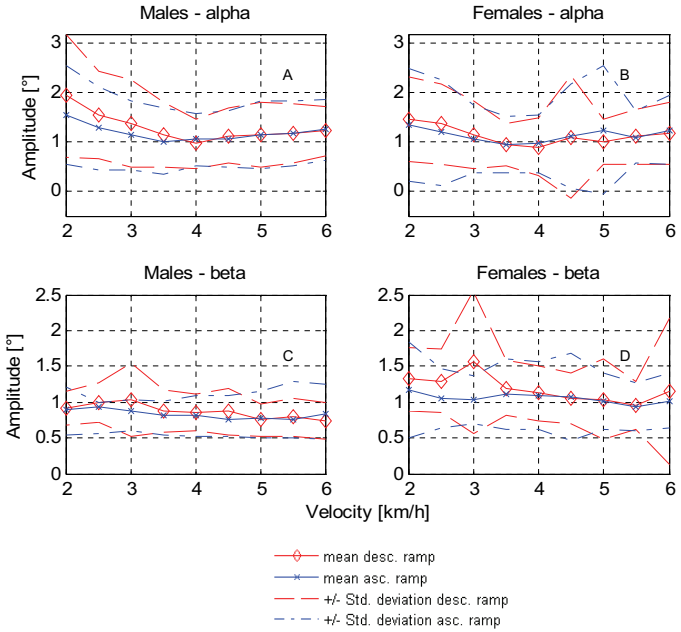

Figure 3- 10 Lateral tilt (A & B) and frontal tilt (C & D) of the thorax of males and females volunteers, related to velocity.

β didn't show significant dependencies on the velocity. Only on males will it be observed that β tends to decrease with the velocity.

For thoracic lateral tilt α of males values arise between 1° and 2°, those of the females, values between 1° and 1,5°.

For frontal tilt β of males values between 0,75° and 1°, in females arise values about 1°.

Figure 3-11 (A and B) show respectively, the axial rotation of the thorax γ of males and females, related to velocity. (C and D) show the thoracic translation in X direction (sagittal axis) of males resp. females, related to velocity.

Men diminish their axial rotation γ (figure 3-11 A) with speed increments until 4 km/h. After that, no significant variations can be observed. Women (figure 3-11 B) show similar paths of γ related to velocity, in this case the decrement ends at 3,5 km/h.

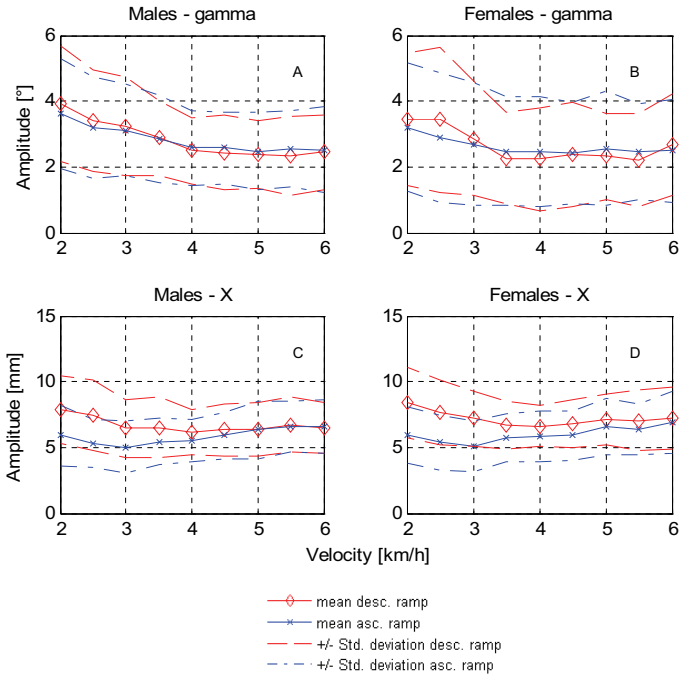

Figure 3- 11 Thorax rotations of males and females volunteers around the longitudinal axis (upper left and right) and translations in the sagittal axis (bottom left and right), related to velocity.

Minimal and maximal values of γ are: 2,21° at 5,5 km/h resp. 3,45° at 2 km/h (females) and 2,33° at 5,5 km/h resp. 3,92° at 2 km/h (males).

The thoracic translations X (in sagittal axis) show different behaviours on males and females for ascending and descending ramp. Males and females start the ascending ramp with a negative slope up to the inflexion point at 3 km/h. From this speed, the slope of males and females became positive. For the descending ramp, males and females show again similar paths. Amplitudes diminish from 2 km/h to 4 km/h, after that no significant variations are observed.

Minimal and maximal values of X for the ascending ramp are: 5,08 mm at 3 km/h resp. 6,94 mm at 6 km/h (females) and 5 mm at 3 km/h resp. 6,62° at 6 km/h (males).

Minimal and maximal values of X for the descending ramp are: 6,64 mm at 4 km/h resp. 8,39 mm at 2 km/h (females) and 6,16 mm at 4 km/h resp. 7,46 mm at 6 km/h (males).

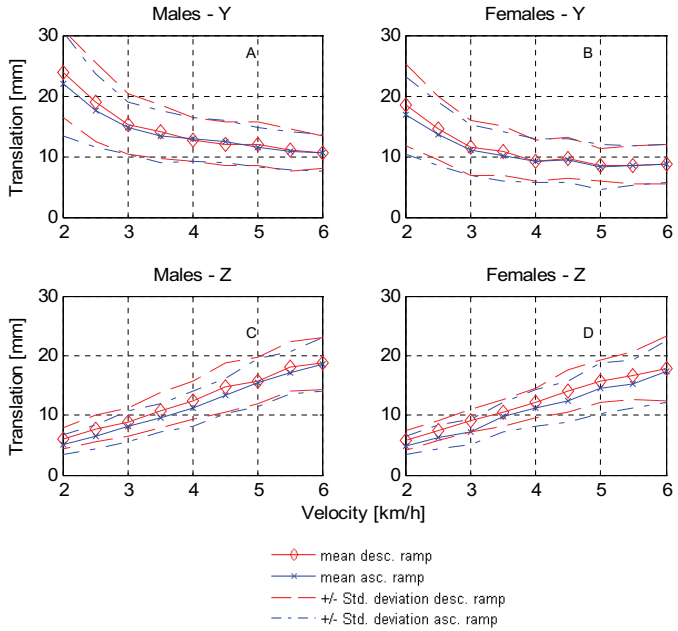

Figure 3- 12 Thoracic translations of male and female volunteers in the transverse axis (upper left and right) and in the longitudinal axis (bottom left and right), related to velocity.

Fig. 3-12 shows the means and std. deviations of the thoracic translations in the transversal (Y) and longitudinal axis (Z) of males and females, related to velocity. Like in the case of the pelvis, the mean of the translation's amplitudes in Y of males and females (upper left and right) descend with the velocity, while the amplitude of the translations in Z (bottom) increase linear with the velocity.

The mean of the minimal and maximal female's thoracic translation arise in Y direction: 8,44 mm at 5,5 km/h resp. 18,5 mm at 2 km/h, in Z direction: 4,89 mm at 2 km/h resp. 17,8 mm at 6 km/h. For males, these values are: in Y direction: 10,6 mm at 6 km/h resp. 23,43 mm at 2 km/h and in Z: 5,08 mm at 2 km/h resp. 18,71 mm at 6 km/h.

Table 3- 7 Thoracic rotations and translations (males)

		Speed	2 km/h	2,5 km/h	3 km/h	3,5 km/h	4 km/h	4,5 km/h	5 km/h	5,5 km/h	6 km/h
Thoracic rotations and translations (males)	Asc. Profile	Alpha [°]	1,55	1,28	1,15	1,02	1,05	1,05	1,15	1,17	1,25
		Std. deviation	1,00	0,84	0,70	0,68	0,54	0,57	0,69	0,66	0,62
		n	51	50	48	51	50	52	51	52	52
	Desc. Profile	Alpha [°]	1,96	1,55	1,38	1,15	0,97	1,13	1,16	1,18	1,22
		Std. deviation	1,28	0,90	0,89	0,67	0,49	0,57	0,66	0,60	0,50
		n	52	54	53	53	52	49	51	53	50
	Asc. Profile	Beta [°]	0,90	0,93	0,87	0,82	0,81	0,76	0,77	0,75	0,85
		Std. deviation	0,36	0,37	0,28	0,27	0,29	0,25	0,26	0,25	0,36
		n	51	50	48	51	49	52	51	52	52
	Desc. Profile	Beta [°]	0,91	1,00	1,03	0,87	0,86	0,87	0,75	0,79	0,74
		Std. deviation	0,24	0,27	0,51	0,29	0,26	0,32	0,22	0,26	0,26
		n	52	54	53	53	52	49	51	53	50
	Asc. Profile	Gamma [°]	3,61	3,20	3,13	2,84	2,57	2,58	2,48	2,55	2,52
		Std. deviation	1,68	1,54	1,40	1,34	1,13	1,09	1,19	1,16	1,30
		n	51	50	48	51	50	52	51	52	52
	Desc. Profile	Gamma [°]	3,92	3,41	3,24	2,88	2,49	2,44	2,37	2,33	2,45
		Std. deviation	1,74	1,55	1,49	1,14	1,01	1,14	1,03	1,20	1,15
		n	51	54	53	53	52	49	51	53	50
	Asc. Profile	X [mm]	5,90	5,31	5,03	5,42	5,50	5,90	6,33	6,55	6,62
		Std. deviation	2,27	1,82	1,95	1,78	1,59	1,74	2,20	1,93	2,02
		n	51	50	48	51	51	52	51	52	52
	Desc. Profile	X [mm]	7,86	7,46	6,47	6,52	6,16	6,34	6,36	6,72	6,50
		Std. deviation	2,54	2,67	2,19	2,32	1,66	2,00	2,01	2,07	1,91
		n	52	54	53	53	52	49	51	53	50
	Asc. Profile	Y [mm]	21,46	17,50	14,67	13,29	12,86	12,42	11,50	10,92	10,59
		Std. deviation	7,68	6,06	4,35	4,36	3,61	3,46	3,34	3,18	3,01
		n	50	50	48	51	51	52	51	52	52
	Desc. Profile	Y [mm]	23,43	18,47	15,33	14,09	12,75	12,07	12,03	11,07	10,69
		Std. deviation	7,02	5,81	5,08	4,39	3,57	3,63	3,58	3,53	2,73
		n	51	53	53	53	52	49	51	53	50
	Asc. Profile	Z [mm]	5,09	6,41	8,15	9,54	11,13	13,23	15,43	17,11	18,59
		Std. deviation	1,68	2,03	2,63	2,32	2,99	2,95	3,98	3,54	4,43
		n	51	50	48	51	51	52	51	52	52
	Desc. Profile	Z [mm]	6,09	7,77	8,93	10,81	12,42	14,72	15,82	18,09	18,72
		Std. deviation	1,81	2,19	2,32	2,93	3,17	4,10	4,01	4,12	4,34
		n	52	54	53	53	52	49	51	53	50

In tables 3-7 and 3-8, the values of the means and the standard deviations of the thoracic rotations and translation for each speed are shown, in addition to the amount of data used to calculate them.

Table 3- 8 Thoracic rotations and translations (females)

		Speed	2 km/h	2,5 km/h	3 km/h	3,5 km/h	4 km/h	4,5 km/h	5 km/h	5,5 km/h	6 km/h
Thoracic rotations and translations (females)	Asc. Profile	Alpha [°]	1,36	1,20	1,05	0,96	0,97	1,13	1,25	1,10	1,24
		Std. deviation	1,15	1,08	0,69	0,57	0,58	1,05	1,30	0,53	0,70
		n	49	47	48	49	49	49	47	48	48
	Desc. Profile	Alpha [°]	1,47	1,36	1,14	0,95	0,90	1,11	1,01	1,11	1,17
		Std. deviation	0,85	0,82	0,68	0,43	0,59	1,25	0,47	0,57	0,63
		n	49	48	47	48	49	49	47	45	48
	Asc. Profile	Beta [°]	1,17	1,05	1,03	1,11	1,09	1,07	1,02	0,93	1,02
		Std. deviation	0,66	0,41	0,33	0,49	0,47	0,60	0,39	0,34	0,38
		n	49	47	48	49	49	49	46	48	48
	Desc. Profile	Beta [°]	1,32	1,30	1,56	1,20	1,12	1,05	1,04	0,96	1,15
		Std. deviation	0,44	0,45	1,00	0,39	0,39	0,35	0,57	0,34	1,03
		n	49	48	48	48	49	49	47	45	48
	Asc. Profile	Gamma [°]	3,21	2,90	2,70	2,48	2,46	2,41	2,57	2,47	2,49
		Std. deviation	1,93	1,98	1,87	1,65	1,67	1,54	1,75	1,47	1,57
		n	48	47	48	48	49	48	47	48	48
	Desc. Profile	Gamma [°]	3,45	3,43	2,86	2,26	2,23	2,39	2,32	2,22	2,67
		Std. deviation	2,03	2,22	1,74	1,39	1,56	1,58	1,30	1,41	1,55
		n	49	47	47	47	49	48	47	44	48
	Asc. Profile	X [mm]	5,97	5,37	5,08	5,71	5,84	5,93	6,58	6,37	6,94
		Std. deviation	2,17	2,06	1,93	1,85	1,96	1,89	2,11	1,95	2,34
		n	49	47	48	49	49	49	48	48	48
	Desc. Profile	X [mm]	8,39	7,63	7,19	6,72	6,64	6,80	7,11	7,06	7,23
		Std. deviation	2,68	2,46	2,07	1,83	1,53	1,82	1,89	2,28	2,40
		n	49	48	48	48	49	49	47	45	48
	Asc. Profile	Y [mm]	16,79	13,70	11,02	10,05	9,28	9,38	8,26	8,45	8,74
		Std. deviation	6,33	5,25	4,26	4,06	3,60	3,61	3,63	3,25	3,13
		n	49	47	48	49	49	49	48	48	48
	Desc. Profile	Y [mm]	18,52	14,58	11,41	10,89	9,27	9,71	8,58	8,57	8,67
		Std. deviation	6,76	5,19	4,60	4,14	3,34	3,37	2,68	3,22	3,26
		n	49	48	48	48	49	49	47	45	48
	Asc. Profile	Z [mm]	4,89	6,34	7,29	9,71	11,15	12,34	14,56	15,24	17,42
		Std. deviation	1,50	2,02	2,16	2,52	3,06	3,45	4,24	4,07	5,15
		n	49	47	48	49	49	49	48	48	48
	Desc. Profile	Z [mm]	5,79	7,45	9,11	10,43	12,06	14,07	15,65	16,65	17,84
		Std. deviation	1,57	1,74	1,90	2,24	2,51	3,48	3,50	4,07	5,50
		n	49	48	48	48	49	49	47	45	48

Frequencies

Figs. 3-13 to 3-15 introduce the frequency means and the standard deviations of the oscillations' principal mode of the thoracic rotations and translations of male and female volunteers, related to velocity.

Fig. 3-13 shows that the frequencies of the lateral tilt α (in males and females) as well as those of the frontal tilt β (in males and females) increase with the increment of the velocity.

Minimal and maximal frequency values of the lateral tilt α are: 0,66 Hz at 2 km/h resp. 1,11 Hz at 6 km/h (females) and 0,63 Hz at 2 km/h resp. 1,15 Hz at 6 km/h (males)

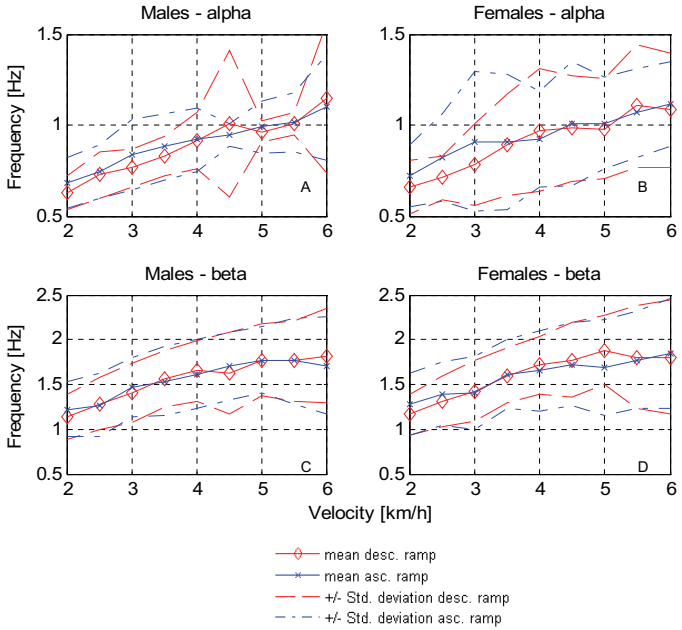

Figure 3- 13 Frequencies of the oscillations' principal mode of the frontal tilt (bottom left and right) and the lateral tilt (upper left and right) of the thorax of males and females volunteers, related to velocity.

Minimal and maximal frequency values of the frontal tilt β are: 1,16 Hz at 2 km/h resp. 1,84 Hz at 6 km/h (females) and 1,22 Hz at 2 km/h resp. 1,82 Hz at 6 km/h (males).

In figs. 3-14 (A and B), the frequencies of the thoracic axial rotation γ of males and females, related to velocity, are shown. Figures 3-14 (C and D) show the frequencies of the translation in the sagittal axis (X) of the thorax of males and females, related to velocity.

In figs. 3-14 (A and B) can be seen, that not only the frequencies of the axial rotation γ but also the translation in X direction grow with the increment of the velocity in both men and women.

Minimal and maximal frequency values of the axial rotation γ of the thorax are:

0,63 Hz at 2 km/h resp. 1,05 Hz at 6 km/h (females) and 0,61 Hz at 2 km/h resp. 1,05 Hz at 6 km/h (males).

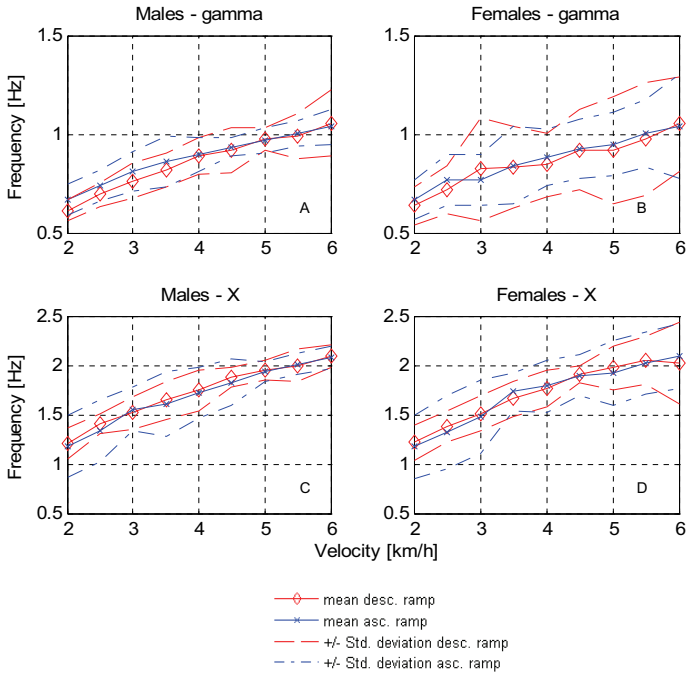

Figure 3- 14 Frequencies of the oscillations' principal mode of the thoracic axial rotations (upper left and right) and translations in the sagittal axis (bottom left and right) of males and females volunteers, related to velocity.

Minimal and maximal frequency values of the translation in X direction of the thorax are: 1,17 Hz at 2 km/h resp. 2,09 Hz at 6 km/h (in both males and females).

In figures 3-15 (A and B), the frequencies of the translations in the transverse axis (Y) of males and females, related to velocity, are shown. Figures 3-15 (C and D) show the frequencies of the translations in the longitudinal axis (Z) of the thorax of males and females, related to velocity.

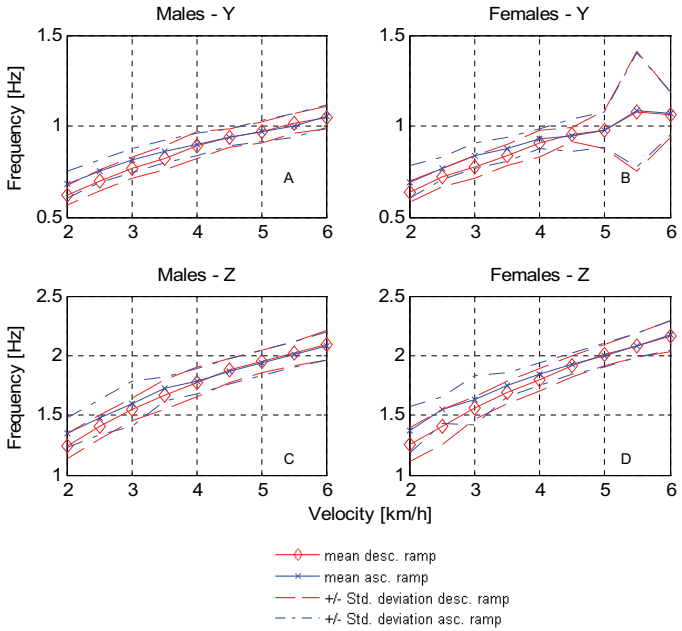

Figure 3- 15 Frequency oscillations' principal mode of the thoracic translation in the transverse (upper left and right) and in the longitudinal axis (bottom left and right) of males and females volunteers, related to velocity.

Males and females show a linear increment of the frequency in both Y and Z translations, related to speed. Only the females in their transversal translation Y and during speed interval 5,5 km/h - 6 km/h show a different behaviour (fig. 3-15 B). In this interval a decrement of the frequency is observed as speed increments.

Minimal and maximal frequency values of the translation of the thorax in Y direction are: 0,636 Hz at 2 km/h resp. 1,09 Hz at 5,5 km/h (females) and 0,622 Hz at 2 km/h resp. 1,05 Hz at 6 km/h (males).

Minimal and maximal frequency values of the translation of the thorax in Z direction are: 1,25 Hz at 2 km/h resp. 2,17 Hz at 6 km/h (females) and 1,24 Hz at 2 km/h resp. 2,09 Hz at 6 km/h (males).

In tables 3-9 and 3-10, the values of the means and the standard deviations of the different thoracic frequencies for each speed are shown, in addition to the amount of data used to calculate them.

Table 3- 9 Frequencies of thoracic rotations and translations (males)

		Speed	2 km/h	2,5 km/h	3 km/h	3,5 km/h	4 km/h	4,5 km/h	5 km/h	5,5 km/h	6 km/h
Frequencies of thoracic rotations and translations (males)	Asc. Profile	Alpha [Hz]	0,68	0,74	0,84	0,88	0,92	0,95	0,99	1,01	1,10
		Std. deviation	0,14	0,15	0,20	0,18	0,18	0,06	0,15	0,16	0,29
		n	52	51	49	51	51	52	51	52	52
	Desc. Profile	Alpha [Hz]	0,63	0,72	0,77	0,83	0,91	1,01	0,97	1,01	1,15
		Std. deviation	0,09	0,12	0,10	0,11	0,15	0,41	0,06	0,06	0,41
		n	52	54	53	53	52	49	51	53	50
	Asc. Profile	Beta [Hz]	1,22	1,27	1,47	1,53	1,62	1,71	1,78	1,76	1,71
		Std. deviation	0,30	0,35	0,34	0,39	0,38	0,38	0,38	0,48	0,54
		n	52	51	49	51	51	52	51	52	52
	Desc. Profile	Beta [Hz]	1,13	1,28	1,40	1,56	1,65	1,62	1,77	1,76	1,82
		Std. deviation	0,25	0,29	0,33	0,31	0,34	0,46	0,40	0,45	0,53
		n	52	54	53	53	52	49	51	53	50
	Asc. Profile	Gamma [Hz]	0,67	0,74	0,81	0,86	0,90	0,94	0,97	1,00	1,04
		Std. deviation	0,08	0,08	0,10	0,13	0,08	0,05	0,06	0,06	0,09
		n	52	51	49	51	51	52	51	52	52
	Desc. Profile	Gamma [Hz]	0,61	0,69	0,76	0,82	0,89	0,92	0,97	0,99	1,06
		Std. deviation	0,05	0,06	0,09	0,08	0,09	0,11	0,06	0,12	0,17
		n	52	54	53	53	52	49	51	53	50
	Asc. Profile	X [Hz]	1,18	1,34	1,55	1,61	1,72	1,83	1,94	2,01	2,08
		Std. deviation	0,31	0,31	0,22	0,32	0,26	0,24	0,10	0,11	0,12
		n	52	51	49	51	51	52	51	52	52
	Desc. Profile	X [Hz]	1,21	1,40	1,52	1,65	1,75	1,88	1,95	2,00	2,09
		Std. deviation	0,16	0,10	0,17	0,19	0,21	0,10	0,10	0,17	0,12
		n	52	54	53	53	52	49	51	53	50
	Asc. Profile	Y [Hz]	0,68	0,75	0,81	0,86	0,90	0,94	0,97	1,00	1,05
		Std. deviation	0,07	0,06	0,07	0,06	0,06	0,05	0,06	0,06	0,06
		n	52	51	49	51	51	52	51	52	52
	Desc. Profile	Y [Hz]	0,62	0,70	0,77	0,82	0,89	0,94	0,97	1,02	1,05
		Std. deviation	0,05	0,06	0,06	0,06	0,07	0,05	0,06	0,05	0,06
		n	52	54	53	53	52	49	51	53	50
	Asc. Profile	Z [Hz]	1,35	1,48	1,59	1,72	1,79	1,87	1,94	2,01	2,08
		Std. deviation	0,13	0,14	0,19	0,10	0,10	0,10	0,10	0,11	0,12
		n	52	51	49	51	51	52	51	52	52
	Desc. Profile	Z [Hz]	1,24	1,40	1,55	1,67	1,78	1,88	1,95	2,02	2,09
		Std. deviation	0,11	0,10	0,09	0,12	0,13	0,10	0,10	0,10	0,12
		n	52	54	53	53	52	49	51	53	50

Table 3- 10 Frequencies of thoracic rotations and translations (females)

Frequencies of thoracic rotations and translations (females)		Speed	2 km/h	2,5 km/h	3 km/h	3,5 km/h	4 km/h	4,5 km/h	5 km/h	5,5 km/h	6 km/h
	Asc. Profile	Alpha [Hz]	0,72	0,82	0,91	0,91	0,92	1,00	1,01	1,07	1,12
		Std. deviation	0,17	0,24	0,38	0,37	0,27	0,34	0,25	0,24	0,23
		n	49	47	48	49	49	49	48	48	48
	Desc. Profile	Alpha [Hz]	0,66	0,71	0,78	0,89	0,97	0,98	0,98	1,11	1,08
		Std. deviation	0,15	0,12	0,22	0,28	0,34	0,29	0,27	0,34	0,32
		n	49	48	48	48	49	49	47	45	48
	Asc. Profile	Beta [Hz]	1,28	1,40	1,41	1,62	1,65	1,72	1,69	1,77	1,84
		Std. deviation	0,34	0,36	0,41	0,39	0,45	0,46	0,54	0,55	0,61
		n	49	47	48	49	49	49	48	48	48
	Desc. Profile	Beta [Hz]	1,16	1,31	1,43	1,60	1,72	1,77	1,88	1,80	1,81
		Std. deviation	0,23	0,29	0,34	0,31	0,32	0,42	0,39	0,57	0,64
		n	49	48	48	48	49	49	47	45	48
	Asc. Profile	Gamma [Hz]	0,67	0,77	0,77	0,84	0,88	0,92	0,95	1,00	1,04
		Std. deviation	0,10	0,13	0,13	0,20	0,14	0,15	0,16	0,17	0,26
		n	49	47	48	49	49	49	48	48	48
	Desc. Profile	Gamma [Hz]	0,64	0,72	0,82	0,83	0,84	0,92	0,92	0,98	1,05
		Std. deviation	0,10	0,12	0,26	0,21	0,16	0,20	0,27	0,29	0,24
		n	49	48	48	48	49	49	47	45	48
	Asc. Profile	X [Hz]	1,17	1,32	1,47	1,73	1,79	1,90	1,92	2,02	2,09
		Std. deviation	0,32	0,37	0,37	0,20	0,27	0,21	0,32	0,32	0,32
		n	49	47	48	49	49	49	48	48	48
	Desc. Profile	X [Hz]	1,22	1,38	1,51	1,66	1,77	1,91	1,97	2,04	2,02
		Std. deviation	0,18	0,16	0,18	0,18	0,19	0,09	0,22	0,24	0,41
		n	49	48	48	48	49	49	47	45	48
	Asc. Profile	Y [Hz]	0,69	0,77	0,84	0,87	0,93	0,95	0,98	1,09	1,07
		Std. deviation	0,09	0,06	0,07	0,06	0,05	0,09	0,10	0,32	0,12
		n	49	47	48	49	49	49	48	48	48
	Desc. Profile	Y [Hz]	0,64	0,72	0,78	0,84	0,90	0,95	0,98	1,08	1,06
		Std. deviation	0,06	0,05	0,06	0,06	0,07	0,04	0,11	0,33	0,12
		n	49	48	48	48	49	49	47	45	48
	Asc. Profile	Z [Hz]	1,38	1,54	1,63	1,76	1,85	1,93	2,00	2,08	2,17
		Std. deviation	0,20	0,12	0,20	0,10	0,09	0,09	0,10	0,10	0,13
		n	49	47	48	49	49	49	48	48	48
	Desc. Profile	Z [Hz]	1,25	1,40	1,56	1,69	1,80	1,91	2,00	2,09	2,16
		Std. deviation	0,14	0,14	0,10	0,09	0,09	0,09	0,09	0,10	0,13
		n	49	48	48	48	49	49	47	45	48

Phases

Figs. 3-16 to 3-18 present the means and the std. deviations of the phase shift angles between the thoracic rotations and translations of male and female volunteers, related to velocity.

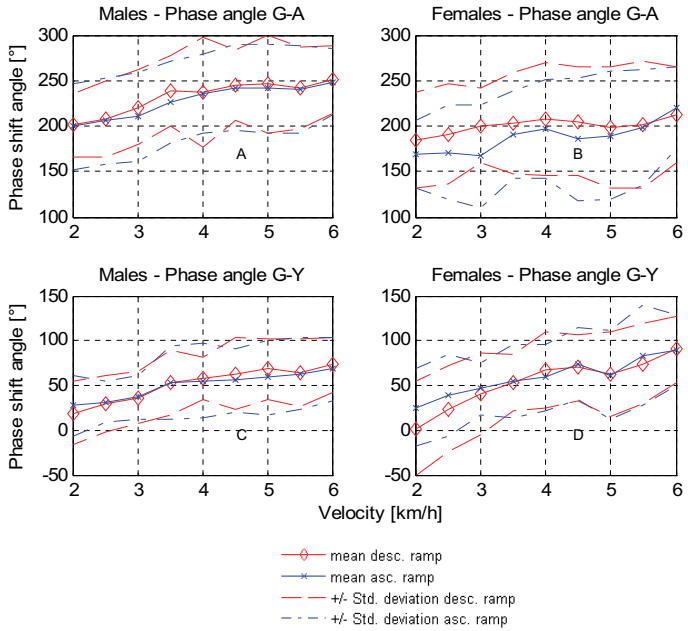

Figure 3- 16 Thoracic phase shift angle between the rotations around longitudinal and sagittal axis (Upper left and right) and pelvic phase shift angle between axial rotations and translations in the transverse axe (Bottom left and right).

Figure 3-16 (upper) shows the means and the std. deviations of the phase shift angles between thoracic axial rotation γ (as base) and thoracic lateral tilt α of males and females, related to velocity. Bottom shows the means and the std. deviations of the phase shift angles between thoracic axial rotation γ (as base) and the translation of the thorax in Y direction of males and females, related to velocity.

Phase shift angle γ–α of males (fig. 3-16 A) grows up to 4,5 km/h and then remains without significant variations. Females (fig. 3-16 B) show different curve shapes in ascending and descending ramps, but the tendency is the same. Up to 4 km/h it grows, after that remains, like in the male's case, without significant variations. On the other hand, phase shift angle γ–Y show for males and females a linear increment with the increment of the speed (fig. 3-16 C-D).

Minimal and maximal values of phase γ-α obtained for female volunteers, are: ascending ramp (168,35° at 2 km/h resp. 220,55° at 6 km/h); descending ramp (184,34° at 2 km/h respectively 212,64° at 6 km/h).

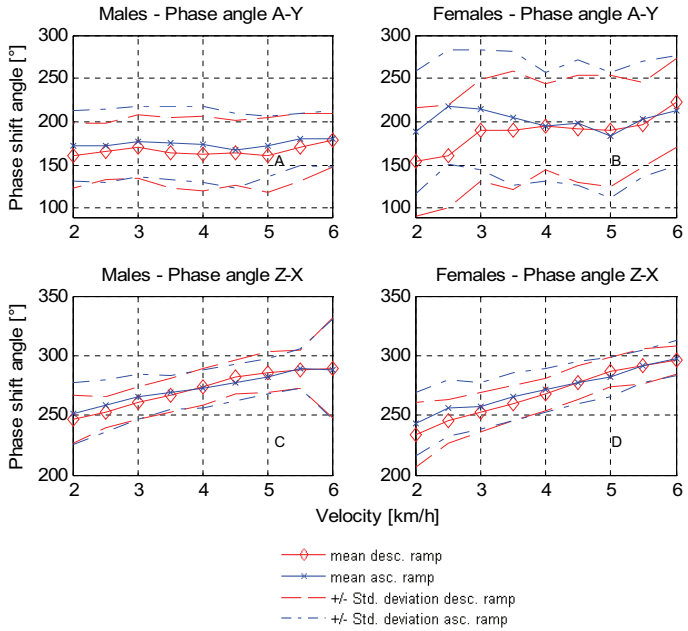

Figure 3- 17 Thoracic phase shift angles, between the rotations around the sagittal axis and the translations in Y direction, related to speed (Upper left and right). (Bottom left and right) thoracic phase shift angle between (Z) translations and (X) translations, related to speed.

Minimal and maximal values of phase γ-α obtained for male volunteers, are: 199,76° at 2 km/h resp. 250,9° at 6 km/h.

Minimal and maximal values of phase γ-Y are: 1,74° at 2 km/h resp. 90,61° at 6 km/h (females) and 18,7° at 2 km/h resp. 72,87° at 6 km/h (males).

Figure 3-17 (A & B) show the means and the std. deviations of the phase shift angles between thoracic lateral tilt α (as base) and thoracic translation in Y direction of males and females, related to velocity. Bottom (C & D) show the means and the std. deviations of the phase shift angles between thoracic translation in Z direction (as base) and the translation of the thorax in X direction for males and females, related to velocity.

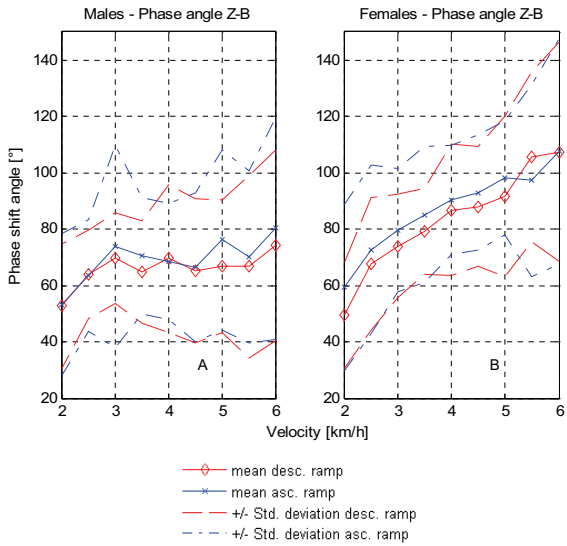

Figure 3- 18 Phase shift angles between thoracic translations in the longitudinal axis Z and thoracic frontal tilt β, related to speed.

Phase shift angle α–Y of males (fig. 3-17 A) is not related to velocity. Its values oscillated between 160° and 180°. Females (fig. 3-17 B) start whit an ascending slope until 3 km/h, then it remains constant up to 5 km/h. From this point it is again ascending. On the other hand, phase shift angle Z-X shows for males and females a linear increment with the increment of the speed (fig. 3-17 C-D).

Minimal and maximal values of phase α–Y obtained for female volunteers, are: 153,52° at 2 km/h resp. 222,07° at 6 km/h.

Minimal and maximal values of phase Z-X are: 233,56° at 2 km/h resp. 297,82° at 6 km/h (females) and 246,52° at 2 km/h resp. 289,52° at 6 km/h (males).

Figure 3-18 shows the mean and the standard deviation of the phase shift angles between the longitudinal translations Z of the thorax (as base) and thoracic frontal tilt β, of males and females, related to velocity. Women increment the angle of phase Z - β, when they increase the velocity. Men start with an increment up to 3 km/h, and then until 5,5 km/h a plateau can be observed. After that it tends to grow again.

Minimal and maximal values of phase Z- β are: 49,45° at 2 km/h resp. 107,8° at 6 km/h (females) and 52,65° at 2 km/h resp. 80,26° at 6 km/h (males).

In tables 3-11 and 3-12, the values of the means and the standard deviations of the phases between rotations and translation for each speed are shown, in addition to the amount of data used to calculate them.

Table 3- 11 Phase shift angles between thoracic rotations and translations (males)

		Speed	2 km/h	2,5 km/h	3 km/h	3,5 km/h	4 km/h	4,5 km/h	5 km/h	5,5 km/h	6 km/h
Phases between thoracic rotations and translations (males)	Asc. Profile	φ(γ–α) [°]	199,76	205,84	210,59	226,53	235,74	242,13	241,24	239,89	248,36
		Std. deviation	47,23	46,97	48,75	45,43	43,73	47,09	48,62	47,83	36,18
		n	47	44	43	46	48	47	45	47	47
	Desc. Profile	φ(γ–α) [°]	201,17	207,65	220,39	238,28	237,33	245,17	246,28	242,14	250,86
		Std. deviation	34,71	42,51	41,22	38,59	60,29	39,04	54,37	45,04	37,09
		n	49	49	46	48	48	38	45	43	46
	Asc. Profile	φ(γ–Y) [°]	27,42	31,74	36,85	52,44	55,14	55,78	58,75	63,30	68,66
		Std. deviation	33,42	23,45	24,29	41,02	42,00	35,33	42,00	40,67	35,42
		n	49	48	45	46	47	51	49	52	49
	Desc. Profile	φ(γ–Y) [°]	18,70	29,08	36,32	53,34	57,48	63,17	68,77	63,93	72,87
		Std. deviation	35,46	31,71	28,80	36,73	23,99	39,64	33,91	37,67	30,96
		n	47	50	46	49	47	42	48	46	48
	Asc. Profile	φ(α–Y) [°]	172,21	172,06	177,44	175,13	174,34	166,58	171,70	179,66	180,41
		Std. deviation	39,89	41,70	40,88	42,39	44,12	43,67	34,73	29,95	32,51
		n	48	42	43	45	46	48	47	47	46
	Desc. Profile	φ(α–Y) [°]	160,53	165,39	170,94	164,59	163,22	164,52	161,54	170,79	178,85
		Std. deviation	37,92	32,14	36,34	40,67	42,38	37,55	43,26	39,33	30,84
		n	46	48	46	48	49	41	48	45	46
	Asc. Profile	φ(Z-X) [°]	251,37	258,18	265,34	269,11	272,09	277,35	282,63	289,50	288,52
		Std. deviation	26,51	21,72	19,21	13,67	16,07	15,01	15,10	16,35	42,13
		n	39	41	45	46	47	49	51	52	51
	Desc. Profile	φ(Z–X) [°]	246,67	252,52	260,47	266,65	274,09	282,03	286,02	288,54	289,52
		Std. deviation	19,68	12,69	13,61	13,92	15,04	13,69	17,15	15,53	42,07
		n	46	52	49	51	50	49	50	52	49
	Asc. Profile	φ(Z–β) [°]	53,27	63,62	73,91	70,59	68,62	66,54	76,20	70,05	80,27
		Std. deviation	25,28	19,71	35,82	20,65	20,60	26,40	32,00	30,61	39,34
		n	41	35	41	40	39	44	43	40	35
	Desc. Profile	φ(Z–β) [°]	52,65	64,06	69,74	64,86	69,66	65,32	66,81	66,69	74,28
		Std. deviation	21,96	15,77	16,22	18,19	26,14	25,55	23,46	32,41	33,83
		n	42	44	41	46	43	37	39	40	35

Table 3- 12 Phase shift angles between thoracic rotations and translations (females)

		Speed	2 km/h	2,5 km/h	3 km/h	3,5 km/h	4 km/h	4,5 km/h	5 km/h	5,5 km/h	6 km/h
Phases between thoracic rotations and translations (females)	Asc. Profile	φ(γ–α) [°]	168,35	171,22	166,77	190,92	197,61	185,72	189,36	198,25	220,55
		Std. deviation	37,15	52,12	56,90	47,56	54,20	67,16	70,57	63,59	44,83
		n	38	35	29	30	36	39	34	40	37
	Desc. Profile	φ(γ–α) [°]	184,34	191,02	200,62	202,42	208,15	205,37	199,05	201,52	212,64
		Std. deviation	52,34	55,26	40,50	55,87	62,02	59,02	66,56	70,11	52,80
		n	42	38	37	32	31	35	33	28	37
	Asc. Profile	φ(γ–Y) [°]	24,95	38,74	46,09	55,14	58,90	73,91	61,60	83,54	89,13
		Std. deviation	43,27	45,52	29,08	40,90	37,41	40,09	49,20	55,57	39,91
		n	40	41	36	34	40	41	36	37	37
	Desc. Profile	φ(γ–Y) [°]	1,75	23,70	40,21	53,38	67,50	69,88	62,49	74,11	90,62
		Std. deviation	53,29	47,84	45,25	31,74	41,96	37,01	47,15	45,26	36,89
		n	41	43	38	37	37	42	31	29	40
	Asc. Profile	φ(α–Y) [°]	188,13	217,35	213,93	203,96	194,35	198,98	184,38	202,99	212,98
		Std. deviation	70,98	66,35	69,18	77,50	62,88	72,03	71,88	67,24	63,69
		n	36	35	38	30	35	39	37	38	43
	Desc. Profile	φ(α–Y) [°]	153,52	160,34	189,76	190,00	194,20	191,42	189,43	196,90	222,07
		Std. deviation	62,24	59,47	58,52	68,49	50,04	61,70	64,03	49,34	50,99
		n	36	40	35	35	29	37	32	31	35
	Asc. Profile	φ(Z-X) [°]	242,57	256,46	257,74	265,47	271,04	277,29	281,98	291,05	297,82
		Std. deviation	27,02	23,44	19,55	20,52	18,20	17,67	16,13	13,34	14,94
		n	35	35	38	47	47	47	45	45	46
	Desc. Profile	φ(Z–X) [°]	233,56	244,98	252,69	259,95	267,53	277,43	286,29	290,95	296,06
		Std. deviation	27,48	17,93	16,72	14,50	13,62	14,50	12,18	14,41	11,78
		n	47	40	45	45	46	48	44	43	44
	Asc. Profile	φ(Z–β) [°]	59,28	72,78	79,60	85,17	90,44	92,95	98,12	97,20	107,80
		Std. deviation	29,56	29,86	21,77	24,27	19,37	20,34	20,31	34,22	40,13
		n	39	39	33	41	38	40	35	36	37
	Desc. Profile	φ(Z–β) [°]	49,45	67,75	74,04	79,30	86,84	87,97	91,63	105,51	107,49
		Std. deviation	18,81	23,46	18,27	15,32	23,25	21,34	28,32	30,16	38,92
		n	42	40	39	41	42	42	39	33	36

3.1.3 Head

Rotations and translations

Figs. 3-19 to 3-21 show the means and the std. deviations of head's rotations and translations of males and females. All values in both ascending and descending profiles, related to velocity, are shown.

Figs. 3-19 A and B display the amplitudes of the lateral tilt motion α of the head of males respectively females volunteers, related to velocity. In figs. 3-19 C and D, the amplitudes of the frontal tilt motion β of the head of males respectively females volunteers are presented.

Amplitudes of head's lateral tilt α of males and females start with a descending slope. In male volunteers it remains until 4 km/h is reached, then means oscillate about 0,7°. Woman show similar but little more unstable paths, because the different speed in the minimal values for ascending and descending ramps.

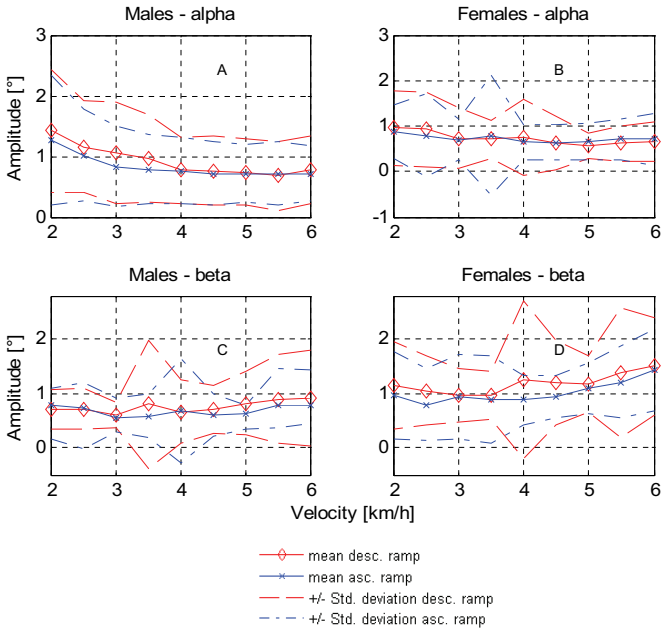

Figure 3- 19 Lateral tilt (A & B) and frontal tilt (C & D) of the head of males and females volunteers, related to velocity.

No significant interdependencies between speed and frontal tilt β of the head of males can be observed (fig. 3-19 C). Amplitudes oscillate between 0,66° and 0,92°. Women show first after 3,5 km/h (descending ramp) and 4km/h (ascending ramp) dependencies on velocity. Minimal and maximal calculated values of head's frontal tilt β of female volunteers during gait are: 0,79° at 2,5 km/h resp. 1,5° at 6 km/h.

Figures 3-20 A and B show the amplitudes of head's axial rotation γ of male resp. female volunteers, related to velocity. In figures 3-20 C and D, amplitudes of the head's translations in the sagittal axis of male resp. female volunteers, related to velocity are shown.

Head's axial rotation γ (fig. 3-20 A and B), in both males and females, diminish with increment of the velocity. In females' case, γ has its minima not at 6 km/h but at 4,5 km/h and 5km/h for ascending resp. descending ramp.

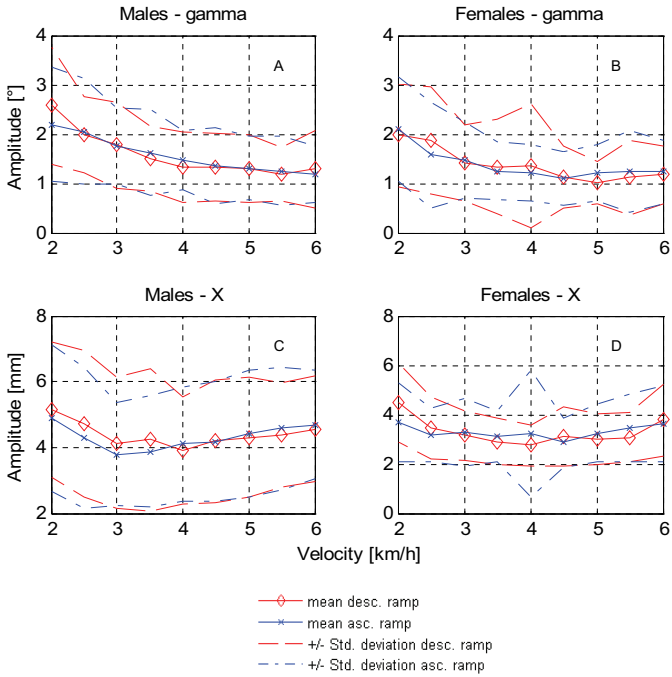

Figure 3- 20 Head axial rotations (A & B) and translations in the sagittal axis (C & D) of male and female volunteers, related to velocity.

After these velocities γ tends to increase again.

Minimal and maximal values of head's axial rotation measured during gait are: 1° at 5 km/h resp. 2,1° at 2 km/h (females) and 1,17 ° at 6 km/h and 2,57° at 2 km/h (males).

Female and male volunteers show similar curve shapes for the head translations in the sagittal axis X (fig. 3-20 C and D). In all cases, the curves descend first up to an inflexion point, which occurs at different velocities for the ascending and descending profiles, and then ascend again. Maximal amplitudes have been reached always at slowest velocities.

Minimal and maximal values of head's translations in X direction measured during gait are: 2,76 mm at 4 km/h resp. 4,5 mm at 2 km/h (females) and 3,87 mm at 3,5 km/h resp. 5,15 at 2 km/h (males).

Figs. 3-21 A and B show the means and std. deviations of the translation amplitudes in the transverse axis Y of the head of male respectively female volunteers, related to velocity.

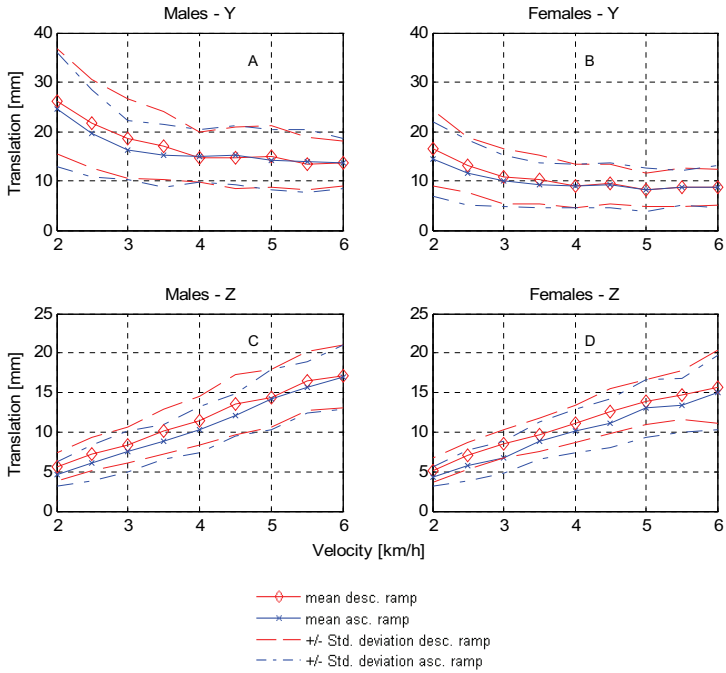

Figure 3- 21 Translations in the transverse axis (A & B) and translations in the longitudinal axis (C & D) of the head of male and female volunteers, related to velocity.

Figures 3-21 C and D introduce means and std. deviations of the amplitudes of head's translations in the longitudinal axis Z of male and female volunteers related to velocity.

The shape of the translation curves in Y and Z directions do not differ with those of pelvis and thorax.

In the head, like in pelvis and thorax's cases, translation amplitudes in the transverse axis Y (figure 3-21 A and B) show a descending slope related to velocity. The most important diminishment takes place until 4km/h, after that, the amplitude's means remain without significant variations.

Translations in the longitudinal axis Z (figure 3-21 C and D) show again almost a linear ascending slope, related to velocity.

Minimal and maximal amplitude values of head's translations in Y direction during gait are: 8,21 mm at 5 km/h respectively 16,6 mm at 2 km/h (females) and 13,5 mm at 5,5 km/h respectively 26,17 mm at 2 km/h (males).

Minimal and maximal amplitude values of head's translations in Z direction during gait are: 4,36 mm at 2 km/h and 15,71 mm at 6 km/h (females) and 4,65 mm at 2 km/h and 17,05 mm at 6 km/h (males).

Table 3- 13 Head's rotations and translations (males).

		Speed	2 km/h	2,5 km/h	3 km/h	3,5 km/h	4 km/h	4,5 km/h	5 km/h	5,5 km/h	6 km/h
Head's rotations and translations (males)	Asc. Profile	Alpha [°]	1,27	1,01	0,84	0,78	0,77	0,72	0,72	0,72	0,72
		Std. deviation	1,08	0,75	0,65	0,57	0,56	0,53	0,47	0,53	0,45
		n	52	51	48	51	51	51	50	52	51
	Desc. Profile	Alpha [°]	1,42	1,16	1,06	0,97	0,77	0,77	0,74	0,68	0,77
		Std. deviation	1,00	0,76	0,84	0,72	0,54	0,56	0,54	0,57	0,56
		n	52	54	52	53	52	49	50	53	50
	Asc. Profile	Beta [°]	0,80	0,73	0,54	0,59	0,67	0,61	0,63	0,78	0,78
		Std. deviation	0,65	0,74	0,25	0,41	0,96	0,38	0,29	0,42	0,32
		n	52	51	48	50	51	51	50	52	51
	Desc. Profile	Beta [°]	0,71	0,72	0,60	0,80	0,67	0,72	0,82	0,90	0,92
		Std. deviation	0,37	0,37	0,23	1,17	0,58	0,44	0,58	0,83	0,88
		n	52	54	52	53	52	49	50	53	50
	Asc. Profile	Gamma [°]	2,20	2,05	1,76	1,62	1,47	1,36	1,31	1,25	1,18
		Std. deviation	1,16	1,07	0,76	0,87	0,59	0,77	0,64	0,70	0,58
		n	51	50	48	50	50	50	50	52	51
	Desc. Profile	Gamma [°]	2,58	1,98	1,77	1,50	1,34	1,33	1,30	1,18	1,29
		Std. deviation	1,19	0,77	0,86	0,65	0,72	0,68	0,69	0,54	0,79
		n	52	54	51	52	52	49	50	51	50
	Asc. Profile	X [mm]	4,89	4,29	3,79	3,88	4,10	4,18	4,42	4,59	4,69
		Std. deviation	2,24	2,13	1,56	1,70	1,72	1,82	1,92	1,86	1,64
		n	52	51	49	51	51	52	51	52	52
	Desc. Profile	X [mm]	5,15	4,71	4,14	4,24	3,92	4,19	4,31	4,37	4,57
		Std. deviation	2,05	2,23	1,98	2,16	1,63	1,88	1,81	1,60	1,59
		n	52	54	53	53	52	49	51	53	50
	Asc. Profile	Y [mm]	24,49	19,65	16,21	15,09	15,04	15,11	14,28	13,92	13,53
		Std. deviation	11,56	8,88	6,00	6,38	5,26	6,01	6,09	6,35	5,17
		n	52	51	49	51	51	52	51	52	52
	Desc. Profile	Y [mm]	26,17	21,62	18,51	17,05	14,76	14,77	15,01	13,50	13,53
		Std. deviation	10,61	8,91	8,02	6,86	5,04	6,22	6,21	5,29	4,60
		n	52	54	53	53	52	49	51	53	50
	Asc. Profile	Z [mm]	4,65	6,04	7,54	8,78	10,33	12,15	14,13	15,69	16,96
		Std. deviation	1,56	2,30	2,54	2,21	2,88	2,70	3,75	3,27	4,07
		n	52	51	49	51	51	52	51	52	52
	Desc. Profile	Z [mm]	5,54	7,28	8,35	10,07	11,49	13,48	14,34	16,48	17,05
		Std. deviation	1,78	2,13	2,23	2,87	3,07	3,84	3,63	3,67	3,97
		n	52	54	53	53	52	49	51	53	50

Tables 3-13 and 3-14 introduce the complete information of head rotations and translations of males respectively females at each velocity.

Table 3- 14 Head's rotations and translations (females).

Head's rotations and translations (females)		Speed	2 km/h	2,5 km/h	3 km/h	3,5 km/h	4 km/h	4,5 km/h	5 km/h	5,5 km/h	6 km/h
	Asc. Profile	Alpha [°]	0,86	0,80	0,70	0,80	0,65	0,63	0,65	0,71	0,71
		Std. deviation	0,59	0,91	0,46	1,32	0,38	0,39	0,41	0,44	0,57
		n	49	47	48	49	48	49	48	48	48
	Desc. Profile	Alpha [°]	0,96	0,94	0,72	0,71	0,75	0,64	0,57	0,61	0,66
		Std. deviation	0,82	0,82	0,67	0,42	0,85	0,59	0,28	0,38	0,44
		n	49	48	48	48	49	49	47	45	48
	Asc. Profile	Beta [°]	0,98	0,80	0,94	0,88	0,89	0,94	1,10	1,21	1,44
		Std. deviation	0,81	0,66	0,78	0,81	0,45	0,40	0,47	0,66	0,75
		n	49	47	48	49	48	49	48	48	48
	Desc. Profile	Beta [°]	1,15	1,06	0,96	0,97	1,26	1,20	1,18	1,39	1,51
		Std. deviation	0,81	0,64	0,49	0,44	1,47	0,77	0,51	1,19	0,89
		n	49	48	48	48	49	49	47	45	48
	Asc. Profile	Gamma [°]	2,11	1,58	1,47	1,24	1,22	1,10	1,21	1,24	1,23
		Std. deviation	1,06	1,07	0,77	0,59	0,57	0,53	0,56	0,84	0,63
		n	49	47	48	48	48	49	48	48	48
	Desc. Profile	Gamma [°]	1,98	1,87	1,42	1,33	1,35	1,13	1,01	1,12	1,18
		Std. deviation	1,05	1,09	0,78	0,96	1,25	0,64	0,43	0,76	0,58
		n	48	47	48	48	49	49	47	45	48
	Asc. Profile	X [mm]	3,69	3,16	3,27	3,11	3,24	2,86	3,25	3,46	3,64
		Std. deviation	1,61	1,09	1,37	1,04	2,58	1,01	1,19	1,37	1,56
		n	49	47	48	49	49	49	48	48	48
	Desc. Profile	X [mm]	4,50	3,45	3,16	2,91	2,76	3,10	2,99	3,08	3,78
		Std. deviation	1,60	1,25	1,01	0,95	0,83	1,20	1,03	0,99	1,45
		n	49	48	48	48	49	49	47	45	48
	Asc. Profile	Y [mm]	14,50	11,68	9,95	9,16	8,96	9,10	8,21	8,61	8,81
		Std. deviation	7,54	6,62	5,13	4,60	4,33	4,51	4,41	3,57	4,28
		n	49	47	48	49	49	49	48	48	48
	Desc. Profile	Y [mm]	16,60	13,19	10,88	10,21	8,94	9,38	8,22	8,69	8,76
		Std. deviation	7,68	5,61	5,52	4,96	4,39	4,11	3,46	3,91	3,57
		n	49	48	48	48	49	49	47	45	48
	Asc. Profile	Z [mm]	4,36	5,73	6,78	8,90	10,18	11,15	12,99	13,40	14,94
		Std. deviation	1,18	1,98	2,02	2,38	2,78	3,04	3,68	3,39	4,71
		n	49	47	48	49	49	49	48	48	48
	Desc. Profile	Z [mm]	5,18	7,02	8,52	9,70	11,06	12,62	13,82	14,67	15,71
		Std. deviation	1,51	1,70	1,85	2,11	2,33	2,87	2,89	3,13	4,63
		n	49	48	48	48	49	49	47	45	48

Frequencies

Figs. 3-22 to 3-24 present the means and the standard deviations of the frequencies of the oscillations' principal mode of head's rotations and translations of male and female volunteers, related to velocity.

In figs. 3-24 (A,B,C,D) can be observed, that lateral tilt frequencies α as well as frontal tilt frequencies β of the head of males and females, will be increased with speed increments by normal gait. From fig. 3-24 can be seen, that while men show a virtually ascending slope from 2 km/h to 6km/h (figs. 3-24 A & C), women seem to reach the maximal frequency at slower speeds (4,5 km/h for α and 5 km/h for β)

Minimal and maximal values of head's lateral tilt frequencies of male and female volunteers during gait are: 0,657 Hz at 2 km/h resp. 1,28 Hz at 5,5 km/h (females) and 0,64 Hz at 2 km/h resp. 1,2 Hz at 5,5 km/h (males).

Minimal and maximal values of head's frontal tilt frequencies measured in male and female volunteers during gait, are: 0,99 Hz at 2 km/h resp. 1,71 Hz at 6 km/h (females) and 0,87 Hz at 2 km/h resp. 1,68 Hz at 6km/h (males).

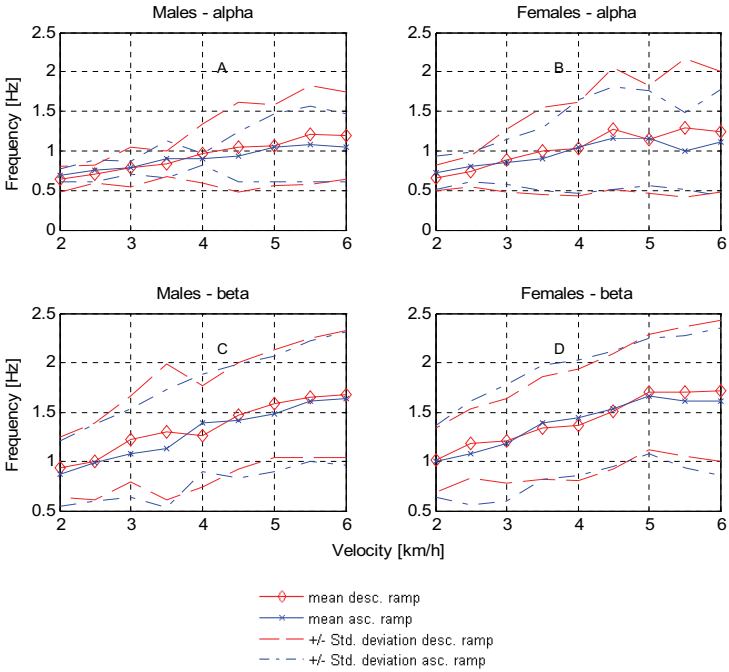

Figure 3- 22 Frequency of the oscillations' principal mode of lateral tilt (upper left and right) and frontal tilt (bottom left and right) of the head from males and females volunteers, related to the velocity.

In figures (3-23 A and B), frequencies of axial rotation γ of the head of males and females, related to velocity are shown. Figures (3-23 C and D) show the frequencies of the head's translations in the sagittal axis X of males and females, related to velocity.

In fig (3-23 A and B) are shown, that the frequencies of the head's axial rotation γ grow with the increment of the speed in both men and women.

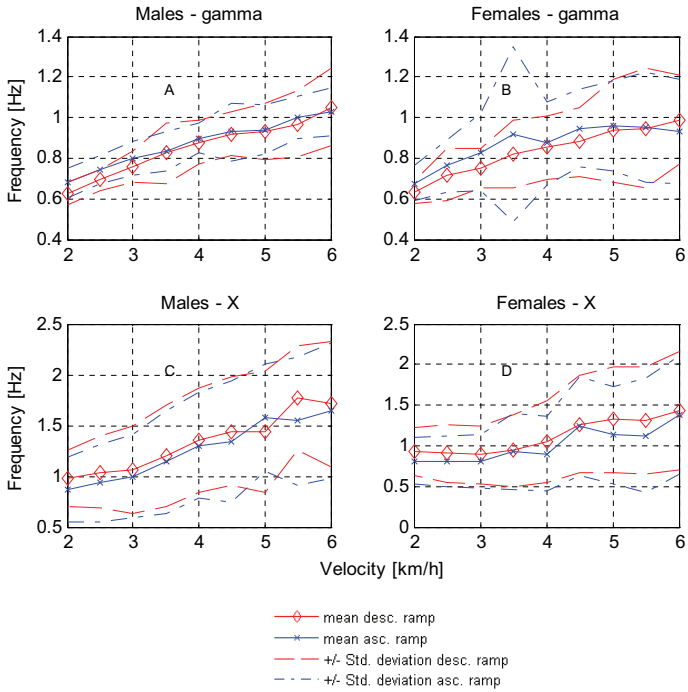

Figure 3- 23 Frequencies of the oscillations' principal mode of axial rotations (upper left and right) and sagittal translations (bottom left and right) of the head of males and females volunteers, related to velocity.

Frequencies of head translations in X direction from males show linear dependencies on the speed (fig. 3-23 C). Although females show an ascending tendency for their translations in X related to speed (fig. 3-23 D), it is not too linear like in men's case.

Minimal and maximal frequency values of head's axial rotation γ of are: 0,63 Hz at 2 km/h resp. 0,988 Hz at 6 km/h (females) and 0,62 Hz at 2 km/h resp. 1,05 Hz at 6 km/h (males).

Minimal and maximal frequency values of head translations in X direction are: 0,81 Hz at 2 km/h resp. 1,42 Hz at 6 km/h (females) and 0,86 Hz at 2 km/h resp. 1,77 Hz at 6 km/h (males).

In figs. 3-24 (A and B), frequencies of translations in the transverse axis Y of males and females related to velocity, are shown. Figs. 3-24 (C and D) display the frequencies of translation in the longitudinal axis Z of the head of males and females,

related to velocity. Males and females show not only a linear increment of head frequencies in transverse translations Y, related to speed but also a very small std. deviation.

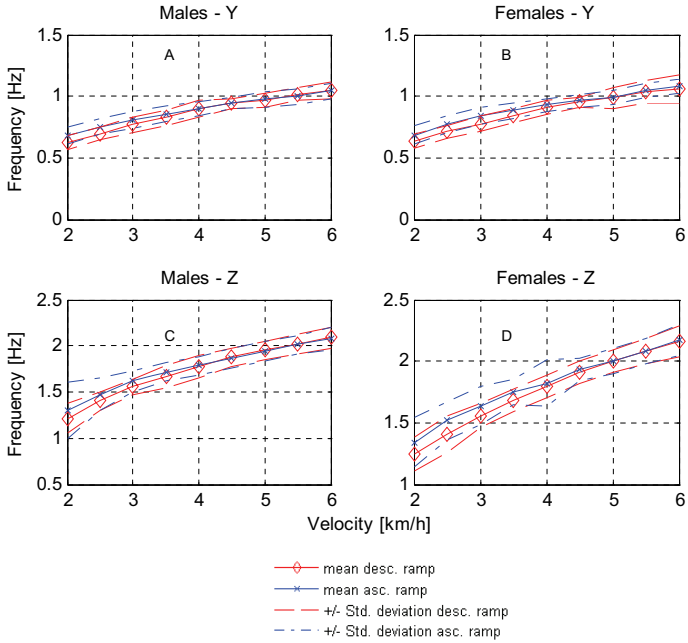

Figure 3- 24 Frequencies of the oscillations' principal mode of head transverse translations (upper left and right) and the longitudinal translations (bottom left and right) of males and females volunteers, related to velocity.

The frequencies of the longitudinal translations of the head Z show also a linear increment related to velocity, and again very small std. deviations. As expected, the frequency values arise as twice as the double step frequency.

If the frequencies of the translations in X, Y and Z are compared, it will be seen, that the most important frequency variations, in males and females, occur along the X axis, even when they were post processed with the same filters.

Table 3- 15 Frequencies of head rotations and translations (males).

		Speed	2 km/h	2,5 km/h	3 km/h	3,5 km/h	4 km/h	4,5 km/h	5 km/h	5,5 km/h	6 km/h
Frequencies of the rotations and translations of the head (males)	Asc. Profile	Alpha [Hz]	0,69	0,75	0,79	0,90	0,89	0,93	1,04	1,09	1,04
		Std. deviation	0,09	0,14	0,09	0,24	0,07	0,32	0,44	0,48	0,43
		n	52	51	49	51	51	52	51	52	52
	Desc. Profile	Alpha [Hz]	0,64	0,70	0,79	0,83	0,97	1,05	1,07	1,20	1,19
		Std. deviation	0,17	0,12	0,25	0,16	0,37	0,57	0,51	0,63	0,56
		n	52	54	53	53	52	49	51	53	50
	Asc. Profile	Beta [Hz]	0,87	0,98	1,08	1,13	1,39	1,41	1,48	1,61	1,64
		Std. deviation	0,33	0,39	0,45	0,60	0,49	0,58	0,58	0,61	0,67
		n	52	51	49	51	51	52	51	52	52
	Desc. Profile	Beta [Hz]	0,94	1,00	1,22	1,30	1,26	1,46	1,59	1,65	1,68
		Std. deviation	0,30	0,39	0,43	0,69	0,51	0,54	0,55	0,60	0,64
		n	52	54	53	53	52	49	51	53	50
	Asc. Profile	Gamma [Hz]	0,68	0,74	0,80	0,83	0,90	0,93	0,94	1,00	1,03
		Std. deviation	0,07	0,07	0,09	0,10	0,07	0,14	0,12	0,10	0,12
		n	52	51	49	51	51	52	51	52	52
	Desc. Profile	Gamma [Hz]	0,62	0,69	0,76	0,82	0,88	0,92	0,93	0,97	1,05
		Std. deviation	0,06	0,05	0,07	0,15	0,11	0,11	0,14	0,16	0,19
		n	52	54	53	53	52	49	51	53	50
	Asc. Profile	X [Hz]	0,87	0,93	1,00	1,14	1,31	1,34	1,58	1,54	1,65
		Std. deviation	0,32	0,38	0,41	0,51	0,52	0,59	0,53	0,63	0,66
		n	52	51	49	51	51	52	51	52	52
	Desc. Profile	X [Hz]	0,98	1,04	1,07	1,20	1,36	1,44	1,44	1,77	1,71
		Std. deviation	0,28	0,35	0,43	0,50	0,51	0,53	0,60	0,51	0,62
		n	52	54	53	53	52	49	51	53	50
	Asc. Profile	Y [Hz]	0,68	0,75	0,81	0,86	0,90	0,94	0,97	1,00	1,04
		Std. deviation	0,07	0,06	0,07	0,06	0,06	0,05	0,06	0,06	0,06
		n	52	51	49	51	51	52	51	52	52
	Desc. Profile	Y [Hz]	0,62	0,70	0,77	0,82	0,89	0,94	0,97	1,02	1,05
		Std. deviation	0,05	0,05	0,06	0,06	0,07	0,04	0,06	0,06	0,06
		n	52	54	53	53	52	49	51	53	50
	Asc. Profile	Z [Hz]	1,31	1,48	1,62	1,72	1,79	1,87	1,94	2,01	2,08
		Std. deviation	0,31	0,18	0,12	0,10	0,10	0,10	0,11	0,11	0,12
		n	52	51	49	51	51	52	51	52	52
	Desc. Profile	Z [Hz]	1,22	1,40	1,55	1,67	1,78	1,88	1,95	2,02	2,09
		Std. deviation	0,16	0,10	0,09	0,12	0,13	0,10	0,10	0,10	0,12
		n	52	54	53	53	52	49	51	53	50

Minimal and maximal frequency values of head translations in Y direction are: 0,63 Hz at 2 km/h resp. 1,08 Hz at 6 km/h (females) and 0,622 Hz at 2 km/h resp. 1,047 Hz at 6 km/h (males).

Minimal and maximal frequency values of head translations in Z direction are: 1,25 Hz at 2 km/h resp. 2,17 Hz at 6 km/h (females) and 1,2 Hz at 2 km/h resp. 2,08 Hz at 6 km/h (males).

Tables 3-15 and 3-16 introduce the complete information of the frequency of head rotations and translations of males resp. females at each velocity.

Table 3- 16 Frequencies of head rotations and translations (females).

		Speed	2 km/h	2,5 km/h	3 km/h	3,5 km/h	4 km/h	4,5 km/h	5 km/h	5,5 km/h	6 km/h
Frequencies of the rotations and translations of the head (females)	Asc. Profile	Alpha [Hz]	0,72	0,80	0,85	0,90	1,05	1,16	1,16	1,00	1,11
		Std. deviation	0,21	0,19	0,29	0,40	0,60	0,65	0,60	0,49	0,67
		n	49	47	48	49	49	49	48	48	48
	Desc. Profile	Alpha [Hz]	0,66	0,74	0,88	1,00	1,02	1,28	1,14	1,29	1,24
		Std. deviation	0,16	0,19	0,40	0,55	0,59	0,77	0,68	0,87	0,77
		n	49	48	48	48	49	49	47	45	48
	Asc. Profile	Beta [Hz]	1,00	1,08	1,19	1,39	1,44	1,53	1,67	1,60	1,60
		Std. deviation	0,36	0,53	0,59	0,58	0,58	0,59	0,59	0,66	0,75
		n	49	47	48	49	49	49	48	48	48
	Desc. Profile	Beta [Hz]	1,01	1,18	1,21	1,34	1,37	1,51	1,70	1,71	1,71
		Std. deviation	0,32	0,35	0,42	0,52	0,57	0,59	0,59	0,66	0,71
		n	49	48	48	48	49	49	47	45	48
	Asc. Profile	Gamma [Hz]	0,68	0,76	0,83	0,92	0,87	0,95	0,96	0,95	0,93
		Std. deviation	0,09	0,13	0,19	0,43	0,20	0,19	0,22	0,27	0,26
		n	49	47	48	49	49	49	48	48	48
	Desc. Profile	Gamma [Hz]	0,63	0,72	0,75	0,82	0,85	0,88	0,94	0,95	0,99
		Std. deviation	0,06	0,13	0,10	0,17	0,16	0,17	0,25	0,29	0,22
		n	49	48	48	48	49	49	47	45	48
	Asc. Profile	X [Hz]	0,82	0,82	0,80	0,93	0,90	1,24	1,13	1,13	1,38
		Std. deviation	0,29	0,31	0,33	0,47	0,46	0,60	0,60	0,70	0,73
		n	49	47	48	49	49	49	48	48	48
	Desc. Profile	X [Hz]	0,93	0,90	0,89	0,94	1,05	1,26	1,32	1,31	1,43
		Std. deviation	0,29	0,35	0,36	0,44	0,51	0,60	0,65	0,66	0,73
		n	49	48	48	48	49	49	47	45	48
	Asc. Profile	Y [Hz]	0,69	0,78	0,84	0,88	0,93	0,97	0,99	1,05	1,08
		Std. deviation	0,08	0,07	0,07	0,06	0,05	0,05	0,06	0,06	0,06
		n	49	47	48	49	49	49	48	48	48
	Desc. Profile	Y [Hz]	0,63	0,71	0,77	0,84	0,91	0,95	0,99	1,04	1,06
		Std. deviation	0,06	0,05	0,06	0,06	0,06	0,04	0,09	0,09	0,12
		n	49	48	48	48	49	49	47	45	48
	Asc. Profile	Z [Hz]	1,34	1,52	1,64	1,76	1,82	1,93	2,00	2,08	2,17
		Std. deviation	0,20	0,16	0,15	0,10	0,19	0,09	0,10	0,10	0,13
		n	49	47	48	49	49	49	48	48	48
	Desc. Profile	Z [Hz]	1,25	1,41	1,56	1,68	1,80	1,91	2,00	2,08	2,16
		Std. deviation	0,14	0,15	0,10	0,09	0,09	0,09	0,09	0,11	0,13
		n	49	48	48	48	49	49	47	45	48

Phases between rotations and translations

Following the same way to show the computed data, in fig.3-25 to 3-27 means and std. deviations of the phases between head rotations and translations of males and females are presented.

Figs. 3-25 (A and B) show the phase shift angles between axial rotations and lateral tilt of the head of male resp. female volunteers, related to velocity. Females show dependencies of the phase $\gamma-\alpha$ (positive slope) on the speed only for the ascending ramp (fig. 3-25 B). For the descending ramp, no easy identifiable interdependencies on the speed are observed.

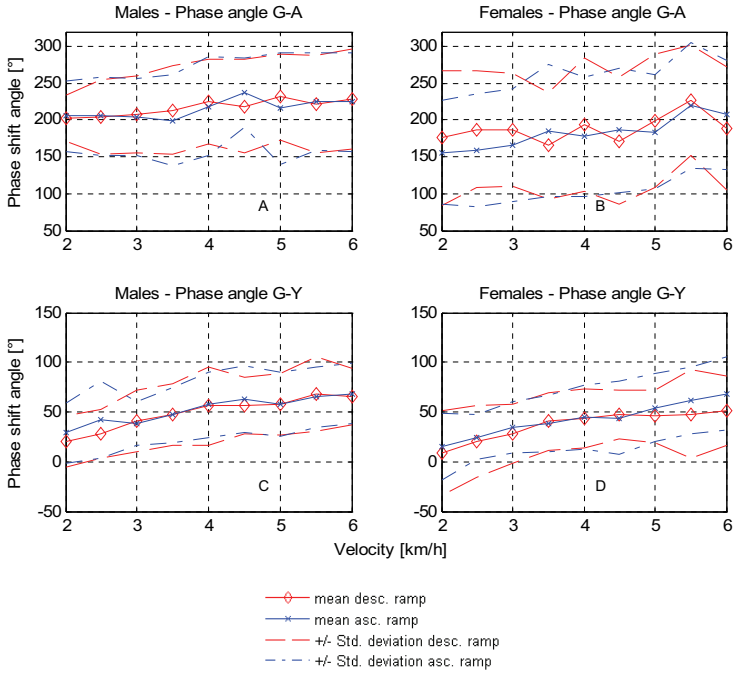

Figure 3- 25 Head phase shift angles between the rotations around longitudinal and sagittal axis (Upper left and right) and head phase shift angles between axial rotations and translations in the transverse axe (Bottom left and right).

Male volunteers tend to increase the phase shift angles $\gamma-\alpha$ with the speed, but as in fig. 3-25 (A) can be observed, this increment is mostly carried out between 3 km/h and 5,5 km/h. Outside this interval, the phase remain almost constant.

Phase shift angles γ-Y show similar paths for males and females as those observed for the thorax. As displayed in fig. 3-25 (C and D), the phase shift angle γ-Y will be increased in males and females with the increment of the speed. Only women show in the descending ramp a plateau between 4,5 km/h and 6 km/h, which does not correspond to the linear increment observed for men (in both ramps) and woman (ascending ramp).

Minimal and maximal values of phase γ-α obtained for female volunteers are: 156,04° at 2 km/h resp. 226,9° at 5,5 km/h.

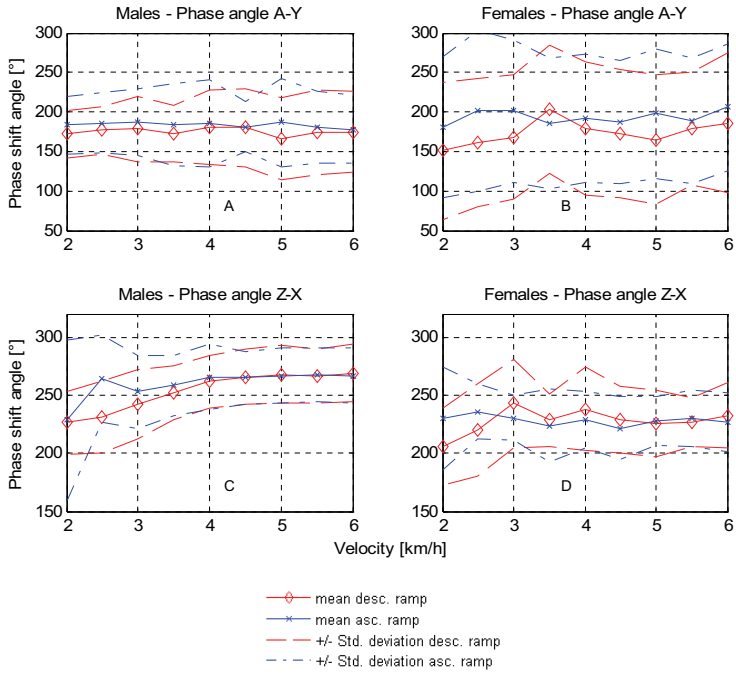

Figure 3- 26 Phase shift angles between the head rotations around sagittal axis and head translations in transverse axis (Upper left and right) and phase shift angles between head translations in longitudinal and in sagittal axis (Bottom left and right).

Minimal and maximal values of phase γ-α obtained for male volunteers, are: 202,11° at 2 km/h resp. 231,27° at 5 km/h. For the phase shift angle γ-Y, minimal and maximal values are: 9,2° at 2 km/h resp. 68,5° at 6 km/h (females) and 20,2° at 2 km/h resp. 68,37° at 6 km/h (males).

By observing the phase shift angle α-Y of males and females (figs. 3-26 A and B), it will be clear that it does not vary with the velocity, but between males and females. Indeed while for males it oscillates about 180°, for females it arises 200°.

Phase Z-X of males (fig. 3-26 C) starts with an ascending slope up to 4 km/h, after that no dependencies on the speed can be observed. Females do not display easy identifiable relationships between phase Z-X and velocity (fig. 3-26 D).

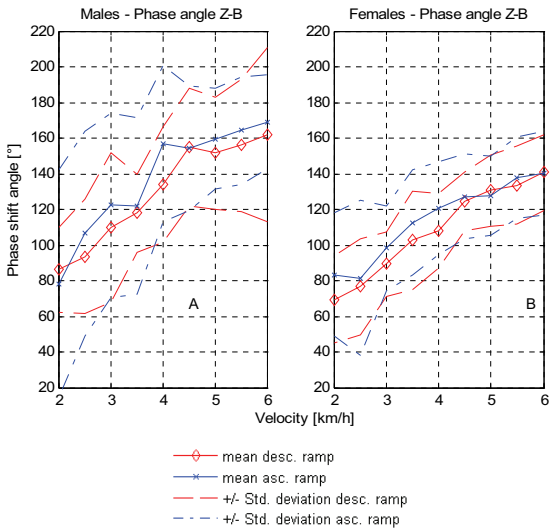

Figure 3- 27 Head phase shift angles between translations in the longitudinal axis and frontal tilt.

Values of the phase Z-X oscillate between 220° and 230°. Again means of males and females differ.

Figs. 3-27 (A and B) present means of phase shift angles between translations in the longitudinal axis (as basis) and frontal tilt of the head of males respectively females.

As shown, the phases Z-β will be increased almost in a linear way with the velocity in males and females. It must be noted, that in males most of the increments of the phase are carried out from 2 km/h to 4,5 km/h. After that the slope remains positive but inclination became smaller. As presented below, means of phase Z-β for males display always larger values than those for females.

Minimal and maximal values of phase shift angles Z- β arise: 69,51° at 2 km/h resp. 140,7° at 6 km/h (females) and 86,15° at 2 km/h resp. 172,86° at 6 km/h (males).

Complete information about the phase Z-β related to velocity is presented in tables 3-17and 3-18.

Table 3- 17 Phase shift angles between head rotations and translations (males).

		Speed	2 km/h	2,5 km/h	3 km/h	3,5 km/h	4 km/h	4,5 km/h	5 km/h	5,5 km/h	6 km/h
Phases between head rotations and translations (males)	Asc. Profile	φ(γ–α) [°]	205,18	205,21	204,70	199,60	218,67	237,35	215,65	225,45	224,79
		Std. deviation	48,09	53,25	52,40	61,54	67,30	46,83	75,23	66,01	67,18
		n	43	40	41	39	43	37	39	38	35
	Desc. Profile	φ(γ–α) [°]	202,11	204,62	207,38	213,60	225,65	218,58	231,27	222,03	228,23
		Std. deviation	31,35	50,73	52,06	60,40	57,44	63,81	58,19	66,26	67,61
		n	45	44	40	43	37	32	39	34	41
	Asc. Profile	φ(γ–Y) [°]	28,73	42,70	38,22	47,24	57,44	63,30	57,66	65,08	68,38
		Std. deviation	29,94	38,53	21,77	27,58	32,63	33,45	32,58	30,42	30,11
		n	45	48	44	44	47	46	45	45	47
	Desc. Profile	φ(γ–Y) [°]	20,20	27,83	40,81	47,43	56,13	56,56	57,63	68,16	66,00
		Std. deviation	25,34	24,45	30,78	31,44	39,38	28,79	31,01	37,85	28,39
		n	49	46	46	45	45	41	44	40	45
	Asc. Profile	φ(α–Y) [°]	183,34	186,35	187,18	184,18	185,33	181,36	186,39	181,13	177,99
		Std. deviation	36,98	38,84	41,72	52,34	55,23	32,12	56,34	45,23	43,00
		n	50	41	42	41	47	37	41	38	36
	Desc. Profile	φ(α–Y) [°]	171,80	176,84	178,54	172,58	180,70	180,48	166,19	174,56	174,88
		Std. deviation	29,80	30,53	41,33	35,21	47,30	49,36	52,56	53,82	51,68
		n	45	44	44	43	36	32	42	38	40
	Asc. Profile	φ(Z-X) [°]	228,80	264,20	252,88	258,61	265,42	264,90	266,84	267,45	266,91
		Std. deviation	68,91	38,03	31,71	25,82	28,15	23,06	23,93	23,37	23,53
		n	15	18	16	23	27	28	35	34	36
	Desc. Profile	φ(Z–X) [°]	226,43	230,85	241,77	252,02	261,61	265,90	267,83	266,92	268,77
		Std. deviation	27,06	30,71	29,95	23,59	22,24	24,04	24,89	23,27	24,94
		n	28	27	23	28	31	30	27	43	35
	Asc. Profile	φ(Z–β) [°]	94,55	127,80	122,32	121,85	156,78	154,41	159,68	164,13	168,99
		Std. deviation	65,38	74,24	51,92	49,39	44,05	34,81	28,07	29,95	26,26
		n	22	17	16	15	24	30	31	34	35
	Desc. Profile	φ(Z–β) [°]	86,15	93,64	109,71	117,97	133,95	155,21	151,46	156,02	172,86
		Std. deviation	23,76	31,82	42,02	21,80	32,37	33,04	31,34	37,02	50,38
		n	20	23	28	20	21	29	32	38	33

Table 3- 18 Phase shift angles between head rotations and translations (females).

		Speed	2 km/h	2,5 km/h	3 km/h	3,5 km/h	4 km/h	4,5 km/h	5 km/h	5,5 km/h	6 km/h
Phases between head rotations and translations (females)	Asc. Profile	φ(γ–α) [°]	156,04	159,00	166,01	185,42	177,22	186,22	183,94	220,05	206,86
		Std. deviation	70,83	77,08	77,24	89,36	81,29	84,42	77,43	85,96	73,92
		n	27	29	31	29	22	28	23	25	20
	Desc. Profile	φ(γ–α) [°]	175,54	187,37	186,51	165,07	193,66	171,68	198,79	226,97	187,73
		Std. deviation	91,04	79,40	77,07	72,78	90,99	85,92	90,35	75,25	83,62
		n	37	30	31	23	22	25	22	18	26
	Asc. Profile	φ(γ–Y) [°]	15,31	24,84	34,81	38,69	44,90	43,72	54,31	61,88	68,51
		Std. deviation	33,67	23,07	25,54	28,73	32,73	36,81	34,13	33,46	36,43
		n	40	39	40	39	31	42	36	31	32
	Desc. Profile	φ(γ–Y) [°]	9,21	20,79	28,01	40,38	43,89	46,99	45,74	47,62	51,08
		Std. deviation	42,58	36,30	29,81	28,81	29,97	24,73	26,60	44,44	35,10
		n	41	40	40	37	37	36	32	31	39
	Asc. Profile	φ(α–Y) [°]	180,20	202,24	201,14	185,50	191,93	187,56	198,39	188,99	206,35
		Std. deviation	89,50	102,18	90,62	83,42	80,87	78,30	81,95	79,33	80,47
		n	30	34	31	29	29	33	27	26	27
	Desc. Profile	φ(α–Y) [°]	151,11	161,33	168,23	203,37	178,96	172,33	165,11	178,72	186,34
		Std. deviation	86,51	80,82	78,32	81,01	84,40	81,32	82,32	71,02	89,24
		n	41	30	32	27	21	28	22	19	29
	Asc. Profile	φ(Z-X) [°]	229,79	236,05	230,52	223,54	229,10	221,52	227,76	230,25	226,93
		Std. deviation	43,93	24,15	19,01	31,43	23,96	27,08	21,16	24,21	25,36
		n	13	7	7	12	9	19	14	16	23
	Desc. Profile	φ(Z–X) [°]	205,93	219,84	242,86	228,84	238,25	229,07	225,42	226,74	232,37
		Std. deviation	33,28	39,62	38,34	22,68	35,72	28,68	28,60	21,41	28,21
		n	24	16	10	11	13	22	22	19	24
	Asc. Profile	φ(Z–β) [°]	83,46	101,52	98,12	112,69	120,53	127,24	127,47	137,87	140,53
		Std. deviation	34,69	57,48	24,06	29,49	26,11	23,66	22,13	22,87	23,56
		n	25	18	24	28	29	33	34	30	30
	Desc. Profile	φ(Z–β) [°]	69,51	76,63	89,40	102,58	108,13	124,37	130,69	133,53	140,69
		Std. deviation	24,57	26,86	18,22	27,56	21,00	16,59	20,05	21,77	21,29
		n	25	27	27	29	28	31	36	33	33

3.2 Relative motions

In previous sections, the absolute motions of the pelvis, thorax and head have been presented. That means that the motions of each segment have been computed in relationship to the laboratory or main frame. In the following sections, the relative motions between these segments will be presented, where the upper one was always used as reference frame.

3.2.1 Pelvis – thorax

Rotations

The relative motions between pelvis and thorax have been computed using the function *cardan2* (see pag. 26). As mentioned above, the Cardan angles [α, β, γ] have been calculated using thorax as reference frame, where α represents the

lateral- flexion or lateral tilt, β the flexion-extension or frontal tilt and γ the torsion of the trunk.

Figs. 3-28 (A and B) show means and std. deviations of the lateral flexion of the trunk of males resp. females, related to velocity.

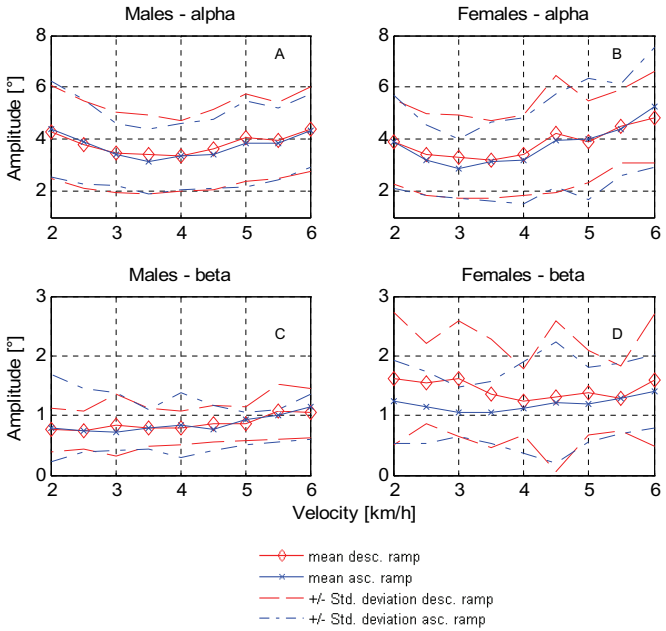

Figure 3- 28 Lateral flexion (upper left and right) and flexion-extension (bottom left and right) of the trunk of males and females volunteers, related to velocity.

Males and females display similar lateral- flexion paths. The curves start descending up to an inflexion point, which coincides with the energetic optimal velocity (3,5 km/h to 4 km/h from Cavagna et al. 1977), after that, they ascend again until the speeds 4,5 km/h and 5 km/h (females resp. males) are reached. At these points, females and males show a plateau for an interval of 0,5 km/h, followed by a linear ascending slope. Males show almost the same lateral flexions at 2 km/h and 6 km/h and larger values than those of the women up to 4,5 km/h. First after this velocity are the lateral flexions of female volunteers larger.

Figs. 3-28 (C and D) present means and std. deviations for trunk's flexion- extension of males respectively females related to velocity.

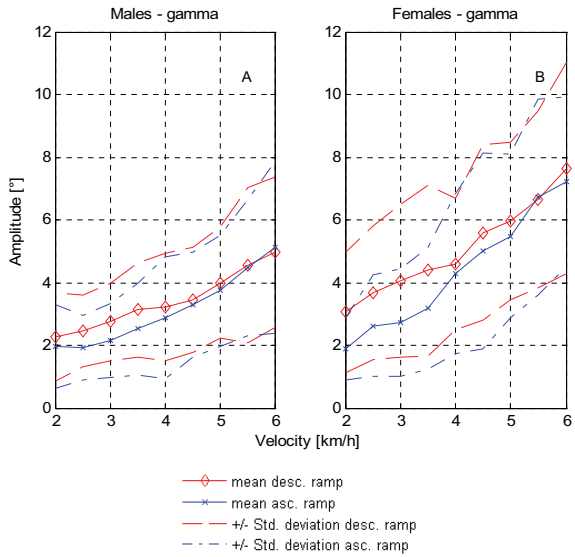

Figure 3- 29 Torsion of the trunk of males and females volunteers, related to velocity.

Male's flexion- extension values remain almost constant up to 5 km/h (from 0,7° to 0,8°), above this speed the amplitudes grow to a maximum of 1,15° at 6 km/h.

In females' case, the shape of flexion-extension curves for the asc. and desc. ramp are totally different and not even one shows dependencies on the velocity. Amplitudes oscillate between 1° and 1,6°.

Torsion of the trunk of males and females show significant dependencies on the velocity (see figs. 3-29 A & B). As presented in previous studies (Witte & Hoffmann, 2001; Witte et al. 2004), torsion of trunk of females is larger than those of males.

At this point it should be useful to remember that the torsion of trunk is related to instant relative positions of thorax and pelvis at each velocity and, as presented in previous sections, while the axial rotation of the pelvis grows with the speed, those of the thorax decrease. So, why does the torsion grow so strong with the speed? The first answer is that the increment of the pelvis rotation is bigger than the decrease of thorax rotation and the second one is the variation of the phase shift angles between pelvis and thorax.

Minimal and maximal trunk torsions are: 1,88° at 2 km/h resp. 7,65° at 6 km/h (females) and 1,92° at 2,5 km/h resp. 5,12° at 6 km/h (males).

Tables 3-19 and 3-20 present the complete information of the relative motions of pelvis and thorax of males and females at each velocity.

Table 3- 19 Trunk rotations (males).

		Speed	2 km/h	2,5 km/h	3 km/h	3,5 km/h	4 km/h	4,5 km/h	5 km/h	5,5 km/h	6 km/h
Trunk rotations (males)	Asc. Profile	Alpha [°]	4,39	3,90	3,42	3,14	3,34	3,43	3,84	3,82	4,32
		Std. deviation	1,86	1,64	1,20	1,26	1,28	1,33	1,65	1,38	1,41
		n	52	50	48	51	50	52	51	52	52
	Desc. Profile	Alpha [°]	4,27	3,81	3,48	3,39	3,36	3,61	4,04	3,95	4,39
		Std. deviation	1,79	1,67	1,55	1,52	1,38	1,53	1,68	1,48	1,61
		n	52	54	53	53	52	49	51	53	50
	Asc. Profile	Beta [°]	0,79	0,75	0,73	0,80	0,84	0,76	0,94	1,01	1,15
		Std. deviation	0,56	0,36	0,32	0,36	0,54	0,34	0,43	0,45	0,54
		n	51	50	48	51	50	52	51	52	52
	Desc. Profile	Beta [°]	0,76	0,76	0,84	0,80	0,79	0,86	0,86	1,06	1,04
		Std. deviation	0,36	0,32	0,51	0,33	0,28	0,30	0,29	0,46	0,41
		n	52	53	53	53	52	49	51	53	50
	Asc. Profile	Gamma [°]	1,96	1,92	2,15	2,52	2,88	3,28	3,73	4,47	5,12
		Std. deviation	1,33	1,02	1,19	1,46	1,93	1,68	1,77	2,17	2,74
		n	51	50	48	51	50	52	51	52	52
	Desc. Profile	Gamma [°]	2,28	2,46	2,75	3,13	3,22	3,45	3,98	4,54	4,97
		Std. deviation	1,41	1,15	1,23	1,49	1,70	1,69	1,77	2,47	2,41
		n	52	54	53	53	52	49	51	53	50

Table 3- 20 Trunk rotations (females).

		Speed	2 km/h	2,5 km/h	3 km/h	3,5 km/h	4 km/h	4,5 km/h	5 km/h	5,5 km/h	6 km/h
Trunk rotations (females)	Asc. Profile	Alpha [°]	3,92	3,21	2,87	3,12	3,17	3,94	4,02	4,38	5,24
		Std. deviation	1,79	1,37	1,15	1,52	1,67	1,80	2,35	1,76	2,32
		n	49	47	48	49	49	49	47	48	47
	Desc. Profile	Alpha [°]	3,90	3,42	3,33	3,20	3,39	4,21	3,91	4,48	4,83
		Std. deviation	1,65	1,56	1,58	1,49	1,57	2,26	1,58	1,42	1,76
		n	49	48	47	48	49	49	47	45	46
	Asc. Profile	Beta [°]	1,23	1,14	1,06	1,06	1,13	1,23	1,18	1,29	1,41
		Std. deviation	0,70	0,60	0,41	0,51	0,76	1,02	0,62	0,59	0,62
		n	49	46	48	49	49	49	46	48	48
	Desc. Profile	Beta [°]	1,63	1,54	1,62	1,37	1,24	1,32	1,38	1,28	1,60
		Std. deviation	1,11	0,67	0,97	0,90	0,55	1,26	0,70	0,54	1,11
		n	48	46	46	47	48	48	46	44	47
	Asc. Profile	Gamma [°]	1,89	2,62	2,73	3,19	4,29	5,00	5,48	6,73	7,22
		Std. deviation	0,99	1,62	1,71	1,96	2,55	3,12	2,60	3,14	2,70
		n	48	47	47	48	49	49	44	47	44
	Desc. Profile	Gamma [°]	3,06	3,68	4,04	4,38	4,59	5,60	5,97	6,65	7,66
		Std. deviation	1,92	2,13	2,43	2,71	2,09	2,81	2,52	2,81	3,36
		n	49	47	47	48	49	48	47	43	46

Frequencies

For each relative Cardan angle [α, β, γ] between pelvis and thorax, the frequencies of the principal vibration mode of oscillation of each volunteer using FFTs were computed (means and std. deviations at each speed).

The results of these calculations are presented in figs. (3-30 & 3-31)

Figs. 3-30 (A and B) display the frequencies of the lateral flexion of males resp. females, related to velocity. In males, frequencies of the lateral trunk flexion increase from 0,62 Hz at 2 km/h to 1,05 Hz at 6 km/h.

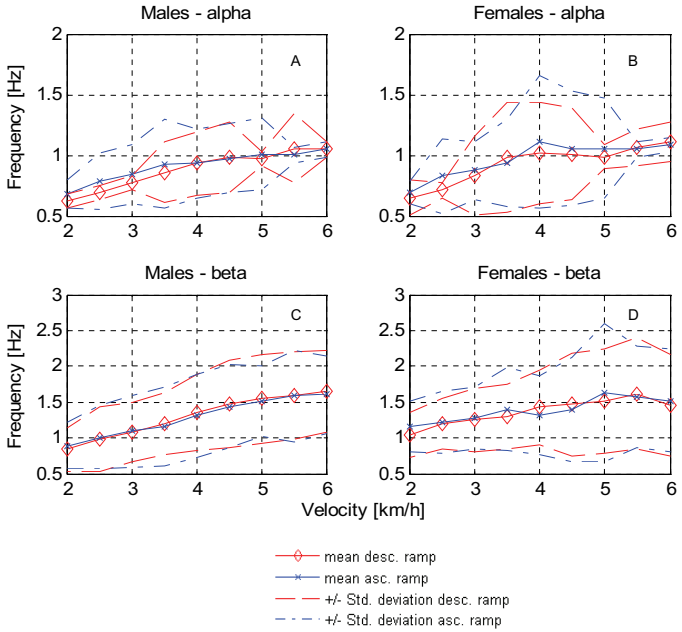

Figure 3- 30 Principal mode of oscillation of the trunk's lat. tilt (A and B) and frontal tilt (B and C) of male resp. female volunteers, related to velocity.

In females, the curve starts with 0,64 Hz at 2 km/h and ascends up to 1,1 Hz at 4 km/h. At higher velocities no evidence of dependence on the velocity is given.

Frequencies of the trunk's flexion extension are displayed in fig. 3-30 (C and D). The variation of the trunk flexion extension's frequency of male volunteers evidences a linear relationship to the speed. It starts with 0,83 Hz at 2 km/h and reaches 1,64 Hz at 6 km/h. Females start with larger frequency values (1,04 Hz at 2 km/h) and reach

maximal values at 5 km/h and 5,5 km/h (about 1,62 Hz) for the ascending resp. descending ramps.

Figs. 3-31 (A and B) present the frequencies of the trunk's torsion of males resp. females, related to velocity. Like in the case of the lateral flexion frequencies, females reach their maximal frequency values at slower velocities than males. To illustrate this behaviour, it will be enough to observe that females at 4 km/h choose values larger than 1 Hz, males between 0,87 Hz and 0,95 Hz.

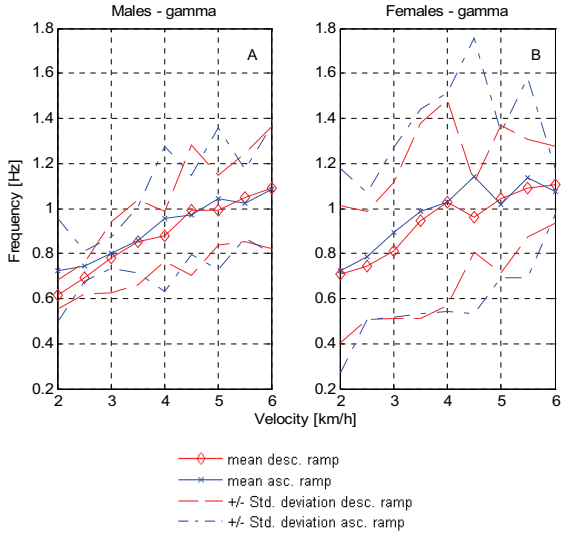

Figure 3- 31 Principal mode of oscillation of the trunk's torsion of male (A) and female (B) volunteers, related to velocity.

As we change the speed from 4 km/h to 6 km/h, frequencies of male volunteers increase continuously, while those of the females are not highly defined, with higher standard deviations. Finally, at 6 km/h, both reach frequencies about 1,1 Hz.

Females display almost the same minimal frequencies for ascending and descending ramps (about 0,7 Hz). In contrast, males show significant differences (0,72 Hz and 0,61 Hz) for ascending resp. descending ramps.

Complete information about frequencies and velocities of males and females are introduced in tables 3-21 and 3-22.

Table 3- 21 Frequencies of trunk rotations (males).

		Speed	2 km/h	2,5 km/h	3 km/h	3,5 km/h	4 km/h	4,5 km/h	5 km/h	5,5 km/h	6 km/h
Frequencies of trunk rotations (males)	Asc. Profile	Alpha [Hz]	0,68	0,78	0,84	0,93	0,93	0,98	1,01	1,00	1,05
		Std. deviation	0,11	0,23	0,25	0,37	0,28	0,28	0,30	0,06	0,06
		n	52	51	49	51	51	52	51	52	52
	Desc. Profile	Alpha [Hz]	0,62	0,69	0,77	0,86	0,93	0,98	0,97	1,06	1,05
		Std. deviation	0,05	0,06	0,06	0,25	0,26	0,29	0,06	0,28	0,06
		n	52	54	53	53	52	49	51	53	50
	Asc. Profile	Beta [Hz]	0,89	1,01	1,09	1,17	1,31	1,44	1,51	1,59	1,61
		Std. deviation	0,33	0,45	0,50	0,55	0,59	0,58	0,49	0,64	0,55
		n	52	51	49	51	51	52	51	52	52
	Desc. Profile	Beta [Hz]	0,84	0,98	1,09	1,20	1,36	1,47	1,54	1,59	1,65
		Std. deviation	0,30	0,45	0,42	0,43	0,53	0,61	0,62	0,61	0,57
		n	52	54	53	53	52	49	51	53	50
	Asc. Profile	Gamma [Hz]	0,73	0,74	0,80	0,86	0,95	0,97	1,05	1,02	1,09
		Std. deviation	0,23	0,07	0,07	0,15	0,32	0,18	0,32	0,15	0,28
		n	52	51	49	51	51	52	51	52	52
	Desc. Profile	Gamma [Hz]	0,62	0,69	0,78	0,85	0,88	0,99	0,99	1,05	1,09
		Std. deviation	0,07	0,07	0,16	0,19	0,11	0,29	0,15	0,20	0,27
		n	52	54	53	53	52	49	51	53	50

Table 3- 22 Frequencies of trunk rotations (females).

		Speed	2 km/h	2,5 km/h	3 km/h	3,5 km/h	4 km/h	4,5 km/h	5 km/h	5,5 km/h	6 km/h
Frequencies of trunk rotations (female	Asc. Profile	Alpha [Hz]	0,69	0,83	0,87	0,94	1,11	1,06	1,05	1,05	1,09
		Std. deviation	0,09	0,31	0,24	0,36	0,55	0,47	0,41	0,06	0,06
		n	49	47	48	49	49	49	48	48	48
	Desc. Profile	Alpha [Hz]	0,65	0,71	0,83	0,98	1,02	1,01	0,99	1,07	1,11
		Std. deviation	0,15	0,06	0,33	0,45	0,42	0,38	0,10	0,15	0,16
		n	49	48	48	48	49	49	47	45	48
	Asc. Profile	Beta [Hz]	1,16	1,21	1,28	1,40	1,32	1,39	1,63	1,58	1,52
		Std. deviation	0,35	0,44	0,43	0,58	0,55	0,73	0,96	0,71	0,72
		n	49	47	48	49	49	49	48	48	48
	Desc. Profile	Beta [Hz]	1,04	1,20	1,25	1,30	1,43	1,47	1,51	1,62	1,45
		Std. deviation	0,31	0,36	0,44	0,46	0,52	0,72	0,72	0,78	0,71
		n	49	48	48	48	49	49	47	45	48
	Asc. Profile	Gamma [Hz]	0,72	0,79	0,89	0,99	1,03	1,14	1,02	1,14	1,08
		Std. deviation	0,45	0,28	0,38	0,45	0,49	0,61	0,32	0,44	0,10
		n	49	47	48	49	49	49	48	48	48
	Desc. Profile	Gamma [Hz]	0,71	0,75	0,81	0,95	1,03	0,96	1,04	1,09	1,11
		Std. deviation	0,30	0,24	0,30	0,43	0,46	0,15	0,33	0,22	0,17
		n	49	48	48	48	49	49	47	45	48

Trunk phase shift angles

In this section, an analysis will be made for the phase shift angles between the rotations of thorax (as base) and pelvis in three motion planes. The variations of phases are related to velocity and will be displayed as phases of lateral tilt and sagittal tilt and axial rotation.

Figs. 3-32 (A y B) display variations of phases between thorax (as base) and pelvis around the longitudinal axis (axial rotation) of males resp. females. The shapes of the

curves of both sexes are similar but those of females show values which are 20°-30° higher.

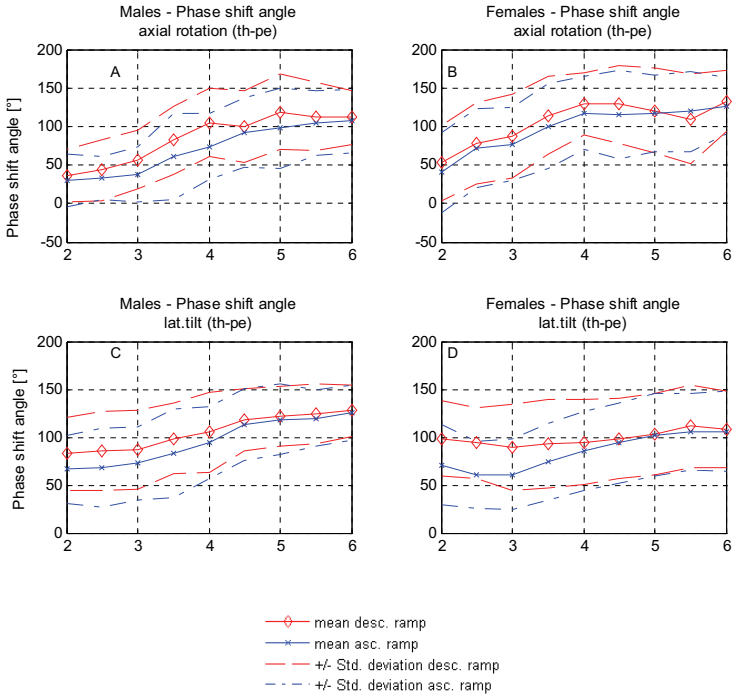

Figure 3- 32 Phase shift angles between thorax (as base) and pelvis. (A and B) phases between pelvic and thoracic axial rotation of males resp. females. (C and D) phases between pelvic and thoracic lat. tilt of males resp. females.

Females (fig. 3-32 B) start at a phase shift angle of 40° and increase their phases very fast until 4 km/h, soon the inclination of the curve diminishes and reaches the maximal value at 6 km/h (133°). Those of males (fig. 3-32 A) start at about 30°. For the ascending ramp, the maximal value of phase shift angle is reached at 6 km/h (107°), on the other hand, the descending ramp shows a maximum at 5 km/h (119°).
The gender variations of the phase shift angles on the sagittal axis (lat. tilt) between thorax (as base) and pelvis are introduced in fig. 3-32 (C and D).
In figs. 3-32 (C & D) is displayed, that phase shift angles for males and females show significant dependencies on the velocity for the ascending ramp.

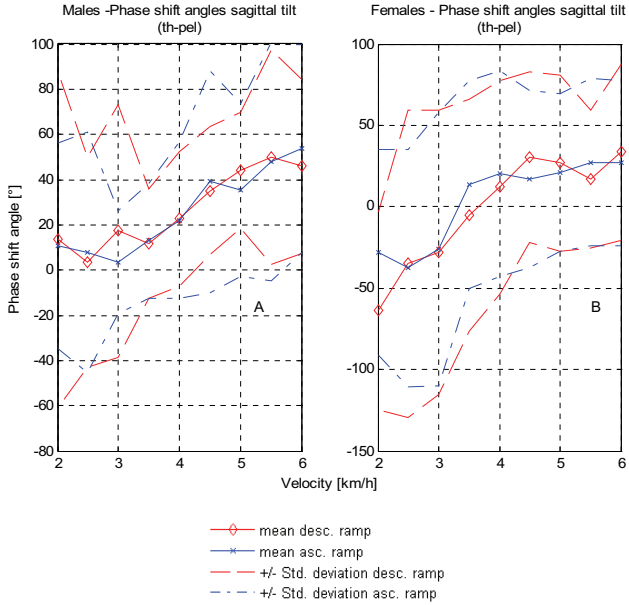

Figure 3- 33 Phase shift angles between thorax (as base) and pelvis. (A and B) phases between pelvic and thoracic frontal tilt of males resp. females.

On the other hand, females do not show these significant dependencies for the descending ramp (see fig. 3-32 D). Minimal and maximal phase shift values for the ascending profile: 71° at 2 km/h and 106° at 6 km/h, respectively.

Male volunteers (fig. 3-32 C) started with a phase of 66° showing an ascending slope in their phase shift angles related to speed. Maximal values are observed at 5 km/h for the ascending profile (119°) and at 6 km/h for the descending one (125°).

The behaviour of the phases shift angle's curves for the frontal tilt of males and females is similar (see fig. 3-33 A and B). Males (fig. 3-33 A) start with a mean of 11° and a descending slope, which after 3 km/h is ascending until 6 km/h, where the curve reaches the maximal value of 54°. Females start with negative phases (about -30°). The phase became positive after 3,5 km/h. At higher velocities than 4 km/h, the mean oscillates between 20° and 30°. At 2km/h, phase mean values for the ascending ramp differ significantly in relation to those for the descending ramp.

Complete information about phases, at each velocity, between thorax and pelvis can be found in tables (3-23 and 3-24).

Table 3- 23 Phase shift angles between trunk rotations (males)

Phase shift angles of trunk rotations (males)		Speed	2 km/h	2,5 km/h	3 km/h	3,5 km/h	4 km/h	4,5 km/h	5 km/h	5,5 km/h	6 km/h
	Asc. Profile	Axial rotation [°]	30,58	33,43	37,65	61,12	74,04	91,41	97,84	104,44	106,98
		Std. deviation	34,04	28,28	35,18	55,22	43,19	44,96	52,28	42,00	40,97
		n	47	47	42	46	44	48	45	50	48
	Desc. Profile	Axial rotation [°]	36,50	43,28	57,14	82,12	105,12	99,79	119,06	112,86	111,70
		Std. deviation	34,40	38,95	37,74	44,75	44,48	46,10	48,39	43,96	35,12
		n	49	48	46	48	43	42	45	45	46
	Asc. Profile	Lateral tilt [°]	66,48	68,11	72,56	83,12	94,16	112,55	118,52	119,73	125,72
		Std. deviation	35,72	41,31	37,70	45,96	37,82	37,48	37,10	29,37	28,73
		n	45	39	42	43	47	46	46	45	46
	Desc. Profile	Lateral tilt [°]	83,01	85,36	86,96	98,47	105,20	118,20	121,88	124,20	127,53
		Std. deviation	38,21	41,28	41,24	36,83	41,62	32,82	30,94	30,97	27,06
		n	46	43	45	48	45	40	47	44	45
	Asc. Profile	Frontal tilt [°]	10,81	7,84	3,65	13,02	22,09	39,04	35,43	47,94	53,94
		Std. deviation	45,35	53,16	22,80	25,39	34,76	49,28	38,29	52,79	45,92
		n	32	29	31	29	31	30	28	28	26
	Desc. Profile	Frontal tilt [°]	13,40	3,62	17,34	11,71	22,71	35,13	44,16	49,81	45,86
		Std. deviation	74,35	46,36	55,80	23,99	29,68	28,26	25,53	47,54	38,39
		n	30	31	25	27	28	25	25	34	27

Table 3- 24 Phase shift angles between trunk rotations (females)

Phase shift angles of trunk rotations (females)		Speed	2 km/h	2,5 km/h	3 km/h	3,5 km/h	4 km/h	4,5 km/h	5 km/h	5,5 km/h	6 km/h
	Asc. Profile	Axial rotation [°]	40,61	71,99	81,14	100,61	117,63	115,25	116,76	119,82	126,86
		Std. deviation	52,17	51,44	48,64	55,89	47,42	57,17	49,26	51,84	35,94
		n	35	34	29	33	40	42	39	39	37
	Desc. Profile	Axial rotation [°]	52,73	77,77	87,46	114,05	129,13	128,98	120,80	109,66	132,99
		Std. deviation	48,68	52,96	53,62	50,69	40,50	50,82	55,24	58,65	39,82
		n	39	43	41	37	35	42	34	30	38
	Asc. Profile	Lateral tilt [°]	71,20	60,93	61,25	74,26	85,46	94,17	102,43	105,73	106,21
		Std. deviation	41,82	35,31	37,48	39,73	41,22	41,95	42,96	40,27	41,90
		n	34	35	37	31	36	41	37	40	41
	Desc. Profile	Lateral tilt [°]	98,74	93,87	88,91	92,98	94,98	98,50	102,91	111,45	108,22
		Std. deviation	39,03	36,85	45,07	46,66	44,59	42,02	42,40	43,29	39,78
		n	33	37	34	35	30	35	34	34	34
	Asc. Profile	Frontal tilt [°]	-28,23	-37,54	-26,05	13,87	20,45	17,13	21,08	27,22	26,94
		Std. deviation	63,18	72,85	83,95	63,86	63,24	54,55	48,48	51,50	50,75
		n	27	23	19	20	24	22	22	23	24
	Desc. Profile	Frontal tilt [°]	-63,83	-34,94	-27,83	-5,16	12,02	30,23	27,02	17,18	33,61
		Std. deviation	60,95	94,40	87,26	71,26	65,27	52,30	54,05	42,49	54,00
		n	27	21	19	22	17	20	22	16	25

3.2.2 Thorax – head

Rotations

As mentioned before (p. 86), the upper segment was always used as reference frame, when relative motions were computed. For this reason, the head was set as reference frame to calculate the relative rotations between thorax and head. Like in the case of the relative motion pelvis-thorax, the definitions of the Cardan angles are: α (lateral flexion), β (flexion- extension) and γ (torsion).

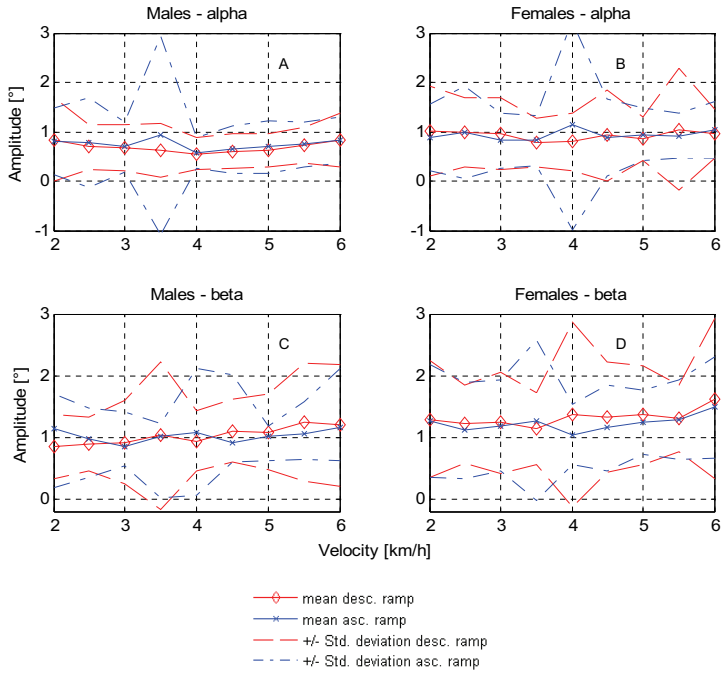

Figure 3- 34 Lateral flexion (A and B) and flexion-extension (C and D) of the trunk of male resp. female volunteers, related to velocity.

Cervical lateral flexion and flexion-extension seem to be rather independent from speed variations. As shown in fig. 3-34, amplitudes of these motions always stay close to 1°. But if we look closer at the graphics of the lat. tilt of males and females, it is possible to find, at first gender differences, and afterwards a very fine variation of lat. flexion in males related to speed.

Males and females show different paths for their cervical torsions, related to speed (see figs. 3-35 A and B). In males cervical torsions start with values close to 2°. After 3 km/h these values decrease to 1,6°. From this velocity to 6 km/h no significant variations in torsion amplitudes are observed. Females start also with a mean of about 2°. Immediately it descends to a minimum of 1,72° at 3,5 km/h. Then ascends again to a maximum of 2,17° at 6 km/h.

To obtain the complete information about means, std. deviations and the number of volunteers used to compute the data, see tables 3-25 and 3-26

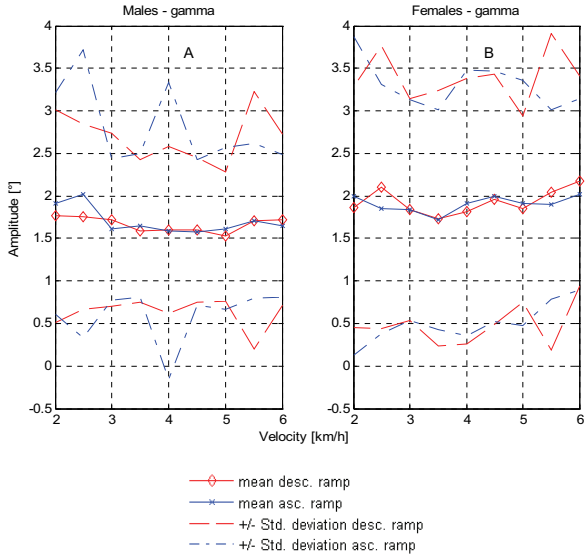

Figure 3- 35 Torsion between thorax and head of male and female volunteers, related to velocity.

Table 3- 25 Cervical rotations (males)

		Speed	2 km/h	2,5 km/h	3 km/h	3,5 km/h	4 km/h	4,5 km/h	5 km/h	5,5 km/h	6 km/h
Cervical rotations (males)	Asc. Profile	Alpha [°]	0,81	0,78	0,69	0,93	0,57	0,64	0,69	0,74	0,82
		Std. deviation	0,68	0,92	0,50	2,01	0,31	0,48	0,53	0,45	0,47
		n	52	51	48	51	50	52	50	52	52
	Desc. Profile	Alpha [°]	0,84	0,69	0,68	0,63	0,55	0,61	0,62	0,73	0,83
		Std. deviation	0,83	0,46	0,46	0,54	0,33	0,35	0,34	0,36	0,56
		n	52	54	53	53	52	49	50	53	50
	Asc. Profile	Beta [°]	1,15	0,97	0,86	1,01	1,08	0,91	1,02	1,06	1,16
		Std. deviation	0,97	0,61	0,32	1,00	1,03	0,32	0,39	0,41	0,54
		n	51	50	47	51	50	51	50	52	51
	Desc. Profile	Beta [°]	0,85	0,90	0,92	1,03	0,94	1,10	1,09	1,25	1,19
		Std. deviation	0,52	0,43	0,67	1,19	0,49	0,51	0,61	0,95	0,98
		n	52	54	52	53	52	49	50	53	50
	Asc. Profile	Gamma [°]	1,91	2,02	1,61	1,65	1,59	1,57	1,62	1,71	1,65
		Std. deviation	1,31	1,69	0,83	0,84	1,75	0,86	0,95	0,91	0,84
		n	51	50	47	50	50	51	50	52	51
	Desc. Profile	Gamma [°]	1,77	1,76	1,72	1,59	1,60	1,60	1,53	1,71	1,72
		Std. deviation	1,25	1,09	1,01	0,83	0,98	0,85	0,76	1,51	1,01
		n	52	54	51	52	52	49	50	53	50

Table 3- 26 Cervical rotations (females)

		Speed	2 km/h	2,5 km/h	3 km/h	3,5 km/h	4 km/h	4,5 km/h	5 km/h	5,5 km/h	6 km/h
Cervical rotations (females)	Asc. Profile	Alpha [°]	0,87	1,00	0,83	0,83	1,15	0,89	0,94	0,92	1,04
		Std. deviation	0,67	0,94	0,56	0,50	2,13	0,78	0,53	0,45	0,58
		n	49	47	48	49	49	49	47	48	48
	Desc. Profile	Alpha [°]	1,01	0,99	0,96	0,77	0,80	0,93	0,86	1,05	0,96
		Std. deviation	0,92	0,71	0,73	0,50	0,58	0,93	0,44	1,24	0,48
		n	49	48	48	48	49	49	47	45	48
	Asc. Profile	Beta [°]	1,27	1,11	1,19	1,28	1,05	1,15	1,25	1,29	1,49
		Std. deviation	0,92	0,78	0,74	1,31	0,49	0,70	0,52	0,64	0,82
		n	49	47	48	49	48	49	46	48	48
	Desc. Profile	Beta [°]	1,29	1,21	1,24	1,15	1,37	1,33	1,36	1,31	1,63
		Std. deviation	0,95	0,63	0,82	0,58	1,49	0,88	0,80	0,53	1,29
		n	49	48	48	48	49	49	47	45	48
	Asc. Profile	Gamma [°]	2,00	1,85	1,84	1,72	1,92	2,00	1,92	1,90	2,02
		Std. deviation	1,87	1,46	1,30	1,29	1,56	1,47	1,44	1,11	1,12
		n	49	47	48	47	49	48	47	48	48
	Desc. Profile	Gamma [°]	1,87	2,10	1,84	1,74	1,82	1,96	1,85	2,05	2,17
		Std. deviation	1,42	1,67	1,31	1,51	1,56	1,47	1,10	1,86	1,24
		n	47	47	46	47	48	49	47	45	47

Frequencies

In the present section, the frequency means of the oscillations' principal mode at each speed from the relative motion thorax-head are introduced.

Figs. 3-36 (A and B) display the frequency variations of the cervical lateral flexion of males resp. females, related to velocity. Those of the flexion-extension and torsion are showed in figs. 3-36 (C and D) resp. figs. 3-37 (A and B).

Only with the exception of the significant differences observed between males and females for their flexion-extension after 4 km/h, the behaviour of frequency variations on the frontal, transverse as well as on the sagittal plane in males and females do not differ much from those already observed in the relative motions pelvis-thorax. This fact shows that the kinematical chain is preserved among the segments.

Thus, the graphs will not be explained in detail. The complete information about means, std. deviations and volunteers' number are condensed in tables 3-27 and 3-28.

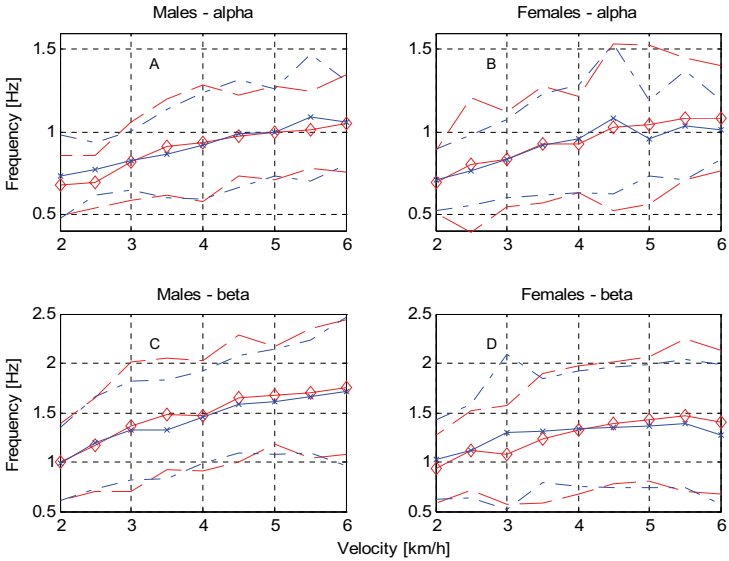

Figure 3- 36 Oscillations' principal mode of the lat. tilt (A and B) and frontal tilt (B and C) of the trunk of male resp. female volunteers, related to velocity.

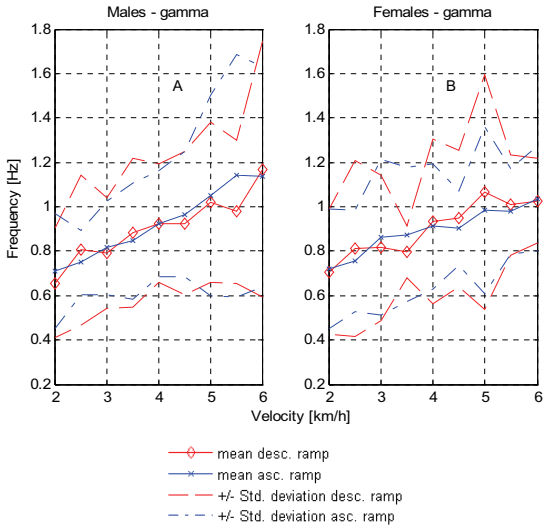

Figure 3- 37 Oscillations' principal mode of the cervical torsion of male (A) and female (B) volunteers, related to velocity.

Table 3- 27 Frequencies of cervical rotations (males)

		Speed	2 km/h	2,5 km/h	3 km/h	3,5 km/h	4 km/h	4,5 km/h	5 km/h	5,5 km/h	6 km/h
Frequencies of cervical rotations (males)	Asc. Profile	Alpha [Hz]	0,73	0,77	0,83	0,87	0,92	0,99	1,00	1,09	1,05
		Std. deviation	0,25	0,16	0,18	0,27	0,32	0,33	0,26	0,39	0,25
		n	52	51	49	51	51	52	51	52	52
	Desc. Profile	Alpha [Hz]	0,67	0,69	0,82	0,91	0,93	0,98	0,99	1,01	1,05
		Std. deviation	0,19	0,16	0,24	0,29	0,36	0,25	0,29	0,23	0,30
		n	52	54	53	53	52	49	51	53	50
	Asc. Profile	Beta [Hz]	0,98	1,20	1,32	1,33	1,46	1,59	1,61	1,66	1,72
		Std. deviation	0,37	0,47	0,50	0,50	0,47	0,49	0,54	0,57	0,75
		n	52	51	49	51	51	52	51	52	52
	Desc. Profile	Beta [Hz]	1,00	1,17	1,36	1,48	1,46	1,64	1,68	1,70	1,76
		Std. deviation	0,39	0,48	0,65	0,57	0,56	0,64	0,49	0,66	0,69
		n	52	54	53	53	52	49	51	53	50
	Asc. Profile	Gamma [Hz]	0,71	0,75	0,82	0,85	0,92	0,97	1,05	1,14	1,14
		Std. deviation	0,26	0,14	0,21	0,26	0,24	0,28	0,45	0,55	0,50
		n	52	51	49	51	51	52	51	52	52
	Desc. Profile	Gamma [Hz]	0,66	0,81	0,79	0,88	0,93	0,93	1,02	0,98	1,17
		Std. deviation	0,25	0,34	0,25	0,34	0,26	0,32	0,36	0,32	0,57
		n	52	54	53	53	52	49	51	53	50

Table 3- 28 Frequencies of cervical rotations (females)

		Speed	2 km/h	2,5 km/h	3 km/h	3,5 km/h	4 km/h	4,5 km/h	5 km/h	5,5 km/h	6 km/h
Frequencies of cervical rotations (females	Asc. Profile	Alpha [Hz]	0,71	0,77	0,83	0,92	0,96	1,08	0,96	1,04	1,01
		Std. deviation	0,19	0,21	0,24	0,31	0,32	0,46	0,23	0,33	0,18
		n	49	47	48	49	49	49	48	48	48
	Desc. Profile	Alpha [Hz]	0,69	0,80	0,83	0,92	0,92	1,03	1,04	1,08	1,08
		Std. deviation	0,19	0,41	0,29	0,35	0,29	0,51	0,48	0,37	0,32
		n	49	48	48	48	49	49	47	45	48
	Asc. Profile	Beta [Hz]	1,02	1,11	1,30	1,32	1,34	1,35	1,36	1,39	1,28
		Std. deviation	0,40	0,48	0,79	0,52	0,59	0,61	0,63	0,65	0,71
		n	49	47	48	49	49	49	48	48	48
	Desc. Profile	Beta [Hz]	0,93	1,12	1,07	1,24	1,32	1,39	1,43	1,47	1,40
		Std. deviation	0,34	0,40	0,49	0,66	0,65	0,61	0,63	0,77	0,73
		n	49	48	48	48	49	49	47	45	48
	Asc. Profile	Gamma [Hz]	0,72	0,76	0,86	0,88	0,91	0,90	0,98	0,98	1,04
		Std. deviation	0,27	0,23	0,35	0,30	0,28	0,17	0,38	0,19	0,23
		n	49	47	48	49	49	49	48	48	48
	Desc. Profile	Gamma [Hz]	0,71	0,81	0,82	0,80	0,93	0,95	1,07	1,01	1,03
		Std. deviation	0,28	0,40	0,33	0,12	0,37	0,31	0,53	0,23	0,19
		n	49	48	48	48	49	49	47	45	48

Cervical phase shift angles

Phase shift angles between rotations of thorax and head were calculated using the head as base. The interval ($-\pi$, π) was chosen, in order to obtain normal distributions at each velocity. Phase variations are displayed as: lateral tilt, sagittal tilt and axial rotation phases between head and thorax.

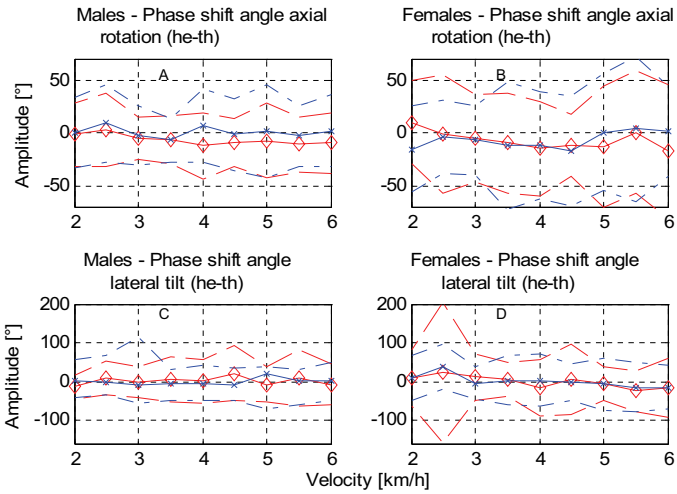

Figure 3- 38 Phase shift angles between head (as base) and thorax. A y B phases between head and thoracic axial rotation of males resp. females. C y D phases between head and thoracic lat. tilt of males resp. females.

Phase shift angles between head and thoracic axial rotations (figs. 3-38 A and B) are almost synchronic motions, with the tendency that head drives the thorax. Paths related to speed can not easily be found. Similar behaviour can be observed for the lat. tilt phases (figs. 3-38 C and D), although some means appear on the positive side, indicating that shoulders can also drive the head.

Motions around the transversal axis also are driven by the head (see figs. 3-39 A and B). From the graphs may be concluded, that the delay in trunk's motion increases with the velocity until 5 km/h. At higher velocities, the phase shift angles decrease in males and females.

As presented in the previous figures, the head does not compensate the motions of the trunk during normal gait. That means that for fixation of far-away objects, the compensation of the motions must be made by the eyes.

All the information about phase shift angles, their std. deviations and volunteer numbers are condensed in tables 3-29 and 3-30.

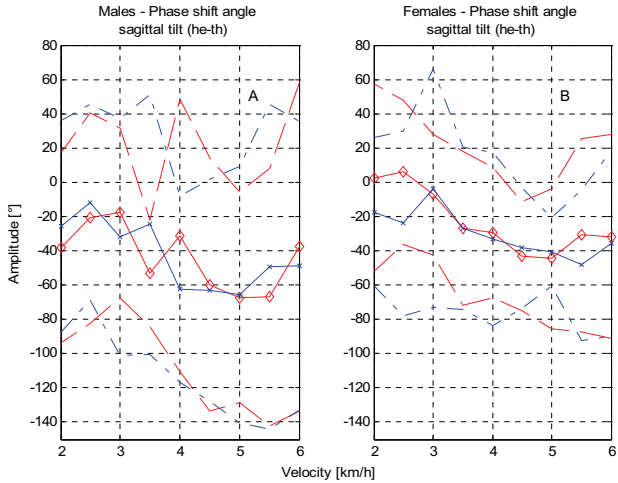

Figure 3- 39 Phase shift angles between sagittal tilt of head (as base) and thorax of male and female volunteers (A resp. B).

Table 3- 29 Phase shift angles between cervical rotations (males)

Phase shift angles of cervical rotations (males)		Speed	2 km/h	2,5 km/h	3 km/h	3,5 km/h	4 km/h	4,5 km/h	5 km/h	5,5 km/h	6 km/h
	Asc. Profile	Axial rotation [°]	-0,37	8,75	-2,62	-6,99	6,50	-1,86	1,76	-3,04	1,73
		Std. deviation	33,17	36,91	27,50	20,44	34,92	33,84	43,99	28,77	33,93
		n	44	47	43	45	48	45	45	46	47
	Desc. Profile	Axial rotation [°]	-1,57	2,74	-5,13	-6,92	-12,49	-9,40	-7,49	-11,13	-9,50
		Std. deviation	30,23	34,37	19,69	22,93	31,80	22,09	35,14	26,23	28,58
		n	48	50	42	46	45	40	43	38	44
	Asc. Profile	Lateral tilt [°]	2,77	-1,85	-8,76	-6,17	-4,50	-9,24	20,94	3,41	3,63
		Std. deviation	44,71	33,79	47,99	41,53	44,66	40,23	93,15	63,79	52,88
		n	46	36	36	35	42	34	39	38	35
	Desc. Profile	Lateral tilt [°]	-13,58	7,97	-2,62	5,24	0,34	20,73	-7,27	9,63	-8,05
		Std. deviation	31,51	43,80	40,10	58,71	57,67	71,33	45,53	73,94	52,48
		n	43	44	44	40	36	31	39	37	38
	Asc. Profile	Frontal tilt [°]	-25,45	-11,64	-31,87	-24,56	-62,58	-62,96	-65,38	-49,47	-48,66
		Std. deviation	61,61	56,84	69,23	75,61	54,10	64,92	74,71	94,63	84,06
		n	15	20	14	15	25	27	30	30	29
	Desc. Profile	Frontal tilt [°]	-38,41	-20,77	-17,81	-52,81	-31,15	-59,68	-67,22	-67,01	-37,61
		Std. deviation	55,48	61,42	49,32	31,21	79,53	74,00	61,55	75,14	95,81
		n	23	27	26	18	22	24	30	33	28

Table 3- 30 Phase shift angles between cervical rotations (females)

Phase shift angles of cervical rotations (female		Speed	2 km/h	2,5 km/h	3 km/h	3,5 km/h	4 km/h	4,5 km/h	5 km/h	5,5 km/h	6 km/h
	Asc. Profile	Axial rotation [°]	-15,40	-3,78	-6,81	-11,88	-12,26	-17,40	0,21	3,63	0,98
		Std. deviation	40,71	34,69	32,60	60,00	50,65	52,08	55,36	69,30	42,69
		n	37	36	34	39	32	41	34	30	35
	Desc. Profile	Axial rotation [°]	9,48	-1,21	-5,46	-9,66	-15,25	-12,09	-13,58	0,47	-16,95
		Std. deviation	39,34	55,65	41,12	47,28	45,07	29,69	57,06	57,98	62,82
		n	39	39	36	32	36	32	34	27	38
	Asc. Profile	Lateral tilt [°]	9,11	37,99	-3,84	2,98	2,31	-1,83	-6,86	-14,83	-14,81
		Std. deviation	59,45	57,49	40,75	62,97	67,60	47,34	66,30	64,83	55,21
		n	31	28	27	23	25	30	26	21	22
	Desc. Profile	Lateral tilt [°]	8,65	23,86	11,41	5,37	-16,81	4,85	-4,92	-24,29	-14,78
		Std. deviation	71,72	181,27	58,94	43,77	73,30	90,34	43,48	53,03	76,32
		n	32	31	26	23	17	24	18	20	23
	Asc. Profile	Frontal tilt [°]	-17,24	-23,98	-3,55	-26,94	-33,20	-38,25	-40,59	-48,31	-35,44
		Std. deviation	43,21	54,10	69,26	47,35	50,29	35,19	20,00	44,13	54,32
		n	22	18	20	27	28	28	26	24	25
	Desc. Profile	Frontal tilt [°]	2,55	5,91	-7,16	-27,00	-29,59	-43,24	-44,40	-30,87	-31,77
		Std. deviation	54,65	41,97	35,40	44,77	37,96	31,74	40,81	56,50	59,47
		n	27	28	22	26	24	27	34	26	27

3.3 Anthropometry

The results of the descriptive statistics, performed on the anthropometrical data, display a normal distributed cohort of test-persons. As an example of that fact, the following histograms introduce the distribution of three different anthropometrical measurements. In addition, the mean and std. deviations of these measurements were compared to those published by Flügel, Greil & Sommer (1986) and presented in table 3-31. The complete series of histograms involving all anthropometrical measurements are presented in Appendix A.

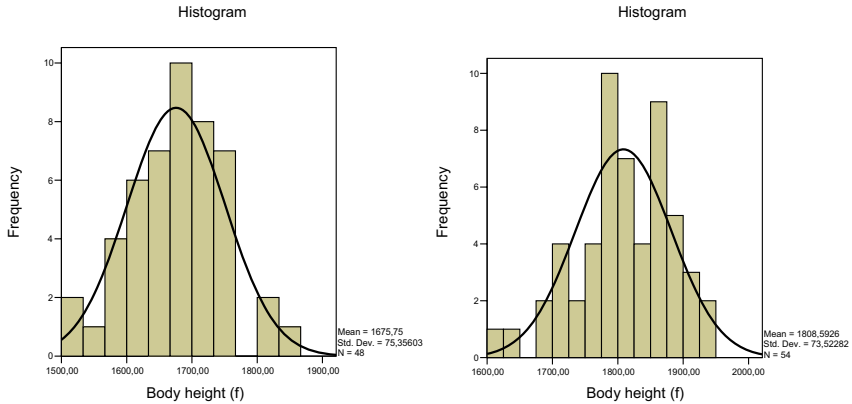

Figure 3- 40 Body height histograms obtained from own sample data. Left females, right males.

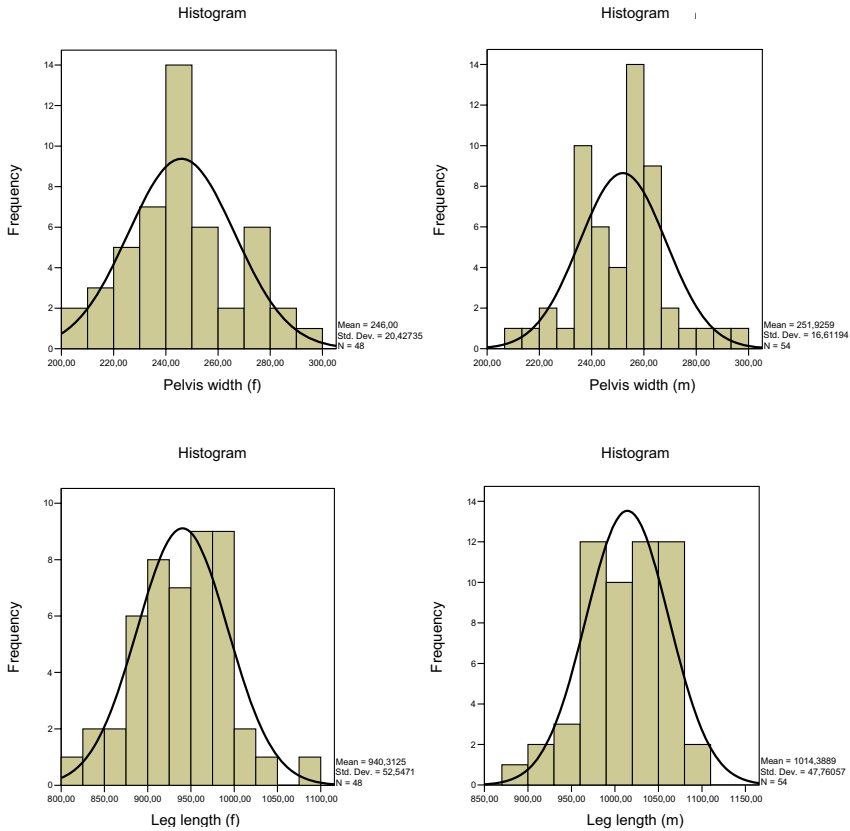

Figure 3- 41 Histograms. Upper left and right, pelvis width of female resp. male volunteers. Bottom left and right, leg length of female resp. male volunteers.

Table 3- 31 Comparison of own samples and data from Flügel/Greil/Sommer (1986)

All measurements in [mm]	Females, own sample	Females, reference	Males, own sample	Males, reference
Body height	1676 +/- 75	1644	1809 +/- 74	1763
Pelvis width (bicristal)	246 +/- 20	284	252 +/- 17	299

"…all things have form, all things are form, and all forms can be defined by numbers"
Pythagoras

Chapter 4: Interdependencies of trunk motion and anthropometry in humans

4.1 Introduction

During human walking the trunk interacts with its extremities. At the energetically optimal speed for each person (3,5 - 4 km/h from Cavagna et al. 1977) appears a dent in the shape of the torsion's curve of the trunk (see Witte 1996), indicating the use of the resonance phenomena. Following the mechanical concepts of resonant systems currently under discussion for human locomotion (suspended, inverted and torsion pendulums, spring-mass systems) and observing their frequency and motions equations, **a high correlation between kinematics and anthropometry may be hypothesised**.

In order to prove this assumption, statistical tests were performed involving kinematical and biometrical data from the 106 volunteers at the energetically optimal velocity (4 km/h). The tests performed included linear and non-linear correlations, linear regressions, uni-and multivariate ANOVAs. All tests were performed using SPSS® 12 and 13.

This chapter presents the results of these calculations in a similar way used to show the results of kinematical data (chapter 3), that means divided in pelvis, thorax and pelvis-thorax, but this time separated in males and females.

Because of the abundance of computed data, not all results can be displayed. We will focus on the statistical test presentation to the relations between kinematical and biometrical data, related to the actual models of bipedal walking. The fact that other parameters are not shown, does not mean that tests were not performed. It means that those tests did not show any kind of correlation.

4.2 Pelvis

Based on the already discussed bipedal models like ballistic walking or inverted pendulum, pelvic rotations, translations and frequencies may be related to anthropometrical data like leg length, pelvis width, sqr. root of leg length, body height or segmental mass properties.

As explained in previous chapters, the meanings of the Cardan angles for pelvis are: α= axial rotation, β= frontal tilt and γ= lateral tilt. Translations are: x= in sagittal axis, y= in transversal axis and z= longitudinal axis. In the scatter plots, angles are in degrees [°], translations and biometrical data in mm, and frequencies in [Hz].

4.2.1 Females

In following scatter plots (figs. 4-1 and 4-2) it may be observed, that there is no easy connection between females' biometry and their pelvic motions. In addition, different models like sq. root from leg length with the frequency or inertial moments did not show any correlation. Only when motions were compared, some correlations were observed.

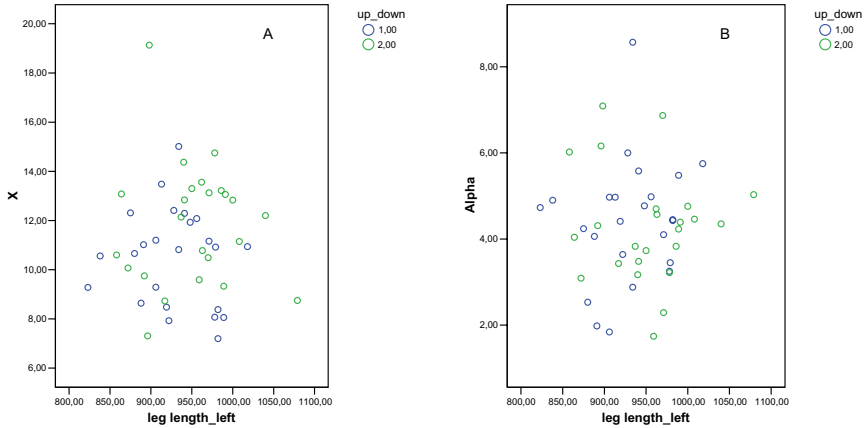

Figure 4- 1 Scatter plots A: pelvic translations in sagittal axis related to leg length. B: pelvic lat. tilt related to leg length.

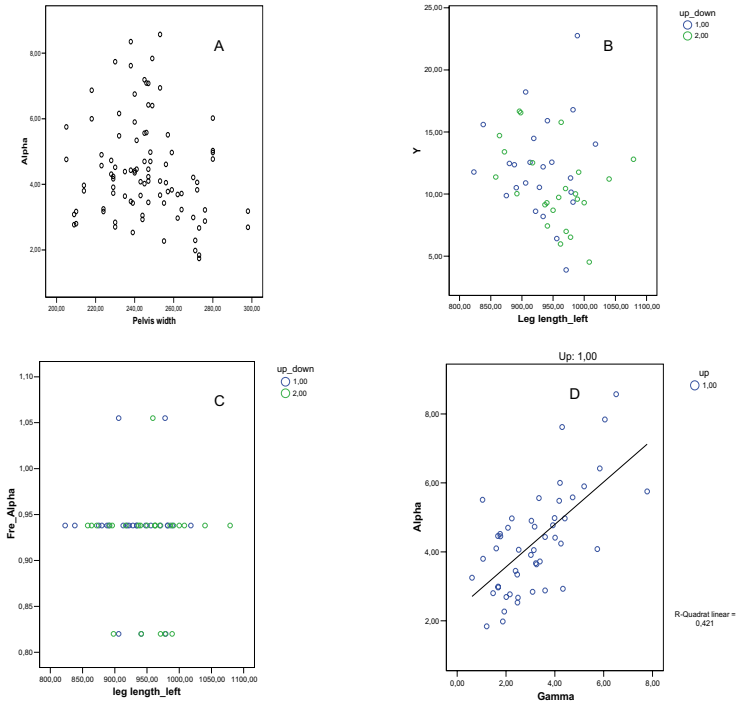

Figure 4- 2 Scatter plots A: pelvic lat.tilt, related to pelvis width. B: pelvic translation in transversal axis, related to leg length. C: Lat. tilt pelvic frequencies, related to leg length. D: Pelvic lat. tilt related to pelvic axial rotation.

For instance between lat. flexion (alpha) and axial rotation (gamma), indicating a linear interconnection between these rotations. The larger the pelvic axial rotations are, the larger are their lat. tilts (see fig. 4-2 D).

To get a more general and complete view of the relations between pelvic motions and anthropometry in both profiles, tables 4-1 to 4-6 introduce first correlations between rotation and translation amplitudes, after that, those between rotation and translation frequencies, followed by correlations between motion amplitudes and motion frequencies. The tables 4-7 to 4-10 display correlation coefficients between anthropometry and motion frequencies and between anthropometry and motion amplitudes.

The tables were filled out following the bellows mentioned criteria:

Only correlations with significant values lower than p=0,05 were included.

Fields not fulfilling the above mentioned criteria were painted in grey.

Table 4- 1 correlations between pelvic rotations and translations (females, profile: upwards)

upwards		Alpha_B	Beta_B	Gamma_B	X_B	Y_B	Z_B
Alpha_B	Corr.	1		0,649			
	Sig	0,000		0,000			
Beta_B	Corr.		1		0,350		0,288
	Sig		0,000		0,012		0,045
Gamma_B	Corr.	0,649		1	0,330		
	Sig.	0,000		0,000	0,021		
X_B	Corr.			0,330	1		
	Sig			0,021	0,000		
Y_B	Corr.					1	0,337
	Sig					0,000	0,018
Z_B	Corr.		0,288			0,337	1
	Sig.		0,045			0,018	0,000

Table 4- 2 correlations between pelvic rotations and translations (females, profile: downwards)

downwards		Alpha_B	Beta_B	Gamma_B	X_B	Y_B	Z_B
Alpha_B	Corr.	1		0,555		0,394	
	Sig	0,000		0,000		0,006	
Beta_B	Corr.		1				
	Sig		0,000				
Gamma_B	Corr.	0,555		1			
	Sig.	0,000		0,000			
X_B	Corr.				1		0,364
	Sig	0,394			0,000		0,011
Y_B	Corr.	0,006				1	
	Sig					0,000	
Z_B	Corr.				0,364		1
	Sig.				0,011		0,000

In tables 4-1 and 4-2 can be observed, that only with the exception of the correlations between pelvic lat. flexion and axial rotation, relations between pelvic motions vary depending on their profiles. That could display an adaptation mechanism in which the volunteer changes motion relations depending whether velocities are going faster or slower. On the other hand, relations between motion frequencies (tables 4-3 and 4-4) did not show significant variations related to profiles. These tables display also, that pelvic frontal tilt frequencies do not correlate with the others.

Table 4- 3 correlations between frequencies of pelvic rotations and translations (females, profile: upwards)

Upwards		Fre_A_B	Fre_B_B	Fre_G_B	Fre_X_B	Fre_Y_B	Fre_Z_B
Fre_A_B	Corr.	1		0,345	0,726	0,915	0,726
	Sig	0,000		0,015	0,000	0	0,000
Fre_B_B	Corr.		1				
	Sig		0,000				
Fre_G_B	Corr.	0,345		1	0,413	0,333	0,413
	Sig.	0,015		0,000	0,003	0,019	0,003
Fre_X_B	Corr.	0,726		0,413	1	0,726	1,000
	Sig	0,000		0,003	0,000	0,000	0,000
Fre_Y_B	Corr.	0,915		0,333	0,726	1	0,726
	Sig	0		0,019	0,000	0,000	0,000
Fre_Z_B	Corr.	0,726		0,336	1,000	0,726	1
	Sig.	0,000		0,018	0,000	0,000	0,000

Table 4- 4 correlations between frequencies of pelvic rotations and translations (females, profile: downwards)

Downwards		Fre_A_B	Fre_B_B	Fre_G_B	Fre_X_B	Fre_Y_B	Fre_Z_B
Fre_A_B	Corr.	1		0,376	0,607	0,924	0,614
	Sig	0,000		0,008	0,000	0,000	0,000
Fre_B_B	Corr.		1				
	Sig		0,000				
Fre_G_B	Corr.	0,376		1	0,515	0,382	0,495
	Sig.	0,008		0,000	0,000	0,007	0,000
Fre_X_B	Corr.	0,607		0,515	1	0,614	0,983
	Sig	0,000		0,000	0,000	0,000	0,000
Fre_Y_B	Korr.	0,924		0,382	0,614	1	0,623
	Sig	0,000		0,007	0,000	0,000	0,000
Fre_Z_B	Corr.	0,614		0,480	0,983	0,623	1
	Sig.	0,000		0,000	0,000	0,000	0,000

Table 4- 5 correlations between pelvic rotations and translations and their frequencies (females, profile: upwards)

upwards		Fre_A_B	Fre_B_B	Fre_G_B	Fre_X_B	Fre_Y_B	Fre_Z_B
Alpha_B	Corr.						
	Sig						
Beta_B	Corr.						
	Sig						
Gamma_B	Corr.			-0,321			
	Sig.			0,024			
X_B	Corr.	-0,477		-0,301	-0,563	-0,494	-0,563
	Sig	0,001		0,035	0,000	0,000	0,000
Y_B	Corr.						
	Sig						
Z_B	Corr.						
	Sig.						

Tables 4-5 and 4-6 show that the pelvic motion frequencies are only related to the translation of the pelvis in the sagittal axis. That could mean that this motion generates the trunk oscillations' principal mode and all other frequencies related to the variations of this motion. Another conclusion is: the smaller sagittal translation

amplitudes are, the higher the frequencies will be. This fact is directly related to the step length.

Table 4- 6 correlations between pelvic rotations and translation and their frequencies (females, profile: downwards)

downwards		Fre_A_B	Fre_B_B	Fre_G_B	Fre_X_B	Fre_Y_B	Fre_Z_B
Alpha_B	Corr.					0,279	
	Sig					0,055	
Beta_B	Corr.						
	Sig						
Gamma_B	Corr.						
	Sig.						
X_B	Corr.	-0,408			-0,414	-0,401	-0,454
	Sig	0,004			0,003	0,005	0,001
Y_B	Corr.		0,352				
	Sig		0,014				
Z_B	Corr.						
	Sig.						

Table 4- 7 correlations between pelvic frequencies and anthropometry (females, profile: upwards)

upwards		Body height	Shoulder_height	Leg length	waist width
Fre_A_B	Corr.	-0,545	-0,516	-0,526	-0,347
	Sig	0,000	0,000	0,000	0,017
Fre_B_B	Corr.				
	Sig				
Fre_G_B	Corr.				-0,312
	Sig.				0,033
Fre_X_B	Corr.	-0,572	-0,556	-0,547	-0,544
	Sig	0,000	0,000	0,000	0,000
Fre_Y_B	Corr.	-0,638	-0,591	-0,598	-0,414
	Sig	0,000	0,000	0,000	0,004
Fre_Z_B	Corr.	-0,572	-0,556	-0,547	-0,544
	Sig.	0,000	0,000	0,000	0,000

Table 4- 8 correlations between pelvic frequencies and anthropometry (females, profile: downwards)

downwards		Body height	Shoulder_height	Leg length	waist width
Fre_A_B	Corr.	-0,451	-0,436	-0,474	
	Sig	0,001	0,002	0,001	
Fre_B_B	Corr.				
	Sig				
Fre_G_B	Corr.	-0,510	-0,483	-0,517	-0,321
	Sig.	0,000	0,001	0,000	0,028
Fre_X_B	Corr.	-0,543	-0,505	-0,551	-0,374
	Sig	0,000	0,000	0,000	0,010
Fre_Y_B	Corr.	-0,435	-0,421	-0,48	
	Sig	0,002	0,003	0,001	
Fre_Z_B	Corr.	-0,530	-0,487	-0,480	-0,374
	Sig.	0,000	0,003	0,001	0,010

In tables 4-7and 4-8 the results of the correlations between pelvic frequencies and anthropometry are introduced. Only with the exception of the pelvic frontal tilt, which did not show any correlation, frequencies of pelvic motions seem to follow the inverted pendulum laws. That means higher people make larger steps and consequently need lower frequencies for a determinate speed than small people.
Correlations between anthropometry and motion amplitudes (table 4-9 and 4-10) showed only for the ascending ramp some very small correlation coefficients related to the pelvic sagittal translations. On the other hand, if we take a look to the desc. ramp (table 4-10), no correlations will be found. With this evidence, it must be concluded that the pelvic motion arrangement of females can not be predicted form the anthropometry.

Table 4- 9 correlations between pelvic rotations and translations and anthropometry (females, profile: upwards)

upwards		Body height	Shoulder_height	Leg length	waist width
Alpha_B	Corr.				
	Sig				
Beta_B	Corr.				
	Sig				
Gamma_B	Corr.				
	Sig.				
X_B	Corr.	0,326	0,358	0,346	
	Sig	0,025	0,013	0,017	
Y_B	Corr.				
	Sig				
Z_B	Corr.				
	Sig.				

Table 4- 10 correlations between pelvic rotations and translations and anthropometry (females, profile: downwards)

downwards		Body height	Shoulder_height	Leg length	waist width
Alpha_B	Corr.				
	Sig				
Beta_B	Corr.				
	Sig				
Gamma_B	Corr.				
	Sig.				
X_B	Corr.				
	Sig				
Y_B	Corr.				
	Sig				
Z_B	Corr.				
	Sig.				

4.2.2 Males

Following tables display correlation coefficients among pelvic motions, frequencies and anthropometry of male volunteers, in the same way already introduced for the females.

By observing the correlations between pelvic rotations and translations of male volunteers (tables 4-11 and 4-12), it will be clear that only one correlation is present in both profiles. While in females this was between lat. tilt and axial rotation, in males it is related to translations in sagittal and longitudinal axes. In males relations between lat. tilt and axial rotations are only observed for the desc. ramp. In this case, it can also be inferred that volunteers change motions arrangement, depending whether velocity are going up or down.

Relations among pelvic motion frequencies show similar behaviours in both profiles (tables 4-13 and 4-14). If we compare pelvic frequency correlations of males with those of females, pelvic axial rotation's frequencies of males are not (table 4-13) or less (table 4-14) related to other motion frequencies than those showed by females (tables 4-5 and 4-6). On the other hand, lat. tilt rotations' frequencies show very significant correlation coefficients with all translation frequencies. Finally, it can also be seen that translations frequencies in sagittal, frontal and transverse planes are strong linked.

Table 4- 11 correlations between pelvic rotations and translations (males, profile: upwards)

Upwards		Alpha_B	Beta_B	Gamma_B	X_B	Y_B	Z_B
Alpha_B	Corr.	1					
	Sig	0,000					
Beta_B	Corr.		1		0,350		
	Sig		0,000		0,012		
Gamma_B	Corr.			1		0,456	
	Sig.			0,000		0,001	
X_B	Corr.		0,350		1		0,474
	Sig		0,012		0,000		0,000
Y_B	Corr.			0,456		1	
	Sig			0,001		0,000	
Z_B	Corr.				0,474		1
	Sig.				0,000		0,000

Table 4- 12 correlations between pelvic rotations and translations (males, profile: downwards)

Downwards		Alpha_B	Beta_B	Gamma_B	X_B	Y_B	Z_B
Alpha_B	Corr.	1		0,344			
	Sig	0,000		0,012			
Beta_B	Corr.		1				
	Sig		0,000				
Gamma_B	Corr.	0,344		1			
	Sig.	0,012		0,000			
X_B	Corr.				1		0,612
	Sig				0,000		0,000
Y_B	Corr.					1	
	Sig					0,000	
Z_B	Corr.				0,612		1
	Sig.				0,000		0,000

Table 4- 13 correlations between frequencies of pelvic rotations and translations (males, profile: upwards)

Upwards		Fre_A_B	Fre_B_B	Fre_G_B	Fre_X_B	Fre_Y_B	Fre_Z_B
Fre_A_B	Corr.	1			0,743	0,962	0,727
	Sig	0,000			0,000	0,000	0,000
Fre_B_B	Corr.		1				
	Sig		0,000				
Fre_G_B	Corr.	0,345		1			
	Sig.	0,015		0,000			
Fre_X_B	Corr.	0,743			1	0,744	0,987
	Sig	0,000			0,000	0,000	0,000
Fre_Y_B	Corr.	0,962			0,744	1	0,726
	Sig	0,000			0,000	0,000	0,000
Fre_Z_B	Corr.	0,727			0,987	0,726	1
	Sig.	0,000			0,000	0,000	0,000

Table 4- 14 correlations between frequencies of pelvic rotations and translations (male, profile: downwards)

Downwards		Fre_A_B	Fre_B_B	Fre_G_B	Fre_X_B	Fre_Y_B	Fre_Z_B
Fre_A_B	Corr.	1		0,307	0,740	0,952	0,821
	Sig	0,000		0,025	0,000	0,000	0,000
Fre_B_B	Corr.		1				
	Sig		0,000				
Fre_G_B	Corr.	0,307		1		0,311	
	Sig.	0,025		0,000		0,024	
Fre_X_B	Corr.	0,740			1	0,733	1,000
	Sig	0,000			0,000	0,000	0,000
Fre_Y_B	Corr.	0,952		0,311	0,733	1	0,817
	Sig	0,000		0,024	0,000	0,000	0,000
Fre_Z_B	Corr.	0,821			1,000	0,817	1
	Sig.	0,000			0,000	0,000	0,000

Tables 4-15 and 4-16 show again that pelvic motion frequencies are related to pelvic translations in sagittal axis. They display also correlations with the translations in the longitudinal axis, but this can be related with the high correlation coefficients between sagittal and longitudinal translation frequencies (see table 4-13 and 4-14). Negative

correlation coefficients display agreement with the inverted pendulum frequency equations.

Table 4- 15 correlations between pelvic rotation and translation's frequencies (males, profile: upwards)

Upwards		Fre_A_B	Fre_B_B	Fre_G_B	Fre_X_B	Fre_Y_B	Fre_Z_B
Alpha_B	Corr.			-0,322			
	Sig			0,021			
Beta_B	Corr.						
	Sig						
Gamma_B	Corr.						
	Sig.						
X_B	Corr.	-0,609			-0,604	-0,615	-0,621
	Sig	0,000			0,000	0,000	0,000
Y_B	Corr.						
	Sig						
Z_B	Corr.	-0,482			-0,483	-0,400	-0,495
	Sig.	0,000			0,000	0,004	0,000

Table 4- 16 correlations between pelvic rotation and translation's frequencies (males, profile: downwards)

Downwards		Fre_A_B	Fre_B_B	Fre_G_B	Fre_X_B	Fre_Y_B	Fre_Z_B
Alpha_B	Corr.			-0,297			
	Sig			0,031			
Beta_B	Corr.						
	Sig						
Gamma_B	Corr.						
	Sig.						
X_B	Corr.	-0,589			-0,561	-0,593	-0,561
	Sig	0,000			0,000	0,000	0,000
Y_B	Corr.						
	Sig						
Z_B	Corr.	-0,367			-0,367	-0,376	-0,336
	Sig.	0,007			0,008	0,006	0,014

Table 4- 17 correlations between pelvic frequencies and anthropometry (males, profile: upwards)

Upwards		Body height	Shoulder height	Leg length	Pelvis width	Weigth Stand
Fre_A_B	Corr.		-0,291	-0,338		
	Sig		0,043	0,018		
Fre_B_B	Corr.				0,293	0,273
	Sig				0,041	0,058
Fre_G_B	Corr.					
	Sig.					
Fre_X_B	Corr.	-0,337	-0,366	-0,463		
	Sig	0,018	0,010	0,001		
Fre_Y_B	Corr.		-0,303	-0,358		
	Sig		0,034	0,012		
Fre_Z_B	Corr.	-0,337	-0,366	-0,463		
	Sig.	0,018	0,010	0,001		

In tables (4-17 and 4-18) the correlation coefficients between pelvic frequencies and anthropometry are introduced. By observing the tables can be also inferred, that pelvic motion frequencies are related to the inverted pendulum laws. Pelvic axial rotation frequencies of males showed that they are neither related to other frequencies nor to anthropometry.

Only with the exception of two very weak correlation coefficients obtained for the ascending ramp, no correlation coefficients among anthropometry and motion amplitudes could be found (tables 4-18 and 4-19). Like in female's case, pelvic motions of male volunteers can not be inferred form the anthropometry.

Table 4- 18 correlations between pelvic frequencies and anthropometry (males, profile: downwards)

Downwards		Body height	Shoulder height	Leg length	Pelvis width	Weigth Stand
Fre_A_B	Corr.	-0,292	-0,276	-0,412		
	Sig	0,038	0,050	0,003		
Fre_B_B	Corr.				0,314	
	Sig				0,025	
Fre_G_B	Corr.					
	Sig.					
Fre_X_B	Corr.	-0,364	-0,36	-0,452		
	Sig	0,009	0,010	0,001		
Fre_Y_B	Corr.	-0,308	-0,307	-0,45		
	Sig	0,028	0,028	0,001		
Fre_Z_B	Corr.	-0,302	-0,298	-0,412		
	Sig.	0,031	0,034	0,003		

Table 4- 19 correlations between pelvic rotations, translations and anthropometry (males, profile: upwards)

Upwards		Body height	Shoulder height	Leg length	Pelvis width	Weigth Stand
Alpha_B	Corr.					0,281
	Sig					0,050
Beta_B	Corr.					
	Sig					
Gamma_B	Corr.					
	Sig.					
X_B	Corr.					
	Sig					
Y_B	Corr.					0,264
	Sig					0,067
Z_B	Corr.					
	Sig.					

Table 4- 20 correlations between pelvic rotations, translations and anthropometry (males, profile: downwards)

Downwards		Body height	Shoulder height	Leg length	Pelvis width	Weigth Stand
Alpha_B	Corr.					
	Sig					
Beta_B	Corr.					
	Sig					
Gamma_B	Corr.					
	Sig.					
X_B	Corr.					
	Sig					
Y_B	Corr.					
	Sig					
Z_B	Corr.					
	Sig.					

4.3 Thorax

In thorax Cardan angles and translations have the same meaning as in pelvic motions. The tables were also fulfilled using the same criteria used for pelvic motions.

4.3.1 Females

In the following section, the correlations among thoracic motions, frequencies and body anthropometry of females will be explored.

By observing tables (4-21 and 4-22), it can be easily be seen, that thoracic rotations seem to be related between each other, that the same behaviour occurs among pelvic translations, but also that rotational motions are not related to the translational ones.

Table 4- 21 correlations between thoracic rotations and translation (females, profile: upwards)

		Ampl_alf_S	Ampl_bet_S	Ampl_gam_S	Ampl_x_S	Ampl_y_S	Ampl_z_S
Ampl_alf_S	Corr.	1	0,501	0,415			
	Sig.		0,000	0,003			
	N	49	49	49	49	49	49
Ampl_bet_S	Corr.	0,501	1	0,371			
	Sig.	0,000		0,009			
	N	49	49	49	49	49	49
Ampl_gam_S	Corr.	0,415	0,371	1			
	Sig.	0,003	0,009				
	N	49	49	49	49	49	49
Ampl_x_S	Corr.				1		0,657
	Sig.						0,000
	N	49	49	49	49	49	49
Ampl_y_S	Corr.					1	0,476
	Sig.						0,001
	N	49	49	49	49	49	49
Ampl_z_S	Corr.				0,657	0,476	1
	Sig.				0,000	0,001	
	N	49	49	49	49	49	49

Table 4- 22 correlations between thoracic rotations and translations (female, profile: downwards)

		Ampl_alf_S	Ampl_bet_S	Ampl_gam_S	Ampl_x_S	Ampl_y_S	Ampl_z_S
Ampl_alf_S	Corr.	1		0,640		0,303	
	Sig.			0,000		0,034	
	N	49	49	49	49	49	49
Ampl_bet_S	Corr.		1	0,404			
	Sig.			0,004			
	N	49	49	49	49	49	49
Ampl_gam_S	Corr.	0,640	0,404	1			
	Sig.	0,000	0,004				
	N	49	49	49	49	49	49
Ampl_x_S	Corr.				1		0,492
	Sig.						0,000
	N	49	49	49	49	49	49
Ampl_y_S	Corr.	0,303				1	0,318
	Sig.	0,034					0,026
	N	49	49	49	49	49	49
Ampl_z_S	Corr.				0,492	0,318	1
	Sig.				0,000	0,026	
	N	49	49	49	49	49	49

Table 4- 23 correlations among thoracic rotations, translations and their frequencies of female volunteers (profile: upwards)

		Freq_alf_S	Freq_bet_S	Freq_gam_S	Freq_x_S	Freq_y_S	Freq_z_S
Ampl_alf_S	Corr.						
	Sig.						
	N	49	49	49	49	49	49
Ampl_bet_S	Corr.	-0,251					
	Sig.	0,082					
	N	49	49	49	49	49	49
Ampl_gam_S	Corr.			0,278			
	Sig.			0,053			
	N	49	49	49	49	49	49
Ampl_x_S	Corr.			-0,333		-0,277	-0,509
	Sig.			0,019		0,054	0,000
	N	49	49	49	49	49	49
Ampl_y_S	Corr.		-0,321				
	Sig.		0,024				
	N	49	49	49	49	49	49
Ampl_z_S	Corr.			-0,275			
	Sig.			0,056			
	N	49	49	49	49	49	49

Table 4- 24 correlations among thoracic rotations, translations and their frequencies of female volunteers (profile: downwards)

		Freq_alf_S	Freq_bet_S	Freq_gam_S	Freq_x_S	Freq_y_S	Freq_z_S
Ampl_alf_S	Corr.						
	Sig.						
	N	49	49	49	49	49	49
Ampl_bet_S	Corr.	-0,396					
	Sig.	0,005					
	N	49	49	49	49	49	49
Ampl_gam_S	Corr.	-0,334		0,413			
	Sig.	0,019		0,003			
	N	49	49	49	49	49	49
Ampl_x_S	Corr.						-0,427
	Sig.						0,002
	N	49	49	49	49	49	49
Ampl_y_S	Corr.		-0,278				-0,322
	Sig.		0,053				0,024
	N	49	49	49	49	49	49
Ampl_z_S	Corr.				-0,306		-0,264
	Sig.				0,033		0,066
	N	49	49	49	49	49	49

In tables 4-23 and 4-24, the relations between motion amplitudes and motion frequencies are introduced. Only axial rotations are related to their frequencies. These coefficients are positive. Pelvic translations in the sagittal axis display correlations to pelvic longitudinal translation frequencies. On the other hand, thoracic rotation frequencies did not show significant correlations with biometrical data, some very small correlation coefficients appear in one, but not in both profiles (tables 4-25 and 4-26). Only translations in transversal and longitudinal axis show more interesting correlations coefficients. For these thoracic frequencies the most important factor seems to be the body height in inverted relation. This fact agrees also with the inverted pendulum laws.

Table 4- 25 correlations between thoracic frequencies and anthropometry (females, profile: upwards)

		Body height	Shoulder height_ri	Leg length_le	Shoulder width	Weight stand	Waist circumf.	Finger gipfel heigth_le	Waist width	Spine length	Thoracic circumf.
Freq_alf_S	Corr.				0,263						
	Sig.				0,074						
	N	47	47	47	47	47	47	47	47	47	47
Freq_bet_S	Corr.										
	Sig.										
	N	47	47	47	47	47	47	47	47	47	47
Freq_gam_S	Corr.						-0,249			-0,249	
	Sig.						0,091			0,092	
	N	47	47	47	47	47	47	47	47	47	47
Freq_x_S	Corr.								-0,245		
	Sig.								0,097		
	N	47	47	47	47	47	47	47	47	47	47
Freq_y_S	Corr.	-0,607	-0,565	-0,582	-0,386	-0,460	-0,290	-0,508	-0,349	-0,484	-0,248
	Sig.	0,000	0,000	0,000	0,007	0,001	0,048	0,000	0,016	0,001	0,093
	N	47	47	47	47	47	47	47	47	47	47
Freq_z_S	Corr.	-0,572	-0,556	-0,547	-0,368	-0,352	-0,329	-0,518	-0,544	-0,425	
	Sig.	0,000	0,000	0,000	0,011	0,015	0,024	0,000	0,000	0,003	
	N	47	47	47	47	47	47	47	47	47	47

Table 4- 26 correlations between thoracic frequencies and anthropometry (females, profile: downwards)

		Körperhöhe	Schulterhöhe_rechts	Beinhöhe_links	Schulterbreite	Gewicht_stehend	Beckenumfang	Fingerspitzenhöhe_links	Beckenbreite	Rumpfhöhe	Brustumfang
Freq_alf_S	Corr.										
	Sig.										
	N	47	47	47	47	47	47	47	47	47	47
Freq_bet_S	Corr.	-0,277			-0,312			-0,339			
	Sig.	0,059			0,033			0,020			
	N	47	47	47	47	47	47	47	47	47	47
Freq_gam_S	Corr.										
	Sig.										
	N	47	47	47	47	47	47	47	47	47	47
Freq_x_S	Corr				-0,354		-0,475		-0,372		-0,370
	Sig.				0,015		0,001		0,010		0,011
	N	47	47	47	47	47	47	47	47	47	47
Freq_y_S	Corr.	-0,294	-0,277	-0,270						-0,322	
	Sig.	0,045	0,059	0,066						0,027	
	N	47	47	47	47	47	47	47	47	47	47
Freq_z_S	Corr.	-0,530	-0,487	-0,523	-0,312	-0,414	-0,346	-0,499	-0,374	-0,474	
	Sig.	0,000	0,001	0,000	0,033	0,004	0,017	0,000	0,010	0,001	
	N	47	47	47	47	47	47	47	47	47	47

Tables 4-27 and 4-28 show that only thoracic translations are correlated with biometrical data. Furthermore, only thoracic translations in the transversal axis present relations in both profiles, where the most important factor seems to be the weight in standing position.

Table 4- 27 correlations among thoracic rotations, translations and anthropometry (females, profile: upwards)

		Body height	Shoulder height_ri	Leg length_le	Shoulder width	Weight stand	Waist circumf.	Finger gipfel heigth_le	Waist width	Spine length	Thoracic circumf.
Ampl_alf_S	Corr.				-0,326						
	Sig.				0,026						
	N	47	47	47	47	47	47	47	47	47	47
Ampl_bet_S	Corr.										
	Sig.										
	N	47	47	47	47	47	47	47	47	47	47
Ampl_gam_S	Corr.										
	Sig.										
	N	47	47	47	47	47	47	47	47	47	47
Ampl_x_S	Corr.					0,262	0,331				
	Sig.					0,075	0,023				
	N	47	47	47	47	47	47	47	47	47	47
Ampl_y_S	Corr.	0,254	0,262	0,288		0,481	0,420	0,355			0,343
	Sig.	0,085	0,076	0,050		0,001	0,003	0,014			0,018
	N	47	47	47	47	47	47	47	47	47	47
Ampl_z_S	Corr.					0,358	0,416				
	Sig.					0,014	0,004				
	N	47	47	47	47	47	47	47	47	47	47

a. Profil = 1,00

Table 4- 28 correlations among thoracic rotations, translations and anthropometry (females, profile: downwards)

		Body height	Shoulder height_ri	Leg length_le	Shoulder width	Weight stand	Waist circumf.	Finger gipfel heigth_le	Waist width	Spine length	Thoracic circumf.
Ampl_alf_S	Corr.										
	Sig.										
	N	47	47	47	47	47	47	47	47	47	47
Ampl_bet_S	Corr.										
	Sig.										
	N	47	47	47	47	47	47	47	47	47	47
Ampl_gam_S	Corr.										
	Sig.										
	N	47	47	47	47	47	47	47	47	47	47
Ampl_x_S	Corr.										
	Sig.										
	N	47	47	47	47	47	47	47	47	47	47
Ampl_y_S	Corr.		0,252	0,317		0,441	0,387	0,275	0,260		
	Sig.		0,088	0,030		0,002	0,007	0,061	0,077		
	N	47	47	47	47	47	47	47	47	47	47
Ampl_z_S	Corr.										
	Sig.										
	N	47	47	47	47	47	47	47	47	47	47

4.3.2 Males

While women did not display relations between thoracic rotations and translations, in males these relations are significant. As shown in tables 4-29 and 4-30, thoracic lateral flexions are not only related to other rotations but also with translations. Furthermore, axial rotations show correlations in both profiles with transversal translations and even frontal tilt display it self related to sagittal and longitudinal translations (desc. ramp). Another important point is the strong relations observed between sagittal and longitudinal translations. This fact was already observed for women too.

As observed for the relations between thoracic motions, thoracic frequencies are more related to each other for the downward profile (tables 4-31 and 4-32).

Table 4- 29 correlations between thoracic rotations and translation (males, profile: upwards)

Upwards		Alpha_S	Beta_S	Gamma_S	X_S	Y_S	Z_S
Alpha_S	Corr.	1		0,415		0,442	
	Sig	0,000		0,003		0,001	
Beta_S	Corr.		1				
	Sig		0,000				
Gamma_S	Corr.	0,415		1		0,283	
	Sig.	0,003		0,000		0,046	
X_S	Corr.				1		0,602
	Sig				0,000		0,000
Y_S	Corr.	0,442		0,283		1	
	Sig	0,001		0,046		0,000	
Z_S	Corr.				0,602		1
	Sig.				0,000		0,000

Table 4- 30 correlations between thoracic rotations and translation (males, profile: downwards)

Downwards		Alpha_S	Beta_S	Gamma_S	X_S	Y_S	Z_S
Alpha_S	Corr.	1	0,330	0,466	0,265	0,429	0,265
	Sig	0,000	0,016	0,000	0,055	0,001	0,055
Beta_S	Corr.	0,330	1		0,425		0,360
	Sig	0,016	0,000		0,002		0,008
Gamma_S	Corr.	0,466		1		0,377	
	Sig.	0,000		0,000		0,005	
X_S	Corr.	0,265	0,425		1		0,721
	Sig	0,055	0,002		0,000		0,000
Y_S	Corr.	0,429		0,377		1	
	Sig	0,001		0,005		0,000	
Z_S	Corr.	0,265	0,360		0,721		1
	Sig.	0,055	0,008		0,000		0,000

Table 4- 31 correlations between thoracic rotations and translations' frequencies (males, profile: upwards)

Upwards		Fre_A_S	Fre_B_S	Fre_G_S	Fre_X_S	Fre_Y_S	Fre_Z_S
Fre_A_S	Corr.	1		0,551		0,467	0,397
	Sig	0,000		0,000		0,001	0,004
Fre_B_S	Corr.		1	0,366			
	Sig		0,000	0,008			
Fre_G_S	Corr.	0,551	0,366	1		0,732	0,526
	Sig.	0,000	0,008	0,000		0,000	0,000
Fre_X_S	Corr.				1		
	Sig				0,000		
Fre_Y_S	Corr.	0,467		0,732		1	0,718
	Sig	0,001		0		0,000	0,000
Fre_Z_S	Corr.	0,397		0,526		0,718	1
	Sig.	0,004		0,000		0,000	0,000

Table 4- 32 correlations between of thoracic rotations and translations' frequencies (males, profile: downwards)

Downwards		Fre_A_S	Fre_B_S	Fre_G_S	Fre_X_S	Fre_Y_S	Fre_Z_S
Fre_A_S	Corr.	1		0,383	0,279	0,521	0,48
	Sig	0,000		0,005	0,043	0,000	0,000
Fre_B_S	Corr.		1			0,292	0,328
	Sig		0,000			0,034	0,017
Fre_G_S	Corr.	0,383		1	0,338	0,641	0,643
	Sig.	0,005		0,000	0,013	0,000	0,000
Fre_X_S	Corr.	0,279		0,338	1	0,433	0,512
	Sig	0,043		0,013	0,000	0,001	0,000
Fre_Y_S	Corr.	0,521	0,292	0,641	0,433	1	0,809
	Sig	0,000	0,034	0,000	0,001	0,000	0,000
Fre_Z_S	Corr.	0,480	0,328	0,643	0,512	0,809	1
	Sig.	0,000	0,017	0,000	0,000	0,000	0,000

Tables 4-33 and 4-34 introduce the results of correlations performed between motion amplitudes and their frequencies. Just a few correlations could be found, from these few ones, only the thoracic sagittal translations show correlation coefficients in both profiles with the same frequency. This frequency does not correspond to the sagittal translation but to longitudinal translation.

With the exception of the thoracic frontal tilt frequencies, all others show correlations with the anthropometrical data (tables 4-35 and 4-36) and with the expected negative coefficient, related to inverted pendulum laws. By means of these results can be conclude that the most important biometrical factors related to thoracic frequency variations seem to be leg length and shoulder height.

Even though thoracic rotation amplitudes like lat. tilt and frontal tilt show some interesting correlation coefficients (only for the ascending profile). Correlations between motions amplitudes and anthropometry show again that motions amplitudes are not simply defined by mass distribution or mass lengths (see tables 4-37 and 4-38).

Table 4- 33 correlations among thoracic rotations, translations and their frequencies (males, profile: upwards)

Upwards		Fre_A_S	Fre_B_S	Fre_G_S	Fre_X_S	Fre_Y_S	Fre_Z_S
Alpha_S	Corr.						
	Sig						
Beta_S	Corr.						
	Sig						
Gamma_S	Corr.						
	Sig.						
X_S	Corr.			-0,333			-0,509
	Sig			0,019			0
Y_S	Corr.		-0,321				
	Sig		0,025				
Z_S	Corr.						
	Sig.						

Table 4- 34 correlations among thoracic rotations, translations and their frequencies (males, profile: downwards)

Downwards		Fre_A_S	Fre_B_S	Fre_G_S	Fre_X_S	Fre_Y_S	Fre_Z_S
Alpha_S	Corr.						
	Sig						
Beta_S	Corr.	-0,396					
	Sig	0,005					
Gamma_S	Corr.	-0,334		0,413			
	Sig.	0,019		0,003			
X_S	Corr.						-0,427
	Sig						0,002
Y_S	Corr.						-0,322
	Sig						0,024
Z_S	Corr.				-0,306		
	Sig.				0,033		

Table 4- 35 correlations between thoracic frequencies and anthropometry (males, profile: upwards)

Upwards		Should. Height	Body height	Leg length	Spine length	Waist width	Weigth Stand
Fre_A_S	Corr.	-0,300					
	Sig	0,036					
Fre_B_S	Corr.						
	Sig						
Fre_G_S	Corr.	-0,373	-0,302	-0,394	-0,293		
	Sig.	0,008	0,035	0,005	0,041		
Fre_X_S	Corr.	-0,399	-0,343	-0,370		-0,391	-0,363
	Sig	0,005	0,016	0,009		0,005	0,010
Fre_Y_S	Corr.			-0,328			
	Sig			0,021			
Fre_Z_S	Corr.	-0,349	-0,318	-0,450			
	Sig.	0,014	0,026	0,001			

Table 4- 36 correlations between thoracic frequencies and anthropometry (males, profile: downwards)

Downwards		Body height	Shuold. height	Leg length	Spine length	Finger height
Fre_A_S	Corr.	-0,312	-0,321	-0,385		-0,278
	Sig	0,026	0,022	0,005		0,048
Fre_B_S	Corr.					
	Sig					
Fre_G_S	Corr.	-0,360	-0,315	-0,427	-0,317	
	Sig.	0,010	0,024	0,002	0,023	
Fre_X_S	Corr.	-0,274		-0,339		
	Sig	0,052		0,015		
Fre_Y_S	Corr.	-0,284	-0,277	-0,430		
	Sig	0,043	0,049	0,002		
Fre_Z_S	Corr.	-0,287	-0,283	-0,394		
	Sig.	0,041	0,044	0,004		

Table 4- 37 correlations among thoracic rotations, translations and anthropometry (males, profile: upwards)

Upwards		Body height	Shuold. height	Leg length	Spine length	weigth stand	Finger height
Alfa_S	Corr.	-0,352	-0,268	-0,278	-0,301		
	Sig	0,014	0,066	0,056	0,038		
Beta_S	Corr.	-0,413	-0,446	-0,424	-0,413		-0,408
	Sig	0,004	0,001	0,003	0,004		0,004
Gama_S	Corr.						
	Sig.						
X_S	Corr.					-0,328	
	Sig					0,023	
Y_S	Corr.						
	Sig						
Z_S	Corr.					-0,276	
	Sig.					0,058	

Table 4- 38 correlations among thoracic rotations, translations and anthropometry (males, profile: downwards)

Downwards		Finger heigth	Should. Height	Leg length	Spine length	Waist width	Weigth stand
Alfa_S	Corr.						
	Sig						
Beta_S	Corr.						
	Sig						
Gama_S	Corr.					-0,295	
	Sig.					0,036	
X_S	Corr.						-0,296
	Sig						0,035
Y_S	Corr.						
	Sig						
Z_S	Corr.						
	Sig.						

4.4 Relative motion pelvis-thorax

In previous sections (absolute motions of pelvis and thorax) was demonstrated that the motion arrangement of pelvis and thorax are not defined by mass distributions or mass lengths. It was also corroborated, that although motion frequencies display correlation coefficients according to the inverted pendulum laws, these coefficients are not strong enough, to permit the construction of regression models. Finally, it was verified that same rotations and translations are related to each other.
In the present section and in order to certificate the results obtained for the absolute motions from pelvis and thorax, the relative motions between them were analysed following the same proceedings. In addition, the phase shift angles between pelvis and thorax were correlated with the most important factors and their results are also presented.
The relative motions between pelvis and thorax were already discussed in section 3.2. In this section, it will be only necessary to re-explain the definition of the Cardan angles for the relative motions pelvis-thorax. [α] represents the lat. flexion, [β] the flexion-extension and [γ] the torsion between pelvis and thorax. The criteria used to fill the correlation tables are the same as those explained in p. 107.

4.4.1 Females

If correlations between absolute motions were difficult to find, we will see in the following tables, that those of the relative motions are even harder.
Relative rotations of female volunteers are very poor or not related to each other. They are also not related to pelvic or thoracic translations. Only the lat. flexion shows some correlations, but just for the downward profile, with flexion-extension and the thoracic translation in the transversal axis (see tables 4-39 and 4-40).
Relative rotations display also very weak correlations, if existent, with motion frequencies (table 4-41 and 4-42).

Table 4- 39 correlations between relative rotations (pelvis-thorax) and pelvic and thoracic translations (females, profile: upwards)

		Ampl_alf_S_B	Ampl_bet_S_B	Ampl_gam_S_B	Ampl_x_B	Ampl_y_B	Ampl_z_B	Ampl_x_S	Ampl_y_S	Ampl_z_S
Ampl_alf_S_B	Corr.	1						-0,264		
	Sig.							0,066		
	N	49	49	49	49	49	49	49	49	49
Ampl_bet_S_B	Corr.		1							
	Sig.									
	N	49	49	49	49	49	49	49	49	49
Ampl_gam_S_B	Corr.			1						
	Sig.									
	N	49	49	49	49	49	49	49	49	49

Table 4- 40 correlations between relative rotations (pelvis-thorax) and pelvic and thoracic translations (females, profile: downwards)

		Ampl_alf_S_B	Ampl_bet_S_B	Ampl_gam_S_B	Ampl_x_B	Ampl_y_B	Ampl_z_B	Ampl_x_S	Ampl_y_S	Ampl_z_S
Ampl_alf_S_B	Corr.	1	0,350						0,339	
	Sig.		0,014						0,017	
	N	49	49	49	48	48	48	49	49	49
Ampl_bet_S_B	Corr.	0,350	1							
	Sig.	0,014								
	N	49	49	49	48	48	48	49	49	49
Ampl_gam_S_B	Corr.			1						
	Sig.									
	N	49	49	49	48	48	48	49	49	49

Table 4- 41 and Table 4- 42 correlations between relative rotations (pelvis-thorax) and their frequencies (females, profiles: upwards resp. downwards)

		Freq_alf_S_B	Freq_bet_S_B	Freq_gam_S_B
Ampl_alf_S_B	Corr.	-0,367	-0,275	
	Sig.	0,010	0,056	
	N	49	49	49
Ampl_bet_S_B	Corr.			
	Sig.			
	N	49	49	49
Ampl_gam_S_B	Corr.	0,338		-0,254
	Sig.	0,017		0,078
	N	49	49	49

		Freq_alf_S_B	Freq_bet_S_B	Freq_gam_S_B
Ampl_alf_S_B	Corr.	-0,256		
	Sig.	0,075		
	N	49	49	49
Ampl_bet_S_B	Corr.			
	Sig.			
	N	49	49	49
Ampl_gam_S_B	Corr.			
	Sig.			
	N	49	49	49

Frequencies of the relative motions between pelvis and thorax are not determined by body mass and lengths (tables 4-43 and 4-44). Trunk's lat. flexion frequencies display only for the desc. ramp one significant correlation coefficient, which is related to shoulder width. But it must also be said, that these correlation coefficient is not a very weightily one.

Table 4- 43 and Table 4- 44 correlations between rotation frequencies (pelvis-thorax) and anthropometry (females, profiles: upwards resp. downwards)

		Body height	Shoulder hight_ri	Leg length_ri	Shoulder width	Pelvis width	Spine length
Freq_alf_S_B	Corr.						
	Sig.						
	N	47	47	47	47	47	47
Freq_bet_S_B	Corr.						
	Sig.						
	N	47	47	47	47	47	47
Freq_gam_S_B	Corr.						
	Sig.						
	N	47	47	47	47	47	47

		Body height	Shoulder hight_ri	Leg length_ri	Shoulder width	Pelvis width	Spine length
Freq_alf_S_B	Corr.				-0,345	-0,262	-0,266
	Sig.				0,018	0,075	0,071
	N	47	47	47	47	47	47
Freq_bet_S_B	Corr.						
	Sig.						
	N	47	47	47	47	47	47
Freq_gam_S_B	Corr.						
	Sig.						
	N	47	47	47	47	47	47

Table 4- 45 and Table 4- 46 correlations between relative rotations (pelvis-thorax) and anthropometry (females, profiles: upwards resp. downwards)

		Body height	Shoulder hight_ri	Leg length_le	Shoulder width	Pelvis width	Spine length
Ampl_alf_S_B	Corr.						
	Sig.						
	N	47	47	47	47	47	47
Ampl_bet_S_B	Corr.	-0,257			-0,256		
	Sig.	0,081			0,083		
	N	47	47	47	47	47	47
Ampl_gam_S_B	Corr.	-0,269		-0,280			
	Sig.	0,067		0,057			
	N	47	47	47	47	47	47

		Body height	Shoulder hight_ri	Leg length_le	Shoulder width	Pelvis width	Spine length
Ampl_alf_S_B	Corr.						
	Sig.						
	N	47	47	47	47	47	47
Ampl_bet_S_B	Corr.						
	Sig.						
	N	47	47	47	47	47	47
Ampl_gam_S_B	Corr.						
	Sig.						
	N	47	47	47	47	47	47

Not even one significant correlation could be found between trunk relative rotations and anthropometry (see tables 4-45 and 4-46). It must be then concluded that trunk relative motion's amplitudes of females are not predefined by body proportions.

For the asc. ramp, axial rotations' phase shift angles between pelvis and thorax display interesting negative correlation coefficients related to some anthropometrical data, in special leg length or body height. This fact could mean that large people need smaller phase shift angles between pelvis and thorax for the same gait velocity. Unfortunately these relations are not present for the desc. ramp, in which not even any significant correlation is present.

Table 4- 47and Table 4- 48 correlations between phase shift angles of rotations (pelvis-thorax) and anthropometry (females, profiles: upwards resp. downwards)

		Body height	Shoulder hight_ri	Leg length_ri	Shoulder width	Pelvis width	Spine length	Weight standing
Phi_gam_S_B	Corr.	-0,518	-0,521	-0,541			-0,465	
	Sig.	0,001	0,001	0,000			0,003	
	N	38	38	38	38	38	38	38
Phi_alph_S_B	Corr.							
	Sig.							
	N	34	34	34	34	34	34	34
Phi_bet_S_B	Corr.							
	Sig.							
	N	24	24	24	24	24	24	24

		Body height	Shoulder hight_ri	Leg length_ri	Shoulder width	Pelvis width	Spine length	Weight standing
Phi_gam_S_B	Corr.							
	Sig.							
	N	33	33	33	33	33	33	33
Phi_alph_S_B	Corr.					-0,323		
	Sig.					0,094		
	N	28	28	28	28	28	28	28
Phi_bet_S_B	Corr.							
	Sig.							
	N	24	24	24	24	24	24	24

Multivariate analyses

In order to model the influence and relationship of the different factors (like leg length, pelvis width, etc) to the dependent variables and to evaluate whether those variables could be related to the interaction of more factors, multivariate analysis ANOVAs were performed.

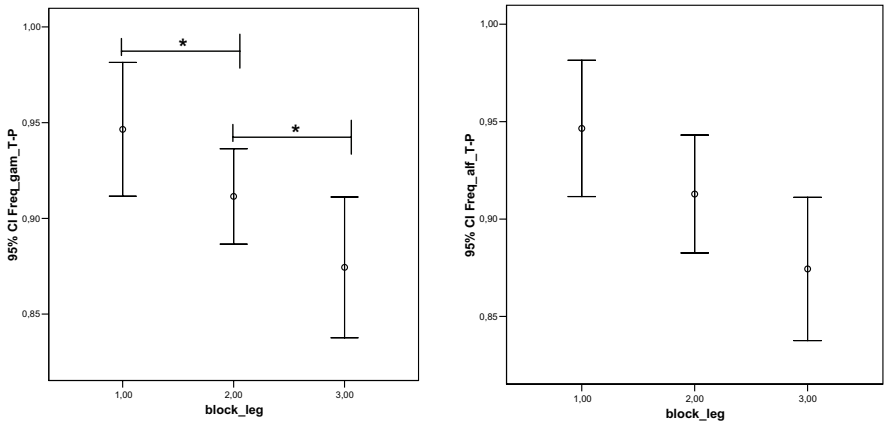

Figure 4- 3 Means and confidence intervals of: A) Freq. of torsion pelvis- thorax and B) Freq. of lat. flexion pelvis- thorax. Frequencies in Hz. Leg length divided in clusters, 1: short, 2: middle, 3: long legs (females).

As displayed before, correlations of pelvic and thoracic motion frequencies showed significant relationships to leg length and therefore to the inverted pendulum models.

On the other hand, trunk motions' frequencies did not show significant correlation coefficients related to anthropometry, but if the factor "leg length" is grouped in clusters like short, middle and long legs, trunk frequencies diminish in agreement to the inverted pendulum laws (see fig. 4-3).

To test the influence of leg length clusters on the trunk frequency variation in females, multivariate analysis were performed using leg length block as factor and the rotational frequencies as dependent variables.

The results of the ANOVA test show clearly that the factor block_leg has a significant influence of grad $p<0,05$ to the frequency variations of the lateral flexion and $p<0,01$ to those of the torsion of females' trunk (table 4-50). On the other hand, the results of the Levene test (table 4-49) display for the torsion frequency significance values below 0,1. This fact reveals that we should suspect that the factor (Freq_gam_SB) does not follow a normal distribution.

Table 4- 49 Levene test

	F	df1	df2	Signif.
Freq_alf_S_B	1,212	2	39	,309
Freq_bet_S_B	,232	2	39	,794
Freq_gam_S_B	3,742	2	39	,033

a Design: Intercept+block_leg

Table 4- 50 ANOVA tests

Source	Dependent variables	Square sum Typ III	df	Square middle	F	Significance
Revised model	Freq_alf_S_B	,034	2	,017	4,506	,017
	Freq_bet_S_B	,090	2	,045	,184	,832
	Freq_gam_S_B	,043	2	,021	7,635	,002
Constant term	Freq_alf_S_B	34,231	1	34,231	9155,378	,000
	Freq_bet_S_B	83,148	1	83,148	340,284	,000
	Freq_gam_S_B	34,303	1	34,303	12243,951	,000
block_leg	Freq_alf_S_B	,034	2	,017	4,506	,017
	Freq_bet_S_B	,090	2	,045	,184	,832
	Freq_gam_S_B	,043	2	,021	7,635	,002

For the lat. flexion frequencies, the Levene test returns values >0,3. That means that this data can be accepted as valid and therefore also the significant influence of the leg length to the lat. flexion's frequency variation. On the other hand, ANOVA tests for amplitudes of rotations and phase shift angles related to clusters like leg length, pelvis length, pelvis width, shoulder height, shoulder width, or body height did not return significant values (p>0,05). In addition, the interaction effect of the already mentioned factors did not show also any other significant influence on the above mentioned dependent variables.

Those results reinforce the already introduced evidence, that trunk motion amplitudes and sequences are not intensely determined by body anthropometry.

4.4.2 Males

In the last part of this chapter, the relations among anthropometry, trunk motions and trunk motion frequencies of male volunteers will be explored. As already presented for females, we will introduce at first the relations in form of correlation tables followed by the multivariate analyses (ANOVA).

Following similar behaviours already observed for women, male's relative rotations between pelvis and thorax are not related to each other. Only the trunk torsion

display significant correlations in both profiles to translations of pelvis and thorax. Lat. flexion show also correlations to translations but in this case only for the downward profile (see tables 4-51 and 4-52).

Table 4- 51 and Table 4- 52 correlations between relative rotations (pelvis-thorax) and pelvic and thoracic translations (females, profiles: upwards resp. downwards)

		Ampl_alf_S_B	Ampl_bet_S_B	Ampl_gam_S_B	Ampl_x_B	Ampl_y_B	Ampl_z_B	Ampl_x_S	Ampl_y_S	Ampl_z_S
Ampl_alf_S_B	Corr.	1								
	Sig.									
	N	50	50	50	50	50	50	50	50	50
Ampl_bet_S_B	Corr.		1							
	Sig.									
	N	50	50	50	50	50	50	50	50	50
Ampl_gam_S_B	Corr.			1		0,423	-0,423		0,389	
	Sig.					0,002	0,002		0,005	
	N	50	50	50	50	50	50	50	50	50

		Ampl_alf_S_B	Ampl_bet_S_B	Ampl_gam_S_B	Ampl_x_B	Ampl_y_B	Ampl_z_B	Ampl_x_S	Ampl_y_S	Ampl_z_S
Ampl_alf_S_B	Corr.	1			0,417	0,261	0,376	0,457		0,351
	Sig.				0,002	0,059	0,006	0,001		0,010
	N	53	53	53	53	53	53	53	53	53
Ampl_bet_S_B	Corr.		1							
	Sig.									
	N	53	53	53	53	53	53	53	53	53
Ampl_gam_S_B	Corr.			1		0,276	-0,313		0,346	
	Sig.					0,045	0,022		0,011	
	N	53	53	53	53	53	53	53	53	53

Tables 4-53 and 4-54 introduce the results of the correlations between relative rotations and their frequencies as well as the correlations between these frequencies. Only with the exception of the flexion extension (profile: downward), which shows a weak correlation coefficient related to the lateral flexion frequency, the correlation tables display clearly, that neither trunk rotation amplitudes are related to their frequencies nor these frequencies between each other.

If we observe the results of the correlations between trunk rotation frequencies and anthropometry (tables 4-55 and 4-56), trunk lateral flexion's frequencies displays dependencies in sense of the inverted pendulum laws. The most influent factors are body height and shoulder height. Trunk torsion's frequencies display also dependencies on anthropometry, but in this case only for the descending ramp. The factor, which seems to have more influence in the variation of trunk torsion's frequencies, is the leg length.

In the results of the correlations between trunk's relative rotations and anthropometry (tables 4-57 and 4-58) appear some unexpected correlation coefficients displaying

interdependencies of trunk flexion extension's amplitudes and factors like leg length, body height or shoulder height. These correlation coefficients are present only for the ascending ramp.

Table 4- 53 and Table 4- 54 correlations between relative rotations (pelvis-thorax) and their frequencies as well as correlations between rotational frequencies (females, profiles: upwards resp. downwards)

		Freq_alf_S_B	Freq_bet_S_B	Freq_gam_S_B
Ampl_alf_S_B	Corr.			
	Sig.			
	N	50	50	50
Ampl_bet_S_B	Corr.			
	Sig.			
	N	50	50	50
Ampl_gam_S_B	Corr.	0,277		
	Sig.	0,052		
	N	50	50	50
Freq_alf_S_B	Corr.	1		
	Sig.			
	N	50	50	50
Freq_bet_S_B	Corr.		1	
	Sig.			
	N	50	50	50
Freq_gam_S_B	Corr.			1
	Sig.			
	N	50	50	50

		Freq_alf_S_B	Freq_bet_S_B	Freq_gam_S_B
Ampl_alf_S_B	Corr.			
	Sig.			
	N	53	53	53
Ampl_bet_S_B	Corr.	0,297		
	Sig.	0,031		
	N	53	53	53
Ampl_gam_S_B	Corr.			0,259
	Sig.			0,061
	N	53	53	53
Freq_alf_S_B	Corr.	1		
	Sig.			
	N	53	53	53
Freq_bet_S_B	Corr.		1	
	Sig.			
	N	53	53	53
Freq_gam_S_B	Corr.			1
	Sig.			
	N	53	53	53

For the descending ramp is the panorama again the same as observed for all the cases before, not even any significant correlation between motion amplitudes and anthropometry. This fact shows again, how important the change of the motion paths between the profiles can be but also that trunk rotation's amplitudes can not be inferred from anthropometry.

To fill the tables 4-59 and 4-60, the results of the phase shift angles between pelvic and thoracic rotations were correlated with biometrical data.

We saw in chapter 3 that phase shift angles between pelvic and thoracic frontal tilt in males at 4 km/h is about 20°, and now adding the results obtained for their correlations with the biometrical data, it will be possible to fulfil the panorama by saying that this phase will be smaller in higher persons.

Axial rotation's phase shift angles display significant correlations with the weight at standing position, but only for the ascending ramp.

Table 4- 55 and Table 4- 56 correlations between rotation frequencies (pelvis-thorax) and anthropometry (males, profiles: upwards resp. downwards)

		Body height	Shoulder height_le	Leg length_ri	Shoulder width	Pelvis width	Spine length
Freq_alf_S_B	Corr.	-0,358	-0,364	-0,332			-0,351
	Sig.	0,013	0,011	0,021			0,015
	N	48	48	48	48	48	48
Freq_bet_S_B	Corr.						
	Sig.						
	N	48	48	48	48	48	48
Freq_gam_S_B	Corr.						
	Sig.						
	N	48	48	48	48	48	48

		Body height	Shoulder height_le	Leg length_ri	Shoulder width	Pelvis width	Spine length
Freq_alf_S_B	Corr.	-0,395	-0,384	-0,377			-0,364
	Sig.	0,004	0,005	0,006			0,009
	N	51	51	51	51	51	51
Freq_bet_S_B	Corr.						
	Sig.						
	N	51	51	51	51	51	51
Freq_gam_S_B	Corr.	-0,273		-0,336			-0,295
	Sig.	0,052		0,016			0,036
	N	51	51	51	51	51	51

Table 4- 57 and Table 4- 58 correlations between rotation amplitudes (pelvis-thorax) and anthropometry (males, profiles: upwards resp. downwards)

		Body height	Shoulder height	Leg lenth_ri	Spine length	Weight standing
Ampl_alf_S_B	Corr.					
	Sig.					
	N	48	48	48	48	48
Ampl_bet_S_B	Corr.	-0,490	-0,502	-0,518	-0,354	-0,316
	Sig.	0,000	0,000	0,000	0,014	0,029
	N	48	48	48	48	48
Ampl_gam_S_B	Corr.					
	Sig.					
	N	48	48	48	48	48

		Body height	Shoulder height	Leg lenth_ri	Spine length	Weight standing
Ampl_alf_S_B	Corr.					
	Sig.					
	N	51	51	51	51	51
Ampl_bet_S_B	Corr.					
	Sig.					
	N	51	51	51	51	51
Ampl_gam_S_B	Corr.					0,257
	Sig.					0,069
	N	51	51	51	51	51

Multivariate analyses

Male's trunk frequencies displayed more correlations with anthropometry than those showed by female volunteers. Therefore it will be important to confirm this evidence with a multivariate analysis, and also to check whether other significant dependencies can be found.

As already done for female volunteers, the leg length of male volunteers was grouped in three clusters. The first includes males with leg lengths up to 970 mm, the second males with leg lengths from 971 mm up to 1020 and the third one, males with leg lengths larger than 1020 mm.

In fig. 4-4, the means and 95 % confidence interval of the lat. flexion and torsion frequencies through the clusters are introduced. As expected, those frequencies show decrements, as we move form short to long legs.

Table 4- 59 and Table 4- 60 correlations between phase shift angles of rotations (pelvis-thorax) and anthropometry (males, profiles: upwards resp. downwards)

		Body height	Shoulder height_le	Leg length_ri	Shoulder width	Pelvis width	Spine length	Weight standing
Phi_gam_S_B	Corr.							0,344
	Sig.							0,026
	N	42	42	42	42	42	42	42
Phi_alph_S_B	Corr.							
	Sig.							
	N	46	46	46	46	46	46	46
Phi_bet_S_B	Corr.	-0,407	-0,421	-0,429				
	Sig.	0,023	0,018	0,016				
	N	31	31	31	31	31	31	31

		Body height	Shoulder height_le	Leg length_ri	Shoulder width	Pelvis width	Spine length	Weight standing
Phi_gam_S_B	Corr.					0,293		
	Sig.					0,057		
	N	43	43	43	43	43	43	43
Phi_alph_S_B	Corr.							
	Sig.							
	N	44	44	44	44	44	44	44
Phi_bet_S_B	Corr.	-0,403	-0,409	-0,358			-0,366	-0,338
	Sig.	0,018	0,016	0,037			0,033	0,051
	N	34	34	34	34	34	34	34

To confirm whether leg length in clusters play a significant role in the variation of the trunk frequencies, multivariate analyses were performed.

The cluster leg length was chosen as factor and the lat. flexion, flexion-extension and torsion frequencies as dependent variables.

Results of the Levene test return for the three dependent variables significance values above 0,1. Therefore there are no reasons to suspect the model (table 4-61).

Table 4- 61 Levene-Test

	F	df1	df2	Signific.
Freq_alf_S_B	1,046	2	46	,360
Freq_bet_S_B	,872	2	46	,425
Freq_gam_S_B	,735	2	46	,485

a Design: Intercept+block_leg

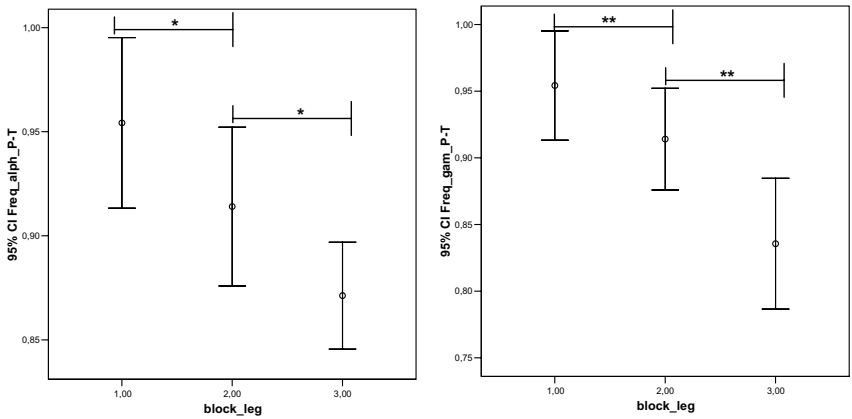

Figure 4- 4 Means and confidence intervals of: A) Freq. of lat. flexion pelvis- thorax and B) Freq. of torsion pelvis- thorax. Frequencies in Hz. Leg length divided in clusters, 1: short, 2: middle, 3: long legs (males).

Results of the multivariate analysis (table 4-62) show that the factor leg length in clusters has a strong influence in the lat. flexion and torsion frequency's variation. The significance level for the lateral flexion frequency is $p<0,05$ and for the torsion frequency $p<0,01$.

As already observed in the female's case, factors like leg length, pelvis width, body height, shoulder width and height or their interactions did not return significant contributions to dependent variables like trunk rotations or phases.

Table 4- 62 ANOVA tests

Source	Dependent variables	Square sum Typ III	df	Square middle	F	Significance
Revised model	Freq_alf_S_B	,042(b)	2	,021	4,531	,016
	Freq_bet_S_B	,637(c)	2	,318	1,099	,342
	Freq_gam_S_B	,104(d)	2	,052	5,676	,006
Constant term	Freq_alf_S_B	28,909	1	28,909	6173,471	,000
	Freq_bet_S_B	69,671	1	69,671	240,490	,000
	Freq_gam_S_B	28,162	1	28,162	3078,505	,000
block_leg	Freq_alf_S_B	,042	2	,021	4,531	,016
	Freq_bet_S_B	,637	2	,318	1,099	,342
	Freq_gam_S_B	,104	2	,052	5,676	,006

Due to the strong evidence accumulated from the results of the correlations and ANOVAS, the hypothesis enunciated at the beginning of this chapter expecting important dependencies between anthropometry and kinematics, must be neglected.

It is a capital mistake to theorize before one has data.
***The adventures of Sherlock Holmes**, 1892*

Chapter 5: Discussion for chapters 2, 3 and 4

In the present chapter, the chapters 2, 3 and 4 will be evaluated and discussed.
In chapter 2 the materials and methods to obtain the kinematics of the spine and body anthropometry were introduced. After that in chapter 3 the results of the kinematical calculations were presented and finally in chapter 4 the interdependencies of trunk motion and anthropometry investigated.
But before the results of the calculations can be taken as reliable data, the validity of the methods must be critically investigated.

5.1 Error discussion

As already explained in chapter 2, the motion analyses were performed using Qualisys® infrared cameras adjusted at a sampling frequency of 120 Hz. The awaited accuracy by using this acquisition method depends of a multiplicity of factors, like:

Room conditions: The light relations, the temperature and changes in the current supply are source of inaccuracies in the measures.
Marker properties: The marker dimensions, their distance to the cameras and also the reflective properties of the markers influence the measures' accuracy. In the case of Qualisys® infrared cameras, the sampling frequency is also a very important factor, because only until 240 Hz the complete pixel matrix is used. After this point, the higher the sampling frequency, the higher measure inaccuracies are.
Room's conformation and cameras layout: There is a significant accuracy difference when the experiment is made in a symmetrical room and the cameras are placed also symmetrically with respect to non-symmetrical rooms and/or non-symmetrical cameras layout. Finally another important point to get the most accurate possible measure is the correct calibration of the equipment.

As discussed in the above mentioned items, there are no fixed error values related to the coordinate axis, these values must be determined from the experiment's own conditions. The manufacturer recommends to measure the noise in the signal of fixed markers and to use this measure as position's error. The problem with this method is that normally, when the experiment is properly designed and constructed, it is not possible to find noise in the signal of the fixed markers. Therefore we have measured the noise in each coordinate of the marker signals of different representative volunteers in standing position.

Table 5- 1 Awaited coordinate error based on the spatial resolution by using Qualisys®

Coordinate	x	y	z
Error in mm	+/-0,227	+/-0,077	+/-0,077

The means of these measures are displayed in table 5-1. From these position errors, those due to the Cardan angles calculation must be computed. In our calculations we have not only relative computations, for instance pelvis-thorax, but also absolute ones like pelvis, thorax or head rotations. So it will be necessary to assess the errors due to absolute and relative calculations.

The method chosen, in order to compute angle errors, is the numerical determination of the influence on the rotation matrix, by changing one element of the position matrix.

In the case of the absolute motions, the markers are 3, which implies 9 coordinates (3 for each marker). To asses the absolute error, the proceeding was the following: first, one sample data was taken and its rotations matrix and Cardan angles calculated. After that, the same sample was computed other nine times, including in each one the expected position error by using Qualisys® (one error in each coordinate at each calculation). Here again, rotation matrix and Cardan angles were computed. The subtraction from the results for the Cardan angles without errors, minus one of those including one error in the coordinate position, return the expected angle error by changing one value in the position matrix. The sum of these nine subtractions will return the expected absolute angle error based on the expected position error.

To asses the errors in the relative rotations between two bodies, the proceedings are the same but with much more computational work. In this case the coordinates are 18, which implies 1 time Cardan angles' calculation without errors and 18 times with

one coordinate error. Then 18 subtractions from the Cardan angles without errors minus those including one coordinate position error and finally the additions of these subtractions results. The maximal expected angle errors for absolute and relative computations are introduced in table 5-2.

The displayed errors show how sensible the Cardan angles are to inaccuracies in the position matrix.

Although the probabilities that the maximal inaccuracies occur in the three axes and at the same time are very small, the worst case should be always considerate as maximal possible errors.

Another important point obtained from these results is the very significant error differences, when relative motions between two bodies are computed, by using relative coordinates, in relation to the use of absolute coordinates' subtraction. From the results can be observed that if we use absolute coordinates to compute relative motions between two bodies, the calculation errors grow to 89,45% for α, 100% for β and 82% for γ.

Table 5- 2 Awaited maximal angle errors in grad based on numerical calculation by using Qualisys®

Angle	α	β	γ
Absolute rotational errors [°]	+/-0,846	+/-1,42	+/-1,22
Relative rotational errors [°]	+/-0,893	+/-1,42	+/-1,34

Markers attached to a segment of interest may not always represent true skeletal locations. These differences are referred to as relative and absolute errors.

Relative marker error is defined as the relative movement of two markers with respect to each other. On the other hand, absolute marker error is defined as the movement of one specific marker with respect to specific bony landmarks of a segment [8].

Three major approaches have been suggested to correct relative marker errors:

Invasive methods provide the most accurate results of bone movement. Bone pins have been used to asses movements of bone elements (Gregersen & Lucas 1967).

A procedure like this is always joined to a great task complexity (radiological controls, local anaesthesia, skin incision) and due to the important accompanying risks is this procedure in Germany not easily approved. In addition, the results of such experiment may not display the normal kinematics of a healthy person.

Mathematical algorithms have been proposed for error reduction in raw data, including skin displacement effects (Woltring 1985; Veldpaus et al., 1988). Smoothing algorithms are base on the assumption that the noise is additive and random with a zero mean value. Errors due to skin displacements, however, may not have zero means [8].
Therefore mathematical algorithms as currently used do not seem to be appropriate approaches for solving the errors due to the skin displacement errors.
Marker attachment systems were proposed to reduce errors due to the relative marker movement. In this method, the markers are not attached to the skin but to frames constructed from thermoplastic material or aluminium, which are then attached to the segment of interest (Ronsky and Nigg, 1993). It is also possible to increase the accuracy of this method by using an array of markers [75]. In this case, the distance between all markers is monitored and those with the minimal change in distance (with respect to the static measure) are used for further calculations. It must be said that this procedure is more convenient to assess kinematics of the extremities but seems not to be applicable to the trunk. First because rigid bodies attached to the trunk can be uncomfortable and therefore may produce changes in the kinematical paths of a person. Second, the trunk must not be considered as a rigid body and therefore a change in the marker reference triplet should produce important changes in the results of the calculations.
Finally, marker arrangements on bony structures like pelvis crest or vertebral column show height correlation coefficients between surface displacement and bone displacement (Drerup & Hierholzer, 1987; Pearcy et al., 1987; Gracovetsky et al., 1995; Saur et al., 1996, Mörl, 2004). Therefore we can expect changes in the amplitudes but no basic changes in the kinematics of the movement.

Motion analyses performed on a treadmill are usually taken as non-physiological movements. Frequently, it is also argued that experiments accomplished under this kind of situations are unfamiliar for the test persons and therefore long acclimatization times are needed to obtain reliable kinematical data. Taylor et al. (1996) showed, however, that pelvic and trunk paths obtained from persons walking on a treadmill, four minutes after they had began, are not significant different than those obtained after long times. This demonstrates that four minutes are enough to obtain reproducible and reliable data.

5.2 Discussion

The study up to here is based on hypothesis 1 (see chapter 1). This, up to date was considered as plausible but not tested. Hypothesis 1 tries to explain trunk kinematics as a direct function of anthropometry.
One point to reinforce this theory is present in earlier studies from Witte (1996) and Hoffmann (2001). In one pilot study, Witte found that the torsion of the trunk has a minimum at the energetically optimal velocity from Cavagna et al. (1977), which agrees with the theory that pelvis and trunk constitute a resonant system. But then this minimum disappears in later studies with cohort of 30 males and females volunteers (Hoffmann, 2001). One answer to this fact could be that this minimum disappears because the differences in the anthropometry of the test-persons build different resonant systems.

Dynamical analyses of the spine and pelvis are normally performed using treadmills or walking lanes. Studies like those performed by Stokes et al., 1989; Crosbie et al., 1997; Vogt & Banzer 1999, Syczewska et al., 1999 were implemented using normally one and up to 3 different velocities, in addition motion, behaviours were analysed during restricted phases of the motion's cycle. Complete phases or more motion cycles have been analysed by Taylor et al., 1999 and Feipel et al. 2000. In these works, however, we will not really find spine kinematics (like torsion or lateral flexion), because they are focussed on pelvic and thoracic oscillations.
Spine kinematics can be found in the works of Wagenaar & Beek (1992), van Emmerik & Wagenaar (1996), Hoffmann (2001) and Witte (2002).
Wagenaar & Beek (1992) examined in their experiment, the transverse plane of the trunk at different velocities (from 0,25 m/s to 1,50 m/s). Their calculations also included the phase shift variation between pelvis and thorax on the transverse plane at the different velocities. It must be said that this examination was performed only with two males and two females as test-persons. This fact introduces many suspects about the representativeness of this study. Emerick & Wagenaar (1996) studied the phase dynamics of the trunk, while the walking velocity was gradually increased and decreased. They found phase changes on the transverse plane from 25° to 110° as speed is increased from slower to higher velocities. Here again the number of subjects is not solid enough (seven healthy persons). Such number must be taken as

very exiguous, in order to make generalizations. A solid cohort of test-subjects can be found in the work of Hoffmann (2001) and Witte (2002). Thirty males and females walked on a treadmill at velocities from 2 km/h to 6 km/h. The motion paths of pelvis and thorax were taken using an ultrasonic system adjusted at a sampling frequency of 24 Hz. Amplitudes, frequencies of pelvic and thoracic motions on transverse and frontal planes have been analysed as well as the relative motions between them. In addition, the phase shift angles between pelvis and thorax on both planes at each velocity were computed.

McGibbon & Krebs et al. (2001) examined pelvic and lower trunk interactions on the sagittal plane from 93 test-persons ranging in age from 20.2 y to 88.8 y old. These subjects performed trials at self-selected speed. In this experiment the phases were calculated as the mean of three pick to pick (pelvis-lower trunk) between two knee flexions.

Head kinematical analyses by walking can be found in the works of Pozzo et al. (1989 & 1990). In these works, ten normal subjects performed four different tasks, like free walking, walking in place, running in place and hopping. Analyses focus on head translations along the vertical axis and rotations on sagittal, vertical and horizontal planes. Three dimensional computations of eyes, head and body interactions were analysed by Imai et al. (2001). This experiment was performed only with 5 subjects walking at preferred velocity. Head and trunk equilibrium strategies while walking forward and backwards under different conditions have been investigated by Nadeau et al. (2003).

The present work presented in chapter 3, introduces source of new kinematical data from pelvis, thorax, head, pelvis-thorax (trunk) and thorax-head. This new kinematical data is not only based in a solid cohort of test-persons (106 subjects, 50 females and 56 males) but also in a very important quantity of new kinematical calculations. These calculations were performed using spherical coordinates and algorithms from the signal analysis (see chapter 2), at each velocity (in total more than 100.000).

To this date, there was no information about the phase shift angles (coupling angles) in pelvis (phases between rotations, translations and rotations-translations), or in thorax or in head and their variation with the velocity. In addition, the present work brings new light in the relative movement thorax-head, related to the velocity. The results are presented in a form that makes possible to observe, not only the different

gender strategies while walking at varied velocities but also their adaptability to the upwards and downwards variations of the speed.

The observed variations of maximal pelvic, thoracic and trunk rotations as a function of walking speed are generally consistent with earlier findings in the literature (e.g. Stokes et al., 1989; Wagenaar & Beek, 1992; van Emmerik & Wagenaar, 1996; Hoffmann and Witte, 2001).

Pelvic axial rotations in males descend to a minimum at 4 km/h, immediately they ascend again. These observations agree with those of Hoffmann & Witte (2001). Pelvic axial rotations in females increase considerably from 3 km/h. Females did not show a minimum. These results display a discrepancy with the results of Hoffmann & Witte (2001), but agree with earlier observations of Wagenaar & Beek (1992) and van Emmerik & Wagenaar (1996). Like presented by Hoffmann (2001) & Witte (2002), female's pelvic axial and lateral tilt rotation amplitudes were larger than those displayed by male volunteers. Pelvic frontal tilt in males and females show constant amplitudes (about 1°) up to 4 km/h, above this speed amplitudes increase.

One of the new calculations included in the present work are the phases between rotations, translations and rotations-translations from the same segment of interest (e.g. pelvis). How these calculations can help us understand relations between different motions at different velocities is introduced below, later thoracic and head motions will be also analysed in the same way.

As pelvic axial rotation and lateral tilt amplitudes increase with the velocity, the phase between these rotations must change. This change is made from about 100° to "in phase-motion", so that the "beauty factor" is neglected by the volunteers, in order to increment motion's speed. At the same time amplitudes of sagittal and transversal translations must decrease to fit these motions with the increasing frequency.

Thoracic axial rotations descend until 4 km/h (1,11 m/s), in agreement with Hoffmann (2001) & Witte (2002), above this velocity these amplitudes stay almost constant. This constant interval agrees with results of Stokes et al. (1989), which depicts constant thoracic amplitudes on the transversal plane from 1,2 mm/s to 2,4 m/s. Wagenaar & Beek (1992) observed also constant amplitudes from 0,25 m/s to 1,5 m/s. Hoffmann & Witte (2001) reported a systematic descent of thoracic amplitudes. Van Emmerik & Wagenaar (1996) reported a slight increase in thoracic rotation up to 0,7 m/s followed by a systematic decrease at higher velocities.

Differences with Hoffmann (2001) & Witte (2002) above 4 km/h can be explained in the difference of the marker paths, the acquisition and calculation methods (for differences see page 13). As explained before, van Emmerik & Wagenaar (1996) used only seven subjects in their experiments, so the change in one person can introduce significant variations in the results. Hoffmann (2001) & Witte (2002) depicted larger pelvic axial rotation amplitudes in females. This difference is not observable in the present work; on the contrary, males display larger amplitudes until 4 km/h, where the amplitudes become almost equal.

As presented by Hoffmann (2001) & Witte (2002), thoracic lateral tilt display a local minimum for males and females at 4 km/h, which can be understood as a resonance dent, supporting the resonance phenomena theory. Gender amplitude differences are not significant.

Females display lager amplitudes for the frontal plane than those of males. As the speed increases, females keep their amplitudes almost constant while those of the males decrease systematically.

Trunk lateral flexions in males and females show a resonance dent close to the energetically optimal velocity (Cavagna et al., 1977). Hoffmann (2001) & Witte (2002) depicted larger amplitudes for males than females. In the present work, this fact can be observed up to 4 km/h, above this velocity, amplitudes of females are slightly larger.

Another coincidence with Hoffmann (2001) and Witte (2002) is present at 5 km/h, where male and female amplitudes are equal (around 4°).

Neither male nor female trunk torsion's curves display resonance dents. Trunk torsion amplitudes for females are significantly larger than those of males. This observation agrees with the results of Hoffmann (2001) & Witte (2002). These gender differences have been explained by Hoffmann (2001) in terms of mass inertial moments. Based on earlier studies by Preuschoft & Witte (1991), Hoffmann postulates that due to the lower sum of mass inertial moments, females must strongly compensate the agent forces by making larger rotations. Another explanation can be proposed, it is well known that females enjoy a significant major flexibility than males, even in subjects with the same relative mass. Then, if we assimilate the trunk as a torsion spring, more flexibility can be represented as a lower spring constant.

The conclusion is then obvious, similar efforts applied to these springs, will conduce to a larger torsion in those which have a lower spring constant.

Separate gender variation of trunk's flexion-extension, related to walking velocity is to this date not presented in the literature, mostly because of the multiplicity of harmonics present in the signal spectrum. The present work introduces this relative motion. Results reveal that trunk's flexion-extension is related to changes in the speed. A slight but systematic increment in males can be observed. This increment is not observed in female's case, but they show significant differences between profiles in females.

As presented in pag. 88 responsible for the increment of the trunk torsion are 1. the increment in the pelvic axial rotation due to the systematic velocity growth and 2. the increment in the phase shift angle between pelvis and thorax. The phase must grow to prevent increasing rotational movement in thorax. Why should the motion of trunk be constrained? Because head axial rotation is strongly related to trunk axial rotation and we know from Grossman et al. (1989) that the restriction of head's angular motion helps the gaze stabilization system the most, by reducing the ocular compensation necessary to maintain gaze on a fixed target.

Trunk phase shift angle on the transverse plane agree with those earlier presented by Wagenaar & Beek (1992), van Emmerik & Wagenaar (1996), Hoffmann (2001) and Witte (2002). Trunk phase shift angles on the frontal plane show that pelvis leads the thorax, in males with a phase of ca. 70° to at 2 km/h to 125° at higher velocities, and in females with a constant phase around 100° for the descending ramp. These results disagree in some form with those of Hoffman (2001) and Witte (2002), which presented larger phase shift angle values. The difference can be founded in the lower acquisition frequency used by Hoffmann (2001), which produces lower accuracy in the calculations of the FFTs.

McGibbon & Krebs (2001) published a study from 93 healthy adults with an age range from 20 to 90 years old. The aim of the study was to investigate age-related changes in lower trunk coordination and energy during gait. Investigations were done between pelvic and lower trunk rotations and angular velocities on the sagittal plane and as explained before, with self-selected speed. They reported in-phase motions for males and females at velocities about 1,2 m/s (4,32 km/h) with the tendency that pelvis leads the thorax. Results from the present work show also almost in-phase motions on the sagital plane at the same speed (20° for males and 12°-20° for

females) but it must be remembered that in our case, phases were computed between pelvis and thorax. Our results suggest also that pelvis leads the thorax at this velocity. However, females walking at velocities below 3,5 km/h display negative phases, which means that at these velocities thorax leads the pelvis.

The present work introduces phase shift angles between the 6 DOF of each body in absolute coordinates and also the relative motion and phases between thorax and head in head coordinate system, at each velocity. Such a great quantity of calculated data allows a very accurate comparison of trunk and head motions.
Comparing the results from absolute thoracic and head rotation curves on frontal and transverse planes, related to velocity (α_{thorax}- α_{head} and γ_{thorax}- γ_{head}), it can easily be seen, that their shapes are very similar, and differences can only be observed in motion amplitudes. Adding to these observations that phase shift angles for their absolute motions are mostly the same or very similar at same velocity, their motions can not be countered. The question is which segment leads the motion?
As explained above, head amplitudes are constrained with respect to those of the thorax, which previously were also constrained in relation to pelvic rotations. This fact shows a systematic damping effect in the oscillations coming from pelvis to head. This damping mechanism was already reported by Prince et al. (1994).

Nadeau et al. (2003) depict positive anchoring indices in head and pelvis, indicating good spatial stabilization in forward and backward locomotion on frontal and sagittal planes. But they also reported a change in the phase of the three spinal segments (upper thoracic, lower thoracic and pelvic), depending on the direction and surfaces. In backward locomotion as well as walking on foam rubber surfaces, the spine adopts a “on block” form. Prince et al. (1994) on the basis of EMG studies have demonstrated a “top-down” anticipatory control, which stabilizes the head first, then the cervical level, followed by the thoracic level and, finally, the lumbar level.
Results from the present work display that in straight walking and gaze on fixed target, thorax and head rotations on the transversal plane are almost “in-phase” motions, but with the tendency that head drives the thorax.
Today there is a great acceptance on the idea that head yaw rotations (axial rotations) are mostly compensated by trunk lateral translations to stabilize gaze in space (Pozzo et al. 1989 & 1990; Imai et al., 2001).

This fact is shown in the counter-phase behaviour displayed by head yaw rotations and thoracic lateral translations.

A prima facie, our results do not agree this hypothesis, but this incoherence is only due to the selected coordinate system. Because in the present work positive X axis is opposite to walking direction, Y positive direction is towards right with respect to the walking direction. Under this constellation, Y translations and head axial rotations are almost in-phase, but motion's meaning is not altered. For example: positive axial rotations of the head are determined by the right-hand rule, and in both coordinate systems are the same (to the left). On the other hand, positive Y translations change between coordinate systems. While in our coordinate system, translations to the right are positive and therefore the phase is cero, they will be negative in the coordinate systems used by Imai et al. (2001), and therefore counter-phase.

In our results it can be observed, that male's head transversal translations are larger than those of the thorax, while female's head and thoracic transversal translations are almost the same. This fact may show, that head jaw rotations in males are compensated by head transversal translations, while those of the females by thoracic transversal translations.

In order to maintain Head fixation point (HFP), head vertical translations are compensated by head rotations on sagittal plane (Grossman et al., 1988; Pozzo et al., 1990). Hirasaki et al. (1999) presented a study with nine subjects, which walked on a treadmill at velocities from 0,6 m/s to 2,2 m/s. The aim of the study was to find relations between head and thoracic frontal tilt and vertical translation of the head as a function of gait velocity. Their results indicate that there is a coordinated vertical translation and pitch of the head during linear locomotion on treadmill at moderate (1,2 m/s -1,8 m/s) to fast (1,8m/s -2,2 m/s) walking that maintained head fixation distance. At slower speeds (0,6 m/s -1,2 m/s), vertical translation was reduced and head pitch in space was almost closely coordinated with trunk pitch rotation to maintain a stable head position in space.

Results of the present work agree with those depicted by Hirasaki et al. (1999), and show how changes are made, in the phase shift angle between Z and beta with velocity variations, to keep the gaze on target (fig. 3.27 A). As speed grows, phase shift angles Z-β increases from circa 90° at 2 km/h to 170° at 6 km/h in males volunteers, which means that at higher velocities and due to the positive increment of

Z, the head is rotated to the front to maintain gaze fixed on target. At the same time, after 3 km/h phase z-β in thorax for males are maintained almost constant, adding to the above explained compensation mechanism reported by Hirasaki et al. (1999).
One finding of the present work is that females, in contrast to males, use systematically trunk compensation mechanisms as velocity grows (cp. fig. 3.18 B & fig. 3.27 B). This fact explains also the depicted lower phase Z-β in head for females at fast velocities (140°). These observations append to the difference depicted for males and females in the above explained compensation mechanism between head jaw rotations and lateral translations.

In order to probe whether kinematical results of the trunk depend on anthropometry, chapter 4 introduce statistical tests between kinematical data from the 106 volunteers at the energetically optimal velocity (4 km/h) and their biometrical data.
Results display that amplitudes of pelvic rotations and translations of males and females do not depend on anthropometry, neither on biometrical data associated to the inverted pendulum and ballistic walking models, nor on linear combinations between them. On the other hand, only with the exception of frontal tilt frequencies in females and axial rotation frequencies in males, pelvic motion frequencies displayed weak to moderate correlation coefficients with anthropometry data in agreement with predictions made by torsion and inverted pendulum models (e.g. leg length, pelvis width or body height).
While correlations between pelvic rotation of females display moderate correlation coefficients between axial rotation and lateral tilt in both profiles, in males correlations between these rotations appears only in the downwards profile and with weak value.
One important point is that not only correlation coefficients vary depending on profiles but also correlations can appear or disappear. This behaviour displays changes in motion strategies depending whether speeds are going faster or slower.
Correlations between thoracic motions of females display moderate correlation coefficients among rotations and also among translations, but these results show also that rotations and translations are not related between each other. On the other hand, thoracic rotations and translations of males display interconnections with weak to moderate correlation coefficients.
Results of the correlations between thoracic frequencies and anthropometry of females displayed significant weak to moderate values, but only for the transverse

and longitudinal translations, while in males, with the only exception of the frontal tilt, rotations and translations displayed weak to moderate dependencies on the anthropometry.

Our findings indicate that thoracic rotation amplitudes of females can not be inferred from anthropometry and that only thoracic Y- translation amplitudes displayed some moderate correlation values. On the other hand, thoracic lateral and frontal tilt of males displayed weak to moderate correlation coefficients with anthropometry but only for the ascending ramp. In the results of the descending ramp, these correlations disappear. For this case, it is difficult to assess whether correlations may exist or not, but if motions are determined by anthropometry, correlations should be more important and be present in both profiles. Therefore we must conclude that thoracic motion amplitudes are not determined by anthropometry.

Results of trunk correlations are even more exiguous; enforcing the conclusion that trunk kinematics are few or not correlated to anthropometry. Therefore the hypothesis, which expected strong dependencies between kinematics and anthropometry, must be neglected.

An important finding, however, reveals that if we divide the legs' length in three clusters (short, middle and long legs) trunk's torsion and lateral flexion frequencies show decrements, as we move from short to long legs. In addition, results of ANOVAs show that the factor leg length in clusters has strong influence in torsion ($p<0,01$) and lat. flexion ($p<0,05$) frequency's variation.

Gracovetsky (1985) presented a coupling model between lateral flexion and torsion of the trunk. The idea behind this model was that thorax and pelvis can not be depicted as two separated rigid planes. He suggests that trunk lateral flexion should produce simultaneously trunk torsion and vice versa. Our results show, however, that trunk's lateral flexion and torsion are not related and, on the contrary, this model is more related to findings in absolute motions of pelvis and thorax.

"The essence of creativity is seeing the problem
in a new way that makes the solution obvious"
***Christopher Barlow**, Co-creativity Institute*

Chapter 6: Functional morphological model of the trunk in walking humans

There is a main statement derived from the results of chapter 4 and it can be expressed in one word: **individuality**. Although in chapter 3 more than 100 kinematical parameters were calculated for 106 test persons in different velocities and profiles, and then in chapter 4 these results for 4 km/h were correlated with 47 anthropometrical data, the reason of why intra- and inter-individual trunk motion's variability is so big could not be answered. However, the relations displayed by the motions between them, the significant dependencies displayed by motion frequencies and some phases on anthropometry helped us understand the reasons to explain, why this question could not be answered.
We think that there are two main factors:

1) The fact that body mass and length can explain part of the observations indicates that the model is correct but incomplete. In this point, the lacking elements are the visco-elastic properties of the musculoskeletal system.
2) Kinematical approaches are oriented to the effects and not to the causes, which are producing these effects.

To solve at the same time the lack of the above enunciated factors, the calculations and models must be analyzed from a dynamical point of view. Naturally, in order to change from kinematics to dynamics, new assumptions must be formulated.
Following hypothesis 2 (see chapter 1), this new assumptions can be expressed as follow:

a) In normal gait and for a given speed, the shapes of the ground reaction forces are a constant.

b) For a defined mass distribution, the variations of amplitudes, frequencies and phases of the trunk are generated due to the changes in the visco-elastic properties of the locomotor system.

In order to test above mentioned new assumptions, a functional morphological model of the trunk based on Hanavan's model is proposed. Functional in this context is referred mechanical and neuronal co-work and also to the concept "intelligent mechanics" (intelligenter Mechanik from Fischer & Witte, 1998). This concept postulates that with an intelligent mechanical design, the necessity of central control decreases. Morphology is the science, which deals with comparative anatomy and includes aspects of historical development (Witte et al. 2004).
The model proposed should be able to show, in case that the hypotheses are true, that by maintaining the shape of the ground reaction forces constant, amplitudes, frequencies and phases are able to be tuned and that can be achieved just manipulating the visco-elastic properties among the segmental bodies.

6.1 Anthropomorphic models

6.1.1 Historical background

Human engineering evaluation models are far more extensive than the simple lengths, diameters, and circumferences used to specify the size of the geometric forms of the early models. Dempster (1955) studied the body as a series of interconnected links that he defined as "straight-line distances between adjacent centers of rotation." This model was an expanded and refined approach of the German infantryman from Braune & Fischer (1889).
Von Meyer (1873), in one of the earliest geometric model, reduced the body to a series of ellipsoids and spheres to arrive at estimated mass and body segments' centers of gravity. In 1960, Simons & Gardner presented a human-model by approximating the body segments as uniform geometric shapes. They represented the appendages, neck, and torso with cylinders and the head as a sphere. Using this model and Barter's (1957) equations for the mass, they computed the inertial parameters for the geometric forms and calculated total-body moments of inertia.

In 1962, Whitsett refined the anthropometric model developed by Simons and Gardner (1960) by increasing the number of body segments from 8 to 14 and by using additional geometric shapes to approximate more closely the shape of the body segments. Whitsett's model included a head, a torso, two upper arms, two lower arms, two hands, two upper legs, two lower legs and two feet. The head was modelled as an ellipsoid, hands as spheres, the upper and lower arms and legs as frustums of circular cones, and finally the feet as rectangular parallelepipeds [96].

The Hanavan model (1964) is made up of fifteen simple geometric solids. In this model the torso was considered as two linked segments. Twenty-five anthropometric measurements were taken from each individual subject and then used to tailor the geometric solids. Hanavan defined the body posture by assigning Euler angles to each of the segment and then calculated the dyadic tensor and the center-of-mass for a specific body in specific positions. The Barter regression equations (Barter, 1957) were used to calculate the segments weights.

Hatze (1980) developed a 17 segment model offering the following improvements over past models. It:

- Includes the shoulders as separate entities,
- Differentiates between male and female subjects,
- Considers actual shape fluctuations of each individual segment,
- Accounts for varying densities across the cross-section and along the longitudinal axis of the segment,
- Adjusts the density of certain segments according to the value of a special subcutaneous fat indicator,
- Does not assume that segments are symmetrical,
- Accounts for body morphological changes such as obesity and pregnancy,
- Is valid for children, and
- Models the lungs at a lower density.

This model assumes that the segments are rigid. Representation of a subject with the model requires 242 separated anthropometric measurements.

Yeadon (1989a, b) introduced an 11 segment model (in fact, segmental inertial parameters can be calculated for 20 separate body segments) using 40 separate solids. Ninety-five anthropometric measurements were taken on an individual and used to define the shape of the model. Yeadon assumed that segments are rigid bodies, that no movement occurs at the neck, wrists or ankles, that the solids

comprising a segment have coinciding longitudinal axes, and that density values are uniform across each solid. In this model, segment masses, location of centroids, and principle moments of inertia about the centroids are calculated based on the geometry of the solid [8, 9, 96].

6.2 Functional morphological model of the trunk

The present model is based on Hanavan's model and it was developed as follows:

- The head was modelled as an elliptical ellipsoid,

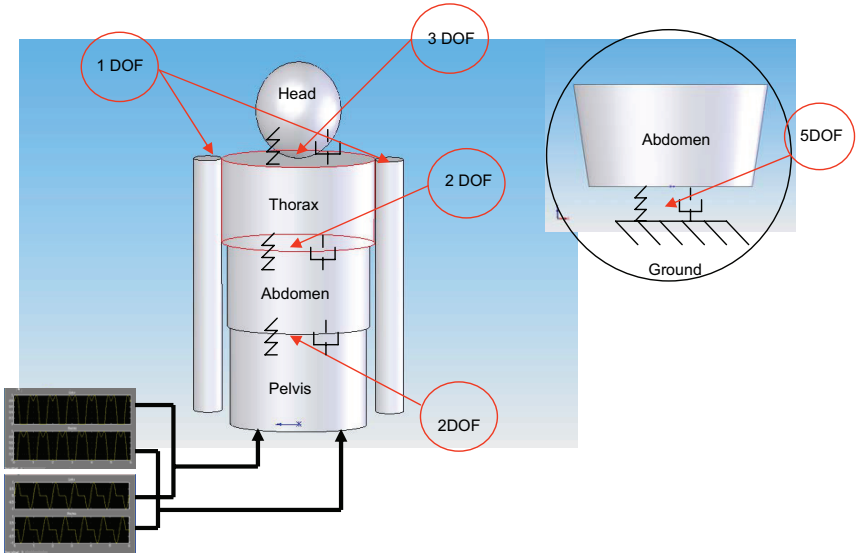

Figure 6- 1 Anthropomorphic model of the trunk

- The trunk was divided in three elliptical cylinders, which represent pelvis, abdomen and thorax.
- 2 DOF rotational joints were placed in the joints pelvis-abdomen and abdomen-thorax. These joints allow rotations about the longitudinal and sagittal axes. At the joint thorax-head, a 3 DOF rotational joint was applied. This joint also allows rotations about the transverse axis.
- The arms were modelled as simple cylinders and coupled to the trunk through 1 DOF rotational joints. These ones allow rotations about the transverse axis.

- The lower part of the abdomen was connected to the ground (global coordinate system) using a 5 DOF joint, which allows the 3 rotations and two out of the three translations. The translational movements were permitted in the longitudinal and in the transverse axis.
- In all rotational joints, for each degree of freedom, torsion spring and damper were mounted. Longitudinal and transverse translations are free.
- The legs were replaced with artificial vertical and anterior-posterior ground reaction forces applied to the hip joints.
- Density values are uniform across each solid and equal to 1,075 gr/cm^3 [8].
- Representation of a subject requires 15 measurements.

6.2.1 Construction of the segmental body parts

In order to compute each geometrical segment based on anthropometrical data, a Matlab® routine was programmed. This routine uses the following anthropometrical data as input:

a = Body height
b = Head height
c = Head width
d = Head depth
e = Shoulder height
f = Bi-acromial width
g = Bi-deltoidal width
h = Arm length
i = Nipples height
j = Ribcage width
k = Ribcage depth
l = Waist height
m1 = Pelvis width
n = Pelvis depth
o = leg length

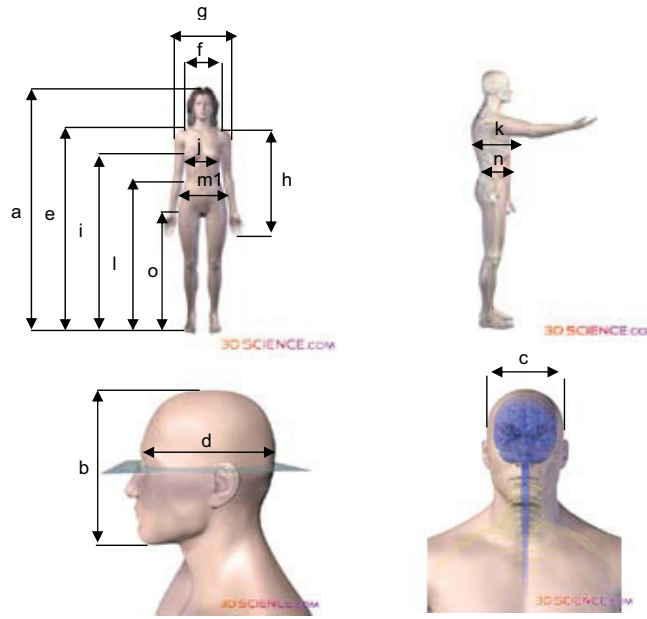

Figure 6- 2 Anthropometrical measures used as input data (Figs courtesy 3D science.com)

The tool chosen to perform the simulations is SymMechanics® from Simulink®. To construct the bodies, SymMechanics® needs the following information:

- Mass
- Moments of inertia about the centroidal axes (x_c,y_c,z_c)
- Position of the center of gravity

Construction of the head

As mentioned before, the head was modelled as an elliptical ellipsoid, therefore its equations are:

$$Volume = \frac{4}{3}\pi bcd \text{ ; eq. (6-1)}$$

$$mass = vol \times 1{,}075 \text{ ; eq. (6-2)}$$

$$I_{xx} = \frac{1}{5}m\left(\left(\frac{b}{2}\right)^2 + \left(\frac{c}{2}\right)^2\right) \text{; eq. (6-3)}$$

$$I_{yy} = \frac{1}{5}m\left(\left(\frac{c}{2}\right)^2 + \left(\frac{d}{2}\right)^2\right) \text{; eq. (6-4)}$$

$$I_{zz} = \frac{1}{5}m\left(\left(\frac{b}{2}\right)^2 + \left(\frac{d}{2}\right)^2\right) \text{; eq. (6-5)}$$

Construction of the thorax, abdomen and pelvis

Thorax, abdomen and pelvis were modelled as elliptical cylinders, therefore their equations can be written as:

For thorax:

$$volumen = \pi \times \frac{f}{2} \times \frac{k}{2} \times (e - i) \text{ ; eq. (6-6)}$$

$$mass = vol \times 1{,}075 \text{ ; eq. (6-7)}$$

$$I_{xx} = \frac{1}{4}m\left(\frac{f}{2}\right)^2 + \frac{1}{12}m(e - i)^2 \text{ ; eq. (6-8)}$$

$$I_{yy} = \frac{1}{4}m\left(\left(\frac{f}{2}\right)^2 + \left(\frac{k}{2}\right)^2\right) \text{; eq. (6-9)}$$

$$I_{xx} = \frac{1}{4}m\left(\frac{k}{2}\right)^2 + \frac{1}{12}m(e-i)^2 \text{; eq. (6-10)}$$

For the abdomen:

$$volumen = \pi \times \frac{j}{2} \times \frac{k}{2} \times (i-l) \text{; eq. (6-11)}$$

$$mass = vol \times 1{,}075 \text{; eq. (6-12)}$$

$$I_{xx} = \frac{1}{4}m\left(\frac{j}{2}\right)^2 + \frac{1}{12}m(i-l)^2 \text{; eq. (6-13)}$$

$$I_{yy} = \frac{1}{4}m\left(\left(\frac{k}{2}\right)^2 + \left(\frac{j}{2}\right)^2\right) \text{; eq. (6-14)}$$

$$I_{zz} = \frac{1}{4}m\left(\frac{k}{2}\right)^2 + \frac{1}{12}m(i-l)^2 \text{; eq. (6-15)}$$

For the pelvis:

$$volumen = \pi \times \frac{m1}{2} \times \frac{n}{2} \times (l-o) \text{; eq. (6-16)}$$

$$mass = vol \times 1{,}075 \text{; eq. (6-17)}$$

$$I_{xx} = \frac{1}{4}m\left(\frac{m1}{2}\right)^2 + \frac{1}{12}m(l-o)^2 \text{; eq. (6-18)}$$

$$I_{yy} = \frac{1}{4}m\left(\left(\frac{m1}{2}\right)^2 + \left(\frac{n}{2}\right)^2\right) \text{; eq. (6-19)}$$

$$I_{zz} = \frac{1}{4}m\left(\frac{n}{2}\right)^2 + \frac{1}{12}m(l-o)^2 \text{; eq. (6-20)}$$

Construction of the arms

The arms were modelled as simple cylinders, for this reason their equations can be written as:

$$volumen = \pi\left(\frac{g-f}{4}\right)^2 \times h \text{ ; eq. (6-21)}$$

$$mass = vol \times 1{,}075 \text{ ; eq. (6-22)}$$

$$I_{xx} = I_{zz} = \frac{1}{4}m\left(\frac{g-f}{4}\right)^2 + \frac{1}{12}mh^2 \text{ ; eq. (6-23)}$$

$$I_{yy} = \frac{1}{2}m\left(\frac{g-f}{4}\right)^2 \text{ ; eq. (6-24)}$$

6.2.2 Artificial ground reaction forces

Models of legged locomotion are widely propagated in biomechanics and robotics. Most problems with these simulations models are due to the very important computational work needed to model the different stand phases during walking. Therefore, these kinds of simulations are normally constrained to a half or one complete cycle. The present work is focussed on the trunk and the head. Their motions are rhythmic oscillations due to the locomotion activity. But until these rhythmic oscillations are reached, a couple of cycles must be performed. That is because, the trunk and the couple trunk-head are not rigid bodies; on the contrary, they build a chain of rigid bodies coupled by visco-elastic elements, and therefore, they need a time-ramp, until the different rotational and translational movement are compensated, and finally, the normal oscillations are reached. For these reasons, it was decided to use artificial ground reaction forces applied to the hip-joint. This approach permits not only to apply one or a combination of more components of the ground reaction forces and observes the reactions on the trunk and head, but also to change the duty-factor.

Components of the reaction forces

In walking two active force peaks are present, the first being associated with deceleration and the second with the acceleration phase. The force component in the a-p (anterior-posterior) direction has two active parts, which are similar in walking and running. In the first half of ground contact, the foot pushes in the anterior direction. Consequently, the reaction force from the force plate is directed in the posterior direction (backwards). In the second half of ground contact the foot pushes

in the posterior direction. Consequently, the reaction force form the force plate is in the anterior direction [8] (see fig 6-3).

The vertical component of the ground reaction forces were modelled using Alexander equations (Alexander & Jayes, 1978):

$$y = 3(\cos\theta - q\cos 3\theta)/(3+q)\text{; eq. (6-25)}$$

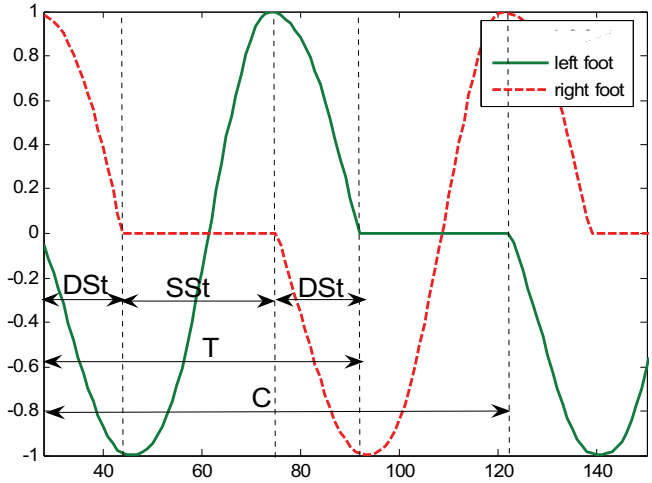

Figure 6- 3 The different phases of gait cycle. DSt: double support phase, SSt: single support phase, T: stand phase, C: double step period

The value of q is determinant for the shape of the curve and depends on the duty factor. For the simulation, the duty factor was chosen at 0,65, which means normal walking. Using the graphs of q against the duty factor from Alexander and Jayes (1978), q can be determined as 0,3.

The a-p reactions forces were modelled as simple cosine functions.

To construct the ground reaction functions, the basic functions (e.g. Alexander or cosines) must be switched with constant zero functions during the swing phase. In fig. 6-3 the basic a-p function is shown. In this fig., SSt represents the left foot's single support phase or right foot's swing phase. DSt represents the double support

phase. T is the searched function period and finally C is the time needed for one foot to make two heel contacts.

In normal walking, the double step frequency (DSf) oscillates between 0,83 and 0,93 Hz. Therefore, C will be:

$$C = \frac{1}{DSf} = T + SSt = 2 \times DSt + 2SSt \text{ ; eq. (6-26, 27, 28)}$$

The duty factor is:

$$Df = 0{,}65 \Rightarrow T = C \times 0{,}65 \text{ ; eq. (6-29)}$$

The simple support phase is

$$SSt = C - T = C - 0{,}65C = 0{,}35C \text{ ; eq. (6-30)}$$

The double support phase shall be

$$DSt = \left(T - SSt\right)/2 \text{ ; eq. (6-31)}$$

T is the period of the artificial function in relation to the double step frequency and the duty factor.

The start point of the simulation was set at the middle of the left foot's single support phase. Under this constellation, the artificial left foot function starts shifted, at t=0, 180 degrees.

$$start\_first\_function = f_{a-p} + 180° \rightarrow t_0 = 0$$

$$swicht\_to\_cero \rightarrow t_{sw1} = SSt/2 + DSt$$

$$\text{sec}ond\_step \rightarrow t_{lf2} = t_{sw1} + SSt$$

$$n\_swicht\_cero \rightarrow t_{sw(n)} = t_{lf(n)} + T$$

$$n\_step \rightarrow t_{lf(n)} = t_{sw(n-1)} + SSt$$

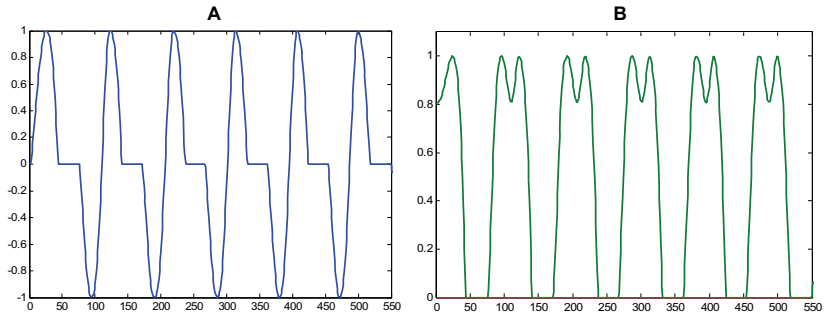

Figure 6- 4 Artificial ground reaction functions. A) anterior-posterior, B) vertical.

At t=0, the right foot is in the middle of the swing phase. Therefore, the a-p reaction forces are zero.

$$cero \rightarrow t_{swr1} = 0$$

The first right heel contact will occur at:

$$first - step = f_{a-p} + 0° \rightarrow t_{rf1} = (SSt/2)$$

$$swicht\_to\_cero \rightarrow t_{swr2} = t_{rf1} + T$$

$$n\_step \rightarrow t_{rf(n)} = t_{sw(n)} + SSt$$

$$n\_swicht\_cero \rightarrow t_{swr(n)} = t_{s(n-1)} + T$$

The construction of the vertical components follows the same logic. The only change is that eq. (6-25) will be used as basic function.

Starting only on the basis of the double step frequency and the duty factor, the Matlab® routine computes the phases and the switch times. These data are introduced in Simulink®, where the functions are created. The generator of ground reaction forces returns the vertical and a-p functions. These functions, however are only basic functions (see fig. 6-4) and therefore, they must be multiplied by the weight. This was already obtained in the same Matlab® routine which calculated the geometric bodies.

The a-p forces arises at most 0,3 times the body weight in normal walking, while vertical ones about 1,3 times the body weight. These coefficients are multiplied by the weight to obtain the ground reaction forces.

6.2.3 Topology of the model

One of the most difficult problem faced in the present simulation, was to fit the motion amplitudes of the thorax in relation to those of the pelvis. In chapter 3 was observed that thoracic rotational amplitudes are strong restricted. Then in chapter 5 this behaviour was explained in terms of head stabilization. Among other things, the present work tries to explain in a mechanical way: how this mechanism works and whether this segmental amplitude motion's reduction produces changes in the phases among the segments.

Two problems should be solved in order to reproduce the motion patterns between pelvis and thorax. The first one is: how many segments should the trunk have?. The second one is the position of the ground (the global frame). In Hanavan's model, the trunk was divided in two segments. With this configuration it is impossible, from a mechanical point of view, to reproduce the kinematics of the spine. One solution to this problem is to divide the pelvis in three segments. But this configuration works only if the connection to the ground is positioned on the right place. That is because the equations of motion vary related to its position.

When observing the motion of the pelvis, this seems to be floating, while the trunk's motion is more constrained. In order to reproduce this behaviour, the ground was located between the abdomen and the pelvis.

The topology of the trunk model is shown in fig. 6-5. The abdomen is linked to the ground by the use of a 5 DOFs joint, which accepts 3 rotations and 2 translations. This joint is the number 1. In the same spatial location, the abdomen is linked to the pelvis by a 2 DOFs joint (number 2). This joint permits only two rotations (axial rotation and lat. tilt)[6].

The above expressed configuration allows larger rotations in pelvis, which are constrained in joint 2, and a more constrained motion of the abdomen, due to the action of joint 1. From this point towards to the head, rotations will be systematically

[6] The fact that joints 1 and 2 appear shifted in fig. 6.5, is only to make the drawing better understandable.

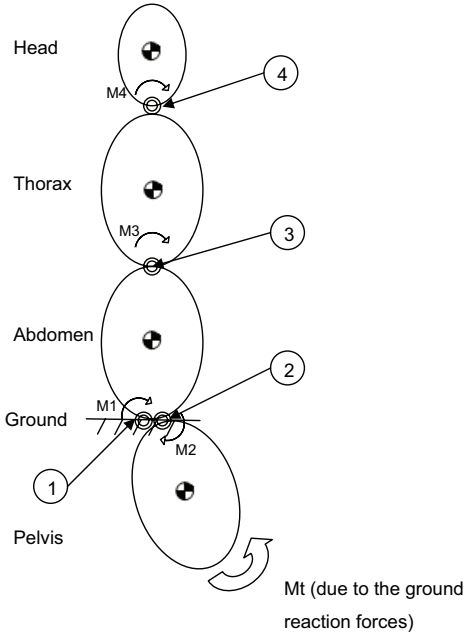

Figure 6- 5 Topology of the trunk model. 1 joint ground-abdomen, 2 joint abdomen-pelvis, 3 joint abdomen-thorax and 4 joint thorax-head.

reduced in joint 3 and 4, in agreement with the depicted results of chapter 3 and the discussions in chapter 5.

The torque in a joint between two bodies is a function of the relative angular displacement and the angular velocity of the bodies. Due to the model's particular topology, the torque equations in joints1 and 2 will be:

$$\tau = -k\theta - b\dot{\theta} \quad \text{eq. (6-32)}$$

This equation must be applied to each rotational degree of freedom. In the joint ground-abdomen, we have three rotations and two translations:

$$r_a = \left[y_a \; z_a \; \alpha_a \; \beta_a \; \gamma_a \right]^T \quad \text{eq. (6-33)}$$

The abdomen-pelvis joint has only 2 rotational DOFs, therefore:

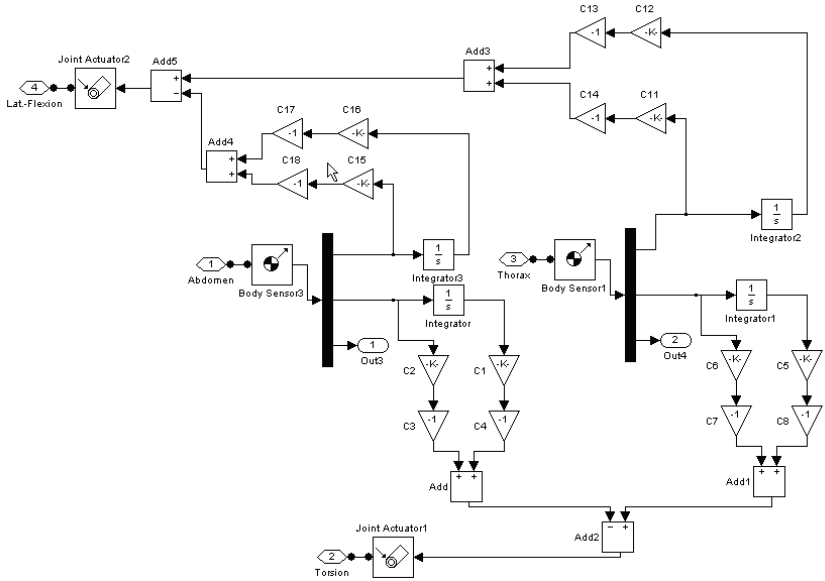

Figure 6- 6 Simulink® diagram of the spring-damper subsystem used in joint 3

$$r_p = \left[\alpha_p \ \gamma_p\right]^T \quad \text{eq. (6-34)}$$

In joints 3 and 4, the rotational spring and damper are modelled as follow:

$$\tau_2 = (-k_1\theta_1 - b_1\dot{\theta}_1) - (-k_2\theta_2 - b_2\dot{\theta}_2) \quad \text{eq. (6-35)}$$

The sub-index “1” represents the body located upper to the joint. This spring-damper configuration is again used for each DOF.

The abdomen-thorax’s joint permits two rotational DOFs.

$$r_t = \left[\alpha_t \ \gamma_t\right]^T \quad \text{eq. (6-36)}$$

While the one between thorax and head permits three DOFs.

$$r_h = \left[\alpha_h \ \beta_h \ \gamma_h\right]^T \quad \text{eq. (6-37)}$$

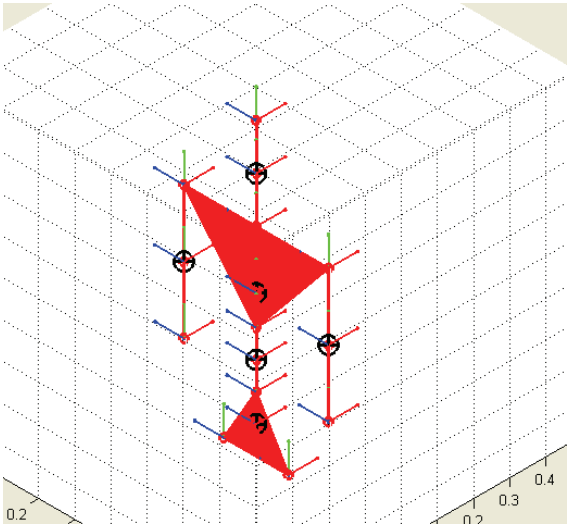

Figure 6- 7 The functional morphological model of the trunk (machine model of SimMechanics®).

Fig. 6-6 introduces the spring-damper model for joint 3. The body sensors measure the angular velocities $[\omega_x\ \omega_y\ \omega_z]^T$ from abdomen and thorax related to the world coordinate system. The velocity is multiplied by the damping constant b and also integrated, to obtain the angular displacement. This is multiplied by the spring constant k. This resultant functions are traduced in torques in the joint actuator and then applied to the joint. The same approach is used in joint 4.

As expressed before, the arms can only rotate above the transversal axis. In this particular case, the torsional spring and damper blocks from SimMechanics® are used.

From the simulations made by Gruber (2004), it is known, that ground reaction forces increase when the arms are fixed in the front of the trunk. In the case of swinging arms, as the gait velocity increases, the distance between acromion and hand decreases. The lower arm is rotated in direction towards to the shoulder. These phenomena produce changes in the arm's moment of inertia and of course in the pendulum length. This procedure is achieved to fit the arm's oscillation frequency to the increasing double step frequency.

In the present model, this behaviour is reproduced in the following way:

The period of a cylinder pendulum is:

$$T = 2\pi \sqrt{\frac{\left(\frac{1}{4}mR^2 + \frac{1}{12}mL^2\right)}{\frac{mLg}{2}} + \frac{L}{2g}} \quad \text{eq. (6-38)}$$

Where T is the period, m is the mass, R the radius and L the length of the cylinder.
By solving the square-root, taking common factors and reorganizing them, we obtain:

$$T^2 L = \frac{2\pi^2}{g}\left(R^2 + \frac{4}{3}L^2\right)$$

Finally, the equation for L will be:

$$\frac{8\pi^2}{3g}L^2 - T^2 L + \frac{2\pi^2 R}{g} = 0 \quad \text{eq. (6-39)}$$

The positive root of eq. (6-39) gives the length of the arm needed to fit the period of the double step frequency, using a radius R.

6.2.4 Methods to assess k & b values

In order to find the visco-elastic parameters (*k* & *b*), related to the motion paths in pelvis, abdomen, thorax and the head, anthropometrical data from one t were used to build the anthropomorphic model. Unfortunately some of the data necessary was not included in the anthropometrical measures introduced in chapter 2, and therefore, they were computed using the values presented in the Anthropometricher Atlas from Flügel, Greil & Sommer (1986). These values are: bi-deltoidal width, nipples height, ribcage depth and pelvis depth.
Due to the amount of DOFs (14), the determination of the *k* & *b* constants was made gradually in each plane starting from the pelvis towards to the head.

Leaving always the upper segments fixed, the motion of the lower segment was fitted in one plane at each time. After that, the following upper segments were fitted in the same way (again one plane at each time), until the mean amplitudes, already introduced in chapter 3, were reached.

The values of *k* & *b* were taken as basis values. Afterwards, these values were tuned up and down, in order to observe, what kind of influence introduces a change in the value of the visco-elastic constants on motions' amplitudes and phases to each segmental body.

In the kinematical analysis (see chapter 2), the motion paths of pelvis, thorax and head were represented using marker triplets. However the motion of the abdomen was not measured. This fact produced one important question: are the abdominal rotations in each plane larger or smaller than those of the thorax? The simulation showed pretty fast that abdominal rotations on the frontal plane have to be smaller than those of the thorax. If this condition is not fulfilled, the simulation becomes unstable and the model fall down. But, what occurs on the trunk? Do these observations on the model represent the behaviour of a real person? To check this behaviour, motion analysis tests involving 2 female subjects, with a mean age of 25 y, has been performed.

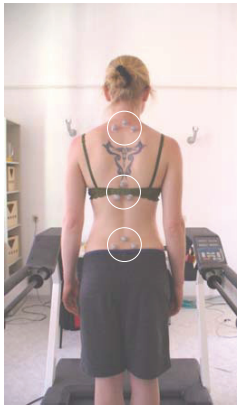

Figure 6- 8 Marker distributions in the motion analysis test.

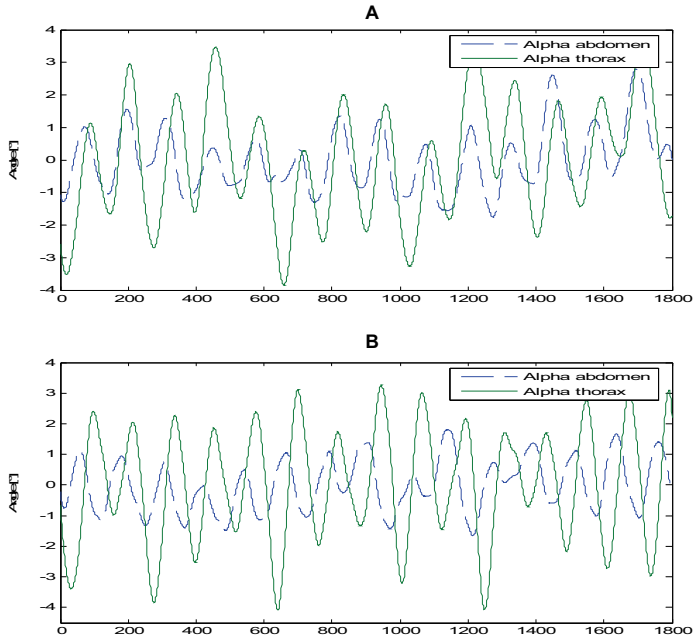

Figure 6- 9 Comparison of lateral tilt in abdomen and thorax. A) subject 1, B) subject 2.

The motion of the thoracic girdle was represented with a marker triplet at the level of C7, the abdominal movement with a marker triplet at the level of T10, and those of the pelvis with a marker triplet over Sacrum (spinal process L4 and Spinae iliacae post. supp.). Fig. 6-8 shows the marker distribution.

The subjects walked on a treadmill at a velocity of 4 km/h for periods of 15 seconds. The motions of the markers representing pelvis, abdomen and thorax were taken using Qualisys® infrared cameras at a sampling frequency of 240 Hz. Calculations were performed using the Matlab® routine already introduced in chapter 2.

Fig. 6-9 introduces the results of these calculations. In both subjects (A & B) it is easy to note, that thoracic lateral tilt amplitudes are significant larger than abdominals. This result is agreement with those obtained by the model.

6.3 Simulation results

6.3.1 Pelvis

In the simulation, the description of the absolute angles (lateral tilt, sagittal tilt and axial rotation) is the same as the one used in previous chapters [α, β, γ].

As expressed before, the joint between pelvis and abdomen allows two rotations. These rotations are around the longitudinal and sagittal axes (α and γ).

The results will be introduced in graphics and tables. The graphics display the smooth effect due by the increment of the damping constants, and the tables, the comparison of amplitudes, frequencies and phases using different value combinations of *k* and *b*.

Six cases are considered, the first one is the approximation to the mean values. In the second one, on the basis of the mean values, only the spring constants were increased. Then in the third one, only damping constants were increased. The fourth one shows the effect due to the increment of both spring and damping constants. In the fifth case, the damping constants were tuned, to explore their impact in the kinematics of the pelvis. Finally the sixth case, the visco-elastic parameters were tuned to obtain phases close to zero.

In case 1, amplitudes were reached by manipulating the spring constants and leaving with relative small values the damping ones. The obtained effect can be appreciated in fig. 6-1A. Lateral tilt rotations display important third harmonic components.

Axial rotations display also harmonic components. By increasing the spring constants (fig. 6-1B) amplitudes decrease, but frequencies and phases remain without changes (see table 6-1). Case three (fig. 6-1C) shows that the increments of damping constants act as a smooth filter. This phenomenon occurs because they constrain the variation of velocities and therefore, they filter higher frequencies. Due to this effect, the oscillation's principal mode is not affected.

Maximal amplitudes decrease with respect to case 1 but the effect is not as significant as the change in the spring constants. The phase γ-α decreases, but is not significantly affected. Case 5 and 6 show the method to decrease the phase α-γ to values close to zero (figs. 6-1E & F).

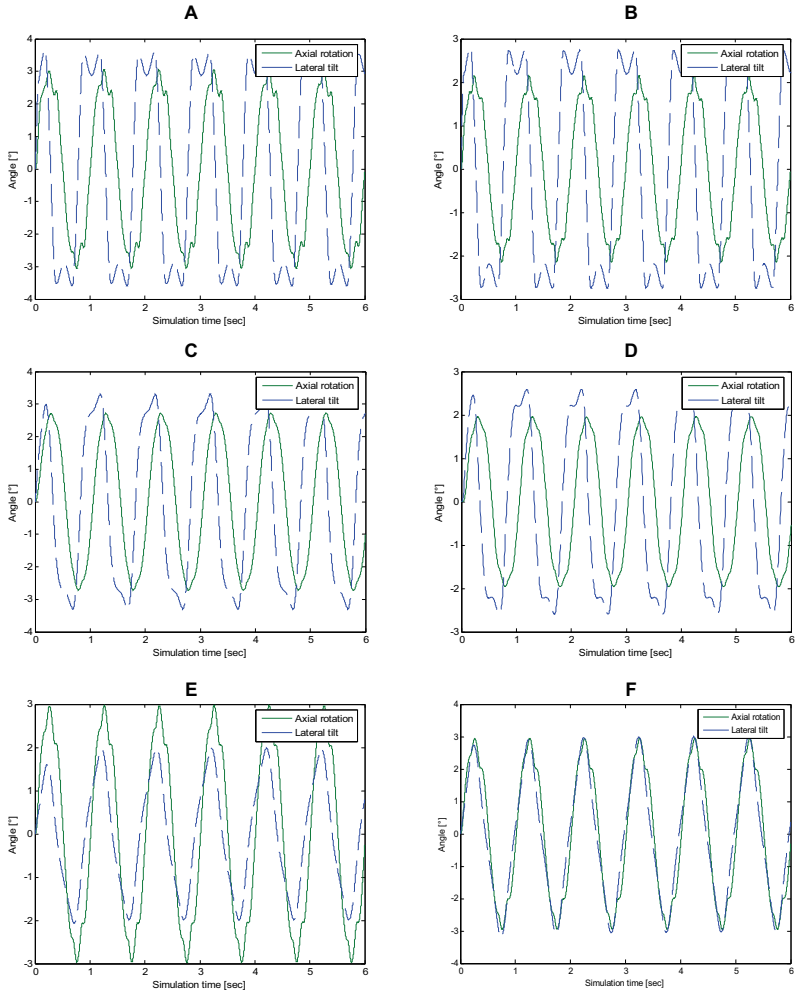

Figure 6- 10 Six studied cases: A) case 1, B) case 2, C) case 3, D) case 4, E) case 5, F) case 6

The most important factors are the relation between the damping effect on the transverse and longitudinal axes (case 5) plus the reduction of the lateral tilt spring constant k-α (case 6).

The results display that motion frequencies are determined by the double step frequency. On the other hand, they also show that amplitudes and phases are defined by the joint's visco-elastic settings.

Table 6- 1 Comparison of the different cases studied for pelvis.

Visco-elastic parameters	Case 1	Case 2	Case 3	Case 4	Case 5-	Case 6
K_2-α_pelvis [Nm/rad]	700	**900**	700	**900**	700	**200**
k_2-γ_pelvis [Nm/rad]	350	**500**	350	**500**	350	350
b_2-α_pelvis [Nms/rad]	20	20	**60**	**60**	**200**	**150**
b_2-γ_pelvis [Nms/rad]	2	2	**20**	**20**	**5**	**6**
Amplitude α	3,84°	2,96°	3,24°	2,64°	1,7°	2,61°
Amplitude γ	2,97°	2,05°	2,75°	1,97°	2,82°	2,8°
Frequency α	0,97 Hz	0,97 Hz	0,97 Hz	0,97 Hz	0,97 Hz	0,97 Hz
Frequency γ	0,97 Hz	0,97Hz	0,97 Hz	0,97 Hz	0,97 Hz	0,97 Hz
Phase γ-α	78,4°	80,1°	76,6°	77,7°	30,2°	10,5°

6.3.2 Abdomen

The joint between ground and abdomen allows 5 DOF (3 rotations and 2 translations). Translations are in the longitudinal and transverse axes.

Results from the pilot study show that abdominal axial rotations can be larger than those of the thorax. This is not a problem for the model, because simulation works with larger as well as smaller abdominal axial rotations.

Table 6-2 display the k & b constant needed on each plane to obtain:

- Abdominal lateral tilt amplitudes smaller than the mean values for thorax.
- Abdominal sagittal tilt and axial rotation amplitudes similar to those of the mean values for thorax.

Lateral tilt and axial rotation frequencies display the same values to those of the pelvis (0,97 Hz). On the other hand, sagittal tilt frequency value is twice the oscillation's principal mode (1,95 Hz). With this constellation, the phase γ-α is 90°.

It has to be noted, that spring constant values for lateral and sagittal tilt are significantly larger than those depicted for pelvis.

Figs. 6-11 introduce abdominal rotations. Due to the relative small damping constants, lateral tilt and axial rotations display important third harmonic components.

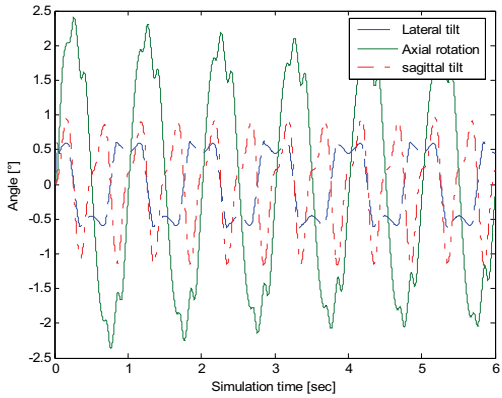

Figure 6- 11 Abdominal rotations

Table 6- 2 Parameters and results for abdomen

Visco-elastic parameters	Case 1
k_1-α_abdomen [Nm/rad]	4500
k_1-β_ abdomen [Nm/rad]	2000
k_1-γ_ abdomen [Nm/rad]	448
b_1-α_ abdomen [Nms/rad]	5
b_1-β_ abdomen [Nms/rad]	3
b_1-γ_ abdomen [Nms/rad]	2
Amplitude α	0,63°
Amplitude β	0,8°
Amplitude γ	2,24°
Frequency α	0,97 Hz
Frequency β	1,95 Hz
Frequency γ	0,97 Hz
Phase γ-α	90°

6.3.3 Thorax

The joint between abdomen and thorax was constrained to two rotational DOFs (lateral tilt and axial rotation).

Table 6- 3 and fig. 6-12 introduce the results for the thorax. These results are only due to the change of visco-elastic parameters on the joint abdomen-thorax. Parameters of pelvis and abdomen are setup always as the first case (see tables 6-1 resp. 6-2).

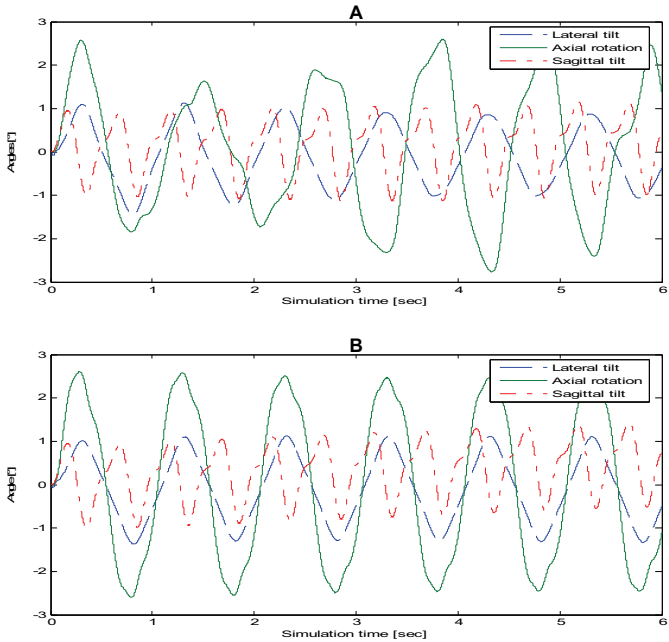

Figure 6- 12 Simulation results for thorax. A) Case 1, B) Case 2

Following the same procedure introduced for pelvis and abdomen, the first case displays again the approximation to the mean values observed in chapter 3. Table 6-3 (Case 1) introduces the *k* & *b* parameters needed. Fig. 6-12A show the evolution of the lateral tilt, sagittal tilt and axial rotation related to time for case 1. The phase γ-α starts almost in phase, but after a ramp of about 2 seconds, the phase changes to counter.

By incrementing k_3-γ (case 2) the phase γ-α reaches values close to 0°, but as shown in table 6-3, the damping constants from both joints thorax-arms have to be incremented to 0,5. If these damping constant are not incremented, the model returns again to a phase γ-α=180°.

Cases 3 and 4 introduce the effects due to the increment of the spring constant for the rotations around the sagittal axis.

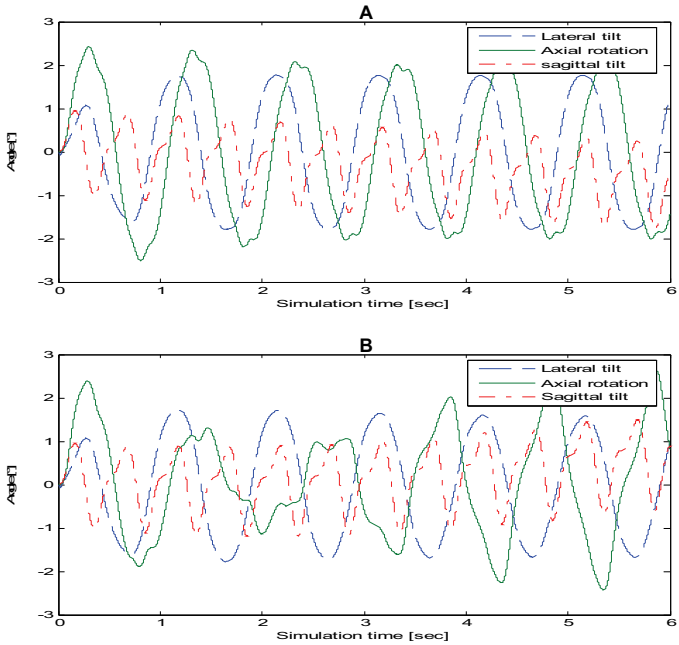

Figure 6- 13 Simulation results for thorax. A) Case 3, B) Case 4

Table 6- 3 Comparison of the different cases studied for thorax.

Visco-elastic parameters	Case 1	Case 2	Case 3	Case 4	Case 5
k_3-α_ thorax [Nm/rad]	40	40	**100**	**100**	40
k_3-γ_ thorax [Nm/rad]	35	**80**	35	35	35
b_3-α_ thorax [Nms/rad]	6	6	6	6	6
b_3-γ_ thorax [Nms/rad]	2	**4**	**4**	**4**	**18**
$b_{5\text{-}6}$-β_ arms [Nms/rad]	0	**0,5**	**0,5**	0	0
Amplitude α	0,82°	1,07°	1,53°	1,6°	
Amplitude γ	2,6°	2,57°	2,39°	1,84°	
Frequency α	0,97 Hz	0,97 Hz	0,97 Hz	0,97 Hz	0,97 Hz
Frequency γ	0,97 Hz	0,97 Hz	0,97 Hz	0,97 Hz	2,93 Hz
Phase γ-α	170°	-14,8°	71°	239°	

The difference between case 3 and 4 is that in case 3, the arms are damped (see table 6-3). Results for case 3 and 4 show that the increment in the spring constant k_3-α produces increments in the amplitude of the lateral tilt, and also that the damped arms produce significant variations on the phase γ-α. Fig. 6-13 (A & B) display the shape of the rotations related to the time for case3 resp. case 4. Comparing both

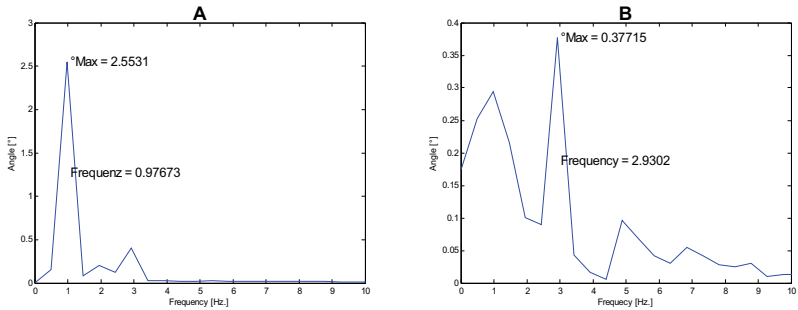

Figure 6- 14 Comparison between thoracic axial rotation spectra of case 1 (A) and case 5 (B)

graphics and those of fig. 6-12, it can be easily noted, that variations on the visco-elastic parameters not only do change the amplitude and phases between the rotations, but also the shape of the curves. The frequencies, however, stay always without changes.

Case 5 (table 6-3) displays the visco-elastic parameters needed to produce variations on the axial rotation oscillation's principal mode. Fig 6-14 A & B introduce the frequency spectra of the thoracic axial rotation for case1 respectively case 5.

The case 5 shows that using very large values of damping constants, the amplitude of the principal frequency decreases to a point, where the harmonic frequencies become larger than the principal oscillation's mode.

6.3.4 Head

In chapter 3 was observed, that the phases between head motions are significantly related to those of the thorax. In the four following cases this relation will be tested. In the cases 1 to 3 (figs. 6-15 A, B & C and table 6-4), the visco-elastic parameters of the joint thorax-head are tuned, while those of the joint abdomen-thorax are set-up as in case1 (thorax, see table 6-3). It has to be remembered that the joint thorax-head has 3 rotational DOF.

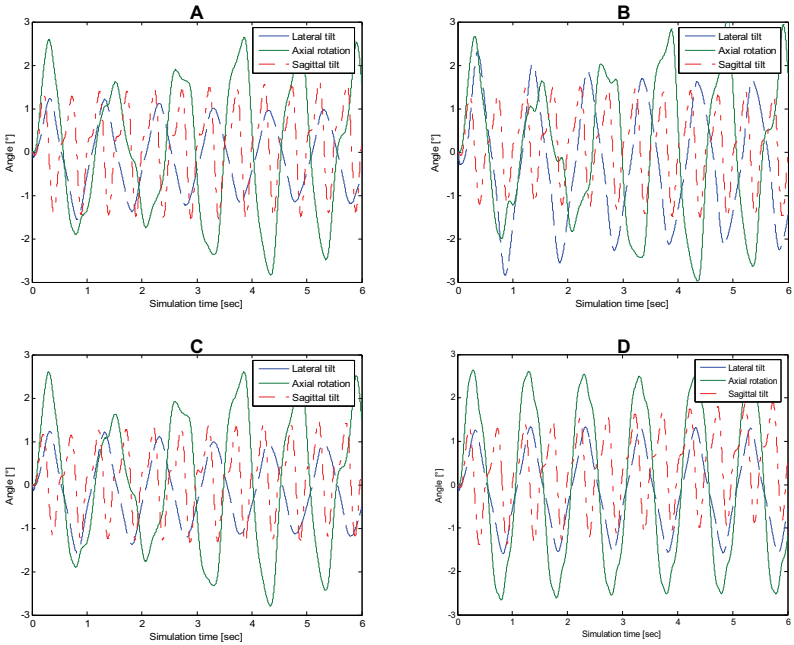

Figure 6- 15 Simulation results for head. A) case1, B) case 2, C) case 3, D) case 4.

Case 4 introduces results using 3rd case's set-up (head) and case 2 (thorax). Fig. 6-15 D and table 6-4 display the results for case 4.

The comparison among the cases 1 to 3 (table 6-4) shows that the lateral and sagittal tilt amplitudes can be tuned by changing the spring constants (case 2) or the damping constant (case 3). On the other hand, axial rotations seem to be independent from the different tuned parameters and they reach the same values as those for the thorax.

The phase γ-α for cases 1 and 3 is the same as the phase γ-α for thorax. Case 2 show a reduction of the phase γ-α related to the case 1 (head and thorax).

Phase γ-Y for cases 1 to 3 display changes but they are not that significant. These phase values agree with those of chapter 3. Case 4 shows how dependent phase γ-α and γ-Y on trunk kinematics are. The phase γ-α changes from 172° to -14,4°, which is the same value as the one observed for the thorax. The phase γ-Y changes 180°. On the other hand, phases Z-β seem to be constant in all cases.

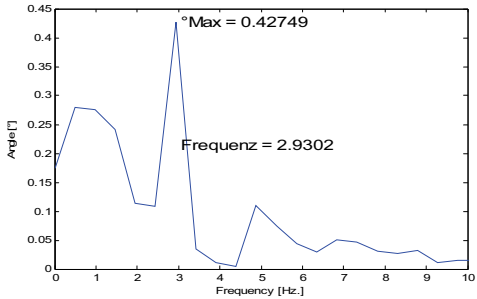

Figure 6- 16 Frequency spectrum of head's axial rotation

Frequencies display the same values as those already introduced for pelvis abdomen and thorax. Fig. 6-16 introduces the spectrum of head's axial rotation produced by the set-up 5th case of the thorax. This example shows again that head's axial rotations depend directly on those of the thorax (cp. with fig. 6-14 B) .

Table 6- 4 Different cases studied for the head, using case 1 and 2 of the thorax

Visco-elastic parameters	**Case 1** (case 1 thorax)	**Case 2** (case 1 thorax)	**Case 3** (case 1 thorax)	**Case 4** (case 2 thorax)
k_4-α_head [Nm/rad]	20	**10**	20	20
k_4-β_head [Nm/rad]	30	**20**	30	30
k_4-γ_ head [Nm/rad]	10	**5**	10	10
b_4-α_ head [Nms/rad]	1	1	**12**	**12**
b_4-β_head [Nms/rad]	5	5	**8**	5
b_4-γ_ head [Nms/rad]	0,5	0,5	**2**	**2**
Amplitude α	1,52°	1,75°	0,99°	1,22°
Amplitude β	1,12°	1,07°	0,95°	1,02°
Amplitude γ	2,7°	2,81°	2,61°	2,6°
Frequency α	0,97 Hz	0,97 Hz	0,97 Hz	0,97 Hz
Frequency α	1,95 Hz	1,95 Hz	1,95 Hz	1,95 Hz
Frequency γ	0,97 Hz	0,97 Hz	0,97 Hz	0,97 Hz
Phase γ-α	172,3°	147,3°	172°	-14,4°
Phase γ-Y	25,6°	17,5°	34,8°	205,7°
Phase Z-β	225,7°	222,2°	233,4°	222,9°

6.3.5 Pelvis-thorax

In previous sections, it has been shown that phases within body motions are controlled by visco-elastic constants. The present section will try to explain, how visco-elastic properties have to be tuned, in order to produce changes in the phase between pelvis and thorax (e.g. from in phase to counter motions).

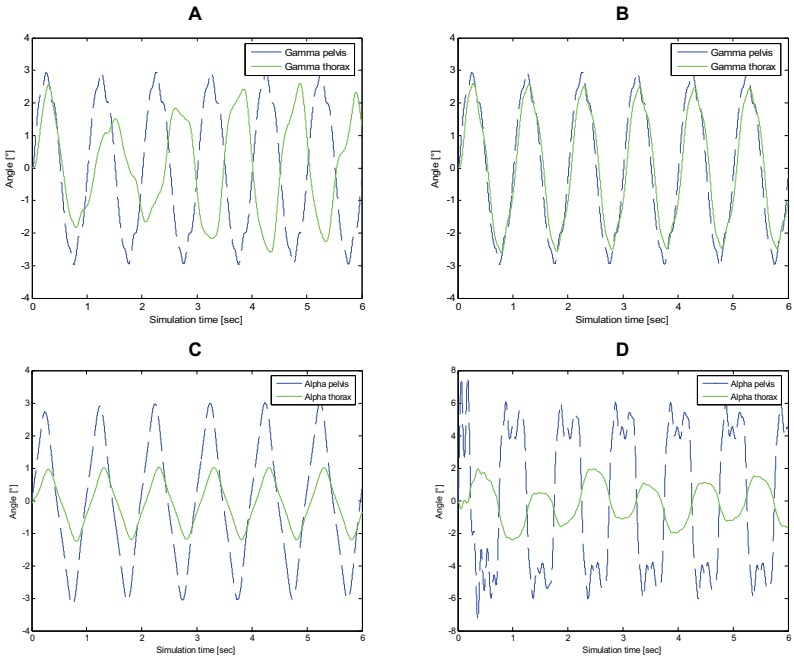

Figure 6- 17 Simulations of pelvic and thoracic motions. A & B around the longitudinal axis, C & D around the sagittal axis.

Figs. 6-17 A & B display pelvic (dashed line) and thoracic axial rotation curves. Fig. 6-17 A shows counter motions between thorax and pelvis. In order to obtain this behaviour, case 1 has to be used for thorax and pelvis. On the other hand, fig. 6-17 B display motions in phase between pelvic and thoracic axial rotations. To produce this phase relations, the visco-elastic parameters form case 2 (thorax) along to those of case1 (pelvis) have to be chosen.

Figs. 6-17 C & D show the effects due to the tuning of visco-elastic parameters on the frontal plane. Fig. 6-17 C shows that to reach phases close to cero pelvic (dashed line) and thoracic lateral tilt motions have to be strong damped, for instance using case 6 for pelvis and case 2 for thorax. The opposite introduces fig. 6-17 D. To reach counter motions, damper parameters on pelvis and thorax have to be very small (close to cero).

The simulation results reveal that the phenomena of amplitudes', frequencies' and phases' variations can be explained in terms of visco-elastic parameters.

6.4 Parameters optimization

In previous sections, visco-elastic parameters based on mean amplitudes have been introduced. These sections also introduced the motion behaviours due to the action of the damping elements. As shown, these elements produce high frequencies filtering and also, with very larger values, phase variations.

Fig. 6-18 A & B introduce pelvic and thoracic axial rotation and lateral tilt motions of a female test-person. These figures display that the shape of the curves are very weak or not smoothed, showing that damping constants have to be very small. Based on these observations, we can assume that the main task in tuning amplitudes and phases may be performed by the spring elements and the fine tuning by the damping ones.

The present section introduces two methods based on segmental amplitudes and fixed damping values to find personalized visco-elastic parameters. Both methods are based on linear relationships depicted on the model. The first one is applicable to joints 1 and 2 (see fig.6-5) and equations like (6-32). The second method is used to fit motions in joints 3 and 4 and respond to equation (6-35).

It has to be noted, that the methods described below do not try to control the motions, they are only oriented to find the values of the spring constant *k*.

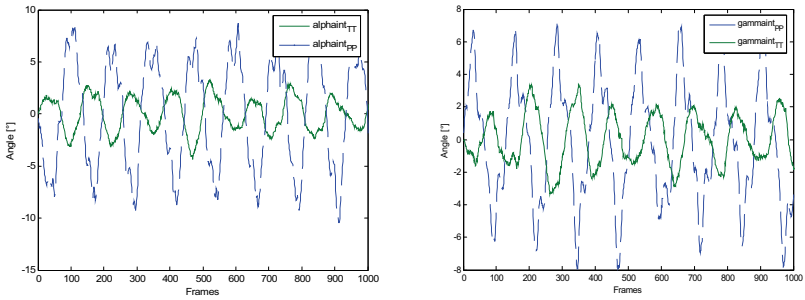

Figure 6- 18 Pelvis and thoracic motion paths of a female test-person. A) Lateral tilt, B) axial rotation

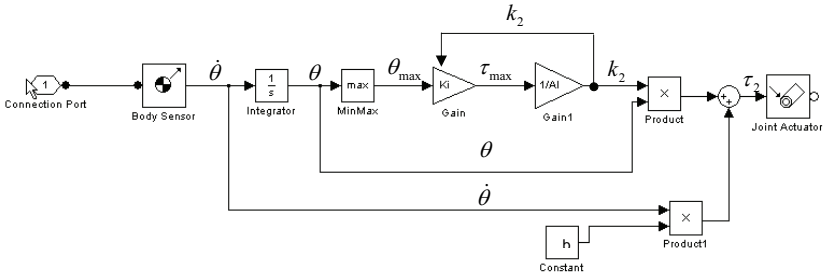

Figure 6- 19 Simulink® diagram for method 1

Fig. 6-19 shows the Simulink® diagram for method 1. As already mentioned this method is based on eq. (6-32). In this case we have three initial values: the spring constant (k_i), the damping constant (b) and the desired amplitude (A_i). The operation mode is the following: The body sensor measures the angular velocities around each axis. These velocities are integrated to obtain the rotations. The maximal rotational amplitudes are measured and then multiplied by the initial spring constant (k_i), in order to obtain τ_{max} by means of the value of (k_i). The relation τ_{max}/A_i returns the new spring constant k_2. This new constant (k_2) replaces (k_i) and is multiplied by the angular displacement to obtain $k_2\theta$ and then summed with $b\dot{\theta}$, in order to obtain the new torque (τ_2). This torque is applied to the joint using a joint actuator. This process is repeated until the difference between current and wanted amplitude is<0,01°.

Fig. 6-20 introduces the Simulink® diagram for method 2. This method is based on eq. (6-35). As before mentioned, the motion fitting is performed from lower to upper segments. That means that for joints like abdomen-thorax, the lower segment (abdomen) has been fitted before (using method 1). Therefore, it is only necessary to match the motion of the upper segment (thorax). In order to do that, we measure both segmental accelerations (lower and upper segments) but we change the spring constant only in relation to the variation of upper segment's amplitude.

Method 2 has the same three initial values, k_i, b, and A_i.

Input 1 and 2 receive angular accelerations form the upper respectively lower segments. These accelerations are, like in method 1, integrated to get the angular displacement. Then, using a maximal amplitude block, the maximal angular amplitude for the upper segment is measured.

In this case the relation to get the k_2 will be:

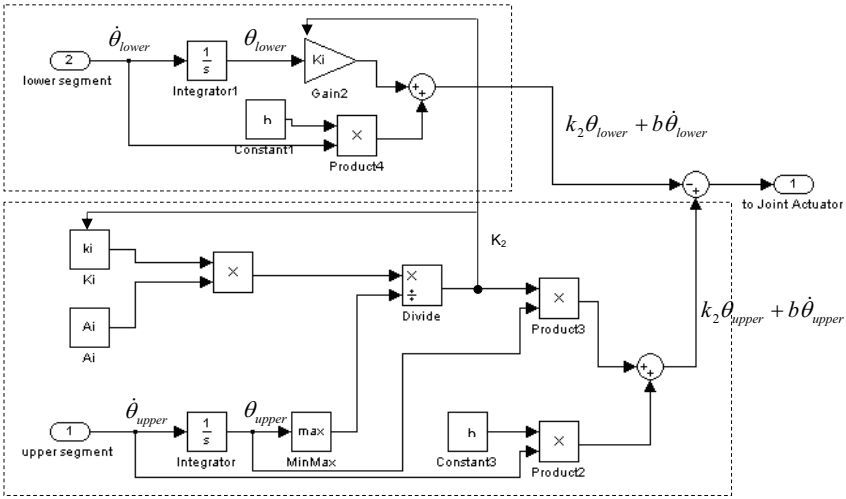

Figure 6- 20 Simulink® diagram for method 2

$$k_2 = \frac{k_i \times A_i}{A_{\max c}} \quad \text{eq. [6-40]}$$

This new k_2 replaces k_i in both segments. Following eq. (6-35), τ will be:

$$\tau = \tau_{upper} - \tau_{lower} = \left(k_2\theta_{upper} + b\dot{\theta}_{upper}\right) - \left(k_2\theta_{lower} + b\dot{\theta}_{lower}\right)$$

The torque is applied to the joint using a joint actuator. This process is repeated until the difference between current and wanted amplitude is < 0,1°.

It has to be remembered, that subsystems like those introduced in figs. 6-19 & 6-20 represent only one DOF. That means, one subsystem is necessary for each rotational DOF.

Finally, fig. 6-21 introduces the complete simulation's module. This module is composed by three m.files (Matlab®) and two trunk models (Simulink®). The first m.file generates the data needed to build the model, as already introduced in section 6.2.1. It then generates the constants also needed to construct the artificial ground reaction forces, using the relations depicted in section 6.2.2 and finally load the initial visco-elastic parameters for each joint.

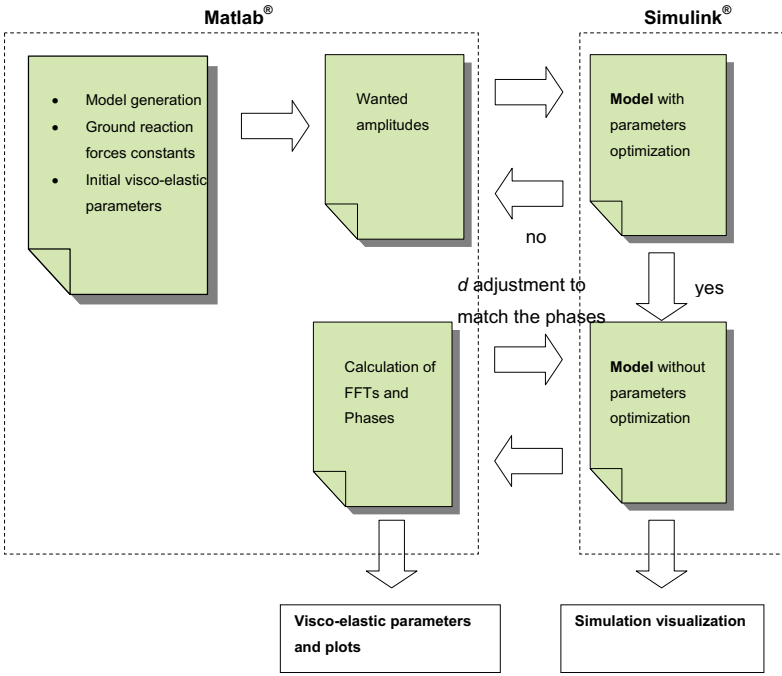

Figure 6- 21 Simulation's module to assess visco-elastic parameters.

The second m.file loads the wanted segmental amplitudes and calls the model with parameters optimization subsystems. Following the method already introduced in section 6.2.4, the m.file activates systematically the parameters optimization subsystem from pelvis towards to the head. In the m.file, each joint DOF is a buckle. Within this buckle the m.file calls the model and switches its correspondent parameter optimization subsystem on. As soon the amplitude is under the tolerance threshold, come out from the buckle and switches this subsystem off. From this point, the fitted joint uses the optimized spring constant. The task continues with the next DOF in the next buckle, which repeats the same operation. Once all segments have been matched, the m.file reruns the process, in order to be sure that all the amplitudes stay under the tolerance. If some segment's amplitude comes out of the tolerance, the optimization process is reloaded. When all amplitudes are under the tolerance, the m.file loads the optimized spring constants and run the second model. This model is the same as the first one, but without the optimization subsystem and is prepared to export the motion matrixes to Matlab®. Once the simulation has been

done, the third m.file plots the motions and computes the FFTs and the phases between them. To calculate FFTs and phases, the m.file uses the functions already developed and introduced in chapter 2. Comparing these results with the real ones, it will be possible to decide, whether damping constants need some adjustments or not. Finally when shapes of curves, amplitudes, frequencies and phase have been matched, the module returns the visco-elastic parameters and the visualization of the simulation.

"It has become appallingly obvious
that our technology has exceeded our humanity".
Albert Einstein

Chapter 7: Applications

7a Non-invasive tool for diagnostic of trunk diseases and their rehabilitation control.

Until today, physicians and therapists discuss, which method should be applied, in order to obtain objective and precise diagnostics in back-pain pathologies. Studies involving clinical or radiological examinations, EMG test and motion analyses on subjects with different back pain pathologies were performed, in order to compare the predictability from each approach. Their results showed that motion analyses are able to return the same predictive values as for clinical or radiological examinations, but also that these predictive values can only be used to differentiate subjects with chronic back pain pathologies from healthy ones (see Andrada & Witte et al. 2006). Another conclusion expresses that neither radiological nor EMG nor motion analysis studies can be used to identify or separate different back-pain pathologies or their causes (Andrada & Witte et al. 2006; Anders et al. 2006).
It is well know that the trunk is systematically deformed and used for the locomotion (Witte et al 2002, 2004). Pathological problems may influence not only these periodical motions, but also the stability of the musculoskeletal system (Andrada & Witte et al. 2006).
Findings of chapter 6 display that visco-elastic parameters can be used to explain changes in amplitudes, frequencies and phases of trunk's segmental parts. Therefore, it is valid to hypothesise that pathological changes on the gait may be explained using visco-elastic parameters as well.
The present section introduces, based on previous studies and our new findings, a new tool for trunk's state diagnosis and rehabilitation's control.

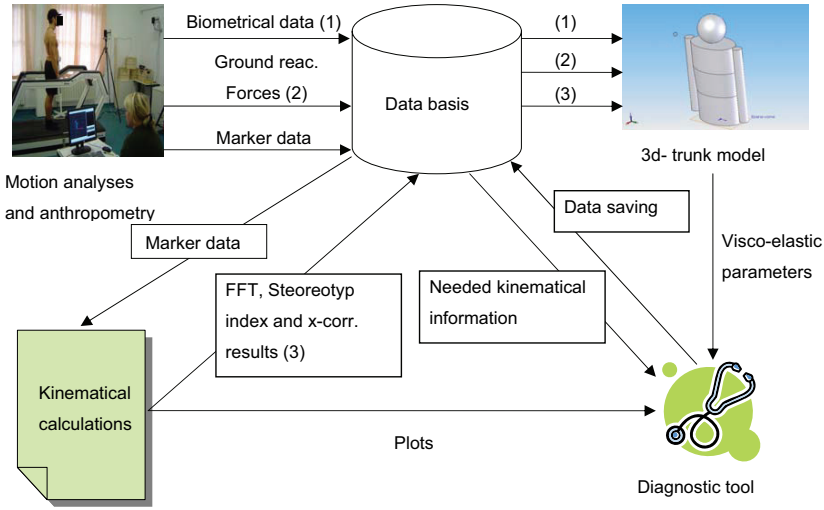

Figure 7- 1 Diagnostic and control process

7a.1 Diagnostic and rehabilitation control process

Fig. 7-1 presents the general diagnostic and rehabilitation control process. The process involves and includes all previous (e.g. stereotype index from Witte et al. 2003) and new findings. It also uses mostly kinematical and simulation tools already introduced in previous chapters.

The general process can be subdivided into four steps. They are:

- Motion analyses and anthropometry
- Kinematical calculations
- Functional model of the trunk
- Diagnostic tool: analyses of kinematical and simulation results

In the following pages, each step of the process will be explained in detail.

7a.1.1 Motion analyses and anthropometry

In the motion analysis test, the subject would walk on a treadmill at a velocity of 4 km/h. The capture of the motion paths of pelvis, abdomen, thorax and head will be performed using marker triplets on sacrum, T10, C7 and head, respectively. All marker triplets have to be attached on the back as shown in fig. 7-2. This arrangement diminishes possible problems with Cardan angle calculations and phase inversions. It permits also a better cameras distribution, which produce a decrement in capture errors.

Figure 7- 2 Marker distribution. They represent the motion of pelvis, abdomen thorax and head.

In order to ensure maximal FFT resolution, sampling periods and sampling frequency should not be smaller than 15 sec. resp. 240 Hz. The data obtained from the motion system will be exported to Matlab® and saved in the data basis.
In chapter 6 was proved that amplitudes, frequencies and phase can be altered using constant ground reaction forces. Nevertheless, they will be measured as well, in order to have more accurately signals for the model. The reaction forces will be saved later as a vector in the data basis.
Finally the 15 anthropometrical parameters needed to construct the model will be measured and saved in the data basis.

7a.1.2 Kinematical calculations

Kinematical calculations will be performed using the routines already programmed and introduced in chapter 2. These routines load the marker data from the data basis, compute the needed data, and then save the results (e.g. absolute and relative amplitudes, frequencies, phases, Stereotyp indexes) again in the data basis. Plots and curve shapes can be directly sent to the diagnostic tool.

7a.1.3 Functional model of the trunk

In this step, the already introduced simulations module will be called (see fig. 6-21). As fig. 7-1 shows, input parameters to construct the model (anthropometrical parameters), kinematical parameters and ground reaction forces are obtained from the data basis. It has to the noted that this simulation's model does not use artificial ground reaction forces, but those from the subject it self. These forces, in form of a vector, will be automatically previously scaled for the model's weight. Out of this difference, the simulations module will perform the same task as those explained in section 6.4 and introduced in fig. 6-21.
When the simulation is ready, visco-elastic parameters and other (if needed) simulation results will be sent to the diagnostic tool and also saved into the data basis.

7a.1.4 Diagnostic and control tool

The diagnostic and control tool is a compendium of kinematical and dynamical information. Amplitudes, offsets, frequencies, phases and Stereotypindex of absolute and relative motions can be displayed and depicted, as well as the visco-elastic parameters among the segments.

How to differentiate sick from healthy persons?

As explained before, Stereotyp-index (Witte et al. 2003) displayed a prediction rate of 95% in separating subjects with chronic back pain pathologies from healthy ones (Andrada & Witte et al 2006). Therefore they can be used for a first approximation. The visco-elastic parameters seem to be significant factors in building motion arrangements. Therefore, if they are responsible for trunk and head motions of healthy subjects, they may also show significant value variations in those subjects with diseases.

Fig. 7-3 introduce a possible element of decision for one DOF. We can suppose that visco-elastic parameters of healthy subjects may follow a normal distribution. Should this be true, visco-elastic parameters outside the Gauss bell may indicate pathologies. Extending this hypothesis, different positions outside the bell (e.g. points 1, 2 and 3 in fig. 7-3) or combination of decision's element patterns for different DOF may also indicate different pathologies.

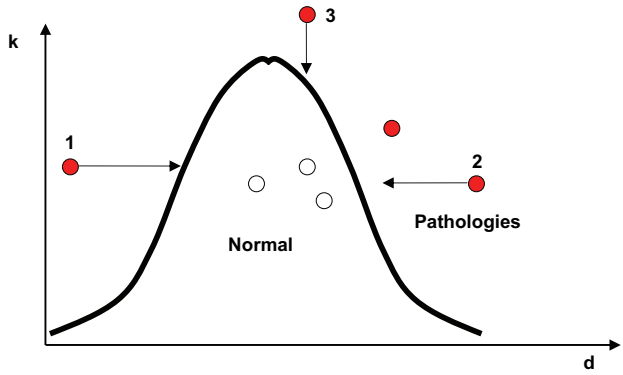

Figure 7- 3 Representation of k in relation to d. Healthy persons should follow a normal distribution, points outside the bell (red points) should signalize pathologies.

Therapy and rehabilitation control

Once the affection's diagnostic was made, the physicians indicate a treatment or therapy. All the decision elements, treatments and therapies can be saved in the data basis.
Until now the success of those treatments or therapies were evaluated in a subjective way (e.g. subject confessions or physicians' impressions). The diagnostic and control tool will offer an objective approach to supervise the course of the treatment. The idea behind is the following: If the treatment impacts positive on the patient, points on the outside (like 1, 2 or 3 in fig. 7-3) should move in direction to the bell, finalizing the treatment when the point is inside the bell. On the other hand if the point does not move, or worst, it moves in the opposite direction. The treatment or therapy does not work or is inadequate.

7b Bionically inspired robots (anthropofunctional machines)

Thanks to the significant technological advances during the last years, bipedal robots (based on anthropomorphic models) today show an impressive high level of humanoid behaviour. In addition, they enjoy autonomy at a relative high degree in sense of information. But out of these (certainly impressive) properties, anthropomorphic based bipedal robots have two main lacks:

a. Energetic autonomy
b. They still appear artificial

Witte & Fischer (et al. 2003, 2004) proposed that robot engineers should observe closer the functional morphology of human walking. With this approach, they can learn from about "*6 Myr beta test period of minimization of power requirements for biped locomotion*" (Witte & Fischer et al. 2004). Indeed if we take a look to the differences between anthropomorphic robots and human beings, it will be easily concluded that the change from anthropomorphic to anthropofunctional machines solves problems a and b at the same time.

The first difference between anthropomorphic robots and humans is that the first use and follow rigid body mechanic laws, human beings those of the elasto-mechanics. The second one is how the control is made. In this item, the control theory in robotics is rather different from motion control in humans. In robots, the control is based on a planed trajectory. Thus to reach a high degree of accuracy in the motion, high performance motors have to be mounted on each motion axis. They produce great moments and also a great friction in the mechanical coupling elements. That kind of constructions conduce to an important power consumption as they have to accelerate and brake each body segment. In addition, because every motion must be planed computed and corroborated, they need a very significant computational work, which conduces to slow and artificial motions. On the other hand, human gait is oriented to minimization of power consumption, which provides autonomy and mobility. This energy efficiency is due to the use of 'energetically optimal velocities' provided by the use of different resonance phenomena and the systematic use of the trunk as a torsional spring.

7b.1 Saving energy and control

The present section introduces a way to save energy and control, based on the findings of chapter 3, 4 and 6.
During this work, it was remembered many times (and shown in chapter 3), that the trunk is used systematically in humans for locomotion. As discussed in chapter 5, the trunk stores mechanical energy as deformation energy in the muscles. As velocity grows, increases the torsion of the trunk as well. In chapter 3 was shown that this mechanism is driven mostly by the change in the phase between the trunk segments. When the maximal deformation was reached, the energy is then restored to the system.

7b.1.1 Using visco-elastic parameters for normal gait

The findings of chapter 6 reveal that:

a) The swing of arms is due to the action of the vertical components of the ground reaction forces, and therefore a passive motion. They must be used,

however, to change the phase shift angles pelvis-thorax on the transverse plane.

b) Visco-elastic parameters explain the change in amplitudes, phases and frequencies of the different body segments in normal walking. They explain also inter and intra individual kinematical variations.
c) No actuators are needed to achieve changes in amplitudes or phases, during normal gait. That means that for walking, the energy obtained from the ground reaction forces is transformed in motions through the mass distribution and their visco-elastic parameters.
d) Motions are poorly damped, which reveals a high conservative system.
e) The relation between motions and visco-elastic parameters is highly linear (for the tolerances described in chapter 6).

Point b introduces that the results of the simulations explain inter and intra individual dispersion in amplitudes and phases. This explanation can be expressed as follows: we have from the beginning of our life, the morphological construction needed for locomotion. We need to learn during the first years how it has to be used (the function). Once we learned to walk correctly, it will not be necessary any more to think about it again. Expressed in visco-elastic parameters, we find the combination of parameters in the trunk with which we can walk stable and autonomic. These “standard settings” are saved and will be always used in straight forward motion (under normal conditions). The intra individual variation of these standard settings added to the particular mass distribution in trunk produces the different gait forms; with them, we recognise for example our friends or family members. By using these learned visco-elastic standard settings, the necessity of central control is reduced and cerebral capacities are liberated for tasks needing more neuronal activity.

Robots designed using the model and the simulations introduced in chapter 6, will be able to enjoy those capabilities. In normal walking, the power consumption will be mostly focuses in moving the legs. In relation to the ground reaction forces, the setting of the visco-elastic parameters in the trunk will be performed. Visco-elastic parameters in technical sense are referred to tuneable spring and damping elements.

As tuneable spring can be used:

- Mechanical springs, in which the change of the k constant is due to the change in spring length.
- Pneumatic springs use the principle of fluid compressibility. Through the compression of gas, the force will be saved as hydrostatic pressure (energy per volume). The variation of the stiffness can be performed altering the initial pressure and/or changing the translation of the piston.

Magnetorheologic fluids (MRF) can be used as tuneable damping elements. The change in the d constant is due to the change in the viscosity of specifically prepared suspension mixtures of iron particles of about 10 microns under the action of a magnetic field.

The use of these tuneable visco-elastic parameters will ensure stability (which will drastically decrease the need of control) and minimization of energy expenditure (in moving arms, trunk and head to be seeing more realistic).
Only when changes in direction or other task (e.g. take some object) are needed, or in case of emergency, the motors will be activated.
As already introduced in Chapter 5, Nadeau et al. (2003) depicted “in block trunk motion strategy” in case of unfamiliar locomotion (like walking with closed eyes, on soft surfaces or backwards walking). From the results of chapter 6, robots using visco-elastic parameters will be able to adopt this strategy to ensure stability without important energy costs.

"The difference between fiction and reality?
Fiction has to make sense".
Tom Clancy

Chapter 8: Discussion for chapters 6 and 7

In the following chapter, the chapters 6 and 7 will be evaluated and discussed.
In order to check hypothesis 2 (see chapter 1), a 14 DOFs functional morphological model of the trunk, based on Hanavan's model, was presented in chapter 6.
As explained before, Hanavan divided the trunk of his model into two cylindrical segments. In the present model, it was necessary to divide the trunk in three segments, because with two it was impossible to achieve motions and phases on the frontal plane between pelvis and thorax. In direct relation to this morphological conformation of the trunk, the link that joins the model with the ground had to be precisely placed above the abdomen. Only when these two requirements were fulfilled, it was possible for the model to represent the observed motion amplitudes and phases. That fact may be a consequence of the surjective relation of mechanics and morphology, which was proposed by Witte et al. (2003) (if you find the morphology, with high probability the mechanics has been described as well).
The change from two to three trunk segments produced an important question: are the abdominal motion amplitudes larger than those of the thorax? The model showed first that those in the frontal plane can not be larger. Indeed if abdominal motions are larger than those of the thorax, spring constant decreases to values, which can not sustain any more the moments produced by thoracic and head motions. This behaviour was depicted later in a locomotion study with two female test-persons. On the other hand, the same study shows larger abdominal amplitudes on the transverse plane than those of the thorax. In this case the simulation did not have problems and worked with larger abdominal axial rotations and with smaller as well.
In the functional morphological model, the legs were replaced by constant ground reaction forces, in order to test whether is possible to obtain different motion frequency and phase patterns only by acting on the visco-elastic parameters.
Although the models did not show stability problems, some adjustments were done in the ground reaction forces when changing between different anthropometrical values.

By using subject's own measured ground reaction forces, that kind of adjustments will be not necessary in the future.

Findings of chapter 6 show that it is possible to model and constrain trunk motions with rotational joints equipped with rotational spring and damper. Result of the simulations could not disprove hypothesis 2. Visco-elastic parameters, which are obtained by the simulations, are a solid base to explain the change in amplitudes, phases and frequencies of the different body segments in normal walking. They also are able to explain inter and intra individual kinematical variations.

The results show also that a systematic amplitude reduction occurs towards to the cranial, cranially which as explained in chapter 5 is used to facilitate gaze fixing in space.

Findings of chapter 6 reveal that the most important reduction of moments is performed in the abdomen. They also introduce that the sagittal tilt frequency (which is twice the oscillation's principal mode) is a consequence of the mechanical construction of the trunk.

In the case of the pelvis, six different visco-elastic combinations were tested. Results show that as pelvic spring constants are increased, motion amplitudes decrease. The effect of the damper constant can be summarised as follow: As damper constants are increased, they act first as a smoothing filter and then, with larger values, reduce the phase from 80° to almost in phase motions. Results from chapter 3 display that the phase γ-α of male volunteers varied form about 100° at 2 km/h to 7° at 6 km/h. At this point, it will be important to ask our self, whether these phase changes may be produced by the increment of the damping constant or may be due to the change in the duty-factor. By observing the graphics of the damped pelvis in the simulation and comparing them with those of the volunteers, we will depict one important difference. The graphics of the volunteers contain important harmonic frequencies, and therefore, they do not look much smoothed. This observation let us hypothesise that the main cause in the change of the phase γ-α may be produced by the variation of the duty-factor.

The movement patterns of the thorax are strongly related to those of the abdomen, our findings show that spring constants are the main cause in changing amplitudes. In the case of thorax, five different visco-elastic configurations were tested. Results of these simulations can be summarized as follow:

Increments in the values of the spring constants conduce to increment in rotational amplitudes. Changes in the thoracic phase γ-α are more related to the variation in the values of damping constants than the change in the values of spring constants. It has to be noted, that trunk phase variation can be achieved actuating either in the visco-elastic parameters on the frontal or transverse planes or both at the same time. The key to solve how much from each plane is given in the phase between thorax and pelvis. Our findings show that to change the phase on the transverse plane, both schoulder-joints have to be damped. On the frontal plane, both spring and damping constants produce changes of phase.
Observations on thoracic frequency spectrum show that by using very large values of damping constant, the amplitude of the principal frequency can be decreased down to a point, where the harmonic frequencies become larger than the principal oscillation's mode.

In chapter 3 was observed that head motions and phases are significantly correlated to those of the thorax. The results of the simulations of chapter 6 add to these observations. One important point is the fact that head axial rotations seem to be independent from visco-elastic parameters (Head axial rotation amplitudes did not vary using different visco-elastic settings and their values were almost the same to those of the thorax). Therefore, axial rotation phase shift angles are close to zero. This fact reveals that in order to have negative phases between head and thorax on the transverse plane (like some displayed in chapter 3), controlled and acted motions are needed.
Chapter 5 discussed the compensation mechanism occurring between head and trunk. In that chapter, compensation mechanisms were also explained in terms of phase shift angles like γ-Y and Z-β. The simulations display that kind of mechanism without acting in any way thorax or head. That may mean that they are a result of the motion's dynamics and not due to an active control.

Simulation results of relative motions between pelvis and thorax show that by manipulating visco-elastic parameters, it is possible to change from "counter" to "in phase motions" on both frontal and transverse planes. They introduce also that the main task is performed in the joint abdomen-thorax, which means changes in the

phase γ-α in thorax. One important point to be addressed is that phase adjustments in one plane do not affect significantly phase shift angles on the other plane.

Chapter 6 also introduces a very robust optimization method to assess values of the spring constants. The method is based on the observation and comparison between the motion patterns of the test-person and the results of the simulations. The pattern of the test-person displayed very weak or not smoothed patterns, which may mean very small damping values and a high conservative system. Therefore, the optimization routine was based in two assumptions:

- Spring elements may perform the main task in tuning amplitudes and phases.
- Damping elements may perform the fine tuning.

From the experience with the model it is possible to make a first approximation of the damping constants (normally very small values). The automatic optimization process for assessing spring constant takes no more than 2 minutes (for the tolerances described in chapter 6) to fit the amplitudes. After obtaining the first results, it takes no more than 10 minutes to achieve the phases as well.

Criteria to change phases between pelvis and thorax on the transverse plane are:

1) Without damping on the shoulder-joints phases stay around 180°,
2) as the damping values in shoulder-joints increase, the phase between pelvis-thorax decreases down to values close to cero (for damping values about 0,5).

Criteria to change phases between pelvis and thorax on the frontal plane are:

1) As explained before, spring constant on the joint abdomen-thorax produces change of phase, therefore, with the amplitude approximation, the phase will be approximated as well. With larger spring values, amplitudes increase and phases decrease. When phases reach values close to cero, the pelvic and thoracic amplitudes display almost same amplitudes. That means they work as one body.
2) Damping values work in a different way than spring values. As damping values increase, both amplitudes and phases decrease. Important to be addressed here is that phases decrease in a more significant way than amplitudes.

This method has to be revised and completely automated in the future using the subject's ground reaction forces.

Chapter 7 introduces two different application fields for the simulations and the visco-elastic parameters. The first one is a medical oriented application, while the second is oriented to bionic inspired robots or morphofunctional machines.
The "Non-invasive tool for diagnostic of trunk diseases and their rehabilitation control" is a method including for the first time both kinematical and dynamical aspects of the spine, during locomotion. It attends to present a new and objective way for diagnosis and therapy control. This method summarizes the programs and simulations used to build this work. It presents also objective decision elements to make diagnosis and to control the rehabilitation.
Due to the marker distribution used for the documentation of trunk and head motions (see chapter 2), the significant kinematical amount of data stored and computed in chapters 3 and 4 can not be used to build the normal distribution of visco-elastic parameters in healthy persons. Therefore, a new study with similar amount subjects (50 males and 50 females) has to be performed. This must also follow the methods described in point 7a.1.1. Once the normal distribution was completed, another study with subjects suffering from different back pain pathologies (using the same set-up) has to be performed. Only after the above mentioned studies have been done, it will be possible to confirm the viability in using visco-elastic parameters as trunk decease predictors.
The decision element introduced in fig. 7-3 (chapter 7) displays one of the possible different ways to achieve a diagnostic. Not only this method, but also the combination of different elements as well as their integration with kinematical data have to be intensively investigated in the future.

In section 7b was introduced and discussed, why the design of biped robots should be based on functional morphology. In that section, two important lacking points in morphological based machines were presented. Visco-elastic parameters were presented as a solution of these problems as well as a bridge between morphological and morphofunctional machines. Finally, technical principles for tunable spring and damper were introduced.

"The only good is knowledge
and the only evil is ignorance".
Socrates

Chapter 9: Conclusion

Since Weber & Weber (1836), biomechanical observations and models of human walking were restricted to the extremities' behaviour. This paradigm has driven biomechanical investigation during the last century. Observing that, it can not surprise that kinematical and dynamical analyses of the trunk started first 15 years ago. After this short period of "dynamical" trunk studies, many kinematical and dynamical aspects about the complex motion arrangement occurring in the trunk during walking stay unexplored. For instance, until today there is not any information about the coupling angles (phase shift angles) concerning absolutes motions of segmental trunk motion.

Questions like: "Can amplitudes or phases be predicted?" "Are the changes in the amplitudes, frequencies or phases a function of anthropometry?" "Why a person has its own gait?" "Could it be possible to find objective parameters in order to describe intra- and inter-individual variations of trunk amplitudes, frequencies and phases?" stay up to here unexplained.

The objective of this work was, from a mechanical point of view, to find answers to these questions. First expanding our kinematical knowledge and relating this to anthropometry and then introducing a new model of the human trunk mechanics in walking.

106 (50 females and 56 males) test-persons (t-p) have participated in the experiment as volunteers. 48 biometrical data hypothesized as relevant have been measured in each t-p. Then they walked on a treadmill with an ascending and descending velocities. The motion of the head, pectoral, and pelvic girdle were tracked with 6 infrared cameras.

More than 100 kinematical parameters were computed for each t-p, including segmental absolute and relative amplitudes, frequencies and phases. Pelvic axial rotations in males and females descend to a minimum at energetically optimal

velocity, immediately they ascend again, those minima can be interpreted as resonance mechanisms. Female's pelvic axial and lateral tilt rotation amplitudes were larger than those displayed by male volunteers. Pelvic frontal tilt in males and females do not show significant dependencies on velocity.

As pelvic axial rotation and lateral tilt amplitudes increase with the velocity, the phase between these rotations change from about 100° to "in phase-motion". At the same time amplitudes of pelvic sagittal and transversal translations must decrease to fit these motions with the increasing frequency.

Thoracic and head kinematics are strong related. Finding of this work show not only similar amplitude patterns related to velocity but also similar coupling angles of absolute translations and rotations for each segment. In addition, head rotations do not compensate thoracic rotations, our result show almost "in phase" rotations on the three planes of motion.

By comparing amplitudes of pelvis, thorax and head, a systematic restriction of absolute segmental amplitudes towards to the head can be depicted. These damping mechanisms occurring on transversal and frontal planes helps the gaze stabilization system, by reducing the ocular compensation necessary to maintain gaze on a fixed target. In addition, finding of the present work show that: 1. Amplitude reductions are stronger for the frontal plane than for the transversal one, 2. damping mechanisms are imprinter in females than in males.

Our results show that coupling angles between translations and rotations vary not only as a function of velocity but also between genders. As a result of that, the present work displays that the so called "compensation mechanism" between head rotations and body or shoulder translations are first velocity dependent, but also that woman and men use different strategies. Indeed, this work introduced for first time results that show that females, in contrast to males, use systematically trunk compensation mechanisms as velocity grows.

Trunk lateral flexions in males and females show a resonance dent close to the energetically optimal velocity, above this, amplitudes of females are slightly larger. Neither male nor female trunk torsion's curves display resonance dents. Trunk torsion amplitudes for females are significantly larger than those of males. Responsible for the increment of the trunk torsion are 1. the increment in the pelvic

axial rotation due to the systematic velocity growth and 2. the increment in the phase shift angle between pelvis and thorax.
All these results display that the trunk is systematically used for locomotion, and introduce also two main tasks due to the change of phase. The phase must grow first to absorb the increasing forces coming from the legs and second, to prevent increasing rotational movement in thorax.

The results of statistical tests performed involving kinematical and biometrical data display that amplitudes of pelvic, thoracic or trunk rotations and translations of males and females are not easily related with anthropometry, neither on biometrical data associated to the inverted pendulum and ballistic walking models, nor on linear combinations between them.
One important point is that correlation coefficients between rotations and translation not only vary depending on profiles but also correlations can appear or disappear. This behaviour displays changes in motion strategies depending whether speeds are going faster or slower.
An important finding, however, reveals that if we divide the legs' length in three clusters (short, middle and long legs) trunk's torsion and lateral flexion frequencies show significant decrements ($p<0,01$ resp. $p<0,05$), as we move from short to long legs. This fact displays the influence of the inverted pendulum.

In order to find the causes of trunk amplitudes, frequencies and phases' variations, a functional morphological model of the trunk based on Hanavan's model was developed.
Our findings show that it is possible to model and constrain trunk motions with rotational joints equipped with rotational spring and damper (visco-elastic elements). Result of the simulations could not disprove that visco-elastic parameters, which are obtained by the simulations, are a solid base to explain the change in amplitudes, phases and frequencies of the different body segments in normal walking. They also are able to explain inter and intra individual kinematical variations.
Simulation results show also that a systematic amplitude reduction occurs towards to the cranial, cranially which as explained is used to facilitate gaze fixing in space. In this direction, our findings reveal that the most important reduction of moments (damping mechanism) is performed in the abdomen. They also introduce that the

sagittal tilt frequency (which is twice the oscillation's principal mode) is a consequence of the mechanical construction of the trunk.
The simulations display head compensation mechanism without acting in any way thorax or head. That may mean that they are a result of the motion's dynamics and not due to an active control. This result complements the kinematical ones, in which it is possible to talk about compensation mechanism only above 4 or 5 km/h.
Based on visco-elastic parameters is possible to find explanations to individual gaits: As heritage from our phylogenetical ancestors, the morphological construction needed to walk is given. During the first years of our life we learnt how it has to be used (the function). Expressed in visco-elastic parameters, we find the combination of parameters in the trunk (muscle activation) to walk stable and autonomic. These "standard settings" are saved and will be always used in straight forward locomotion (under normal conditions). The intra individual variation of these standard settings added to the particular mass distribution in trunk produces the different gait forms; with them, we recognise for example our friends or family members.

The present work introduces two different application fields for the simulations and the visco-elastic parameters. The first one is a medical oriented application, while the second is oriented to bionic inspired robots or morphofunctional machines.
The "Non-invasive tool for diagnostic of trunk diseases and their rehabilitation control" is a method including for the first time both kinematical and dynamical aspects of the spine, during walking. It attends to present a new and objective way for diagnosis and therapy control.
For the bionically inspired robots' application, visco-elastic parameters were presented as a solution for saving energy and control as well as a bridge between morphological and morphofunctional machines.

In further works the here presented model of the human trunk mechanics in walking should be equipped with legs, in order to investigate the energy flow between trunk and extremities. New experiments using the "Non-invasive tool for diagnostic of trunk diseases and their rehabilitation control" must be performed to test whether visco-elastic parameters can be used as disease predictors.

The trunk must be understood as a synthesis of morphology and function. Simplified models of the trunk conduce to complicated control strategies. On the other hand more complicated models do not necessary means complicated control. We have shown that morphofunctional based models not only help us to understand the biomechanics of locomotion, but also that the technical adoption of morphofunctional based models may reduce in a significant way the need of control.

Appendix A

Due to the fact that I have worked with a German version of SPSS®, the histograms are presented in German language. In order to avoid difficulties in understanding the graphics, the following table introduce the English translation for each German term.

Body height	Körperhöhe
Shoulder height (right)	Schulterhöhe_re
Shoulder height (left)	Schulterhöhe_li
Upper arm height (right)	Oberarmhöhe_re
Upper arm height (left)	Oberarmhöhe_li
forearm height (right)	Unterarmhöhe_re
forearm height (left)	Unterarmhöhe_li
Finger pick height (right)	Fingerspitzenhöhe_re
Finger pick height (left)	Fingerspitzenhöhe_li
Leg length (right)	Beinhöhe_re
Leg length (left)	Beinhöhe_li
Knee height, standing (right)	Kniehöhe_re
Knee height, standing (left)	Kniehöhe_li
Ankle height, standing (right)	Knöchelhöhe_re
Ankle height, standing (left)	Knöchelhöhe_li
Scretch of arms	Spannweite
Shoulder width (bi acromial)	Schulterbreite
Ribcage width, standing	Brustkorbbreite
Waist width, standing	Taillenbreite
Pelvis width, standing	Beckenbreite
Foot length, standing (right)	Fußlänge_re
Foot length, standing (left)	Fußlänge_li
Thoracic circumference	Brustumfang
Waist circumference	Taillenumfang
Pelvis circumference	Beckenumfang
Arm circumference (right)	Armumfang_re
Arm circumference (left)	Armumfang_li
Leg circumference (right)	Beinumfang_re
Leg circumference (left)	Beinumfang_li
Spine height (C7)	Rumpfhöhe_sitz
Knee height, sitting (right)	Kniehöhe_re_sitz
Knee height, sitting (left)	Kniehöhe_li_sitz

Ankle height, sitting (right)	Knöchelhöhe_re_sitz
Ankle height, sitting (left)	Knöchelhöhe_li_sitz
Ribcage width, sitting	Brustkorbbreite_sitz
Waist width, sitting	Taillenbreite_sitz
Pelvis width, sitting	Beckenbreite_sitz
Thigh length, sitting (right)	Oberschenkellänge_re_sitz
Thigh length, sitting (left)	Oberschenkellänge_li_sitz
Foot length, sitting (right)	Fußlänge_re_sitz
Foot length, sitting (left)	Fußlänge_li_sitz
Head width	Kopfbreite
Head height	Kopfhöhe
Head depth	Kopftiefe
Weight, standing	Gewicht_stehend
Weight, sitting	Gewicht_sitzend
Frequency	Häufigkeit

A1 Histograms (Females)

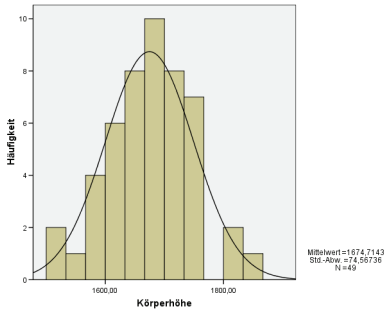

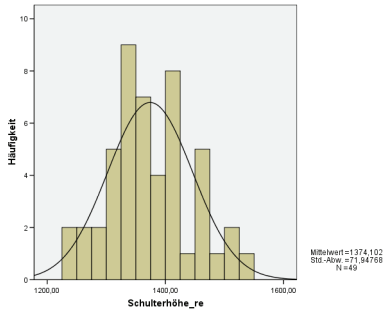

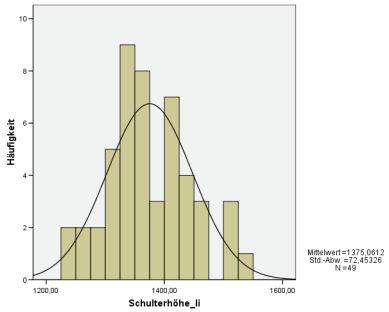

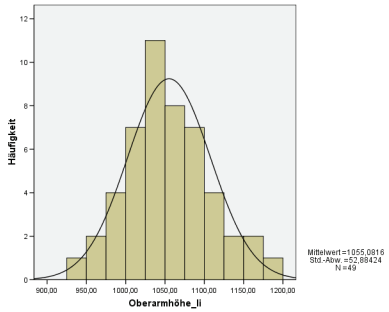

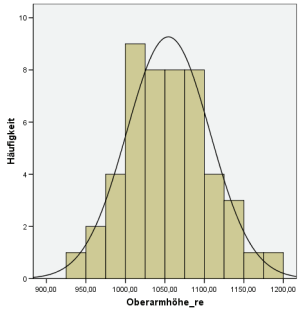
Häufigkeit
Oberarmhöhe_re
Mittelwert=1054,4082
Std.-Abw.=52,72923
N=49

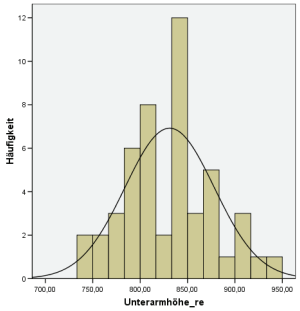
Häufigkeit
Unterarmhöhe_re
Mittelwert=831,0612
Std.-Abw.=47,66618
N=49

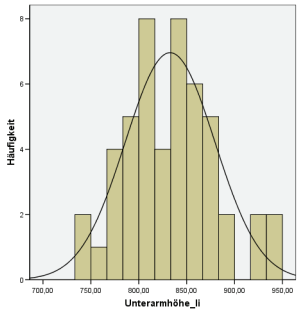
Häufigkeit
Unterarmhöhe_li
Mittelwert=832,6939
Std.-Abw.=46,80509
N=49

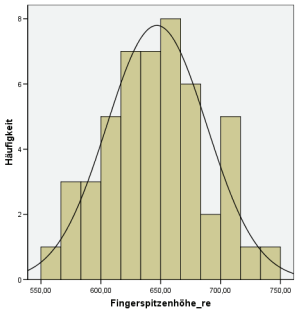
Häufigkeit
Fingerspitzenhöhe_re
Mittelwert=646,7551
Std.-Abw.=41,79341
N=49

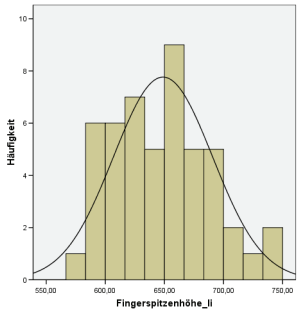
Häufigkeit
Fingerspitzenhöhe_li
Mittelwert=648,7959
Std.-Abw.=41,95284
N=49

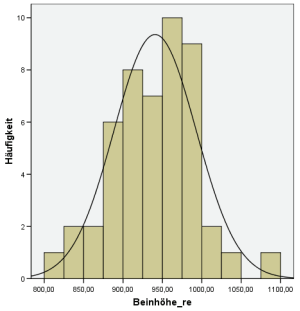
Häufigkeit
Beinhöhe_re
Mittelwert=940,6735
Std.-Abw.=52,22443
N=49

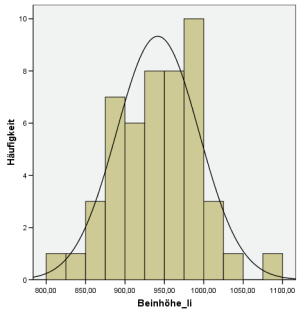
Häufigkeit
Beinhöhe_li
Mittelwert=941,5306
Std.-Abw.=52,37608
N=49

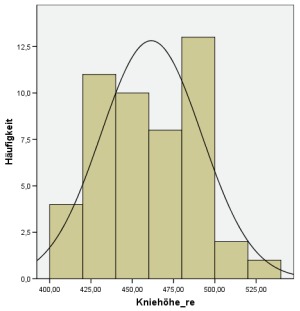
Häufigkeit
Kniehöhe_re
Mittelwert=461,4694
Std.-Abw.=30,50827
N=49

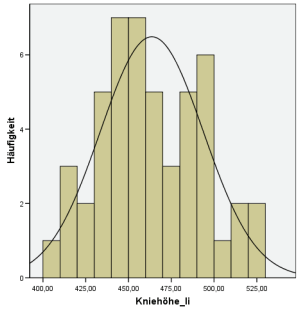
Häufigkeit
Mittelwert=463,6122
Std.-Abw.=30,1336
N=49
Kniehöhe_li

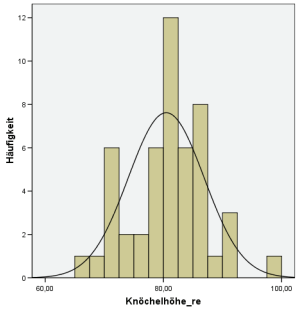
Häufigkeit
Mittelwert=80,4694
Std.-Abw.=6,41646
N=49
Knöchelhöhe_re

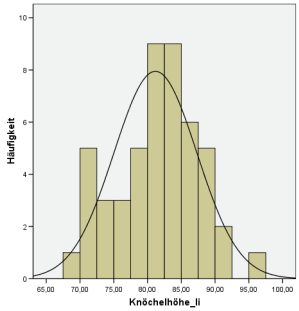
Häufigkeit
Mittelwert=81,1633
Std.-Abw.=6,14867
N=49
Knöchelhöhe_li

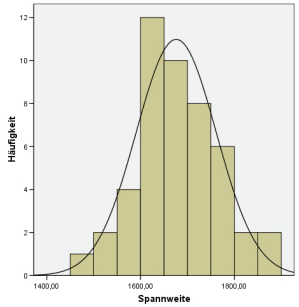
Häufigkeit
Mittelwert=1676,00
Std.-Abw.=85,3624
N=47
Spannweite

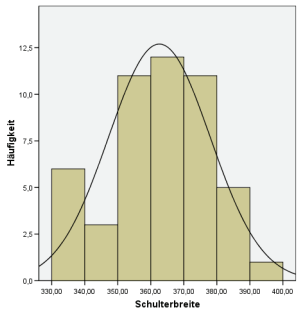
Häufigkeit
Mittelwert=362,5918
Std.-Abw.=15,39605
N=49
Schulterbreite

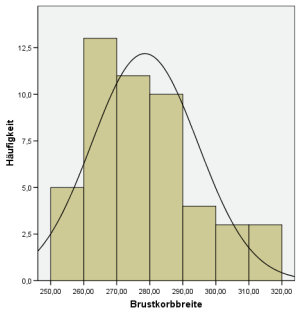
Häufigkeit
Mittelwert=278,4898
Std.-Abw.=16,04307
N=49
Brustkorbbreite

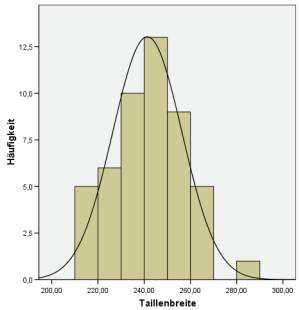
Häufigkeit
Mittelwert=241,3469
Std.-Abw.=14,99799
N=49
Taillenbreite

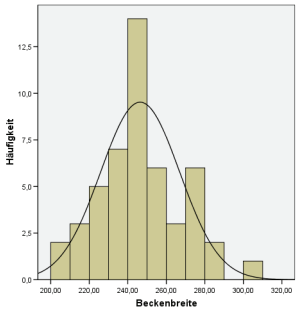
Häufigkeit
Mittelwert=246,4082
Std.-Abw.=20,52125
N=49
Beckenbreite

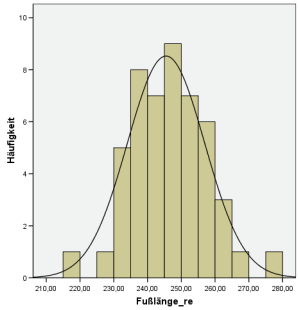
Häufigkeit
Fußlänge_re
Mittelwert=245,4694
Std.-Abw.=11,4639
N=49

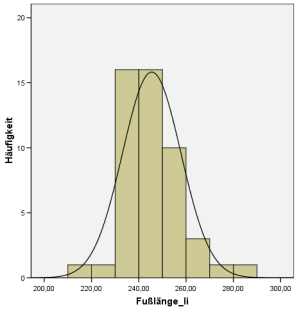
Häufigkeit
Fußlänge_li
Mittelwert=245,4694
Std.-Abw.=12,35432
N=49

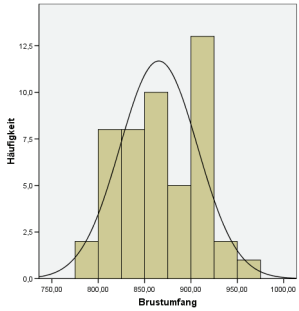
Häufigkeit
Brustumfang
Mittelwert=865,3061
Std.-Abw.=41,83609
N=49

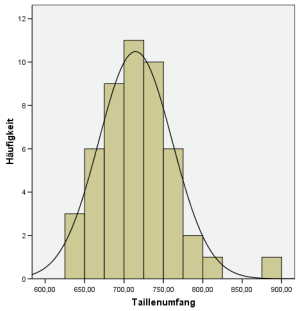
Häufigkeit
Taillenumfang
Mittelwert=714,551
Std.-Abw.=46,62129
N=49

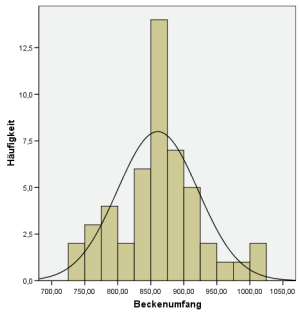
Häufigkeit
Beckenumfang
Mittelwert=860,551
Std.-Abw.=61,0908
N=49

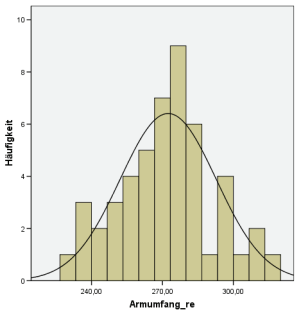
Häufigkeit
Armumfang_re
Mittelwert=272,4286
Std.-Abw.=20,33777
N=49

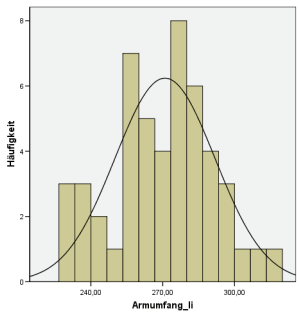
Häufigkeit
Armumfang_li
Mittelwert=270,9388
Std.-Abw.=20,89302
N=49

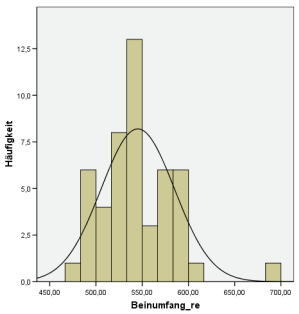
Häufigkeit
Beinumfang_re
Mittelwert=545,2245
Std.-Abw.=39,74464
N=49

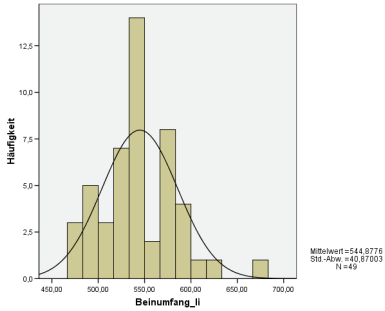
Häufigkeit
Beinumfang_li
Mittelwert = 544,8776
Std.-Abw. = 40,87003
N = 49

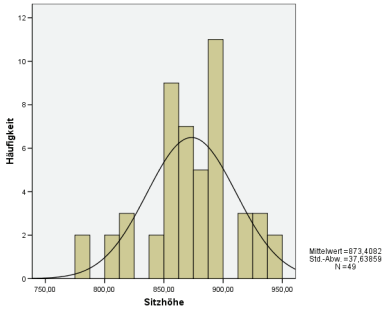
Häufigkeit
Sitzhöhe
Mittelwert = 873,4082
Std.-Abw. = 37,63859
N = 49

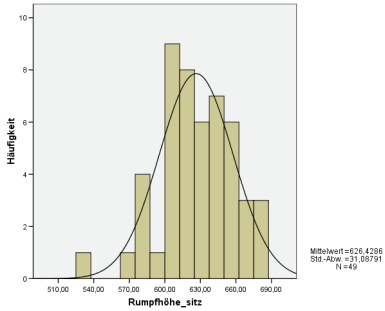
Häufigkeit
Rumpfhöhe_sitz
Mittelwert = 626,4286
Std.-Abw. = 31,08791
N = 49

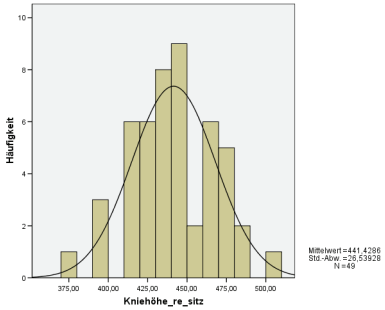
Häufigkeit
Kniehöhe_re_sitz
Mittelwert = 441,4286
Std.-Abw. = 26,53928
N = 49

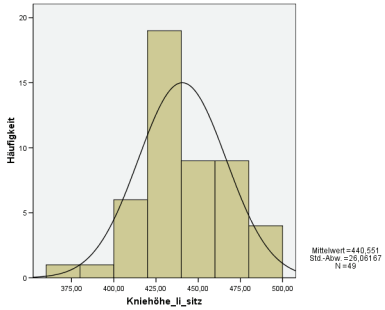
Häufigkeit
Kniehöhe_li_sitz
Mittelwert = 440,551
Std.-Abw. = 26,06167
N = 49

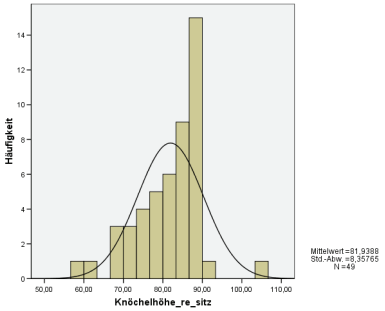
Häufigkeit
Knöchelhöhe_re_sitz
Mittelwert = 81,9388
Std.-Abw. = 8,35765
N = 49

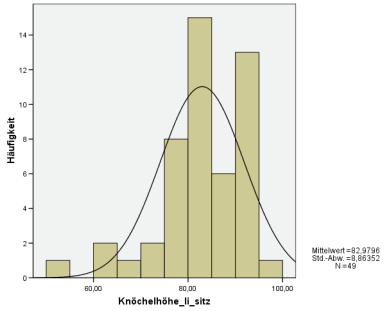
Häufigkeit
Knöchelhöhe_li_sitz
Mittelwert = 82,9796
Std.-Abw. = 9,86352
N = 49

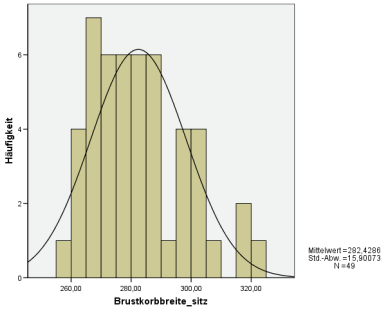
Häufigkeit
Brustkorbbreite_sitz
Mittelwert = 282,4286
Std.-Abw. = 15,90073
N = 49

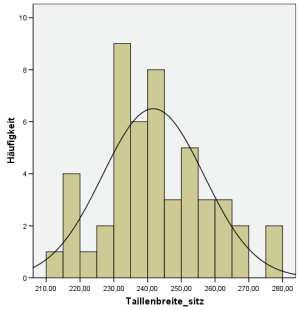
Häufigkeit
Taillenbreite_sitz
Mittelwert=241,6939
Std.-Abw.=15,03635
N=49

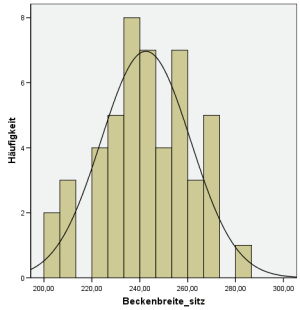
Häufigkeit
Beckenbreite_sitz
Mittelwert=242,5306
Std.-Abw.=18,70172
N=49

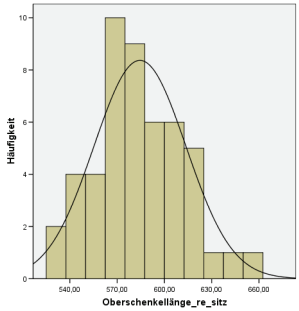
Häufigkeit
Oberschenkellänge_re_sitz
Mittelwert=594,449
Std.-Abw.=29,20193
N=49

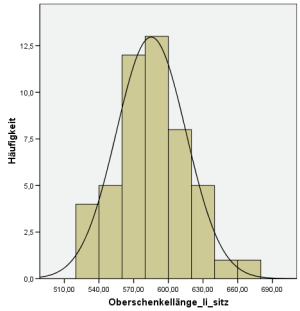
Häufigkeit
Oberschenkellänge_li_sitz
Mittelwert=595,1633
Std.-Abw.=30,15747
N=49

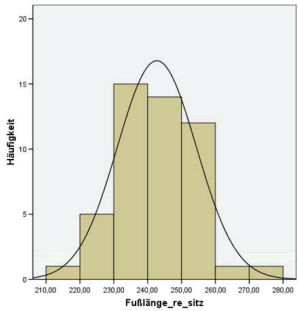
Häufigkeit
Fußlänge_re_sitz
Mittelwert=242,7143
Std.-Abw.=11,64939
N=49

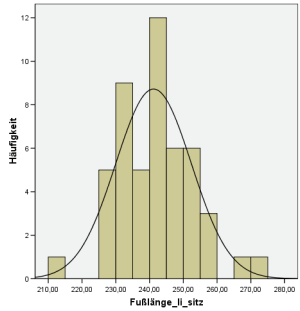
Häufigkeit
Fußlänge_li_sitz
Mittelwert=241,1837
Std.-Abw.=11,20579
N=49

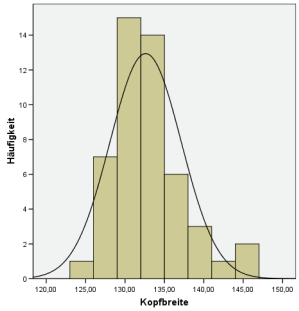
Häufigkeit
Kopfbreite
Mittelwert=132,6122
Std.-Abw.=4,53145
N=49

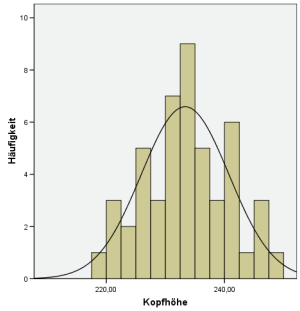
Häufigkeit
Kopfhöhe
Mittelwert=233,3265
Std.-Abw.=7,41448
N=49

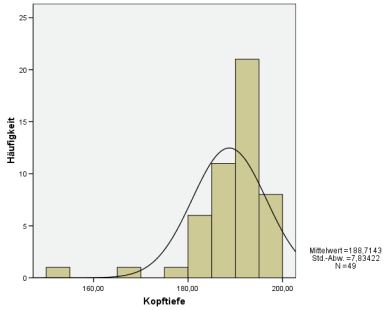

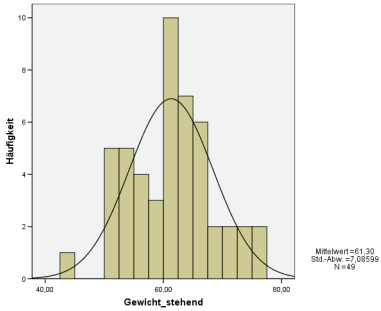

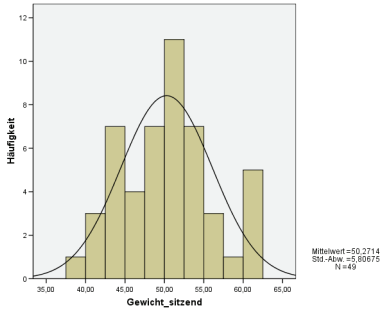

A2 Histograms (Males):

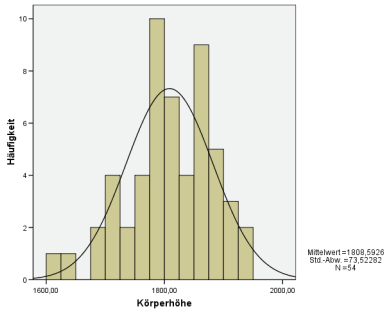

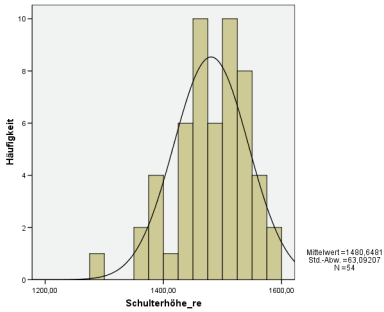

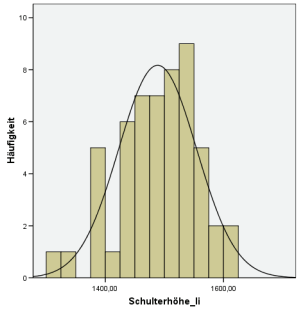
Häufigkeit
Schulterhöhe_li
Mittelwert=1488,5185
Std.-Abw.=65,81087
N=54

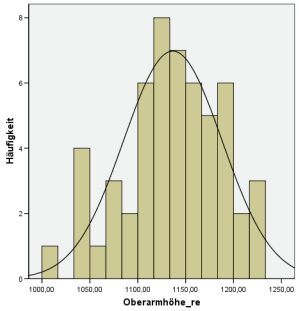
Häufigkeit
Oberarmhöhe_re
Mittelwert=1136,5741
Std.-Abw.=51,45197
N=54

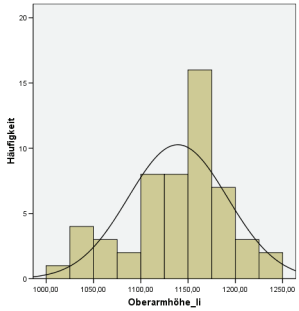
Häufigkeit
Oberarmhöhe_li
Mittelwert=1139,1667
Std.-Abw.=52,44971
N=54

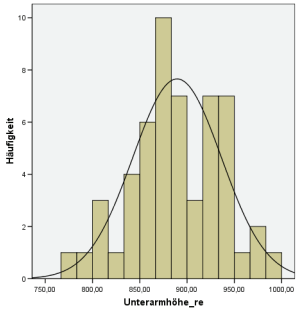
Häufigkeit
Unterarmhöhe_re
Mittelwert=899,4444
Std.-Abw.=46,89477
N=54

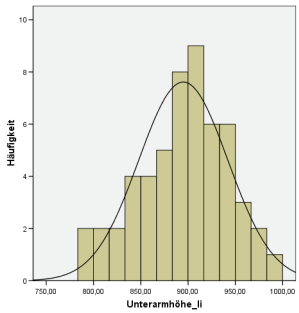
Häufigkeit
Unterarmhöhe_li
Mittelwert=894,9259
Std.-Abw.=47,15044
N=54

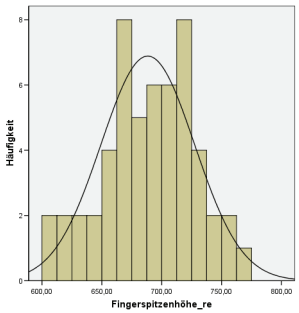
Häufigkeit
Fingerspitzenhöhe_re
Mittelwert=698,3333
Std.-Abw.=39,10171
N=54

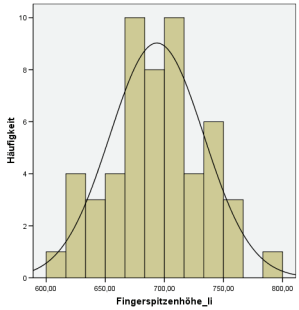
Häufigkeit
Mittelwert =693,6111
Std.-Abw. =39,77456
N =54
Fingerspitzenhöhe_li

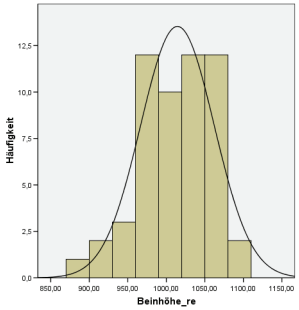
Häufigkeit
Mittelwert =1014,3989
Std.-Abw. =47,76057
N =54
Beinhöhe_re

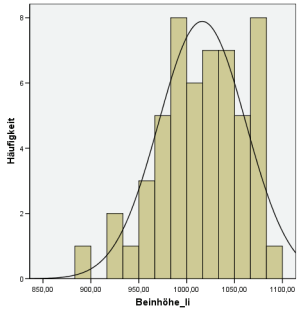
Häufigkeit
Mittelwert =1016,2407
Std.-Abw. =45,50801
N =54
Beinhöhe_li

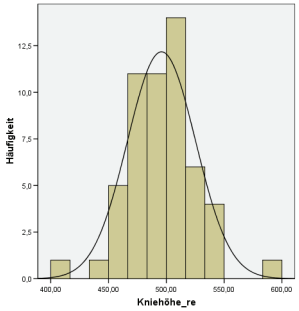
Häufigkeit
Mittelwert =495,9333
Std.-Abw. =29,4892
N =54
Kniehöhe_re

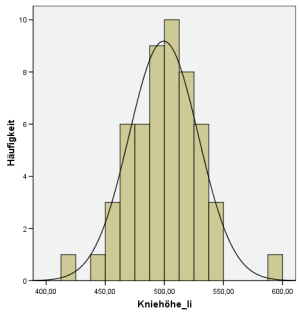
Häufigkeit
Mittelwert =499,3704
Std.-Abw. =29,32402
N =54
Kniehöhe_li

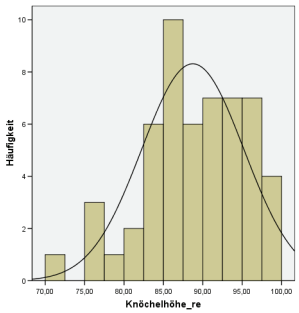
Häufigkeit
Mittelwert =88,7222
Std.-Abw. =6,47904
N =54
Knöchelhöhe_re

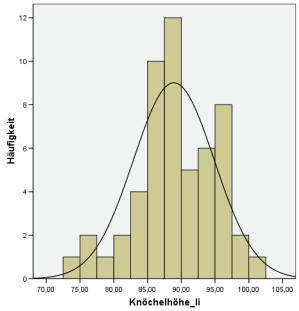
Häufigkeit
Mittelwert =88,8889
Std.-Abw. =5,97689
N =54
Knöchelhöhe_li

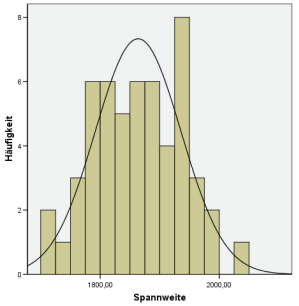
Häufigkeit
Mittelwert =1863,6792
Std.-Abw. =72,06348
N =53
Spannweite

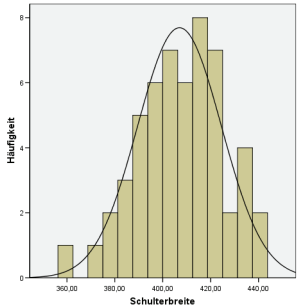
Häufigkeit
Schulterbreite
Mittelwert =407,00
Std.-Abw. =17,50472
N =54

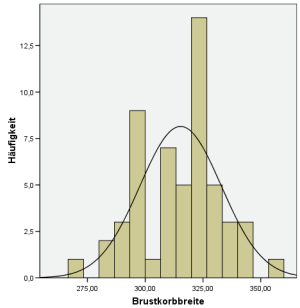
Häufigkeit
Brustkorbbreite
Mittelwert =315,3148
Std.-Abw. =17,62591
N =54

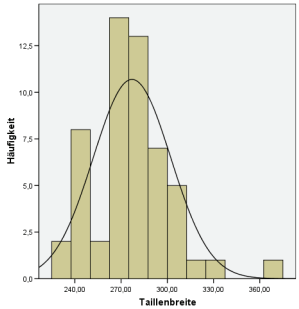
Häufigkeit
Taillenbreite
Mittelwert =277,0741
Std.-Abw. =25,18374
N =54

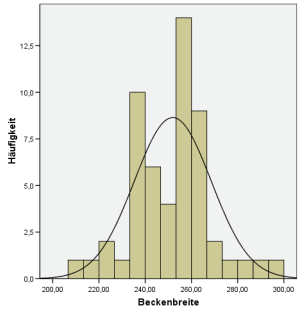
Häufigkeit
Beckenbreite
Mittelwert =251,9259
Std.-Abw. =16,61194
N =54

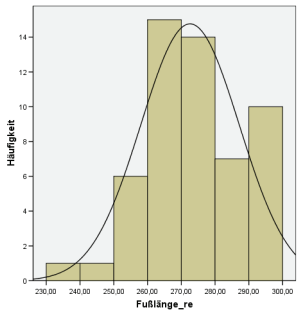
Häufigkeit
Fußlänge_re
Mittelwert =272,5741
Std.-Abw. =14,59077
N =54

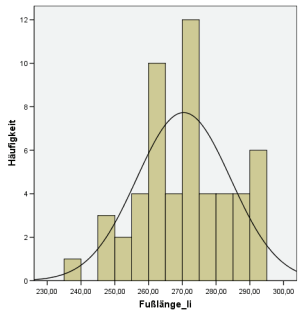
Häufigkeit
Fußlänge_li
Mittelwert =270,3889
Std.-Abw. =13,93031
N =54

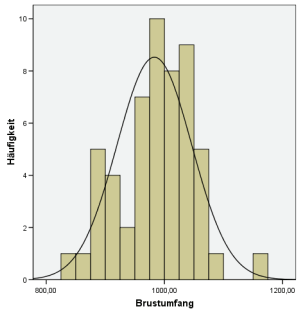
Häufigkeit
Brustumfang
Mittelwert =982,963
Std.-Abw. =63,15986
N =54

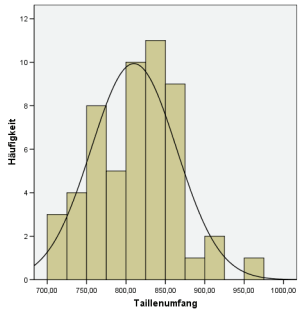
Häufigkeit
Taillenumfang
Mittelwert =809,9815
Std.-Abw. =54,18191
N =54

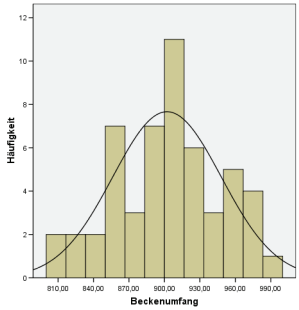
Häufigkeit
Beckenumfang
Mittelwert=902,1698
Std.-Abw.=45,98818
N=53

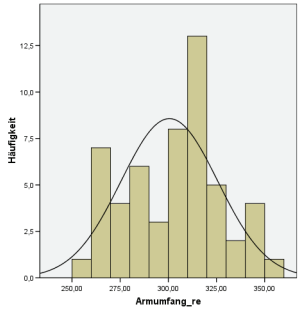
Häufigkeit
Armumfang_re
Mittelwert=300,5556
Std.-Abw.=25,14161
N=54

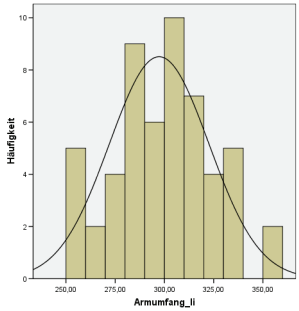
Häufigkeit
Armumfang_li
Mittelwert=297,3148
Std.-Abw.=25,32269
N=54

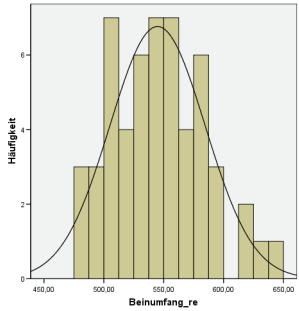
Häufigkeit
Beinumfang_re
Mittelwert=544,8148
Std.-Abw.=39,79858
N=54

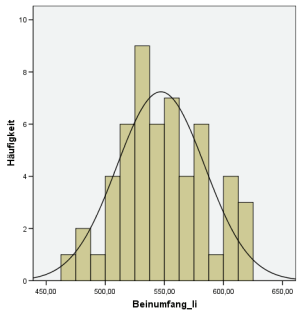
Häufigkeit
Beinumfang_li
Mittelwert=546,9444
Std.-Abw.=37,19425
N=54

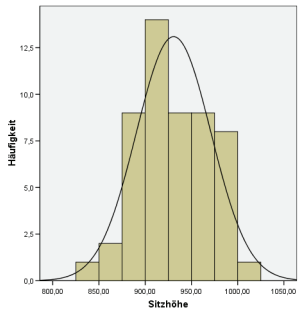
Häufigkeit
Sitzhöhe
Mittelwert=930,7547
Std.-Abw.=40,36702
N=53

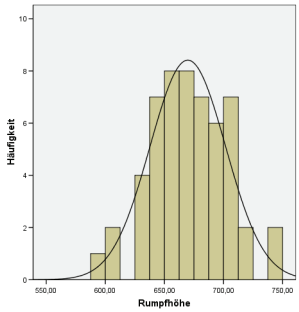
Häufigkeit
Rumpfhöhe
Mittelwert=669,7593
Std.-Abw.=32,00232
N=54

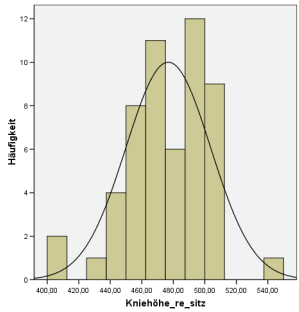
Häufigkeit
Kniehöhe_re_sitz
Mittelwert=476,7963
Std.-Abw.=26,92224
N=54

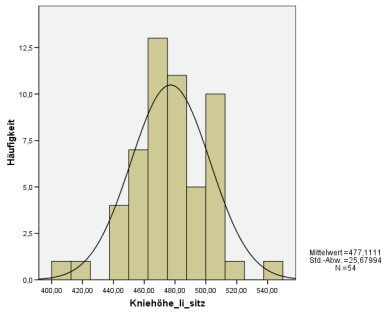
Häufigkeit
Mittelwert=477,1111
Std.-Abw.=25,67894
N=54
Kniehöhe_li_sitz

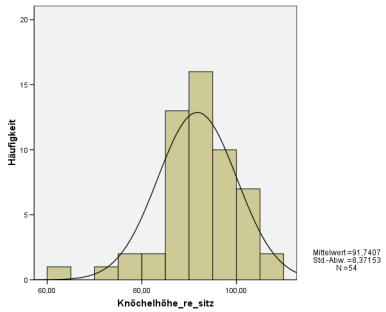
Häufigkeit
Mittelwert=91,7407
Std.-Abw.=8,37153
N=54
Knöchelhöhe_re_sitz

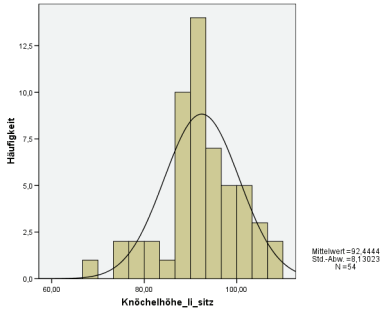
Häufigkeit
Mittelwert=92,4444
Std.-Abw.=8,13023
N=54
Knöchelhöhe_li_sitz

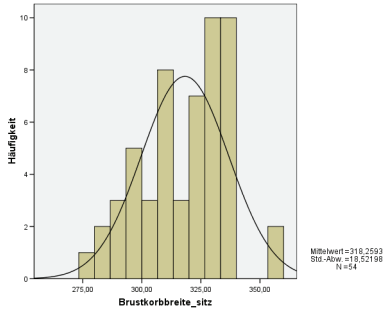
Häufigkeit
Mittelwert=318,2593
Std.-Abw.=18,52198
N=54
Brustkorbbreite_sitz

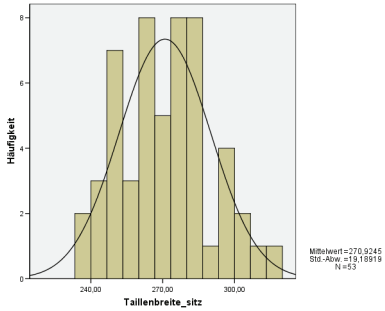
Häufigkeit
Mittelwert=270,9245
Std.-Abw.=19,18919
N=53
Taillenbreite_sitz

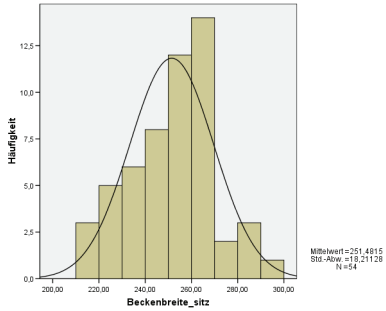
Häufigkeit
Mittelwert=251,4815
Std.-Abw.=18,21128
N=54
Beckenbreite_sitz

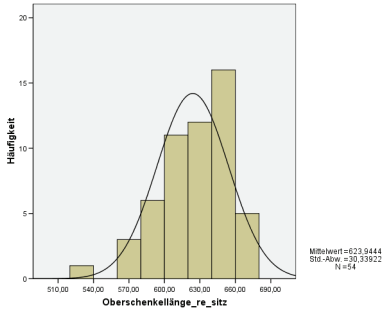
Häufigkeit
Mittelwert=623,9444
Std.-Abw.=30,33922
N=54
Oberschenkellänge_re_sitz

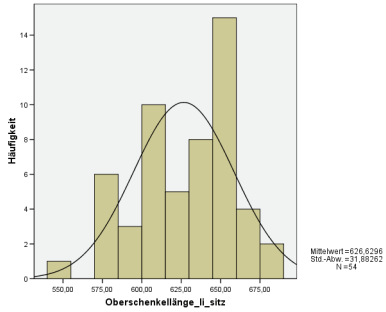
Häufigkeit
Mittelwert=626,6296
Std.-Abw.=31,88262
N=54
Oberschenkellänge_li_sitz

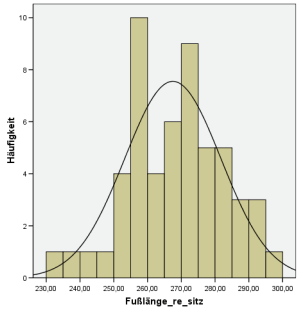
Häufigkeit
Fußlänge_re_sitz
Mittelwert=267,4815
Std.-Abw.=14,26136
N=54

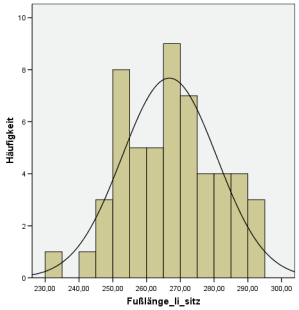
Häufigkeit
Fußlänge_li_sitz
Mittelwert=266,7593
Std.-Abw.=14,02819
N=54

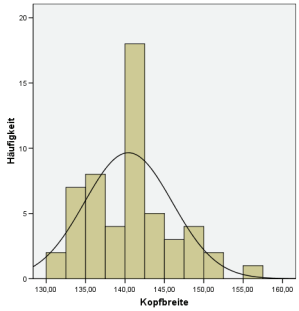
Häufigkeit
Kopfbreite
Mittelwert=140,4259
Std.-Abw.=5,57827
N=54

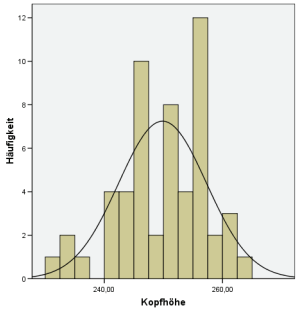
Häufigkeit
Kopfhöhe
Mittelwert=249,8519
Std.-Abw.=7,43375
N=54

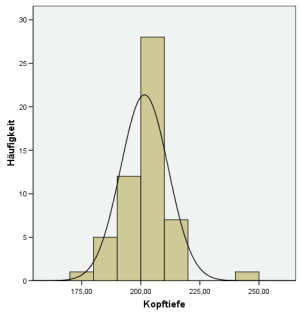
Häufigkeit
Kopftiefe
Mittelwert=201,5556
Std.-Abw.=10,07831
N=54

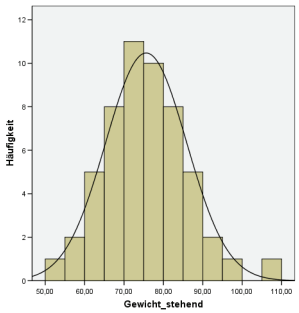
Häufigkeit
Gewicht_stehend
Mittelwert=75,6167
Std.-Abw.=10,28596
N=54

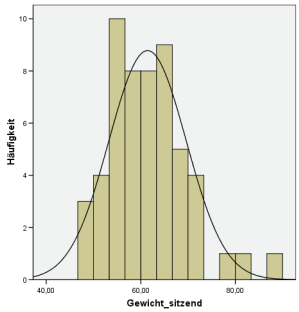
Häufigkeit
Gewicht_sitzend
Mittelwert=61,4296
Std.-Abw.=8,1784
N=54

Bibliography

[1] Abdel-Aziz, Y.I. & Karara, H.M. (1971): Direct linear transformation from comparator co-ordinates into object space co-ordinates. *Proc. ASP/UI Symposium on Close-range Photogrammetry.* Am. Soc. Of Photogrammetry, Falls Church, VA. Pp. 1-18.

[2] Alexander, R.McN. & Jayes A.S. (1978): Vertical movements in walking and running. *J. Zool., Lond*. 185: 27-40.

[3] Analytical Dynamics. Haim Baruh. WCB/ McGraw-Hill, 1999.

[4] Andrada, E., Stadelbauer, B., Carl, K., Voges, D., Witte, H. (2006): How to make better undestandable the mechanical behaviour of the human trunk during locomotion (abstract). *Chinese J. of Pathophysiology.* 22(13): 133.

[5] Andrada, E., Stadelbauer, B., Carl, K., Voges, D., Witte, H. (2006): Zusammenhänge zwischen Rumpfbewegung und Körpermaßen bei Menschen.-In R. Grieshaber, M. Stadeler, H-C. Scholle (Hrsg.). 12. Erfurter Tage. Prävention von arbeitsbedingten Gesundheitsgefahren und Erkrankungen. Verlag Dr. Bussert & Stadeler.

[6] Barter, J.T. (1957): Estiamtion of the mass of body segments. Techincal Report WADC TR 57-260. Wright-Patterson Air Force Base, Ohio.

[7] Biomechanics and biology of movement. Edited by Benno M. Nigg, Brian R. MacIntosh, Joachim Mester. Human Kinetics, 2000.

[8] Biomechanics of the Musculo-skeletal System, second edition. Edited by Benno M. Nigg & Walter Herzog. John Wiley & Sons, 2002.

[9] Braune, W. & Fischer, O. (1889): The center of gravity of the Human body as related to the german Infantryman, Leipzig.

[10] Capozzo, A. (1983): The forces and couples in the human trunk during level walking. *J. Biomech.* 16(4): 265-277.

[11] Cavagna, G.A., Thys, H & Zamboni, A. (1977): Mechanical work in terrestrial locomotion: two basic mechanism for minimizing energy expenditure. *Am. J. Physiol.* 233: 243-261.

[12] Clinical Biomechanics of the Spine, second edition. Augustus A. White III & Manohar M. Panjabi. Lippincott Williams & Wilkins, 1990.

[13] Crawford, N.R., Yamaguchi, G. T. & Dickman, C.A. (1996): Methods for determining spinal flexion/extension, lateral bending, and axial rotation from marker coordinate data: Analysis and refinement. *Human Movement Science.* 15: 55-78.

[14] Crosby, J., Vachalathiti, R. & Smith, R. (1997 a): Patterns of spinal motion during walking. *Gait & Posture* 5: 6-12.

[15] Crosby, J., Vachalathiti, R. & Smith, R. (1997 b): Age, gender and speed effects on spinal kinematics during walking. *Gait & Posture* 5: 13-20.

[16] Dempster, W.T. (1955): Space requirements of the seated operator. Geometrical, kinematic and mechanical aspects of the body with special reference to the limbs. Technical Report WADC 55-159. Wright-Patterson Air Force Base, Ohio.

[17] Drerup, B. & Hierholzer, E. (1987): Movement of the human pelvis and displacement of related anatomical landmarks on the body surface. *J. Biomech.* 20: 971-977.

[18] Dvořák, J. Vadja, E.G., Grob, D. & Panjabi, M.M. (1995): Normal motion of the lumbar spine as related to age and gender. *Eur. Spine J.* 4: 18-23.

[19] Dynamic Systems: Modeling and Analysis. Hung V. Vu, Ramin S. Esfandiari. McGraw-Hill, 1997.

[20] Falk Mörl (2004), 3-D-Bewegungsorganisation der lumbalen Wirbelsäule beim Heben. Dissertation. Friedrich-Schiller-Universität Jena.

[21] Feipel, V., Mesmaeker De, T., Klein, P. & Rooze, M. (2000): Three-dimensional kinematics of the lumbar spine during treadmill walking at different speeds. *Eur. Spine J.* (Online) Springer Verlag.

[22] Fischer, M.S., Witte, H. (1998): The functional morphology of the three-segmented limb of mammals and ist specialities in small and medium-sized mammals. *Proc. European Mechanics Colloquium Euromech*, 375 (Biology and Technology of Walking): 10-17.

[23] Flexible Multibody Dynamics: a finite element approach. M. Géradin, A. Cardona. Wiley, 2001.

[24] Flügel B., Greil H., & Sommer, K. (1986): Anthropometrischer Atlas. Verlag Tribüne Berlin.

[25] Georgopoulos, A.P., Kalaska, J.F., Caminiti, R. and Massey, J.T., Spatial coding of movement: a hypothesis concerning the coding of movement direction by motor cortical populations. In J. Massion, J. Paillard, W. Schultz and M. Wiesendanger, (Eds.), Neural Coding of Motor Performance, Exp. Brain Res., Suppl. 7, 1983, pp. 327-336.

[26] Goel, V.K., Clark, C.R., Harris, K.G., Schulte, K.R. (1988): Kinematics of the cervical spine: Effects of multiple total laminectomy and facet wiring. *J. Orthopaedic Research*. 6: 611- 619.

[27] Gracovetsky, S., Newman, N., Pawlowsky, M., & Al., E. (1995): A database for estimating normal spinal motion derived from noninvasive measurements. *Spine* 20: 1036-46.

[28] GG Gregersen and DB Lucas: An in vivo study of the axial rotation of the human thoracolumbar spine. J Bone Joint Surg Am. 1967;49:247-262

[29] Grillner, S. (1981), Control of locomotion in bipeds, tetrapods, and fish. In *Handbook of physiology: Motor Control.* Sec. 1, vol. II Ed. V.B. Brooks, 1179-236. Baltimore: Williams & Wilkens.

[30] Grood, E.S. & Suntay, W.J. (1983): A joint coordinate system for the clinical description of three dimensional motions: Application to the knee. *J. Biomech. Eng.* 105(2): 136-144.

[31] Grossman, G.E., Leigh, R.J., Abel, L.A., Lanska, D.J. (1988): Frequency and velocity of rotational head perturbations during locomotion. Exp. *Brain Res.* 70: 470-476.

[32] Grossman, G.E., Leigh, R.J., Bruce, E.N., Huebner, W.P., Lanska, D.J. (1989): Performance of the human vestibular reflex during locomotion. *J. Neurophysiol.* 62: 264-272.

[33] Gruber, Stefan. Zur Dynamik und Regelung Zweibeiniger Gehmaschinen. Fortschr.-Ber. VDI Reihe 1 Nr. 374. Düsseldorf: VDI Verlag 2004.

[34] Gunzburg, R., Hutton W. & Fraser, R. (1991): Axial rotation of the lumbar spine and the effect of flexion. An in vitro and in vivo biomechanical study. *Spine* 16(1): 22-8.

[35] Hanavan, E.P. (1964): A mathematical model of the human body. Technical Report AMRL-TR-64-102 (AD 608 463). Wright-Patterson Air Force Base, Ohio.

[36] Hatze, H. (1980): A mathematical model for the computational determination of parameter values of anthropometric segments. *J. Biomech.* 13: 833-843.

[37] Hirasaki, E., Moore, S.T., Raphan, T., & Cohen, B. (1999): Effects of walking velocity on vertical head and body movements during locomotion. *Exp. Brain Res*. 127:117-130.

[38] Hoffmann, H. Eine experimentelle Studie zur Systematik der Nutzung von Rumpfschwingungen beim menschlichen Gehen. Dissertation Bochum 2001.

[39] Imai, T., Moore, S.T., Raphan T., & Cohen, B. (2001): Interaction of the body, head, and eyes during walking and turning. *Exp. Brain Res.* 136: 1-18.

[40] Klassische Mechanik II: Teilchensysteme, Lagrange-Hamiltonsche Dynamik, Nichtlineare Phänomene. Walter Greiner. Harri Deutsch Verlag 2003.

[41] Kumar, S. & Panjabi, M.M. (1995): In vivo axial rotations and neutral zones of the thoracolumbar spine. *J. of Spinal Disorders* 8(4): 253-263.

[42] Kumar, S., Dufresne, R. M. & Schoort, T. van (1995): Human trunk strength profile in lateral flexion and axial rotation. *Spine*20(2): 169-177.

[43] Kummer, B. (1981): Biomechanik der Wirbelgelenke. Die Wirbelsäule in Forschung und Praxis. 87: 29-34.

[44] Macintosh, J.E., Percy, M.J. & Bogduk, N. (1993): The axial torque of the lumbar back muscle: torsion strength of the back muscle. *Aust N Z J. Surg.* 63(3): 205-12.

[45] Marras, W.S. & Granata, K.P. (1995): A biomechanical assessment and model of axial twisting in the thoracolumbar spine. *Spine*20(13): 1440-1451.

[46] Mc Gregor, A.H., Mc Carthy, I.D. & Hughes S.P. (1995): Motion caracteristics of the lumbar spine in the normal population. *Spine* 20(22): 2421-2428.

[47] McGibbon, Ch. A. & Krebs D.E. (2001): Age-related changes in lower trunk coordination and energy transfer during gait. *J. Neurophysiology* 85: 1923-1931.

[48] Meyer, H. von: Statik und Mechanik des menschlichen Knochengerüstes. Leipzig: Engelmann 1873.

[49]Mussa-Ivaldi, F.A. (1998): Do neurons in the motor cortex encode movement direction? An alternative hypothesis. Neuroscience Letters, 91 (106-111).

[50] Nadeau, S., Amblard, B., Mesure, S., Bourbonais, D. (2003): Head and trunk stabilization strategies during forward and backward walking in healthy adults. *Gait & Posture* 18: 134-142.

[51] Nowinsky, G.P., Visarius, H., Nolte, L.P., Herkowitz, H.N. (1993): A biomechanical comparision of cervical laminaplasty and cervical laminectomy with progressive facetectomy. *Spine* 18: 1995-2004.

[52] Oxland, T.R., Lin, R.M. & Panjabi, M.M. (1992): Three-dimensional mechanical properties of the thoracolumbar junction. *J. Orthopaedic Research.* 10: 573-580.

[53] Panjabi, M., Yamamoto, I., Oxland, T. & Crisco, J. (1989): How does posture affect coupling in the lumbar spine? *Spine* 14: 1002-1011.

[54] Panjabi, M., Yamamoto, I., Oxland, T. & Crisco, J. (1994): Mechanical behavior of the human lumbar and lumbosacral spine as shown by three-dimensional load-displacement curves. *J. Bone Joint Surg.* 76-A(3): 413-424.

[55] Panjabi, M.M., Krag, M.H. & Goel, V.K. (1981): A technique for measurement and description of three-dimensional six degree-of-freedom motion of a body joint with an application to the human spine. *J. Biomech.* 14: 447-460.

[56] Panjabi, M.M., Oda, T. , Crisco III, J.J., Dvorák, J. & Grob, D. (1993): Mechanical behavior of the human lumbar and lumbosacral spine as shown by three-dimensional load-displacement curves. *J. of Bone and Joint Surgery.* 76-A, 413-424.

[57] Paul, R.P. (1982): Robot manipulators: mathematics, programming, and control (pp. 45-71). Cambridge: The MIT Press.

[58] Pearcy, Gill, Hindle, and Johnson (1987): Measurement of human back movements in three dimensions by opto-electronic devices. *Clin. Biomech.*

[59] Pearson, K.G. & Rossignol, S. (1991), Fictive motor patterns in chronic spinal cats. *J. Neurophysiol.* 66:1874-87

[60] Pozzo, T., Berthoz, A., Lefort, L. (1989): Head kinematic during various motor task in humans. *Prog. In Brain Research.* 80: 377-83.

[61] Pozzo, T., Berthoz, A., Lefort, L. (1990): Head stabilization during various motor task in humans. I. Normal subjects. *Exp. Brain Research.* 82: 97-106.

[62] Prince, F., Winter, D.A., Stergiou, P., Walt, S.E. (1994): Anticipatory control of upper body balance during human locomotion. *Gait & Posture* 2: 19-25.

[63] Putz, R. Funktionelle Anatomie der Wirbelgelenke. Doerr W., Leonhardt H. (Hrsg): Normale und Pathologische Anatomie, Band 43. Thieme Verlag Sttutgart 1981.

[64] Ronsky, J.L., & Nigg, B.M. (1993): Error in kinematic data due to marker attachment methods. *J. Biomech.*

[65] Rudolf Martin. Lehrbuch der Anthropologie. Jena. Verlag von Gustav Fischer 1914.

[66] Sarton, G (1953) A History of Science: Ancient Science Through the Golden Age of Greece (1-2). W.W. Norton & Company Inc., New York.

[67] Saur, P.M., Ensink, F.B., Frese, K., Seeger, D. & Hildebrandt, J. (1996): Lumbar range of motion: reliability and validity of the inclinometer technique in the clinical measurement of trunk flexibility. *Spine* 21(11): 1332-1338.

[68] Scholle H.Ch., Schumann N.P., Biedermann F., Stegeman, D.F., Graßme, R. Roeleveld, K. et al. (2001): Spatiotemporal surface EMG characteristics from rat triceps brachii muscle during treadmill locomotion indicate selective recruitment of functionally distinct muscle regions. *Exp. Brain Res.*138: 26-36.

[69] Simons, J.C. & Gardner, M.S. (1960): Self-Maneuvering for the orbital worker. Technical Report TR-60-7480. Wright-Patterson Air Force Base, Ohio.

[70] Skalli, W., Lavaste, F. & Descrimes, J.-L. (1995): Quantification of three-dimensional vertebral rotations in scoliosis: What are the true values? *Spine* 20: 546-553.

[71] Stokes, V.P., Andersson, C. & Forssberg, H. (1989): Rotational and translational movement features of the pelvis and thorax during adult human locomotion. *J. Biomech.* 22(1): 43-50.

[72] Syczewska, M., Öberg, T. & Karlsson, D (1999): Segmental movements of the spine during treadmill walking with normal speed. *Clin. Biomech.* 14:384-388.

[73] Taylor, N.F., Evans, O.M. & Goldie, P.A. (1996): Angular movements of the lumbar spine and pelvis can be reliably measured after four minutes of treadmill walking. Clin. Biomech 11: 484-486.

[74] Taylor, N.F., Goldie, P.A. & Evans, O.M. (1999) Angular movements of the pelvis and lumbar spine during self-selected and slow walking speeds. *Gait & Posture*9: 88-94.

[75] Three-dimensional analysis of human locomotion. Edited by P.Allard, A. Cappozzo, A. Lunberg and C.L. Vaughan. John Wiley & Sons 1997.

[76] Thurston, A.J. & Harris, J.D. (1983): Normal kinematics of the lumbar spine and pelvis. *Spine* 8(22): 199-205.

[77] van Emmerik, R.E.A., & Wagenaar, R. C. (1996): Effects of walking velocity on relative phase dynamics in the trunk in human walking. *J. Biomech.* 29(9): 1175-1184.

[78] Veldpaus, F.E., Woltring, H.J. & Dortmans, L.J. (1988): A least-squares algorithm for the equiform transformation from spatial marker co-ordinates. *J. Biomech.* 21(1): 45-54.

[79] Vink, P. & Karssemeijer, N (1988): *Anat. Embryol.* 178: 455-460.

[80] Vink, P., Daanen, H.A.M. & Spoor, C.W. (1989): Elastic strain energy in the low back muscles during walking. *Anat. Embryol.* 180: 99-101.

[81] Vogt, L. & Banzer, W. (1999): Measurements of lumbar spine kinematics in incline treadmill walking. *Gait & Posture* 9: 18-23.

[82] Waagenaar, R.C. & Beek, W.J. (1992): Hemiplegic gait: a kinematical analysis using walking speed as a basis. *J. Biomech.* 25(9): 1007-1015.
[83] Wessel, J., Ford, D. & Driesum, D. v. (1994): Torque of trunk flexion and trunk flexion with axial rotation in healthy men and women. *Spine* 19(3): 329-334.

[84] Whelan, P.J. (1996), Control of locomotion in the decerebrate cat. *Prog. Neurobiol.* 49:481-515.

[85] Whitsett, C.E. (1962): Some Dynamic response characteristics of weightless man. MS thesis. Wright-Patterson Air Force Base, Ohio.

[86] Witte, H. & Günther M.M.: Die Bewegungsanalyse ist das wichtigste Werkzeug der Biomechanik zur Beantwortung klinischer Fragestellungen. Wie wähle ich die richtigen Verfahren und Geräte aus? Rechnergestützte Verfahren in Orthopädie und Unfallchirurgie. Jerosch, Nicol & Peikenkamp (Hrsg.). Steinkopff Darmstadt, 1999.

[87] Witte, H. (2002): Hints for the construction of anthropomorphic robots based on the functional morphology of human walking. -*Journal of the Robotic Society of Japan* 20(3): 247-254.

[88] Witte, H. Beiträge zur funktionellen Anatomie und Biomechanik elastischer Elemente im Bewegungsapparat. Habilitationsschrift Bochum 1996.

[89] Witte, H., Hoffmann, H., Hackert, R., Schilling, C., Fischer, M.S. & Preuschoft, H. (2004): Biomimetic Robotics should be based on Functional Morphology.- *J. Anat.* 204: 331-342.

[90] Witte, H., Voges, D., Schwerda, D., Schilling, N & Fischer, M. S. (2003): Eine Beschreibungsgröße für die Gleichförmigkeit Zyklischer Bewegungen. -In: Grieshaber, R., Schneider, W., Scholle, H.C. (Hrsg.) Prävention von arbeitsbedingten Gesundheitsgefahren und Erkrankungen. 9. Erfurter Tage. Monade Konzept & Kommunikation, Leipzig, 323-336.

[91] Woltring, H.J. (1985): On optimal Smoothing and derivative estimation from noisy displacement data in biomechanics. *Human Movement Science*. 4(3): 229-245.

[92] Woltring, H.J. (1991): Representation and calculation of 3-D joint movement. *Human Movement Science.* 10(5): 603-616.
[93] Wu, G. & Cavanagh, P.R. (1995): ISB recommendations for standardization in the reporting of kinematic data. *J. Biomech*. 28: 1257-1261.

[94] Yeadon, M.R. (1989a): The simulation of aerial movement-II: A mathematical model of the human body. *J. Biomech.* 23(1): 67-74.

[95] Yeadon, M.R. (1989b): The simulation of aerial movement-III:The determination of the angular moment of the human body. *J. Biomech.* 23(1): 75-83.

Internet References:

[96] Ergonomic Models of Anthropometry, Human Biomechanics and Operator-Equipment Interfaces: Proceedings of a Workshop (1988): www.nap.edu/openbook/POD267/html/11.html, 2000 The National Academy of Sciences.

[97] The Mathworks® (www.mathworks.com)

[98] Qualisys® Motion Systems (www.qualisys.com)

[99] 3-D Science® (www.3-dscience.com)

Thesen

Titel: Ein neues Modell der Mechanik des menschlichen Rumpfes beim Gehen

Verfasser: Emanuel Andrada

1 Der Körperstamm besteht aus Rümpf, Hals und Kopf. Die Bewegungen des Rumpfes sind hinreichend zu beschreiben durch die Bewegungen von Schultergürtel, Mittelbauch und Beckengürtel.

2 Die stammesgeschichtlichen Vorfahren des Menschen produzieren bis zu 50 % ihres Raumgewinns bei der Fortbewegung durch Bewegungen des Rumpfes. Diese Bewegungen sind mit jenen der Extremitäten auf ein optimiertes Verhalten des Gesamtsystems abgestimmt [Fischer & Lehmann 1998].

3 Beim menschlichen Gehen interagiert auch der Rumpf systematisch mit den Extremitäten. Aus diesem Grund kann man Änderungen in den Rumpfamplituden, Frequenzen und Phasen als eine Funktion der Fortbewegungsgeschwindigkeit beobachten [Hoffmann 2001]. Diese Änderungen werden aber individuell durchgeführt. Damit bildet sich eine intra- und interindividuelle Variation in der Kinematik des Rumpfes. Die Ursachen dieser Variationen sind bis dato nicht bekannt.

4 Haupt Ziele der Arbeit sollen sein: 1) ein neues Modell des Rumpfes basiert auf morphologische, funktionelle, kinematische und dynamische Studien zu erstellen; und 2) die Ursache der intra- und interindividuellen Variation in der Kinematik des Rumpfes beim Gehen zu erklären.

5 Für die Erklärung der intra- und interindividuellen Variation in der Kinematik des Rumpfes beim Gehen werden zwei Hypothesen getestet: a) Die intra- und interindividuelle Variation der Kinematik des Rumpfes ist eine Funktion der Massenverteilung. Daher erwartet man große Korrelationskoeffizienten zwischen Anthropometrie und Rumpfkinematik; b) Bewegungsamplituden, Frequenzen und Phasen werden nicht nur von den in der Anthropometrie abgebildeten Massenverteilungen bestimmt, sondern auch von den visco-elastischen Eigenschaften des Bewegungsapparates.

6 Als für die Untersuchung notwendiger Probenumfang wird angesehen: Untersucht wurden 56 Männer und 50 Frauen der Altersgruppe 18 bis 30 Jahre ohne bekannte Vorerkrankungen des Bewegungsapparates. Von den Versuchspersonen wurden je 48 anthropometrische Maße erhoben. Bei Laufbandgeschwindigkeiten von 2,0 km/h bis 6,0 km/h (Intervall 0,5 km/h) wurden danach je im auf- und im absteigenden Geschwindigkeitsprofil die Bewegungen von Beckengürtel, Schultergürtel und Kopf mittels Reflexmarkertriplets beobachtet. Dabei wurde mit dem Bewegungsanalysesystem Qualisys® Proreflex® analysiert.

7 Für die mathematische Auswertung war sinnvoll: Interpolation, Filterung, Rotationsberechnung, Frequenzanalyse im Programmpaket MATLAB®. Zur statistischen Auswertung Zusammenführung alle erhobenen Kennwerte (Anthropometrie und FFT-Parameter) im Statistikpaket SPSS®.

8 Bei höherer Geschwindigkeit nehmen die Schwingungsamplituden des Beckens auf die Frontale und Transversale Ebene zu. Gleichzeitig sinkt die Phase zwischen die beiden Bewegungen von 100° bei 2 km/h bis zu „fast in Phase“ ab 4,5 km/h.

9 Thorax und Kopf Kinematik sind mechanisch stark gekoppelt. Dieses Verhalten spiegelt sich in der Amplitudenähnlichkeit und den Phasenmustern bei Änderung der Geschwindigkeit des jeweils Körpersegmentes wieder. Außerdem kompensieren Kopfrotationen weder auf die Transversale noch auf die Frontalebene die Rotationen der Schulter.

10 Erwartungsgemäß ist die Torsionsamplitude des Rumpfes bei den Frauen größer. Hauptursachen für das Inkrement in der Torsion des Rumpfes in Abhängigkeit von der Geschwindigkeit sind: a) die Zunahme der Axialrotation des Beckens und b) das Inkrement des Phasenwinkels zwischen Becken und Thorax.

11 Das Inkrement des Phasenwinkels zwischen Becken und Thorax bei zunehmender Geschwindigkeit leistet zwei wichtige Aufgaben: erstens dient es dazu, die zunehmenden Bodenreaktionskräfte zu dämpfen, zweitens, größere Rotationsbewegungen im Thorax zu verhindern.

12 Die Dämpfungsmechanismen im Körperstamm stabilisieren den Kopf im Raum und minimieren die Notwendigkeit der „Augenkompensation“ für das Sehen beim Gehen. Sie sind ausgeprägter auf die Frontal als auf die Transversalebene. Außerdem, sind die Dämpfungsmechanismen bei den Frauen stärker als bei den Männern.

13 Die so genannten „Kompensationsmechanismen“ zwischen Kopfrotationen und Schultertranslationen dienen dazu, den Blick gezielt zu behalten. Sie sind geschwindigkeitsabhängig. Mit zunehmender Geschwindigkeit nutzen Frauen eher „Schulterkompensation“, während Männer „Kopfkompesation“ betonen.

14 Die Variation der Korrelationskoeffizienten zwischen den Bewegungskomponenten zeigt, dass der Mensch unterschiedliche Bewegungskombinationen nutzt, wenn die Geschwindigkeit schneller oder langsamer wird.

15 Die Clusteranalyse zwischen Beinlänge und Rumpffrequenzen stellt dar, dass große Menschen niedrigere Rumpffrequenzen als mittelgroße, und diese wiederum niedrigere Frequenzen nutzen als kleine Menschen.

16 Die intra- und interindividuelle Variation in der Kinematik des Rumpfes kann allein durch die Anthropometrie der Menschen nicht erklärt werden.

17 Das hier vorgestellte morpho-funktionelle Modell des Rumpfes kann die intra- und interindividuelle Variation in der Kinematik des Rumpfes erklären. Es wurde auf der Basis des Hanavan Modells in Simulink® erstellt. Dieses Modell hat 14 DOF. Segmentalamplituden, Frequenzen und Phasen werden durch visco-elastische Elemente angepasst (Feder und Dämpfer). Die Anpassungsprozesse werden mittels einer Optimierungsroutine durchgeführt.

18 Die unterschiede der Federkonstanten sind die Hauptursache für die Amplitudenvariation in allen Körpersegmenten und für die Phasenvariation auf die Frontalebene.

19 Höhere Dämpfungskonstanten wirken zuerst als Tiefpaß. Bei höheren Werten rufen Phasen und Amplitudevariationen hervor.

20 Die kinematischen Ergebnisse liefern signifikante harmonischen Frequenzen dar. Das ist ein Indiz dafür, dass die Bewegungen schwach gedämpft sind und auch, dass das „System Mensch“ mechanisch annährend konservativ ist.

21 Für die Anpassung der Phasen zwischen Becken und Schultergürtel in der Transversalebene gelten die folgenden Kriterien: a) ohne die Schultergelenke zu dämpfen, nähert sich die Phase 180°; b) mit der Zunahme der Dämpfungskonstanten in den Schultergelenken sinkt die Phase bis zu Werten um die 0° (bei Dämpfungskonstanten um die 0,5 Nm/rad).

22 Für die Anpassung der Phasen zwischen Becken und Schultergürtel in der Frontalebene gilt das folgende Kriterium: Die Variation der Federkonstanten verursacht sowohl Amplituden- als auch Phasenänderungen. Mit der rechnerischen Approximation der Amplituden wird daher die Phase gleichzeitig angepasst.

23 Simulationen zeigen, dass die Hauptarbeit für systematische Amplitudenverringerungen (Dämpfungsmechanismen) nach kranial, im Abdomenbereich geleistet wird.

24 Die doppelte Frequenz der Schwingung in der Sagittaleebene stellt sich in der Simulation ohne zusätzliche Zwangsbedingungen ein.

25 Auf der Grundlage der erstellten Modellergebnisse werden die Kompensationsmechanismen als ein Ergebnis der Bewegungsdynamik interpretiert und nicht unbedingt als die Folge eines aktiven Kontrollmechanismus.

26 Die visco-elastischen Parameter (Feder- und Dämpfungskonstanten) spiegeln die Muskelaktivierung des Körpersegmentes wieder. Diese zeigen, dass die Muskeln nicht nur Kraftelemente sind, sondern auch anpassbare visco-elastische Elemente.

27 Die visco-elastischen Parameter sind eine solide erklärende Kenngröße für die Änderungen der Amplituden, Frequenzen und Phasen der Körpersegmente des Körperstammes beim Gehen.

28 Im Modell werde die visco-elastischen Parameter als Standardeinstellung genutzt. Die Intraindividuelle Variation dieser Standardeinstellungen zusammen mit der eigenen Masseverteilung des Rumpfes bildet die verschiedenen Gangarten.

29 Pathologische Störungen lassen die funktionelle periodische Bewegung des Rumpfes ebensowenig unbeeinflusst wie die strukturelle Stabilität der funktionstragenden Strukturen (Muskeln, Bänder, Gelenke und Knochen). Daher sollten die visco-elastischen Parameter als Krankheitsprädiktoren getestet werden.

30 Das nicht-invasive Tool für Diagnostik und Therapieüberwachung des Rumpfes präsentiert eine neue Methode für die Objektivierung der kinematischen und dynamischen Kenngrößen des Rumpfes beim Gehen.

31 Für bionisch inspirierte Roboter könnten visco-elastische Komponenten dazu dienen, den Bedarf an Energie und Kontrol radikal zu senken. Deren Applikation wird den Sprung von morphologischesähnlichen zu und morpho-funktionellen Maschinen erlauben.